

Dissertation

submitted to the

Combined Faculties for the Natural Sciences and for Mathematics

of the Ruperto-Carola University of Heidelberg, Germany

for the degree of

Doctor of Natural Sciences

presented by

Tillmann Michels, M.Sc.

born in: Tönisvorst, Germany

Oral examination:

.....

A high-throughput RNAi screening identifies olfactory receptor signaling as a novel immune checkpoint in solid tumors

Referees:

Prof. Dr. Philipp Beckhove

Prof. Dr. Michael Boutros

The work described in this thesis was performed from 2012 to 2015 in the Department of Translational Immunology at the National Center for Tumour Diseases – NCT of the German Cancer Research Center - DKFZ in Heidelberg, Germany and from 2016 to 2017 in the department of Interventional Immunology at the Regensburg Center for Interventional Immunology – RCI in Regensburg under the supervision of Prof. Dr. Philipp Beckhove.

Declaration

I herewith declare that I have completed this thesis single-handedly without any unauthorized help of a second party. Any help that I have received in my research work or in the preparation of this thesis has been duly acknowledged.

Heidelberg, 17.12.2017

Tillmann Michels

Parts of this thesis have been published in:

Papers:

Khandelwal N, Breinig M, Speck T, **Michels T**, Kreutzer C, Sorrentino A, Sharma AK, Umansky L, Conrad H, Poschke I, Offringa R, König R, Bernhard H, Machlenkin A, Boutros M, Beckhove P. *A high-throughput RNAi screen for detection of immune-checkpoint molecules that mediate tumor resistance to cytotoxic T lymphocytes*. EMBO Molecular Medicine. 02/2015. DOI:10.15252/emmm.201404414

Sorrentino A, Menevse A, **Michels T**, Volpin V, Jeltsch K, Rhatinasamy A, Werner-Klein M, Breinig M, Mikiety D, Poschke I, Wagner S, Offringa R, Gebhard C, Rheli M, Boutros M, Khandelwal N, Beckhove P. *Cytotoxic T cell attack triggers tumor proliferation through salt-inducible-kinase-3 activation*. **submitted**

Patents:

Philipp Beckhove, **Tillmann Michels**, Nisit Khandelwal, Antonio Sorrentino, Valentina Volpin, Michael Boutros, Marco Breinig. *Immune modulators for reducing immune resistance in melanoma and other proliferative diseases*, filed 10.11.2016

Philipp Beckhove, Nisit Khandelwal, Michael Boutros, Marco Breinig, **Tillmann Michels**. *Modulators of tumor immune resistance for the treatment of cancer*, filed 16.02.2016.

Philipp Beckhove, Nisit Khandelwal, Michael Boutros, Marco Breinig, **Tillmann Michels**. *Modulators of CCR9 for treating tumor resistance to immune responses*, filed 16.02.2016.

Conference presentations:

Michels T. *GPCRs in Immune Evasion of Cancer*. Discovery on Target 09/2017, Boston, USA

Michels T, Hartl CA, Khandelwal N, Breinig M, Sorrentino A, Volpin V, Mäder C, Menevse A, Umansky L, Poschke I, Offringa R, Milenkovic VM, Wetzl C, Boutros M, Eisenberg G, Lotem M, Beckhove P. *Olfactory receptor signaling as a novel immune checkpoint in solid tumors*. Cancer Immunotherapy and Immunomonitoring - CITIM 04/2017, Prague, Czech Republic

Michels T. *Novel Immune Checkpoints Identified by RNAi Screening*. World Preclinical Congress 11/2016, Lisbon, Portugal

Michels T, Hartl CA, Khandelwal N, Breinig M, Sorrentino A, Mäder C, Umansky L, Poschke I, Offringa R, Boutros M, Eisenberg G, Lotem M, Beckhove P. *TiMi1 is a novel immune checkpoint in solid tumors identified via a tumor-infiltrating lymphocyte (TIL)-based RNAi screening*. International Retreat of PhD students in Immunology, 06/2015, Catanzar, Italy

Michels T, Hartl CA, Khandelwal N, Breinig M, Sorrentino A, Mäder C, Umansky L, Poschke I, Offringa R, Boutros M, Eisenberg G, Lotem M, Beckhove P. *TiMi1 is a novel immune checkpoint in solid tumors differentially regulating calcium-depending signaling in tumor-infiltrating lymphocytes*. Cancer Immunotherapy – CIMT 05/2015, Mainz, Germany

Michels T, Hartl CA, Khandelwal N, Breinig M, Sorrentino A, Mäder C, Umansky L, Poschke I, Offringa R, Boutros M, Eisenberg G, Lotem M, Beckhove P. *TiMi1 is a novel immune checkpoint in solid tumors identified via a tumor-infiltrating lymphocyte (TIL)-based RNAi screening*. American Association of Cancer Research annual meeting – AACR 04/2015. Cancer Research 08/2015; 75 (15 Supplement): pp.254

Acknowledgments

First of all, I want to thank Prof. Philipp Beckhove for the opportunity to work on such an interesting topic and for his supervision. When I started I could not imagine the different fields of research and the amount of methods that I would get in contact with over the following years. Working in this lab offered me a unique PhD student experience inside and outside the cell culture. I am especially grateful for the trust that was given me to help starting the company, to set up the immune checkpoint group at the RCI and to interact with other research groups independently. Although often challenging these tasks prepared me for whatever comes next. I want to thank Prof. Michael Boutros and Dr. Marco Breinig for their continuous help in anything related to high-throughput screenings. Furthermore, I want to thank my TAC members Prof. Michael Boutros and Prof. Knut Schäkel for their constructive input on this project.

Special gratitude goes to our amazing collaboration partners from Israel. Dr. Michal Lotem, Dr. Galit Eisenberg, Dr. Arthur Machlenkin and all other members of Dr. Lotems lab made my stay in Jerusalem unforgettable. I am convinced that this fruitful collaboration was crucial for a lot of the scientific success in our lab and will hopefully continue for a long time.

The most important part of any PhD student experience are the colleagues. And I was blessed to have worked among the best. I want to thank Dr. Nisit Khandelwal for all the support over the years and especially at the beginning of my PhD. Our business trips together with Dr. Antonio Sorrentino to different big companies and the presentations in front of important people expanded my horizon beyond academic science. As mentioned, Toni was an important companion during my PhD. I will never forget our non-stop poster presentation at the AACR or all the celebratory events we attended. Of course, I also appreciate the scientific discussions over the years and his input to this project. I want to thank Valentina and Ayse for their constant help with experiments and the fruitful discussions. Without them this project would not have been possible. Special thanks go to Christina Hartl, Christina Mäder, Lora and Katja for their help with important experiments. It was a pleasure to work with such brilliant and motivated students. Christina Hartl pushed this project with an astonishing motivation, scientific knowledge and incredible ideas. I want to thank all our technicians – especially Janine, Karin and Ludmila – for all their help. Any acknowledgments would be incomplete without mentioning Dr. Slava Stamova. She gave valuable input to all scientific questions and fed the

hungry. Outside the lab she organized social events and made sure everybody came home safe. Furthermore, she helped me to get settled in Regensburg. Maria, Anchana, Kathi and Chih-Yeh gave valuable scientific input as well. I want to thank Heiko, Birgitta and Jasmin for all the lab organization. Heiko made our office feel comfy and cozy and showed everybody how to have a good time at the Dult. I want to thank Janine and Jasmin for the fresh energy they brought to our lab and for showing me that Bavarian is really difficult to understand. I want to thank Sabine Termer, Sabine Repp and Mathea for never giving up on trying to tame the organizational chaos that is our lab.

I want to thank all our scientific collaborators. Prof. Christian Wetzel and Dr. Vladimir Milenkovic for the help with single-cell imaging to measure calcium and cAMP signaling and Prof. Stefan Eichmüller for the help with melanoma cultures. Thanks to all former members of D015: Jasmin, Anna-Lena, Noemi, Hans-Henning, Mudita, Felix, Simone, Mariana and Ludmila for their support inside and outside the lab.

I want to thank Adriana for understanding the ups and downs that come along with being a PhD student. I am particularly thankful for the support in the darkest hours.

Special thanks to my friends: Marcel, Robert, Christian, Christian, Patrick, Barbara, Marc and many more. It is always important to be reminded that there is life outside the cell culture.

Last but not least, I would like to express my gratitude to my family for their support and their unconditional love.

“I may not have gone where I intended to go, but I think I have ended up where I needed to be.”

— Douglas Adams

Gewidmet Heinz-Bernd Michels

Summary

Immune checkpoint blockade has revolutionized immunotherapy against cancer with tremendous clinical benefits for patients. Despite these achievements, tumors utilize a plethora of suppressive mechanisms to evade immune destruction which are yet to be understood and matched by today's immunotherapy. Our group developed a high-throughput RNAi screening to unravel the arsenal of immune checkpoints of cancer. We screened a siRNA library (around 2880 kinases and surface-associated genes) with patient-derived tumor cells and HLA-matched tumor-infiltrating lymphocytes (TILs).

The library was reverse-transfected into M579-A2 melanoma cells and these were co-cultured with MART1- and gp100-specific TILs to determine TIL-mediated lysis. We identified 75 genes in tumor cells that impaired TIL-mediated cytotoxicity. Interestingly, we found that several genes and their associated pathways were found in pancreatic adenocarcinoma and multiple myeloma as well. This suggests that different cancer entities might share inhibitory modes of action. In order to distinguish between genes altering tumor susceptibility towards TIL-mediated killing and those impairing TIL activity, we established a secondary screening assaying multiple T cell activation marker, including effector cytokines.

The olfactory receptor OR10H1 was one of the strongest candidates from our primary screening as its knockdown increased TIL-mediated killing in melanoma, PDAC and colorectal carcinoma. Furthermore, TILs were activated stronger after interaction with OR10H1-deficient cells as sensed by the increased secretion of type 1-associated cytokines and a reduced T cell apoptosis. We confirmed the role of OR10H1 as an immune checkpoint *in vivo* using a xenograft mouse model in combination with adoptive T cell transfer.

We performed mode of action analyses in order to understand how OR10H1 affects T cell activity. These analyses revealed that tumor-associated OR10H1 controls cAMP-dependent signaling inside T cells. Inside TILs, cAMP activates protein kinase alpha (PKA) and PKA in turn activates C-terminal Src kinase (Csk). Csk phosphorylates an inhibitory tyrosine residue of Lck impairing its activity and shutting down TCR-associated signaling. Furthermore, PKA activates CREB and thus induces an anergy-associated gene expression profile in TILs. Our data suggest that OR10H1 alters the balance between the inhibitory ($G\alpha_i$) and the stimulatory/olfactory G-Protein alpha ($G\alpha_{s/olf}$) inside tumor cells depending on the encounter

of TILs. This results into increased production of cAMP in tumor cells and its subsequent transport into T cells.

In summary, we established a discovery platform aiding the search for immune checkpoints in cancer. We identified OR10H1 and its associated olfactory receptor signaling as a novel pathway inhibiting TIL responses by inducing cAMP-dependent Lck inhibition.

Zusammenfassung

Die Entwicklung so genannter “Immun-Checkpoint Blockaden” wird als Durchbruch im Kampf gegen Krebs angesehen. Jedoch muss die große Anzahl an Mechanismen, welche von Tumoren genutzt wird um einer Zerstörung durch das Immunsystem zu entgehen, erst noch verstanden werden damit möglichst alle Krebspatienten von den Vorteilen moderner Immuntherapie profitieren können. Unsere Gruppe hat hierzu ein siRNA basiertes Hochdurchsatz-Screening entwickelt um das Arsenal an Immun-Checkpoints verschiedener Tumorentitäten zu entschlüsseln. Wir haben mit dieser Technologieplattform und mit Hilfe von aus Patienten gewonnenen tumorinfiltrierenden Lymphozyten (TILs) und HLA-abgestimmten Primärhautkrebskulturen eine Bibliothek von ca. 2880 Kinasen und Zelloberflächen-assoziierten Genen gescannt.

M579-A2 Melanomzellen wurden mit siRNA transfiziert und anschließend mit MART1- und gp100-spezifischen TILs co-kultiviert um die TIL-vermittelte Lyse zu messen. Das Screening ermittelte 75 Kandidaten, welche die TIL-vermittelte Zytotoxizität negativ beeinflusst haben. Einige dieser Kandidaten wurden auch im Multiplen Myelom und Pankreas-Adenokarzinom als Immun-Checkpoints identifiziert. Dies deutet auf gemeinsam genutzte inhibitorische Signalwege hin. Um den Informationsgewinn unserer Technologieplattform zu erhöhen haben wir ein sekundäres Screening entwickelt, in welchem verschieden Marker der T-Zell-Aktivierung gemessen wurden.

Einer der stärksten Kandidaten aus unserem Screening war der olfaktorische Rezeptor OR10H1. Die Herunterregulierung von OR10H1 erhöhte die TIL Aktivität im Malignen Melanom, Pankreas-Adenokarzinom und kolorektalem Karzinom. Des Weiteren wurde durch die Herunterregulierung von OR10H1 auf den Tumorzellen die Produktion von Typ-1 assoziierten Zytokinen erhöht und das Level an Apoptose in TILs reduziert. Wir konnten die Rolle von OR10H1 als einen Immun-Checkpoint in einem Xenograft Mausmodell in Kombination mit adoptivem Zelltransfer bestätigen.

Unser Ziel war es zu verstehen wie OR10H1 die T-Zell-Aktivität beeinflusst. Diverse Signalweganalysen zeigten, dass OR10H1 die TIL Funktionalität inhibiert indem es cAMP-abhängige Signalwege verändert. Proteinkinase A (PKA) wird durch cAMP aktiviert und aktiviert wiederum C-terminal Src kinase (Csk). Diese inhibiert die lymphocyte-specific protein tyrosine kinase (Lck) durch Phosphorylierung. Unsere Daten zeigen, dass OR10H1 die Balance

zwischen G-Protein alpha I ($G\alpha_i$) und G-Protein alpha S/olfactory ($G\alpha_{s/olf}$) in den Tumorzellen ändert. Dies führt zur Produktion von cAMP und dessen Transport in die T Zelle sowie schlussendlich zur Inhibierung von Lck.

Zusammenfassend haben wir eine Technologieplattform entwickelt um systematisch Immun-Checkpoints ermitteln zu können. Unser neuer Antigen-spezifischer Ansatz führte zur Identifizierung von OR10H1 und dem damit assoziierten Olfaktorischen Signalweg als ein Inhibitionsmechanismus gegen T-Zell-Antworten. Dies geschieht durch die Aktivierung cAMP-abhängiger Signalwege innerhalb der TILs.

Table of Contents

Abbreviations and Definitions	1
1 Introduction	4
1.1 Cancer.....	4
1.2 Antitumor immunity	5
1.3 Cancer immunoediting: Tumor growth despite an antitumor response	7
1.3.1 Elimination (immunosurveillance).....	7
1.3.2 Equilibrium	7
1.3.3 Escape.....	8
1.4 Subsets, dysfunction, and transcriptional regulation of CD8 ⁺ tumor-infiltrating lymphocytes	8
1.4.1 Effector CD8 ⁺ TILs.....	8
1.4.2 Memory CD8 ⁺ T cells	10
1.5 Mechanisms of immune evasion	14
1.5.1 Tumor cell intrinsic immune escape mechanisms	14
1.5.2 Inhibitory tumor microenvironment.....	15
1.5.3 Immune checkpoints: Inhibitory pathways between tumor and T cells.....	19
1.5.4 Inhibitory receptors on T cells	24
1.6 Cancer immunotherapy	24
1.6.1 Cancer vaccines	25
1.6.2 Adoptive cell transfer	25
1.6.3 Immune checkpoint blockade	26
1.7 RNA interference (RNAi) used for gene knockdown	28
1.8 High-throughput screenings dissecting tumor-immune interactions	30
2 Aim and objectives of the thesis.....	32
3 Materials	34
3.1 Laboratory equipment	34
3.2 Stimulation peptides.....	35
3.3 Reagents and consumables.....	35
3.4 Antibodies.....	38
3.5 Primers	39
3.6 shRNA and siRNAs.....	39
3.7 Assay kits	40
3.8 Buffers.....	42

3.9	Media	44
3.10	Mice	45
4	Methods.....	46
4.1	Cell culture methods.....	46
4.1.1	Tumor cell lines.....	46
4.1.2	Generation of stable luciferase transfected M615-luc.....	46
4.1.3	Generation of stable OR10H1 knock-down melanoma cells	46
4.2	Molecular techniques	47
4.2.1	RT-PCR.....	47
4.2.2	Protein extraction	48
4.2.3	Western blotting	48
4.2.4	Transfections.....	49
4.3	TIL generation.....	50
4.3.1	TIL isolation	50
4.3.2	TIL rapid expansion (REP).....	51
4.3.3	TIL activity measurement.....	51
4.3.4	TIL preparations.....	52
4.4	Assays	52
4.4.1	Proliferation assay.....	52
4.4.2	TIL-mediated killing assays.....	52
4.4.3	Flow cytometry	54
4.5	RNAi Screening.....	54
4.5.1	Screening	54
4.5.2	Screening analysis.....	55
4.6	Mode of action analysis.....	56
4.6.1	TIL extraction after co-culture	56
4.6.2	Phosphoprotein analysis.....	57
4.6.3	Calcium imaging	57
4.6.4	cAMP imaging	58
4.6.5	Differential gene expression analysis	58
4.7	Mouse experiments	60
4.8	Statistical evaluation	60
5	Results.....	61
5.1.1	Screening setup.....	61
5.1.2	Characterization of M579 melanoma cultures	61

5.1.3	Tumor-infiltrating lymphocytes 412 kill M579-A2 in an antigen-specific and HLA-restricted manner.....	62
5.1.4	PD-L1 and Galectin-3 protect M579-A2 against TIL412-mediated lysis.....	66
5.2	High-throughput RNAi screen performance.....	68
5.3	The high-throughput RNAi screens reveals novel immune checkpoint candidates in melanoma.....	71
5.4	The immunomodulatory repertoire of solid tumors overlaps.....	75
5.5	OR10H1 inhibits TIL-mediated lysis of solid tumors.....	77
5.5.1	OR10H1 is expressed in solid tumors.....	77
5.5.2	OR10H1 prevents TIL-mediated lysis of melanoma <i>in vitro</i>	78
5.5.3	OR10H1-mediated inhibition of TIL cytotoxicity against melanoma is depending on HLA-A2/TCR interactions.....	80
5.5.4	OR10H1 inhibits TIL-mediated lysis of PDAC and CRC.....	83
5.6	OR10H1 inhibition augments TIL-mediated anti-tumor responses after adoptive T cell transfer <i>in vivo</i>	85
5.6.1	Generation of stable OR10H1 knockdown cell lines.....	86
5.6.2	Adoptive T cell transfer reduced tumor growth in OR10H1 ⁻ melanomas in a xenograft NSG mouse model.....	87
5.7	Tumor-restricted OR10H1 inhibits TIL activity and survival.....	89
5.8	Tumor-restricted OR10H1 induces TIL gene expression associated with negative regulation of T cell activation.....	91
5.8.1	Separation of TIL412 and M579-A2 after co-culture.....	91
5.8.2	OR10H1 induces differential gene expression in TILs.....	92
5.8.3	OR10H1 knockdown increased expression of genes positively associated with immune function downstream of TCR in TILs.....	97
5.9	Tumor-associated OR10H1 impairs anti-tumor activity by activation of CREB and inhibition of Lck in TILs.....	100
5.10	OR10H1-mediated TIL inhibition involves cAMP transport via gap junctions.....	106
5.11	OR10H1 regulates the balance between G α _i and G α _{oif} /G α _s signaling in tumor cells upon TIL encounter.....	108
5.11.1	OR10H1-dependent calcium signaling.....	109
5.11.2	OR10H1-dependent cAMP signaling.....	112
5.12	Improved TIL-mediated lysis of M579-A2 after OR10H1 knockdown can be reversed by cholera toxin (CTX).....	114
6	Discussion.....	116

6.1	High-throughput RNAi screening for tumor-restricted immune checkpoints	116
6.2	Setup and performance of the high-throughput RNAi screen	119
6.3	The immune checkpoint repertoire of cancer	121
6.4	OR10H1 as an immune checkpoint in cancer	123
6.4.1	Olfactory receptors outside of olfactory neurons	123
6.4.2	OR10H1 prevents tumor lysis by inhibiting TIL function.....	127
6.4.3	OR10H1 impairs TCR signaling via PKA-mediated Lck inhibition.....	128
6.4.4	Tumor-associated OR10H1 activation leads to the transport of cAMP via gap junctions	129
6.5	Translational implications of OR10H1 as a target for cancer immunotherapy.....	131
6.5.1	Anti-OR10H1 therapy as monotherapy.....	132
6.5.2	Anti-OR10H1 therapy combined with other immune checkpoint blockades	132
7	Conclusion	134
8	References	135
	Supplementary Data	153

Abbreviations and Definitions

Abbreviation	Name	Abbreviation	Name
%	Percentage	DAMP	Damage-associated molecular pattern
°C	Degree Celsius	DC	Dendritic cell
A2AR	A2A adenosine receptor	DISC	Death inducing signaling complex
AB	Human serum type AB	DMEM	Dulbecco's modified Eagle's medium
ADYC3	Adenylate cyclase 3	DNA	Deoxyribonucleic acid
ACT	Adoptive cell transfer	DR	Death receptor
AP-1	Activator protein 1	E:T	Effector : target
APC	Antigen-presenting cell	EDTA	Ethylenediaminetetraacetic acid
ATF	Activating transcription factor	EGR	Early growth response protein
ATP	Adenosine triphosphate	ELISA	Enzyme-linked immunosorbent assay
BATF	Basic leucine zipper transcription factor, ATF-like	EOMOS	Eomesodermin
BLIMP	B-lymphocyte-induced maturation protein	ERK	Extracellular signal-regulated kinases
bp	Base pair	FACS	Fluorescence-activated cell sorting
Ca ²⁺	Calcium	FCS	Fetal calf serum
CAMK1D	Calcium/calmodulin-dependent protein kinase type 1 delta	FDR	False discovery rate
cAMP	Cyclic adenosine monophosphate	Fluc	Firefly luciferase
Casp-3	Caspase-3	FOXO1	Forkhead box protein O1
CCR9	C-C chemokine receptor type 9	FOXP1	Forkhead box protein P1
CD	Cluster of differentiation	FRET	Förster resonance energy transfer
CEACAM	Carcinoembryonic antigen-related cell adhesion molecule	g	Gram
CLM	Complete lymphocyte medium	Gal-3	Galectin-3
CMM	Complete melanoma medium	GFP	Green fluorescent protein
CO ₂	Carbon dioxide	GJB1	Gap junction beta-1 protein
CRC	Colorectal cancer	GM-CSF	Granulocyte-macrophage colony-stimulating factor
CREB	cAMP response element-binding protein.	gp100	Glycoprotein 100
Csk	C-terminal Src kinase	GPCR	G-protein coupled receptor
CTG	CellTiter-Glo	h	Hours
CTLA-4	Cytotoxic T-lymphocyte-associated protein 4	HLA	Human leukocyte antigen
CX32	Connexin 32	i.v.	Intravenous
		ICAM1	Intercellular adhesion molecule 1
		IFN	Interferon
		IL	Interleukin
		IP3	Inositol trisphosphate

ITIM	Immunoreceptor tyrosine-based inhibitory motif	p70 S6	Ribosomal protein S6 kinase beta-1 (S6K1)
ITSM	Immunoreceptor tyrosine-based switch motif	PBMC	Peripheral blood mononuclear cell
JAK	Janus kinase family	PCR	Polymerase chain reaction
JNK	c-Jun N-terminal kinases	PD-1	Programmed cell death protein 1
kb	Kilobase	PD-L1	Programmed death ligand 1
kd	knockdown	PDAC	Pancreatic ductal adenocarcinoma
L	Liter	PI3K	Phosphoinositide 3-kinase
LAG-3	Lymphocyte-activation gene 3	PKA	Protein kinase alpha
LAT	Linker for activation of T cells	PKC	Protein kinase C
Lck	Lymphocyte-specific protein tyrosine kinase	PMA	4-Methoxyamphetamin
LFA1	Lymphocyte function-associated antigen 1	PRKD2	Protein kinase D2
LOESS	LOcal regrESSion	Ras	Rat sarcoma
m	Meter	RCAS1	Receptor-binding cancer antigen expressed on Siso cells
M	Molar	REP	Rapid expansion protocol
MAPK	Mitogen-activated protein kinase	RISC	RNA-induced silencing complex
MART	Melanoma antigen recognized by T cells 1	RNA	Ribonucleic acid
MCSP	Melanoma-associated chondroitin sulfate proteoglycan	RNAi	RNA interference
MDSC	Myeloid-derived suppressor cell	RT	Room temperature
MHC	Major histocompatibility complex	RT-PCR	Reverse transcription PCR
min	Minutes	s.c.	Subcutaneous
miRNA	microRNA	sc siRNA	Scrambled control siRNA 1
mRNA	Messenger RNA	SEM	Standard error of the mean
NFAT	Nuclear factor of activated T cells	SHP	Src homology region 2 domain-containing phosphatase
NFkB	Nuclear factor 'kappa-light-chain-enhancer' of activated B-cells	shRNA	Short hairpin RNAs
NK	Natural killer cell	siRNA	Small interfering RNA
NSG	Non-obese diabetic (NOD)-severe combined immunodeficient (SCID) Il2rg ^{-/-} gamma	STAT	Signal transducer and activator of transcription
NTS	Non-targeting sequence	Syk	Spleen tyrosine kinase
OR10H1	Olfactory receptor family 10 subfamily H member 1	T-bet	T-box transcription factor
		TAA	Tumor-associated antigen
		TAM	Tumor-associated macrophages
		TC	T cell
		TCGA	The cancer genome atlas
		Tcm	Central memory T cell
		Tconv	Conventional T cell
		TCR	T cell receptor

Tem	Effector memory T cell
TGF-β	Transforming growth factor β
TIL	Tumor-infiltrating lymphocytes
TIM-3	Mucin-domain containing- 3
TME	Tumor microenvironment
TNF	Tumor necrosis factor
TNFR	Tumor necrosis factor receptor
TRAIL	TNF-related apoptosis- inducing ligand
Treg	Regulatory T cells
Tyr	Tyrosine
U	Unit
UBC	Ubiquitin C
ZAP-70	Zeta-chain-associated protein kinase 70

1 Introduction

1.1 Cancer

Cancer is a generic term covering a group of more than two hundred diseases sharing the characteristics of malignant cell transformation, unregulated tumor growth and spreading to other parts of the body [1]. Tumor and metastasis growth impairs the normal functions of healthy organs and thus endangers the survival of the patient. The “world cancer report 2014” (WHO) estimated around 14 million new cases and 8 million cancer-related deaths worldwide in 2012 [2]. In 2016, skin cancer was the most diagnosed cancer type in the United States. Malignant Melanoma, a skin cancer type developing from melanocytes, only accounts for approximately 76,000 new cases a year but caused 10,100 deaths in 2016 (United States) [3]. In the year 2000, Douglas Hanahan and Robert Weinberg defined the development of tumors (tumorigenesis) as a multistep process [4]. This process is summarized by six “hallmarks of cancer”:

- I. Tumor cells grow self-sufficient by providing their own growth signals.
- II. Tumor cells become insensitive to anti-growth signals.
- III. Tumor cells gain the ability to invade local and distant sites (metastasis).
- IV. Tumor cells gain limitless replicative potential.
- V. The growth of blood vessels into the tumor is stimulated in order to extend access to nutrients (angiogenesis).
- VI. Tumor cells develop mechanisms to evade programmed cell death (apoptosis).

These features characterized the malignantly transformed cells as an inert tumor mass overpowering the surrounding healthy cells. Decades of research proved that tumor cells are not inert but interact with, recruit, inhibit or activate a plethora of non-tumor cells inside the so called tumor microenvironment (TME) [5]. Therefore, new hallmarks and characteristics of cancer, associated with the TME were postulated in 2011 [6]:

- VII. Tumor cells deregulate cellular energetic circuits.
- VIII. Genomic instability and mutability drive tumor progression.
- IX. Chronic inflammation inside the TME is tumor-promoting.
- X. Tumor cells and the associated TME prevent the destruction by the immune system.

Researchers are trying to better understand these hallmarks in order to develop therapies against different types of cancer. Studying the way tumors escape recognition by the immune systems is providing us with a basis for establishing promising approaches to improve cancer immunotherapy. Therefore, the present thesis will focus on the mechanisms employed by tumor cells in order to avoid eradication by the adaptive immune system. Chronic inflammation in the TME is an important factor inducing dysfunctional states of immune effector cells (see paragraph 1.4) and needs to be considered.

1.2 Antitumor immunity

Immunosurveillance - a theory developed by Burnet and Thomas – describes the capabilities of an immune system to recognize and destroy transformed cells in early stages of tumor development [7]. It was shown that the innate as well as the adapted branch of the immune system play a key role in the surveillance of tumor growth. The presence and frequency of tumor antigen-specific T cells in cancer patients is widely used as a predictive biomarker for enhanced patient survival [8-10]. T cell-based biomarkers work particularly well in patients with melanoma and colorectal cancer. Another factor determining patient survival is the ratio of CD8⁺ to regulatory T cells (Treg) in the tumor [11]. The induction of an antitumor immunity reaction by the immune system is a complex process described by the “cancer-immunity circle” (**Figure 1**):

- 1) In order to host an effective immune response against cancer, tumor cells have to be distinguished from healthy cells by their antigens. These tumor-associated antigens (TAAs) can be derived from: a) genes overexpressed in tumors, b) products of genes silent in normal tissue, but expressed during development, c) products of tissue (cell lineage) specific gene expression, or d) genes expressed in germ cells (testis-specific) [12]. Recently, it has been shown that mutated tumor-associated antigens trigger a stronger immune response compared to non-mutated antigens [13, 14]. TAAs are released by cell death and can be subsequently taken up, processed and presented by antigen-presenting cells (APC). Some chemotherapeutic or radiation therapies can support this process by inducing immunogenic cell death [15].
- 2) Dendritic cells (DCs) which take up these TAAs and get additionally stimulated by proinflammatory cytokines or receptor/ligand interactions (e.g., TNF (tumor necrosis factor), IFN- α (interferon- α), DAMP (damage-associated molecular pattern molecules)

- released by dying tumor cells, CD40/CD40L interactions) undergo maturation. Matured DCs present tumor-derived antigens on their MHC-I or MHC-II complexes.
- 3) Mature DCs present MHC-bound peptides, in the context of suitable costimulatory signals to naïve T cells in lymph nodes and thus activate tumor antigen-specific T cells mediated immune response against TAAs.
 - 4) After priming in the lymph nodes, CD8⁺ cytotoxic T cells move to the tumor tissue. This movement is governed by chemotaxis (interaction of chemokines and the according chemokine receptors). For example, the chemokines CXCL9 and 10 attract effector T cells to tumors by binding to CXCR3 (reviewed by *Franciszkiewicz et al.*) [16].
 - 5) Endothelial cells have to express adhesion molecules like LFA1, ICAM1 and selectins in order for T cells to cross the endothelial barrier after reaching the tumor tissue. The expression of these adhesion molecules is driven by inflammation inside the tumor tissue.
 - 6) Inside the tumor microenvironment, effector T cells have to recognize and bind their specific TAA presented by MHC-I (for CD8⁺) on the tumor cell surface.
 - 7) The recognition and binding of the MHC-antigen complex induces the activation of the TCR signaling pathway in cytotoxic T cells and results in the secretion of effector cytokines (e.g., IFN- γ , or IL-2 (interleukin-2)) and cytolytic vesicles which contain granzyme B and perforin. These effector mechanisms lead to the lysis of tumor cells (see 1.4.1) and the subsequent secretion of TAAs restarting another cycle of the “cancer-immunity cycle”. The dysfunctional activation and signaling of cytotoxic CD8⁺ T cells (in the tumor microenvironment) is described in the following section.

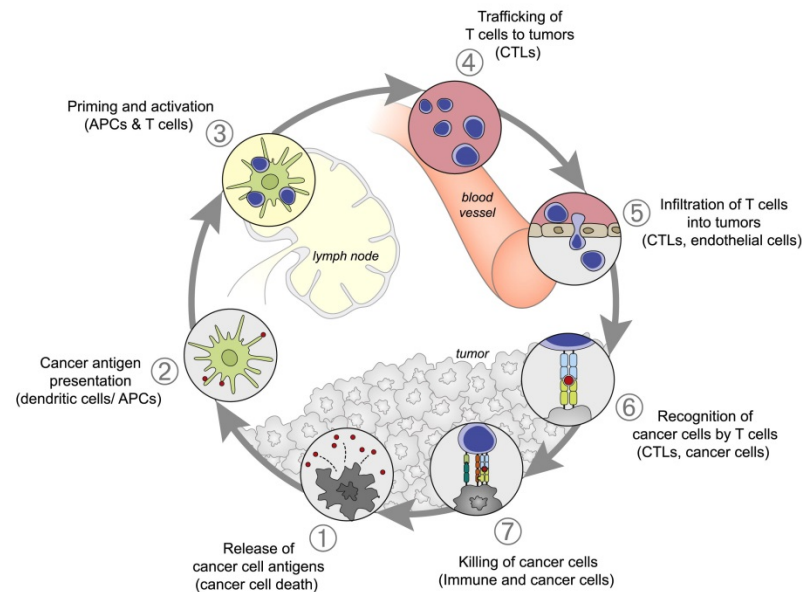


Figure 1: The seven steps of the cancer-immunity cycle involved in the generation of an antigen-specific antitumor immune response. Modified from *Chen et al*, 2013 [17].

1.3 Cancer immunoediting: Tumor growth despite an antitumor response

The first clinical studies using transfer of autologous tumor-reactive T cells failed although these cells could detect and kill tumor cells, setting back immunotherapy for decades [18]. It became clear that tumors oppose the process of immunosurveillance by inducing an escape from immune-mediated destruction (immune evasion). This process – from immune-mediated elimination through an equilibrium and finally to tumor evasion – is called cancer immunoediting [19]. Immunoediting is fueled by the selection pressure of the immune system.

1.3.1 Elimination (immunosurveillance)

In the elimination phase, abnormal cells are recognized and eliminated by the immune system (see section 1.2).

1.3.2 Equilibrium

In this phase, tumor cells are in a long-lasting state of immune system-induced dormancy (reviewed by *Mittal et al.*) [20]. Some tumor cells undergo genetic or epigenetic changes due to constant selection pressure by the immune system, leading to the first development of immune-resistant tumor cell variants. In the equilibrium phase, elimination of tumor cells and growth of “immune-altered” tumor cell variants are in balance.

1.3.3 Escape

Elimination by the immune system exerts selection pressure on the tumor cells which begin to adopt accordingly. This selection pressure leads to a growth advantage of tumor cells which show immune cell interaction-related abnormalities. For example, cells can lose the ability to present antigens on their MHC complexes (e.g., abrogation of MHC complex formation or defects in the antigen processing machinery) or the tumor loses its antigenicity by immune-selection of cancer cells lacking or mutating the respective immunogenic TAA (reviewed by *Beatty and Gladney*) [21]. Ultimately, the accumulation of “immune-altered” tumor cell variants renders the tumor and its microenvironment resistant to the immune systems attack. The tumor can grow uncontrolled and manifests as a clinically apparent disease.

These mechanisms of immune evasion are explained in more detail in section 1.5.

1.4 Subsets, dysfunction, and transcriptional regulation of CD8⁺ tumor-infiltrating lymphocytes

Cytotoxic CD8⁺ tumor-infiltrating lymphocytes (TIL) are an important sub fraction of the lymphocytes found in the tumor microenvironment. CD8⁺ TILs exert an anti-tumor effect by recognition of TAAs on tumor cells and subsequent killing of the transformed cells [22-24]. As mentioned before, the frequency of CD8⁺ TCs inside the tumor correlated strongly with the survival of patients with melanoma, colorectal, lung and breast cancer [8-10, 25, 26]. The CD8⁺ TIL population contains at least six different T cell fates (effector, central and effector memory, exhausted, anergic and senescent T cells) defined by surface markers, transcriptional regulation and effector phenotype (reviewed by *Reiser and Banerjee*) [27].

1.4.1 Effector CD8⁺ TILs

Naïve CD8⁺ T cells undergo differentiation into effector CD8⁺ T cells upon TCR engagement with the according MHC-I-antigen complex and sufficient costimulation from antigen-presenting cells. In cancer, naïve T cells can be activated and differentiated either in tumor-draining lymph nodes or directly in the tumor by tissue-resident APCs or tumor cells [28, 29]. Effector CD8⁺ TILs are characterized by their strong dependency on IL-2 and their high cytotoxicity as well as secretion of IFN- γ , TNF, perforin, and granzyme B after activation [30-32]. There are three main pathways used by cytotoxic T cells to kill target cells (**Figure 2**,

reviewed by *Andersen et al.*) [33]. The first pathway does not involve direct cell-cell contact but is mediated by effector cytokines secreted by T cells (e.g., IFN- γ and TNF). Tumor necrosis factor (TNF) binds to its receptors TNFR1 and 2 and triggers a caspase cascade resulting in cell apoptosis. Recent findings in our lab suggest that this pathway can be altered by tumor cells, resulting in favoring of cell proliferation over cell death (*Sorrentino et al.*, submitted). Interferon- γ (IFN- γ) induces the expression of MHC-I complexes and sensitizes the target cells towards Fas-mediated lysis. The second death-induction pathway depends on the interaction of Fas ligand (FasL) on the CD8⁺ T cell and the death receptor Fas on the target cell. FasL binding to Fas – a member of the tumor necrosis factor receptor family – induces the classical caspase cascade leading to apoptosis. The third pathway utilizes perforin and granzymes stored in cytoplasmic granules. Upon TCR-engagement, those granules are released into the immunological synapse. Killing of target cells by perforin and granzyme B includes the formation of pores (by perforin) and the delivery of granzyme B to the target cell cytosol. The exact modus operandi is being discussed but might involve the entrance of granzyme B through the perforin pore or a process called “endosomolysis” [34].

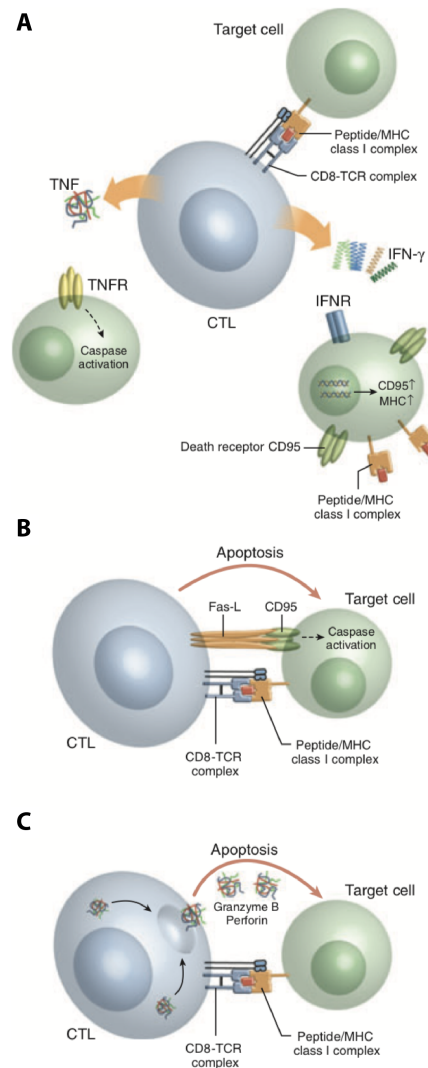


Figure 2: Three pathways of CTL-induced target cell apoptosis. CD8⁺ T cells can induce apoptosis in target cells by cell-cell interaction dependent (B and C) and independent (A) pathways. A. Secreted factors TNF and IFN- γ induce apoptosis in target cells or sensitize them towards other modes of killing. B. Ligand binding to death receptors induce apoptosis. C. Perforin and granzyme B are released in the immunological synapse and induce apoptosis in target cells. Derived from *Andersen et al.*, 2006 [33].

The fate of effector CD8⁺ T cells depends on the duration of the inflammation process. During a “normal” acute infection – after the antigen is cleared – 90-95% of CD8⁺ effector cells undergo apoptosis mediated by the ratio of survival vs. apoptotic factors and a subset of memory CD8⁺ T cells remains [35-37]. However, in a state of chronic inflammation the antigen is not cleared and CD8⁺ TILs become dysfunctional (**Figure 3A**).

1.4.2 Memory CD8⁺ T cells

There are two memory T cell subpopulations (reviewed by *Obar* and *Lefrançois*) [38] defined by the differential expression of CD62L and CCR7. Central memory T cells (T_{CM}) express both

markers whereas effector memory cells (T_{EM}) lack both. As implied by their name, T_{EM} are capable of immediate cytotoxicity and $IFN-\gamma$ production upon reoccurrence of their antigen [39, 40]. T_{CM} produce high levels of IL-2 and can home to secondary lymphoid tissues [40]. T_{CM} are thought to be early differentiated progenitors which pose stem cell features (self-renewal, generate more differentiated progeny) driven by the interleukins 7 and 15 [41]. As mentioned, in a state of chronic inflammation the constant exposure to antigen, negative costimulation and immunomodulation corrupt the generation of memory $CD8^+$ T cell fates.

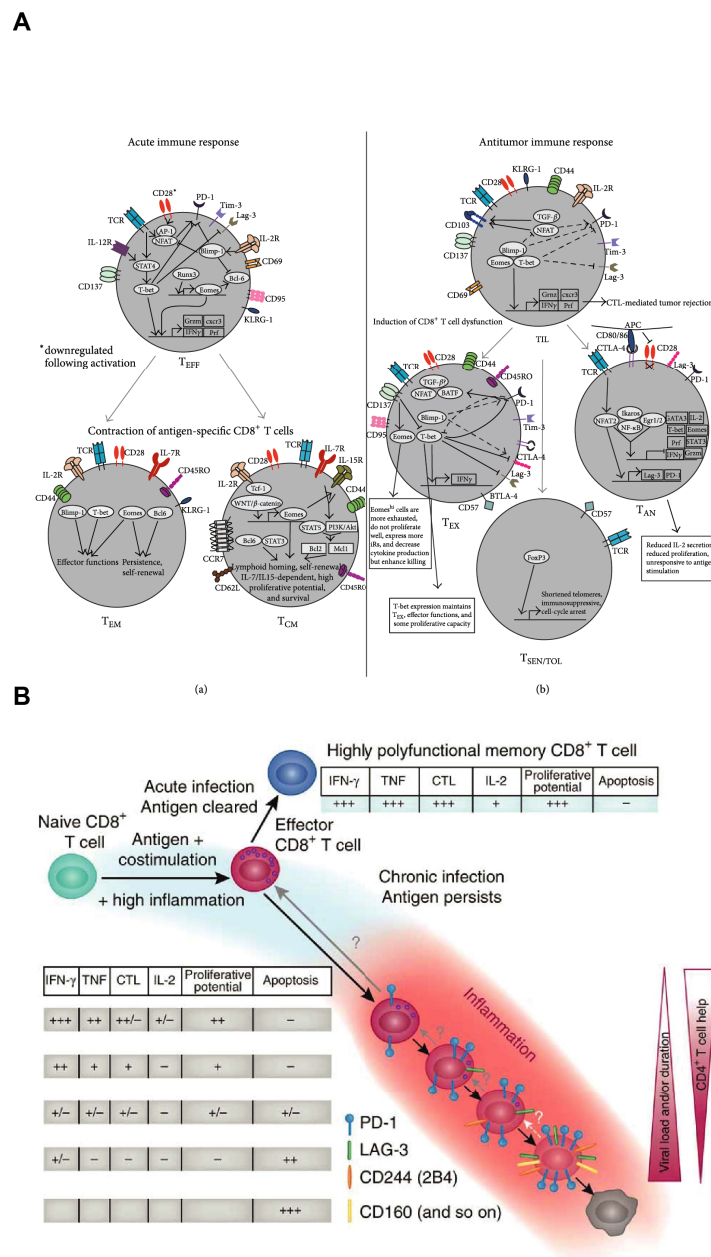


Figure 3: Dysfunctional $CD8^+$ function and transcriptional regulation during chronic inflammation. A. Chronic inflammation and chronic exposure to antigen lead to the onset of dysfunctional $CD8^+$ (memory) phenotypes. T cells can become anergic, senescent or exhausted. B. T cells become exhausted in a hierarchical manner. Modified from Reiser *et al.*, 2016 and Wherry, 2011 [27, 42].

1.4.2.1 Exhaustion

Exhaustion describes a state of T cell dysfunction induced by chronic inflammation and characterized by poor effector function, expression of inhibitory receptors, altered transcription and metabolic derangements (reviewed in [42, 43]). The onset of exhaustion in persistent T cells during chronic inflammation occurs in different steps (**Figure 3B**). In chronic viral infections CD8⁺ T cells first lose their ability to kill target cells and produce IL-2, followed by impaired TNF production. Finally, the production of IFN- γ by CD8⁺ TCs is strongly impaired and a majority of cells undergoes apoptosis [44]. CD8⁺ TCs exhaustion was mainly described in the context of chronic infections but similar observations were made in cancer [42, 45]. The development of exhaustion is accompanied by an increased expression of several receptors mediating inhibitory signaling [46]. Inhibitory receptors as programmed cell death protein 1 (PD-1), cytotoxic T-lymphocyte-associated protein 4 (CTLA-4) or mucin-domain containing-3 (TIM-3) play a major role in CD8⁺ T cell dysfunction as well as tumor immune escape and will be discussed in paragraph 1.5.3 and 1.5.4. Interestingly, the co-expression of PD-1 and TIM-3 define CD8⁺ TILs with a particular high level of exhaustion [47]. These changes in function and cell surface receptor expression hint towards underlying alterations in the transcriptional profile of exhausted CD8⁺ T cells. Antigen-specific CD8⁺ T cells in chronic infections show altered expression of stimulatory, inhibitory and cytokine receptors, transcription factors, signaling molecules and genes involved in metabolism [48]. Such an exhaustion-associated molecular pattern is reported in MART-1-specific T cells from melanoma as well [49]. The two transcription factors T-box transcription factor (T-bet) and eomesodermin (EOMES) are important in exhausted CD8⁺ T cells. In the pool of exhausted CD8⁺ T cells reduced T-bet expression limits their renewal capacity, whereas high expression of EOMES controls the formation of terminally differentiated T cells [50]. Furthermore, in exhausted CD8⁺ T cells, impaired calcium signaling leads to aberrant activation of nuclear factor of activated T-cells (NFAT) similar to that in anergic CD8⁺ T cells. This NFAT-dependent induction of exhausted gene expression pattern is not depending on (and might be opposite to) NFAT cooperation with activator protein 1 (AP-1) [51, 52]. Interestingly, members of the early growth response protein (EGR) family are induced by NFAT in anergic and exhausted CD8⁺ T cells. Other transcription factors important for exhaustion in CD8⁺ cells include BLIMP1 (B-lymphocyte-induced maturation protein 1 [53]), BATF (basic leucine zipper transcription factor, ATF-like [54]), FOXO1 (forkhead box protein O1 [55]) and FOXP1

(forkhead box protein P1 [56]). The state of exhaustion is not only regulated by transcriptional but also by epigenetic changes (reviewed by *Wherry and Karachi*) [43]. A lot of research is dedicated to reverse CD8⁺ TIL exhaustion inside the tumor microenvironment (reviewed by *Zarour* [57]).

1.4.2.2 Anergy

Anergy is another dysfunctional fate of CD8⁺ T cells inside the tumor. Anergy describes the incomplete activation of T cells or TCR activation in an environment lacking costimulation or high in coinhibition resulting in abrogated proliferative and effector functions [58]. Anergy occurs in early stages of tumor progression – driven by activation of CD8⁺ T cells combined with strong coinhibitory signaling – whereas exhaustion is induced during cancer-mediated chronic inflammation over time [27]. Several transcription factors drive the transcriptional profile of anergy. As mentioned before, this profile overlaps in part with exhaustion. Strong antigen-dependent activation of TCR signaling in the absence of costimulatory signaling (or in the presence of strong coinhibitory signaling) leads to impaired calcium signaling without PKC, Ras/MAPK or PI3K/Akt activation (reviewed by *Valdor and Macian*) [59]. Thus, NFAT forms homodimers instead of heterodimers together with AP-1 and induces the expression of anergy-related genes while downregulating the expression of effector cytokines [52]. *Srinivasan et al.* found that the suboptimal calcium signaling in anergic CD8⁺ T cells induces activation of NFAT2 instead of NFAT1 suggesting an isoform-specific process [60].

1.4.2.3 Senescence

Senescent CD8⁺ T cells are defined by the expression of senescence markers (e.g., CD57), the loss of CD28 expression, and permanent cell-cycle arrest. Furthermore, chronic infections (antigen-dependent) accelerate T cell immunosenescence [61, 62]. CD27/CD28-negative CD8⁺ TILs can be found in several tumor entities and show an immune suppressive phenotype [63, 64].

In summary, several mechanisms can lead to a dysfunctional CD8⁺ T cell fate. In individuals without cancer, exhaustion, anergy, or senescence prevent the induction of autoimmunity while allowing the containment of chronic infections. But tumors use these natural occurring processes – driven by immune selection – to prevent antitumor immunity. Therefore, therapies

which prevent or reverse exhaustion, anergy, or senescence are of major importance for antitumor immunotherapy.

1.5 Mechanisms of immune evasion

As mentioned, periphery immune tolerance is an important factor to prevent the onset of autoimmunity mediated by self-reactive T cells. But in a context of cancer, those mechanisms are perverted by the tumors to evade eradication by the immune system. The different mechanisms of immune inhibition by tumors will be grouped into tumor cell intrinsic mechanisms, inhibitory tumor microenvironment, and immune checkpoints.

1.5.1 Tumor cell intrinsic immune escape mechanisms

Tumor cells employ several mechanisms to hide from immune cells or to prevent T cell-mediated cell death.

1.5.1.1 *Loss of antigenicity*

As mentioned before, tumors express tumor-associated antigens which can trigger an immune response. The expression of TAAs in the tumor is heterogeneous and can be selected for by immune destruction. In melanoma, the expression of MART1 and gp100 – both strong TAAs – decreases in line with disease progression [65, 66]. Therefore, tumor cells with less antigenicity become the predominant cell population inside the tumor mass evading destruction. Not only the antigen expression itself but also the expression of HLA class I complex and the antigen presenting machinery can be altered. For example, decreased or absent HLA class I expression is observed in many tumors [67, 68]. Furthermore, a loss of heterozygosity of β_2 -microglobulin was reported [69]. Interestingly, this phenomenon also occurs in patients with a partial response after T cell-based immunotherapy [70]. Other parts of the antigen-presentation pathway that are downregulated in cancer include the proteasome subunits LMP-2 and 7, and the peptide transporters TAP-1 and 2 [71-73].

1.5.1.2 *Resistance to T cell induced apoptosis*

Apoptosis inside tumor cells can be induced via death receptors (extrinsic) or via changes in mitochondria (intrinsic). Unsurprisingly, both pathways can be altered in tumors [74]. Binding of tumor necrosis factor family members Fas ligand (FasL or CD95L) or TNF-related apoptosis-

inducing ligand (TRAIL) – both expressed by cytotoxic T cells – to their receptors Fas (CD95) or death receptor 4/5 (DR4/5) on tumor cells induces apoptosis via the death inducing signaling complex (DISC) [75, 76]. Furthermore, soluble TNF (e.g., secreted by T cells) can bind to Tumor necrosis factor receptor 1 (TNFR1) and trigger downstream signaling leading to apoptosis [77]. It is noteworthy that TNF-induced signaling can trigger several cellular programs including apoptosis and cell survival (reviewed by *Wayant et al.*) [78]. The mitochondrial pathway is activated by the disintegration of the mitochondrial membrane and the subsequent release of pro apoptotic factors cytochrome C, Smac (second mitochondria-derived activator of caspase) or HtrA2 (Omi/high temperature requirement protein A). This leads to the activation of caspase-3 [79]. There are several mechanisms utilized by the tumors to abrogate both the extrinsic and intrinsic apoptosis. Expression of Fas was found to be reduced in several cancers [80-82]. As expected, adoptive immunotherapy with cytotoxic CD8⁺ T cells selects for Fas-resistant tumor variants [83]. Downregulation of TRAIL-associated receptors occurs in tumors as well [84, 85]. Other nodes of extrinsic apoptotic signaling which are altered in tumors include the expression of decoy receptors, upregulation of anti-apoptotic factors (e.g., cFLIP) and inactivation of caspase-8 (reviewed by *Fulda*) [74]. Intrinsic apoptosis can be inhibited by upregulation of Bcl-2, inactivation of Bax or BH3-only proteins or loss of Apaf-1.

1.5.2 Inhibitory tumor microenvironment

The tumor microenvironment not only supports tumor growth but also prevents sufficient antitumor immune responses utilizing several factors.

1.5.2.1 *Immune-suppressive soluble factors*

Tumor cells or the surrounding stroma cells can secrete several immune-suppressive factors (e.g., cytokines and growth factors) impairing a successful antitumor immune response. These factors are summarized in **Table 1**.

Table 1: Immune-suppressive soluble factors in the tumor microenvironment

Soluble factor	Type	Immune-suppressive function
Transforming growth factor β (TGF-β)	Growth factor	Induction of T cell exhaustion [86, 87] and differentiation into Treg [88].
Interleukin 10 (IL-10)	Cytokine	Induction of Treg [89] and impairment of dendritic cell function [90]. Induces the expression of PD-L1 on DCs inducing T cell exhaustion [91].
Gangliosides	Glycosphingolipids	Inhibition of T cell proliferation [92], induction of T cell apoptosis [93], inhibition of cytokine production [94] and, inhibition of granule trafficking in CD8 ⁺ TCs [95].
Prostaglandin E2 (PGE₂)	Prostaglandin	Inhibits natural killer cells, reduces DC ability to present antigen to T cells, impairs T cell function and, induces accumulation and function of immune-suppressive cells [96].

1.5.2.2 Immune-suppressive cell populations inside the tumor microenvironment

As mentioned, the tumor microenvironment contains a plethora of cells possessing anti- or pro-tumor capabilities. Tumors can skew this balance by inducing or deploying cell populations that promote tumor progression and inhibit antitumor immune responses by supporting anergy, exhaustion and suppression in immune cells. Among others, these immune suppressive cells include myeloid-derived suppressor cells (MDSC), tumor-associated macrophages (TAM), tolerogenic dendritic cells (tDC), and regulatory T cells (Treg).

- Myeloid-derived suppressor cells are a group of myeloid progenitor and immature mononuclear cells with a potent immunosuppressive functionality. They are morphologically divided into monocytic and polymorphonuclear MDSCs. The exact mechanisms of MDSC expansion and acquisition of suppressive functions inside the TME is not exactly known but likely involves factors associated with chronic inflammation (e.g., GM-CSF and proinflammatory cytokines). Besides being immunosuppressive, MDSCs support tumor growth by remodeling the TME, establishing a pre-metastatic niche, induction of stemness and facilitation of the epithelial-to-mesenchymal transition (EMT) [97]. MDSCs inhibit T cells by depletion

of arginine and cysteine, production of reactive oxygen species (ROS) and peroxynitrite, induction of Tregs and production of immunosuppressive cytokines [98-101].

- Macrophages are mononuclear phagocytic cells being important for the innate immune system and the induction of adoptive immunity (e.g., presentation of antigens) during inflammation. Depending on the type of activation, macrophages can either have a pro-inflammatory (M1) or an anti-inflammatory phenotype (M2). Macrophages belong to the most abundant non-tumor cells inside the TME. In early stages of cancer these macrophages have an inflammatory (M1) phenotype. During tumor progression, the TME influences tumor-associated macrophages and changes their phenotype towards a more regulatory (M2) phenotype [102]. In such a setting, TAMs can promote tumor growth and inhibit antitumor immunity. Macrophages can inhibit antigen-specific T cells by upregulation of inhibitory ligands, secretion of immunosuppressive cytokines, recruitment of Tregs and depletion of arginine [103].
- Dendritic cells are antigen presenting cells crucial for the activation of the adoptive immune system. They do not only present antigens but also provide co-stimulatory signals and cytokines for T cell activation and differentiation. Inside the TME, DC maturation and normal function is inhibited or reversed. Tumor-infiltrating DCs (TIDC) have an impaired antigen-presenting machinery, express inhibitory ligands, release PGE₂, induce IDO expression and secrete TGF- β and IL-10 [104]. The combination of impaired antigen presentation and the lack of proper costimulatory signals leads to anergy in T cells impairing their antitumor function [105, 106].
- Regulatory T cells are FoxP3⁺ CD25⁺ CD4⁺ T cells that are important for the control of the quality and magnitude of adaptive immune responses. Furthermore, they are important to establish tolerance to self-antigens and prevent autoimmune diseases [107]. Tregs can control a variety of immune cells including TC, B cells, natural killer cells (NK), DCs and macrophages using metabolic disruption, cytokines and cell-cell interactions (**Table 2**) [108]. A high frequency of Tregs can be found in most solid tumors (e.g., melanoma) and is correlated with poor patients' survival [109, 110]. Several factors in the TME either recruit or expand regulatory T cells. Besides their role in immunosuppression, Tregs are also involved in tumor angiogenesis [111].

Table 2: Immunosuppressive functions used by regulatory T cells

Mechanism	Immunosuppressive function
Cytotoxic T-lymphocyte-associated protein 4 (CTLA-4) expression	CTLA-4 on Tregs outcompetes CD38 on conventional T cells for binding of CD80/86 on APCs [108] and leads to downregulation of CD80/86 on DCs [112].
IL-10, TGF-β, IL-35 secretion	Immune suppressive cytokines, which inhibit the function of effector T cells (see paragraph 1.5.2.1) [113].
Cytolysis of effector T cells	Tregs induce apoptosis in effector T cells via granzyme B [114], TRAIL [115] and galectin-1 [116].
Metabolic disruption	CD73 and CD39 hydrolyze ATP to adenosine, which subsequently binds to the adenosine receptor 2A on effector T cells leading to suppression [117]. Furthermore, Tregs can transport cAMP to effector T cells via gap junctions suppressing their function [118].
Targeting DCs	Tregs modulate the maturation and function of DCs and thus attenuate effector T cell function [113].

1.5.2.3 Immunosuppressive metabolism in the tumor microenvironment

Metabolic alterations in cancer and stromal cells are needed to support the energy consumption during tumor growth and progression (see paragraph 1.1). The altered metabolism of cancer cells can impair T cell function.

1.5.2.3.1 Tryptophan catabolism

Local degradation of tryptophan in the TME results in T cell inhibition via two mechanisms. The lack of tryptophan in the extracellular environment is sensed by general control nonderepressible 2 (GCN2) and in combination with mTOR-pathway inhibition mediates proliferative arrest and anergy in T cells [119]. Furthermore, some catabolites (e.g., kynurenine) of the tryptophan catabolism induce T cell apoptosis or differentiation into Treg [120]. Three intracellular enzymes are important in the context of tumor-associated and immune suppressive tryptophan catabolism. Indoleamine 2,3-dioxygenase 1 (IDO1), IDO2 and tryptophan 2,3-dioxygenase (TDO) catalyze the initial step of the kynurenine pathway and their expression in different cancer entities is associated with effector T cell dysfunction [121-123].

1.5.2.3.2 Extracellular adenosine

Intracellular adenosine is mainly involved in metabolism, whereas extracellular adenosine is involved in intercellular signaling. A_{2A} adenosine receptor (A_{2A}AR) is a GPCR, which is predominantly expressed on T cells and stimulated by binding of adenosine [124, 125]. Binding of adenosine to A_{2A}AR leads to the production of cAMP in the T cells, which in turn suppresses TCR-signaling resulting in the inhibition of downstream T cell effector function [126-128]. Extracellular ATP normally serves as a danger signal but in the TME it is degraded to immunosuppressive adenosine by the combined function of the NTPDase CD39 and the ecto-5'-nucleotidase CD73 [129-131]. Thus, adenosine levels can reach micromolar concentrations inside the TME severely dampening the T cell-mediated antitumor response [132, 133].

1.5.3 Immune checkpoints: Inhibitory pathways between tumor and T cells

In the classical “two-signal” concept of T cell activation a first signal is provided by the interaction of the TCR with the antigen/MHC complex, but proper activation is only achieved in combination with a second antigen-independent costimulatory signal. Over time many costimulatory and also coinhibitory signals were found and a “tide” model for T cell activation established [134, 135]. The overall accumulation of stimulatory and inhibitory signals decides the fate of T cell activation. This allows T cell activation but also prevents autoimmunity. As expected, these stimulatory or inhibitory signals do not only prime T cell activation but also regulate effector T cell function [135]. Therefore, it is not surprising that tumor and other cells in the TME hijack inhibitory pathways or prevent signaling via activating pathways to induce anergy, exhaustion and other dysfunctional states in effector immune cells. The following paragraph will review some of the most important so called “immune checkpoint” pathways (inhibitory signals) employed by tumors to avoid destruction by the immune system (focusing on T cells).

1.5.3.1 *The PD-L1/PD-1 axis: The immune checkpoint prototype*

In the 90s both the receptor programmed cell death 1 (PD-1 or CD279) and its ligand programmed death ligand 1 (PD-L1 or B7-H1) were discovered. Soon after, it was shown that the interaction of PD-L1 with PD-1 inhibits T cell function [136-138]. PD-1 – a member of the CD28 coreceptor family – functions as an inhibitory receptor on immune cells and its expression is induced after TCR-mediated activation of NFAT [139]. Interestingly, during

cancer progression and chronic virus infections the PD-1 locus is demethylated in exhausted CD8⁺ T cells allowing for fast re-expression [140, 141]. As a result of its interaction with PD-L1, PD-1 is crosslinked to the TCR complex during antigen recognition (**Figure 4**). There, PD-1 becomes phosphorylated at the immunoreceptor tyrosine-based switch motif (ITSM) which subsequently recruits the tyrosine phosphatase SHP2 (tyrosine-protein phosphatase non-receptor type 11). SHP2 dephosphorylates proximal TCR-associated kinases (e.g., ZAP70) and thus abrogates or skews TCR signaling [142-144]. Other pathways in T cells targeted by PD-1 include PI3K/Akt and Ras/MEK/Erk signaling [145]. Overall, PD-1 mediated signaling inhibits T cell function and plays an important role in T cell exhaustion during chronic inflammation [146]. Notably, this state of exhaustion can be reversed by transient blockade of PD-1-PD-L1 interactions during chronic inflammation [147].

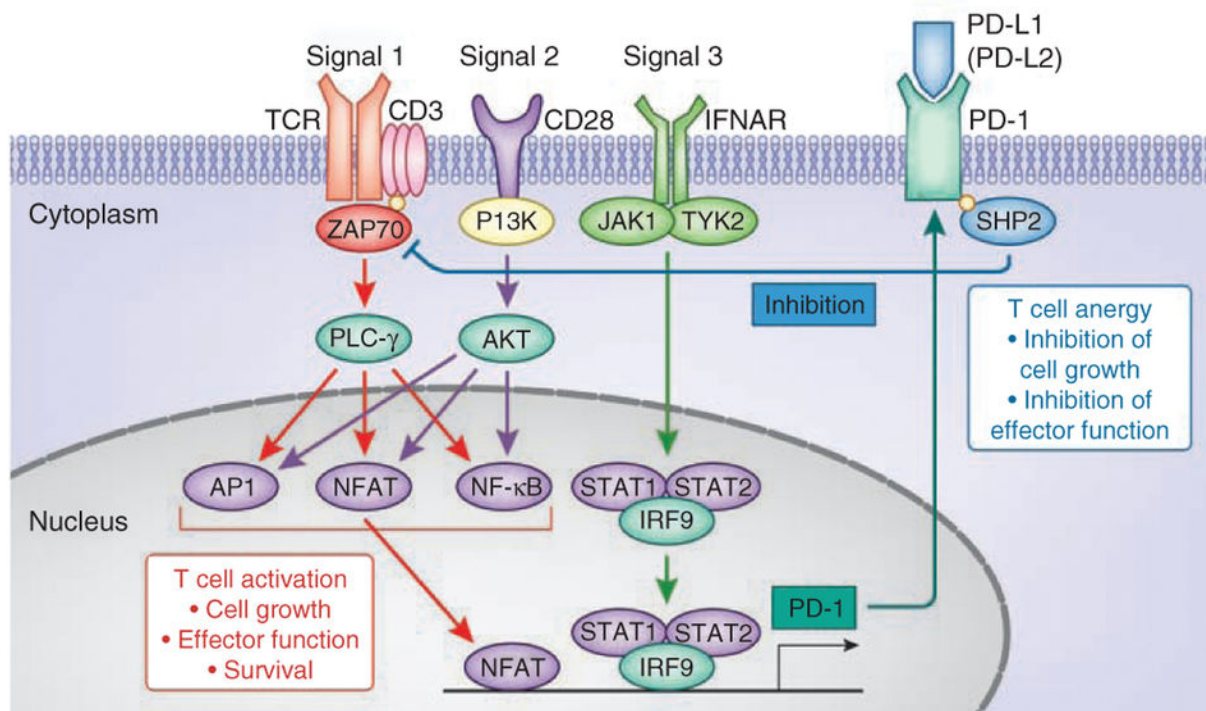


Figure 4: Inhibition of TCR signaling by PD-1 and SHP2. TCR activation induces NFAT-mediated expression of PD-1. Additional factors (e.g., IFN- α) induce prolonged transcription. When bound by PD-L1, PD-1 recruits SHP2, which dephosphorylates kinases (e.g., ZAP70) and abrogates TCR signaling. Modified from *Okazaki et al. 2013* [146].

PD-1 ligands PD-L1 and PD-L2 (B7-DC) are constitutively expressed on APCs and can be induced in epithelial cells during inflammation [148]. Tumors misuse this potent inhibitory pathway in order to avoid destruction by immune cells. PD-L1 is overexpressed in different cancer types including melanoma, multiple myeloma, pancreatic, lung and gastric cancer and it is associated with a poor survival prognosis [149-151]. Several tumor-intrinsic pathways aid

PD-L1 expression but it is also driven by IFN- γ in the TME [152, 153]. For example, TILs secrete IFN- γ upon antigen recognition inducing the upregulation of PD-L1 on tumor cells thus serving as a negative feedback loop (**Figure 5A**). Signaling via the PD-L1/PD-1 axis in tumors can induce T cell exhaustion, anergy and Treg formation and suppress DC function (**Figure 5B**).

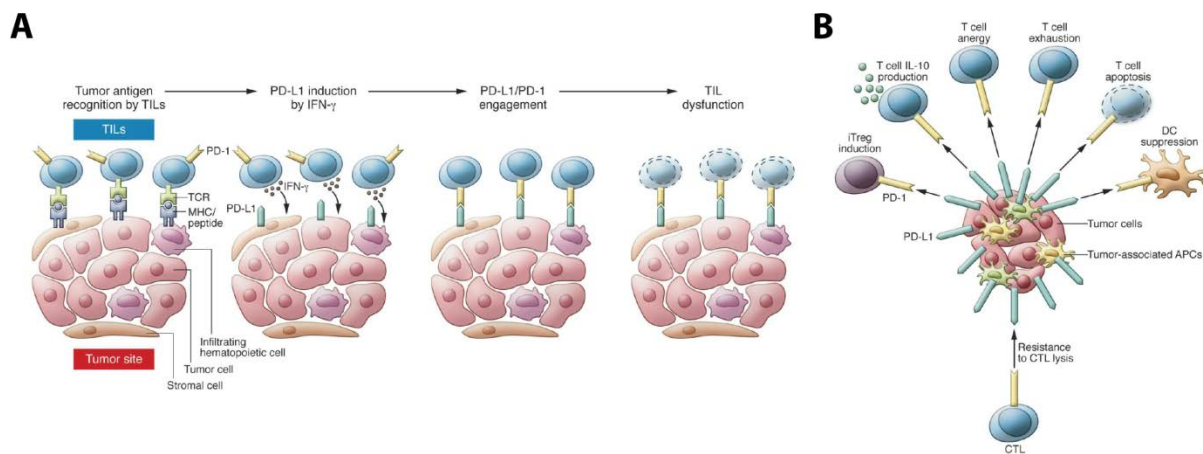


Figure 5: The PD-L1/PD-1 axis in the tumor microenvironment. A. Tumor cells express PD-L1 in a feedback loop induced by TIL-secreted IFN- γ upon antigen recognition. B. Signaling via PD-L1 induces anergy, exhaustion and apoptosis in TILs. Furthermore, it can induce Tregs and suppress DC function. Modified from *Chen et al., 2015*.

1.5.3.2 CTLA-4

As mentioned, functional T cell activation requires costimulatory signals. CD28 binding to its ligands B7-1 (CD80) or B7-2 (CD86) on APCs induces T cell survival and differentiation. Cytotoxic T lymphocyte antigen 4 (CTLA-4) – a CD28 homolog – has a higher binding affinity to B7 and prevents proper T cell activation [154]. Surprisingly, it is still being debated if CTLA-4 possesses the ability to transport an inhibitory signal into the T cell or whether its inhibitory potential is due to ligand competition. Most likely CTLA-4 facilitates its function by reducing the access of CD28 to their shared ligands thus depriving the T cell of the costimulatory signal [155]. **Figure 6** shows different ways in which CTLA-4 can outcompete CD28 and thus prevent proper T cell activation.

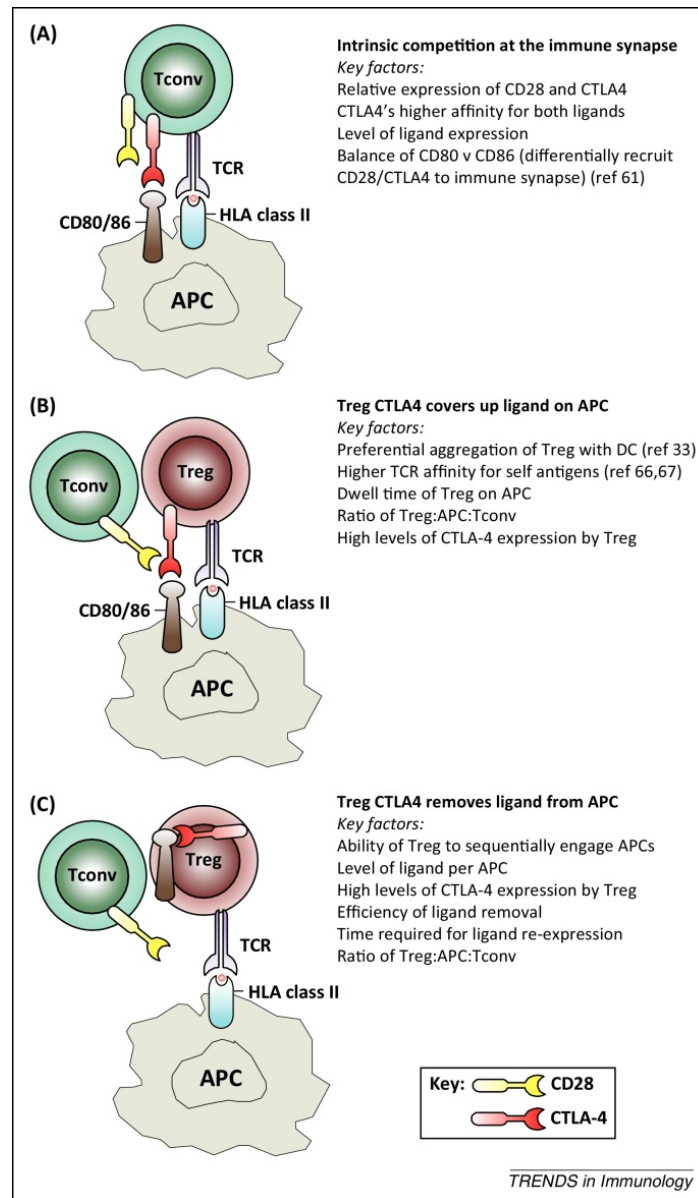


Figure 6: CTLA-4/CD28 ligand competition. CTLA-4 can inhibit T cell activation by competing with CD28 in three different ways. **A.** Tconv intrinsic competition. **B.** Competition of CTLA-4 (on Treg) vs. CD28 on Tconv. **C.** CTLA-4-mediated removal of CD80/86 on APCs. Modified from Walker and Sansom, 2015.

It was shown that blocking the interactions of CTLA-4 resulted in the rejection of tumors indicating an important role for CTLA-4 in tumor-mediated T cell inhibition [156]. Furthermore, CTLA-4 is crucial for the inhibitory function of regulatory T cells. Treg-restricted CTLA-4 can either block the binding of Tconv CD28 to CD80/CD86 or remove these from the surface of APCs [155].

1.5.3.3 *RCAS-1*

Receptor-binding cancer antigen expressed on Siso cells (RCAS1 or EBAG9) is a type II membrane protein expressed in several tumor entities including skin cancer [157]. RCAS1 induces apoptosis in immune cells via a putative receptor [158].

1.5.3.4 *CEACAM1/6*

Carcinoembryonic antigen-related cell adhesion molecule-1 and -6 (CEACAM1/6) belong to a family of surface glycoproteins. In melanoma, CEACAM1 was found to inhibit melanoma-specific T-cell responses [159]. Recently, our laboratory found that CEACAM6 expression on multiple myeloma cells inhibited cytotoxic T cell activation [160]. Blockade or knockdown of CEACAM6 on multiple myeloma cells restored T cell activity. It is hypothesized that both molecules inhibit T cell function through homophilic or heterophilic interactions with CEACAM1 which is expressed on T cells. There, CEACAM1 could recruit SHP1 and subsequently abrogate TCR signaling [161].

1.5.3.5 *Galectin-3*

Galectin-3 is a glycan-binding protein which is expressed in multiple tumor types [162]. Amongst other members of the galectin family, galectin-3 is associated with melanoma growth and metastasis as well as tumor-reactive T cell inhibition [163, 164]. Galectin-3 has several effects on T cells. Galectin-3 induces T cell apoptosis by binding to CD45 and CD71 [165]. Galectin-3 can directly interact with the TCR and thus alter TCR-mediated signaling. Furthermore, galectin-3 alters T cell adhesion and activation [166].

1.5.3.6 *Additional members of the B7-CD28 immune checkpoint family*

After the discovery of PD-L1 (B7-H1) and CTLA-4 a lot of attention was given to other members of the B7-CD28 family. B7 homolog 3 protein (B7-H3) was discovered in 2001 [167]. Interestingly, B7-H3 has co-stimulatory as well as co-inhibitory effects. Although it has been reported that B7-H3 might play an important role in the secretion/production of IFN- γ during T cell activation [167] and it has been shown to activate cytotoxic T lymphocytes [168], it mainly causes inhibition of T cell proliferation and cytokine secretion [169]. The inhibitory effect of B7-H3 is mediated by an unidentified receptor and is based on alteration of NFAT, NF κ B and AP-1 signaling in T cells [168]. B7-H3 expression is associated with disease progression in

melanoma [170], NSCLC [171] and breast cancer [172]. B7x (B7-H4) is another member of the immunoglobulin B7 family. B7x interacts with an unknown receptor on activated T cells [173] and decreases T cell proliferation by decreasing IL-2 [174] and by induction of cell cycle arrest [175]. B7x is expressed in many different human tumors [176]. A recently discovered member of the B7 family with a co-inhibitory function towards T cells is human endogenous retrovirus-H long terminal repeat-associating protein 2 (HHLA2 or B7-H5). A HHLA2 immunoglobulin fusion protein (HHLA2-Ig) decreases the production of several cytokines when incubated with T cells [177].

1.5.4 Inhibitory receptors on T cells

Many immune checkpoint axes exert their inhibitory function via receptors expressed on T cells. For example, PD-L1 binding to the inhibitory receptor PD-1 triggers inhibition of TCR signaling. TIM-3 and LAG-3 are markers of exhaustion in T cells and function as inhibitory receptors on activated T cells. TIM-3 is induced on IFN- γ -secreting CD4⁺ and CD8⁺ T cells under the control of the transcription factor T-bet [178]. It has been shown that crosslinking of TIM-3 by galectin-9 induces its inhibitory function in T cells [179]. Recently, it was also reported that TIM-3-mediated T cell exhaustion is facilitated by cis or trans CEACAM1 [180]. LAG-3 – expressed on CD4⁺ and CD8⁺ T cells – is structurally related to CD4 and binds the MHC-II complex with higher affinity. For CD4⁺ T cells a competition with CD4 could explain the inhibitory function of LAG-3 [181]. In CD8⁺ T cells, LAG-3 might be involved in galectin-3-mediated suppression [182]. Additional inhibitory receptors with a cancer-related inhibitory function in CD8⁺ T cells include T cell immunoreceptor, with Ig and ITIM domains (TIGIT) and CD96 (reviewed by *Dougall et al.* [183]). For many inhibitory ligands, the respective receptors remain unknown.

1.6 Cancer immunotherapy

The discovery that tumors can be recognized and destroyed by the immune system sparked the development of many different approaches to anti-cancer immunotherapy. Unfortunately, many of the approaches failed to induce durable responses in cancer patients [184]. Recent success of immune checkpoint blockade woke immunotherapy from its winter sleep and offers clinical benefit to millions of cancer patients.

1.6.1 Cancer vaccines

Vaccination against cancer was one of the first immunotherapy approaches. In the 1970s, autologous tumor cell vaccination was introduced. Tumor cells were dissected, irradiated and injected back together with immune-stimulatory adjuvants [185, 186]. Other approaches use autologous tumor cell vaccines transduced with GM-CSF (GVAX). This vaccination approach induces the presentation of antigens by DCs and the priming of CD8⁺ T cells. Furthermore, GVAX stimulates the maturation of DCs [187]. Although GVAX showed positive effects in some clinical studies, it failed to show efficacy in a Phase III clinical trial [188]. Injection of allogenic whole tumor vaccines (Canvaxi) significantly improved overall survival in melanoma patients (Phase II trial) but failed in randomized Phase III trials [189]. Other cell-based vaccination approaches use dendritic cells which are loaded with antigens *ex vivo* and treated with adjuvants before reinjection into the individual. The first DC-based vaccine that was approved for clinical usage is sipuleucet-T for prostate cancer [190].

Other cancer vaccines use tumor-associated antigens as therapeutic targets. Here, vaccination can either be performed with proteins/peptides, DNA or RNA [184]. So far vaccinations with TAAs showed limited clinical effect but major improvements in next generation sequencing methods paved the way for personalized vaccine-based immunotherapy [191]. Whole-genome sequencing or transcriptome analysis are used to identify mutated antigens which in turn are used to generate personalized vaccines. In summary, cancer vaccination did not provide major clinical benefits for patients so far but much effort is being put into the discovery of novel TAA as well as novel vaccination approaches in order to improve this immunotherapeutic strategy.

1.6.2 Adoptive cell transfer

The group of Steven A. Rosenberg established adoptive cell transfer (ACT) of *ex vivo* expanded effector TILs into cancer patients as a promising immunotherapy particularly in melanoma [192]. This approach has some benefits in regard to overcoming immune tolerance in the TME. Firstly, TILs are expanded outside of an inhibitory milieu (*ex vivo*) with cytokines and metabolites which restore T cell activity [18]. More advanced expansion protocols generate dramatic increases in expansion rates of TILs [193]. Secondly, most ACT treatments are combined with lymphodepletion which eliminates immunosuppressive cells (e.g., Treg) inside the TME [194]. Several clinical trials showed complete responses in some melanoma patients after adoptive cell therapy with TILs [195, 196]. Unfortunately, melanoma is the only tumor

entity from which TILs can be easily generated and expanded. Furthermore, only a fraction of patients develops durable antitumor responses after ATC [197].

Another approach to ACT is based on genetically altered T cells. T cells can either be genetically engineered to express modified TCRs (specific for TAAs) or protein-fusion-derived chimeric antigen receptors (CAR). Unresponsive T cells can be modified with TCR sequences of reactive T cells [198] or their TCR sequence can be modified to strengthen the interaction (avidity) of the TCR with the target antigen [199]. CARs, on the other hand, are a mixture of antigen-binding domain of antibodies and TCR signaling, thus combining antibody-like recognition with TCR-like activation [200]. Of particular interest is the intracellular signaling domain of these artificial receptors. Usage of the CD3 ζ alone induced anergy [201] whereas combination with the intracellular signaling domains from co-stimulatory signals (e.g., CD28) result in superior T cell activation and therefore produce enhanced tumor-regression [202]. A major benefit of CAR therapies is their independence from HLA-dependent antigen presentation [203]. Furthermore, CARs can target non-peptide antigens such as carbohydrates and glycolipids. So far, clinical trials of CAR therapies focus on CD19-positive leukemia showing high response rates in patients [204]. At this moment, Novartis is awaiting approval from the U.S. Food and Drug Administration (FDA) for their CAR therapy targeting CD19 based on a Phase II clinical trial in acute lymphoblastic leukemia [205].

1.6.3 Immune checkpoint blockade

In recent years tremendous clinical success was achieved by blocking inhibitory pathways between tumor and immune cells. This approach to immunotherapy is revolutionizing decades of fighting against cancer [206]. Unfortunately, a large group of cancer patients cannot benefit from these therapies until today. The search for novel immune checkpoints and the application of combination therapies will be the focus of intensive medical research for the foreseeable future in order to improve immunotherapy. For many cancers, blockade of the PD-L1/PD-1 axis is the most successful immune checkpoint-related therapy currently in the clinic.

In 2015/16/17 several monoclonal antibodies blocking PD-L1/PD-1 interactions were approved by the FDA for the treatment of cancer patients. For example, Nivolumab (Bristol-Meyers Squibb), and Pembrolizumab (Merck) are monoclonal antibodies directed against PD-1 and Avelumab (Merck), Durvalumab (AstraZeneca), and Atezolizumab (Roche) are monoclonal

antibodies directed against PD-L1 [207]. Nivolumab shows significant clinical responses in metastatic melanoma, non-small cell lung cancer (NSCLC), metastatic renal cell carcinoma and metastatic urothelial carcinoma [208-210]. The objective response rates (ORR) of Nivolumab are unmatched with 30-40% in melanoma and 15% in progressive NSCLC (after two-year standard therapy) [211-213]. Pembrolizumab shows comparable results in melanoma, NSCLC and other solid tumors [214]. Avelumab shows good responses in metastatic Merkel cell carcinoma [215], Durvalumab in bladder cancer [216] and Atezolizumab in NSCLC [217]. Other immune checkpoint blockades, which are currently tested are directed against – among others – killer-cell immunoglobulin-like receptor (KIR), CD137 (4-1BB), CD40 and OX40 [218].

As mentioned, the great success of monoclonal antibodies directed against PD-L1/PD-1 benefits only a part of cancer patients. A meta-analysis of 20 studies in melanoma, NSCLC, and genitourinary cancer showed that only a part of tumors is PD-L1 positive (44% in melanoma, 60% in NSCLC and 34% in genitourinary cancer) [219]. Noteworthy, expression of PD-L1 is not a useful biomarker for anti-PD-1/PD-L1 therapy, as PD-L1-negative patients can benefit from the therapy as well. In melanoma patients, 49% of PD-L1-positive and 26.2% of PD-L1-negative tumors react to an anti-PD-L1/PD-1 therapy. For NSCLC, it is 23.2%/14.5% and 29.1%/21% for genitourinary cancer. Thus, a great number of patients cannot benefit from immune checkpoint therapy. Other tumor entities do not respond to anti-PD-L1/PD-1 therapy at all. The great success of immune checkpoint blockade on one hand and the limitations on the other show the need for novel immune checkpoint targets in order to improve immunotherapy. As mentioned, there are several other known immune checkpoints and blocking therapies against them (e.g., CTLA-4, TIM3 and ICOS) are on the market or being developed [220]. These novel therapies could either be used in tumor entities, in which anti-PD-L1/PD-1 therapy is not successful or used to dramatically enhance the effect of anti-PD-L1/PD-1 therapy. As many immune inhibitory pathways do not overlap, combination therapies promise to potentiate the effect of mono therapy [221]. Several clinical studies for the combination of immune checkpoint blockades are currently running. The use of both anti-PD-L1/PD-1 and anti-CTLA-4 antibodies as a combination therapy has great potential as the tumor-mediated T cell inhibition (PD-L1/PD-1 interaction) is reduced and T cells are directly activated (blocking CTLA-4) at the same time [222]. Recent studies showed that this combination dramatically improved the anti-tumor response in melanoma [223, 224]. A

clinical study (phase 2) in untreated melanoma showed an ORR of 61% in patients treated with Nivolumab and Ipilimumab (anti-CTLA-4) against 11% in patients treated with Ipilimumab alone [225]. A complete remission was observed in 22% of the patients from the combinatorial group, whereas Ipilimumab could not induce complete remission. A follow up study (phase 3) showed an increased progression free survival (11.5 month) for combination therapy compared to Nivolumab (6.9 month) or Ipilimumab (2.9 month) alone [224]. In summary, combination of immune checkpoint blockades increases the therapeutic effects and broadens the group of patients benefiting from it. A downside is the onset of severe side effects during combination therapy [225, 226]. More than half of all patients experienced therapy-induced side effects (category 3-4) in the combination group (Nivolumab and Ipilimumab), compared to only 24% in the Ipilimumab-treated group. Furthermore, the side effects in 47% of the combination-treated patients were so severe that the treatment had to be stopped (17% in Ipilimumab only). Therefore, the development of novel immune checkpoint blockades and their combination with known ones could improve the treatment of patients that so far do not benefit from mono or combination therapies and/or could reduce therapy-induced side effects. Particularly, therapy against tumor-restricted immune checkpoints (e.g., PD-L1) might help to reduce systemic side effects.

1.7 RNA interference (RNAi) used for gene knockdown

High-throughput screenings used for the discovery of functional pathways use RNA interference (RNAi) in order to systematically knockdown targets of interest. RNAi is based on the finding that introduction of double-stranded RNA (dsRNA) into cells can target specific genes by sequence homology and was found to interfere with the endogenous function of genes in *Caenorhabditis elegans* [227]. Over time this so-called RNA interference became an important tool in functional assays and high-throughput screenings [228].

The RNAi machinery most probably developed as a defense against genomic parasites [229]. Several RNAi pathways are based on 20-30 nucleotide noncoding RNAs that recruit proteins to the according mRNA and thus control the expression of genes (**Figure 7**) [230]. Endogenous micro RNAs (miRNA) and typically exogenous small interfering RNAs (siRNA) induce pathways converging in the cytoplasm. For siRNAs, the duplex is loaded onto Argonaute and the passenger strand is removed. The guide strand together with the bound Argonaute form the RNA-induced silencing complex (RISC). RISC binds to a complementary mRNA target

sequence which is sliced by Argonaute. For miRNAs, a primary miRNA-hairpin loop is cropped and processed in the same way as siRNAs. Partial complementarity to the target sequence leads to steric inhibition of the RNA translational machinery [231]. Short hairpin RNAs (shRNA) function in a similar fashion as siRNAs but can be stably expressed allowing for the generation of cells with stable and heritable gene silencing (stable knockdown) [232].

The possibility to generate target-specific siRNAs/shRNAs paved the way for high-throughput RNAi screenings in different fields of biological research. For high-throughput siRNA screenings, siRNAs are delivered to cells either by liposomal transfection or electroporation. This approach induces a transient knockdown of the target mRNA without alterations of the genome. Short hairpin RNAs on the other hand are randomly introduced into the genome using viral particles (mainly lentiviral) and mediate transient or stable gene silencing [233]. Both siRNA- and shRNA-based RNAi screens are being employed to dissect cancer-related pathways involved in tumor-growth, invasion, metastasis and resistance to treatments [234-236].

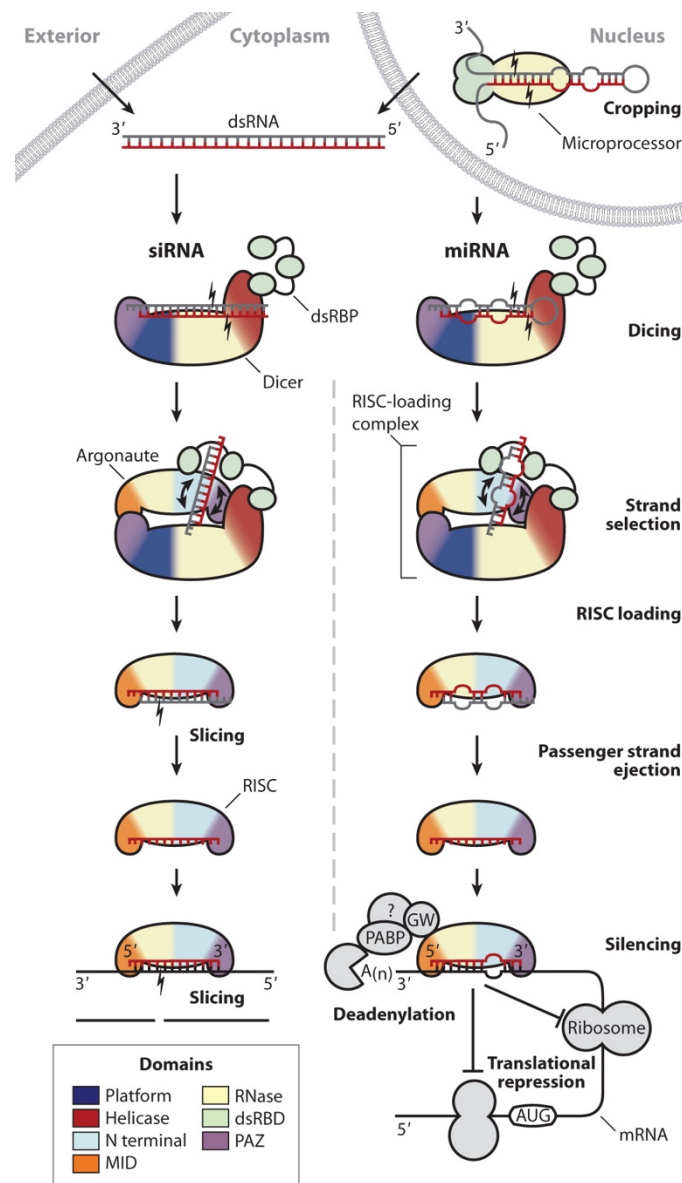


Figure 7: Translational repression mediated by small double-stranded RNA. Exogenous siRNA and endogenous miRNAs guide the RISC complex to target mRNA sequences inducing translational repression. Synthesized siRNAs targeting specific genes are used for functional assays and high-throughput screenings. Modified from *Wilson and Doudna, 2013*.

1.8 High-throughput screenings dissecting tumor-immune interactions

So far, most research done on immune checkpoint was based on the discovery of single genes or gene families involved in immune escape. Only a few groups tried to dissect general pathways of tumor-immune interactions systematically. Bellucci and colleagues developed a high-throughput screening to discover genes mediating melanoma resistance towards NK cell-mediated killing [237]. They transduced melanoma with a lentiviral shRNA library (targeting around 1000 genes) and measured increases in NK cell activity by IFN- γ secretion. Members of

the Janus kinase family (JAK1 and 2) were revealed to reduce susceptibility to NK-mediated killing. Follow up research showed that this effect is mediated by an upregulation of PD-L1 [238]. The group of Kai Wucherpfennig established an elegant *in vivo* discovery platform to find immunotherapy targets in/on T cells [239]. Murine T cells were transduced with a shRNA library and injected into tumor-bearing mice. Subsequently, enriched T cell populations were identified by deep sequencing of the tumor microenvironment. Our group recently utilized an arrayed siRNA library to transiently knockdown targets in breast cancer [240]. Subsequently, the impact of a gene knockdown on T cell-mediated tumor lysis was measured. The chemokine receptor CCR9 was found to impair T cell function *in vitro* and *in vivo*. Systematic dissection of tumor-immune interactions can reveal inhibitory pathways utilized by tumors to avoid destruction by T cells. Using high-throughput screenings allows to reconstruct the “immune modulome” of cancer and aids the generation of novel antitumor immunotherapies.

2 Aim and objectives of the thesis

The discovery of immune checkpoints and the subsequent development of immune checkpoint blockade as a form of antitumor immunotherapy is considered a breakthrough of modern medicine [206]. Blockade of immune checkpoints showed tremendous clinical benefits and the combination of therapies blocking independent inhibitory pathways synergistically improved antitumor responses. Unfortunately, a majority of cancer patients do not benefit from these novel immunotherapies yet. This gives basis for the assumption that only a fraction of all possible immune checkpoints and their underlying pathways has been discovered. Therefore, we aimed to establish an unbiased screening approach to identify novel immune checkpoints in different cancer entities.

We wanted to expand/modify our high-throughput RNAi discovery platform to closely resemble the patient situation. We focused on melanoma as a cancer entity with high immunogenic potential as well as strong immune suppression. The screening and subsequent target validation were performed with patient-derived TILs as well as tumor cultures (**Figure 8**).

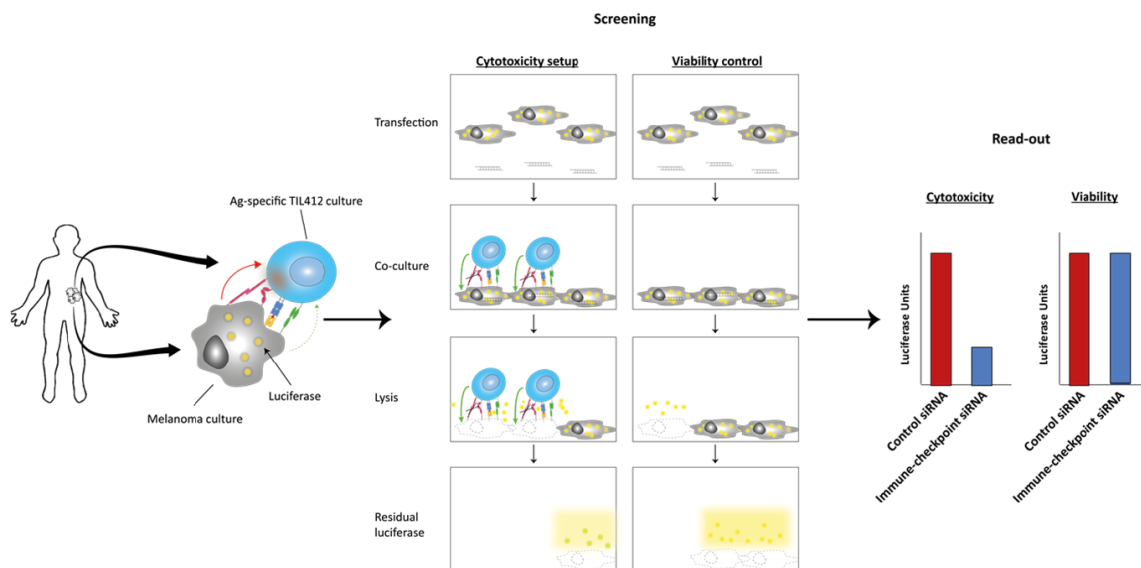


Figure 8: Scheme of the planned high-throughput RNAi screening to discover novel immune checkpoints in melanoma. A setup with patient-derived tumor-infiltrating lymphocytes and HLA-matched melanoma cultures was established. Afterwards, a screening was performed with an arrayed siRNA library targeting as many surface-associated genes as possible. Residual luciferase intensity served as a measure for tumor cell survival. The screening was performed with (cytotoxicity) or without (viability) TILs to exclude genes with a general impact on tumor cell survival.

This project offered an insight into the determinants of tumor-T-cell-interactions in regard to tumor killing. We hoped to find pathways involved in tumor-mediated inhibition of T cell function. In order to discover novel immune checkpoints and dissect their mode of action we planned to:

- Establish a screening system with patient-derived tumor-infiltrating lymphocytes and HLA-matched melanoma cultures.
- Adopt the high-throughput RNAi screening to the aforementioned setup and screen as many surface-associated genes as possible.
- Develop a secondary screening platform to streamline the discovery of genes impacting on TIL function.
- Validate novel immune checkpoints in several cancer entities.
- Validate novel immune checkpoints in a xenograft mouse model.
- Dissect the underlying mechanisms of tumor-mediated inhibition of CD8⁺ TILs.

3 Materials

3.1 Laboratory equipment

Machine	Company
QuantStudio 3 Real-Time PCR System	Thermo Scientific
Agilent 2100 Bioanalyzer	Agilent Technologies
Bandelin Sonorex Super ultrasonic bath	Sigma-Aldrich
Bolt Mini Gel Tank	Life Technologies
Caliper	Carl Roth
Casy cell counter	Innovatis
CTL ImmunoSpot S5 UV analyzer	CTL
Digital caliper gauge	Roth
FACS Canto II Flow cytometer	BD
Gamma Counter (Cobra Packard)	PerkinElmer
Gammacell 1000	Best Theratronics
Spark multimode microplate reader	Tecan
Luminex100 Bio-Plex System	Bio-Rad
Mithras LB 940 microplate Reader	Berthold Technologies
Molecular Imager (ChemiDoc XRS+)	Bio-Rad
MultiDrop Combi I	Thermo Scientific
NanoDrop 2000c UV-Vis Spectrophotometer	Peqlab
Owl EasyCast B2 Mini Gel Electrophoresis Systems	Thermo Scientific

SimpliAmp thermal cycler	Thermo Scientific
myECL documentation system	Thermo Scientific
XCell SureLock Mini-Cell Electrophoresis System	Life Technologies
IncuCyte ZOOM	ESSEN BioScience
ZEISS Observer.Z1 <ul style="list-style-type: none"> • Plan-Apochromat 100x/1.40 Oil (DIC) • LCI Plan-Neofluar 63x/1.3 Imm Korr <ul style="list-style-type: none"> • Fluar 40x/1.30 Oil (DIC) • Plan-Neofluar 20x/0.50 Ph 2 • XBO 75W/2 or XBO 175W light source 	ZEISS

3.2 Stimulation peptides

Peptide	Sequence (amino acids)	Company
MART-1 (26-35, modified) [241]	ELAGIGILTV	ProImmune
gp100 (154-162)	KTWGQYWQV	ProImmune
gp100 (209-217)	ITDQVPFSV	ProImmune
CX32 blockade	SRPTEKTVFTV	Peptide Facility, DKFZ

3.3 Reagents and consumables

Reagent	Company
1 kb DNA ladder (GeneRuler)	Thermo Scientific
AB Serum	Valley Biomedical
Agarose	Life Technologies
Agar	Fluka

Anti-Melanoma (MCSP) MicroBeads, human	Miltenyi Biotech
Aqua ad iniectabilia	Braun
Assay Diluent	BD
ATP	Roche
Benzonase	Merck
Beta-mercaptoethanol	Gibco
Biocoll solution	Biochrom
Cell proliferation reagent WST-1	Roche
CellTrace Far Red DDAO-SE	Life Technologies
Cholera toxin	Sigma-Aldrich
cOmplete Protease inhibitor cocktail tablets	Roche
Conical centrifuge tubes	TPP
Cryogenic vials (2 ml)	Corning
DharmaFECT1, 2 and 4 transfection reagents	Dharmacon, GE
DMSO	Sigma Aldrich
Fura-2-AM	Life Technologies
NuPAGE LDS sample buffer	Invitrogen
Novex 4-12% Bis-Tris SDS polyacrylamide gels	Invitrogen
PageRuler prestained protein ladder	Thermo Scientific
OptiPlate-384	Perkin Elmer
OptiPlate-96	Perkin Elmer
Cell Dissociation Buffer, enzyme-free, PBS	Gibco

3-Isobutyl-1-methylxanthine	Sigma-Aldrich
LumaPlates	Perkin Elmer
Microplates	TPP
Matrigel	BD Bioscience
Pertussis toxin	Sigma-Aldrich
mTurq2Δ_Epac(CD, ΔDEP,Q270E)_td^{cp173}Ven (EPAC_H187; FRET plasmid)	Provided by Kees Jalink; Netherland Cancer Institute
G418	Gibco
Puromycin	Gibco
RPMI (CLM)	Gibco
RPMI	Sigma-Aldrich
DMEM	Sigma-Aldrich
Ham's F12	Thermo Scientific
AIM V	Thermo Scientific
Chemicals for Buffers	Thermo Scientific
pEGFP_{Luc}	Clontech
Polybrene	Sigma-Aldrich
RNAiMAX	Thermo Scientific
jetPEI	Thermo Scientific
GeneJammer	Thermo Scientific
Lipofectamine LTX	Thermo Scientific
Opti-MEM	Gibco
G-Rex cell culture flask	Wilson Wolf

Yoyo-1	Thermo Scientific
Kiovig	Baxter

3.4 Antibodies

Target	Clone	Company
β-actin	mAbcam 8226	Abcam
Galectin-3	Polyclonal	BioLegend
PD-L1	130002	R&D Systems
CREB	48H2	Cell Signaling
pCREB (Ser133)	87G3	Cell Signaling
PKA C-α	Polyclonal	Cell Signaling
pPKA C-α (Thr197)	Polyclonal	Cell Signaling
Lck	73A5	Cell Signaling
pLck (Tyr505)	Polyclonal	Cell Signaling
CX45	Polyclonal	Thermo Scientific
CX32	CX-2C2	Life technologies
Sodium Potassium ATPase	EP1845Y	Abcam
anti-mouse-HRP	Secondary	Santa Cruz
anti-rabbit-HRP	Secondary	Santa Cruz
anti-goat-HRP	Secondary	Santa Cruz

3.5 Primers

Gene	Primer sequence (5' – 3')
β-actin	Forward: AGAAAATCTGGCACCACA Reverse: GGGGTGTTGAAGGTCTCAA
OR10H1	Forward: ACACGCCCATGTACCTCTTC Reverse: CCTTCAGCTCCTTGTTCTG
OR10H1_Qiagen (commercial)	OR10H1 RT ² qPCR Primer Assay
Connexin 32 (GJB1)	Forward: CTGCTCTACCCTGGCTATGCCATG Reverse: CAGGCCGAGCAGCGGTCGCTCTT
CX32_Qiagen (commercial)	GJB1 RT ² qPCR Primer Assay
CX43	Forward: TACCATGCGACCAGTGGTGCCT Reverse: TGAAGGTCGCTGGTCCACAATGGC
GNAL (Bio-Rad, commercial)	qHsaCID0017338
ADCY3 (Bio-Rad, commercial)	qHsaCID0014764

3.6 shRNA and siRNAs

Name	Gene	Sequence (RNA)	Identifier	Company
OR10H1 siRNA 1	26539	GGAGACACCUUGAUGGGCA	D-020479-01	Dharmacon
OR10H1 siRNA 2	26539	AGUAAACUCUACCCAGAAA	D-020479-02	Dharmacon
OR10H1 siRNA 3	26539	GCAGAGAGCCAAUCACUCC	D-020479-03	Dharmacon
OR10H1 siRNA 4	26539	GGUCGUGCACUAUGGCUUU	D-020479-04	Dharmacon
GJB1 siRNA 1	2705	GAUGAGAAAUCUCCUUCA	D-017887-01	Dharmacon
GJB1 siRNA 2	2705	AGAAUGAGAUCAACAAGGCU	D-017887-03	Dharmacon

GJB1 siRNA 3	2705	GAGUAUGGCUCUCGGUCAU	D-017887-17	Dharmacon
GJB1 siRNA 4	2705	GGACCUAUGUCAUCAGCGU	D-017887-18	Dharmacon
PD-L1 siRNA	29126	pool	M-015836-01	Dharmacon
Galectin-3		pool		Dharmacon
CCR9	10803	pool	M-005456-01	Dharmacon
Cell death	---	unknown	SI04381048	Qiagen
Ubiquitin C	7316	pool	M-019408-01	Dharmacon
Negative control 1	---	unknown	AM4611	Ambion
Negative control 2	---	unknown	4390846	Ambion
OR10H1 shRNA 1	NM_013940	G TTCCTGCTGATGTACCTGTT	TRCN0000011786	Sigma Aldrich
OR10H1 shRNA 2	NM_013940	TGCGCTACAACGTGCTCATGA	TRCN0000357706	Sigma Aldrich
OR10H1 shRNA 3	NM_013940	TGGCTTTGCCTCCGTCATTTA	TRCN0000357707	Sigma Aldrich
OR10H1 shRNA 4	NM_013940	TCTGCTGAAGGTCGGAACAAG	TRCN0000357708	Sigma Aldrich
OR10H1 shRNA 5	NM_013940	ACACAAGGAGATCCACCATTT	TRCN0000357775	Sigma Aldrich
Non-targeting Sequence (NTS)	---	Unknown	SHC002V	Sigma Aldrich

3.7 Assay kits

Kit	Company
Agilent RNA 6000 Nano Kit	Agilent technologies

Amersham ECL Prime Western Blotting Detection Reagent	GE Life Science
Bio-Plex Cell lysis kit	Bio-Rad
Mem-PER Plus Membrane Protein Extraction Kit	Thermo Scientific
M-PER Plus Membrane Protein Extraction Kit	Thermo Scientific
Bio-Plex Pro Human Cytokine 27-plex Assay	Bio-Rad
IFN-γ ELISA kit	BD Bioscience
Multi-Pathway Magnetic Bead 9-Plex - Cell Signaling Multiplex Assay (without p38)	Millipore
T-Cell Receptor Signaling Magnetic Bead Kit 7-Plex - Cell Signaling Multiplex Assay	Millipore
QuantiFast SYBR Green PCR kit	Qiagen
Pierce BCA Protein Assay kit	Thermo Scientific
QuantiTect Reverse Transcription Kit	Qiagen
SuperScript IV VILO Master Mix (reverse transcription)	Thermo Scientific
RNeasy Mini Kit	Qiagen
MyTaq HS Red Mix	Bioline
Bio-Plex cell lysis kit	Bio-Rad
Fixable Yellow Dead Cell Stain Ki	Thermo Scientific
Cell-Titer-Glo Luminescent Cell Viability Assay kit	Promega

3.8 Buffers

Buffer	Component	Amount?
B2 buffer	ddH ₂ O	100 ml
	DTT	6.4 g
	ATP	1.82 g
	AMP	0.035 g
BL buffer	ddH ₂ O	100 ml
	HEPES (50 mM)	5 ml
	EDTA (50 mM)	100 µl
	Phenylacetic acid (0.33 mM)	33 µl
	Oxalic acid (0.07 mM)	70 µl
	pH Adjustment to 7.6	
ELISpot washing solution	PBS	500 ml
	Tween-20	1.25 ml
ELISpot blocking solution	RPMI	500 ml
	AB serum	25 ml
FACS Buffer	PBS	49.5 ml
	FCS	0.5 ml
Luciferin solution	ddH ₂ O	8 ml
	D_luciferin (35.7 mM stock)	0.1 g
	Addition of NaOH until color change	
Luciferase buffer	BL buffer	44.35 ml
	B2 buffer	5 ml
	Luciferin solution	650 µl
	MgSO ₄ (1M stock)	751 µl

Luciferase assay lysis buffer	BL buffer	48.5 ml
	10% TritonX-100	1.5 ml
MACS Buffer	PBS	47.5 ml
	EDTA	2.5 ml
	Filtered AB serum	250 μ l
Phosphoplex lysis buffer	Cell lysis buffer	1 ml
	Cell lysis buffer, Factor 1	4 μ l
	Cell lysis buffer, Factor 2	2 μ l
	PMSF	4 μ l
Protein extraction buffer	M-PER Mammalian Protein Extraction Reagent	10 ml
	cOmplete Protease inhibitor cocktail	1 tablet
SDS-PAGE running buffer	MES SDS running buffer (20x)	50 ml
	ddH ₂ O	950 ml
Tris-acetate-EDTA (TAE) buffer (50x)	Tris	242 g (2 M)
	Glacial acetic acid	57.1 ml
	0.5 M EDTA	100 ml
	ddH ₂ O	1 L
	pH	8.5
Western blot transfer buffer (10x)	Tris base	30.3 g
	Glycine	144 g
	ddH ₂ O	1 L
Western blot washing solution (PBS-T)	PBS (10x)	100 ml
	ddH ₂ O	900 ml
	Tween-20	1 ml

Western blot blocking solution	PBS-T	50 ml
	Milk powder	2.5 g
RINGER's solution	ddH ₂ O	1000 ml
	NaCl	6.5 g
	KCL	0.42 g
	CaCl ₂	0.25 g
	Sodium bicarbonat	0.2 g

3.9 Media

Medium	Component	Volume
Complete lymphocyte medium (CLM)	RPMI	500 ml
	AB serum	50 ml
	Pen/Strep (100 x stock)	5 ml
	HEPES (1 M stock)	5 ml
	2-mercaptoethanol (50 mM stock)	50 µl
Complete melanoma medium (CMM)	DMEM	300 ml
	RPMI	100 ml
	Ham's F12 Nutrient Mixture	100 ml
	FCS	50 ml
	Pen/Strep	5 ml
	HEPES	5 ml
Tumor freezing medium	FCS	9 ml
	DMSO	1 ml
Tumor thawing medium	FCS	1 ml
	DMEM	9 ml

RPMI medium	RPMI	500 ml
	FCS	50 ml
	Pen/Strep	5 ml
	HEPES	5 ml
DMEM medium	DMEM	500 ml
	FCS	50 ml
	Pen/Strep	5 ml
	HEPES	5 ml
TIL freezing medium A	AB serum	30 ml
	RPMI	20 ml
TIL freezing medium B	AB serum	40 ml
	DMSO	10 ml
TIL thawing medium	AB serum	1 ml
	RPMI	9 ml
	Benzonase (250 U/ μ l stock)	2 μ l

3.10 Mice

Non-obese diabetic (NOD)-severe combined immunodeficient (SCID) *Il2rg*^{-/-} gamma (NSG) mice were used in this study. Original mouse strain was obtained from the Jackson Laboratory (strain name: NOD.Cg-*Prkdc*^{scid} *Il2rg*^{tm1Wjl}/SzJ) and were bred in-house at the DKFZ Animal Facility. Animal experiments were approved by the regulatory authorities (Karlsruhe). Mice were housed in sterile, individually ventilated cages (IVC). Ethical guidelines were followed according to the local regulations.

4 Methods

4.1 Cell culture methods

4.1.1 Tumor cell lines

M579-A2-luc and M579-A2 melanoma cultures, stably transduced with a HLA-A2 and a luciferase expression construct (HLA-A2 only for M579-A2), were established from melanoma patients as described before [242]. M579, M412, M209 and M615 melanoma cultures were kindly provided by Dr. Michal Lotem, Hadassah Hebrew University Medical Center, Jerusalem, Israel. Melanoma cell lines MaMel 33 and 101 were provided by Prof. Stefan Eichmüller, DKFZ. The colorectal cancer cell line SW480, the PDAC cell line PANC-1 and the multiple myeloma cell line KMM-1 were acquired from the American Type Culture Collection (Wesel, Germany). All melanoma cultures and cell lines were cultured in CMM and maintained at 37 °C and 8% CO₂. M579-A2-luc were maintained in CMM with 0.6 mg/ml G418 (Gibco, UK) and 0.4 µg/ml puromycin (Gibco, UK). SW480 and KMM-1 were cultured in RPMI medium and PANC-1 in DMEM medium at 37 °C and 5% CO₂.

4.1.2 Generation of stable luciferase transfected M615-luc

M615 were transfected with the pEGFPLuc plasmid (Clontech) using the Lipofectamine LTX reagent (as described in 4.2.4.2). After 48 h, the medium was replaced with CMM and incubated for 24 h. Subsequently, the transfected cells were positively selected with 0.6 mg/ml G418. After they reached sufficient confluency, the cells were sorted for high GFP expression using FACS. PANC-1-luc cells were generated in the same manner and kindly provided by Dr. Antonio Sorrentino, DKFZ.

4.1.3 Generation of stable OR10H1 knock-down melanoma cells

M579-A2 cells were transduced with lentiviral particles containing shRNA sequences targeting OR10H1 (Sigma-Aldrich). Non-targeting sequence (NTS) coding particles served as a negative control. Melanoma cells (300,000) were seeded in a 6 well plate overnight. The next day, the medium was replaced with DMEM medium containing 8 µg/ml polybrene (Sigma-Aldrich). The correct multiplicity of infection (MOI) for the lentiviral particles was validated using control GFP lentiviral particles. The optimal MOI found to be 2. 4 hours after culture with

DMEM and polybrene, the lentiviral particles were added (MOI 2) and the cells were incubated for 24 h. Afterwards the medium was replaced with CMM. After additional 24 h the cells were selected using 0.4 µg/ml puromycin. The stable knockdown of OR10H1 was confirmed by RT-PCR.

4.2 Molecular techniques

4.2.1 RT-PCR

Gene expression and mRNA knock-down efficacy of siRNAs and shRNAs were measured using RT-PCR. Tumor cells were harvested and the total RNA was extracted from cell pellets with the RNeasy Micro kit (Qiagen) according to manufacturer's protocol. RNA quality and concentration was analyzed using the RNA 6000 Nano kit (Agilent). RNA (1 µg) was reverse transcribed to cDNA using the QuantiTect reverse transcription kit (Qiagen) according to manufacturer's protocol (including gDNA digestion). For the RT control water was used instead of template RNA. Gene expression or knock-down was validated using traditional PCR. 100 ng of cDNA was amplified in 25 µl final mix with MyTaq HS Red Mix (Bioline) and the according primers (see 3.5).

The PCR reaction was started at 95°C for 3 min, followed by 35 cycles of a 3-step process: denaturation (95°C for 15 s), annealing (60 °C for 15 s) and extension (72°C for 15 s); with the final step at 72 °C for 7 min using the SimpliAmp thermal cycler (Thermo Scientific). The PCR products together with a 1 kb DNA ladder (Thermo Scientific) were run on a 1.5% agarose gel in TAE buffer using a gel electrophoresis system (Thermo Scientific). The DNA bands were visualized using the myECL documentation system (Thermo Scientific).

For low abundance genes (e.g., olfactory receptors) the above technique was modified as described previously [243]. Reverse transcription of 2.5 µg RNA was performed using the SuperScript IV VILO Master Mix kit (Thermo Scientific) as recommended by manufacturer. Shortly, the RNA samples were treated with ezDNase for 2 min at 37 °C. Afterwards, the RT mix together with the ezDNase treated RNA was incubated for 10 min at 25 °C for primer annealing. The reverse transcription took place at 50 °C for 30 min and subsequently the reverse transcriptase was inactivated at 85°C for 5 minutes. Controls for genomic DNA contamination were generated according to manufacturer's protocol. Traditional PCR was performed with 40 cycles of 95 °C, 60 °C and 72 °C at 45 s each.

4.2.2 Protein extraction

4.2.2.1 *General extraction*

Tumor cells were harvested and washed with PBS. Depending on cell numbers ($1-5 \times 10^6$), cells were lysed in 30-50 μ l M-PER (Mammalian Protein Extraction Reagent, Thermo Scientific) containing protease inhibitor cocktail for 20 min on ice. Afterwards, the lysates were spun down (13,000 rpm, 15 min at 4 °C) and the supernatants were either used directly or frozen at -20 °C.

4.2.2.2 *Membrane spanning protein extraction*

Membrane bound proteins (or cytosolic proteins) were extracted using the Mem-PER Plus Protein Extraction kit (Thermo Scientific) according to manufacturer's protocol. Shortly, tumor cells were scraped off the surface and washed twice with cell wash solution. Cells were permeabilized in 350 μ l Permeabilization buffer (containing protease inhibitor) for 10 min at 4 °C (constant mixing). The cells were spun down (15 min, 16,000 g, 4 °C) and the cytosolic proteins in the supernatant were removed and stored on ice. The cell pellets were resuspended in 250 μ l Solubilization buffer (with protease inhibitor) for 30 min at 4 °C (constant mixing). Finally, the lysates were spun down (15 min, 16,000 g, 4 °C) and the supernatants were either used directly or frozen at -20 °C.

4.2.2.3 *Phospho-protein Extraction*

Cells were lysed using the Bio-Plex cell lysis kit (Bio-Rad). Briefly, cells were washed and subsequently resuspended in 100 μ l Phosphoplex lysis buffer (containing protease and phosphatase inhibitors). After 5 min incubation on ice the lysates were frozen at -80 °C, followed by thawing on ice and vortexing. Subsequently, the lysates were incubated 10 min at 4 °C in an ultrasonic bath before being frozen again. Finally, the lysates were thawed on ice, spun down (13,000 rpm, 15 min, 4 °C) and the supernatants were either used directly or frozen at -20 °C.

4.2.3 Western blotting

For immunoblotting analysis, around 20 μ g of protein (less for membrane enrichment or phosphoproteins, see 4.2.2) were reduced in NuPAGE LDS sample buffer (Invitrogen) with DTT for 10 min at 70 °C. Afterwards the samples are separated in denaturing conditions on

Novex 4-12% Bis-Tris SDS polyacrylamide gels with SDS-PAGE running buffer (both from Invitrogen). PageRuler prestained protein ladder (Thermo Scientific) was used for band size determination. The protein bands were blotted onto activated PVDF membranes using 1x Western blot transfer buffer in a wet blotting chamber (400 mA for 45 min at 4 °C, 1 gel). Afterwards, the membranes were blocked with Western blot blocking solution for 20 min at RT. Membranes were incubated with the primary antibody in blocking solution overnight. After three washing steps with PBS-T, the membranes were incubated with the according HRP-conjugated antibody for 1 hour at RT. The membranes were washed again (three times) and protein bands were detected using Amersham ECL Prime western blotting detection reagent (GE Life Science) and a ChemiDoc XRS+ molecular imager.

4.2.4 Transfections

4.2.4.1 *Reverse siRNA transfection*

Gene knock-down in tumor cells was induced using reverse siRNA transfection. Several transfection reagents (HiPerFect, RNAiMAX, Dharmafect 1 and 2) were tested for their transfection efficacy in melanoma. Lipofectamine RNAiMAX (Thermo Scientific) showed the best results and was used for all subsequent experiments. Different reagent amounts depending on plate size were used (**Table 3**). The final siRNA concentration was 50 nM except for the primary screenings (25 nM). The siRNA was diluted in RNase-free water to a 500 nM (250 nM for primary screening) concentration and plated in the wells. RNAiMAX was mixed with RPMI and incubated for 10 min. Then, additional RPMI (ratio 1:1.5) was added and the final mixture was transferred to the siRNA on the plate. After 30 min, the respective number of M579-A2-luc (or other tumor cells) was resuspended in antibiotic-free DMEM supplemented with 10% FCS, seeded on top of the siRNA-lipid complex and incubated for 72 h at 37 °C.

Table 3: Transfection conditions for reverse transfection

Plate size	siRNA (20 μ M stock)	RPMI	Transfection reagent	Cell number (M579-A2-luc)
384 well (per well)	5 μ l	4.95 + 10 μ l	0.05 μ l	5000 in 30 μ l DMEM + FCS
96 well (per well)	10 μ l	9.9 + 20 μ l	0.1 μ l	10000 in 60 μ l DMEM + FCS
6 well (per well)	200 μ l	196 + 400 μ l	4 μ l	4x10 ⁵ in 1200 μ l DMEM + FCS

4.2.4.2 Plasmid transfection

Several transfection reagents (jetPEI, GeneJammer and Lipofectamine LTX with Plus) were tested for optimal plasmid expression. Lipofectamine LTX (Thermo Scientific) showed the best result and was used for all subsequent experiments. Tumor cells (3×10^5 for M579) were seeded in a 6 well plate and incubated at 37 °C overnight. The following day 15 μ l Lipofectamine LTX reagent was diluted in 150 μ l Opti-MEM medium (Gibco). Simultaneously, 3.5 μ g of DNA was diluted in 175 μ l Opti-MEM medium and 3.5 μ l of PLUS Reagent was added. 150 μ l of diluted DNA was added to 150 μ l diluted Lipofectamine LTX (Life Technologies) reagent and incubated for 5 min at RT. DNA-lipid complex was then added to the growth medium of the melanoma cells. Cells were incubated at 37°C for 48 hours before use in other assays.

4.3 TIL generation

4.3.1 TIL isolation

Tumor-infiltrating lymphocyte cultures 209, 412 and 615 were isolated from inguinal lymph nodes of melanoma patients. The TILs were kindly provided by Dr. Michal Lotem, Sharett Institute of Oncology, Hadassah Hebrew University Medical Center, Israel. As described before, tumors were dissected and small pieces were cultured in 24-well tissue culture plates in CLM with 6000 IU/ml IL-2 for 14 days [244]. The wells were checked for dense lymphocyte growth

and subsequently the TILs (each well is considered an independent TIL) were either frozen or expanded directly (section 4.3.2). In parallel, PDAC TIL was generated from a male patient with poorly differentiated pancreatic adenocarcinoma (PDAC). The PDAC TIL was kindly provided by Dr. Isabel Poschke and Dr. Rienk Offringa, DKFZ, Germany.

4.3.2 TIL rapid expansion (REP)

Melanoma and PDAC-derived TILs were rapidly expanded *ex vivo* using a modified version of the Rosenberg protocol [193, 244]. TILs were thawed in RPMI medium with 10% AB serum and 50 U/ml benzonase. Subsequently, they were incubated for 2 days (6×10^5 cells/ml in CLM with 6000 IU/ml IL-2) at 37°C and 5% CO₂. Mitotically inactivated feeder cells were generated from peripheral blood mononuclear cell (PBMC) buffy coats of healthy donors (three different donors) by irradiation with 60 Gy (Gamacell 1000). TILs were co-cultured with feeder cells in a 1:100 ratio (e.g., 2×10^6 TILs and 200×10^6 feeders) in 400 ml expansion medium (CLM/AIM-V 50/50) with 30 ng/ml OKT3 antibody and 3000 IU/ml IL-2 for 5 days without moving in a G-Rex 100 cell culture flask. Afterwards, 250 ml supernatant was replaced with 150 ml of fresh expansion medium supplemented with 3000 IU/ml IL-2 (for the complete 300 ml). On day 7, the TILs were resuspended in the medium and distributed into 3 G-Rex 100. 150 ml of AIM-V with 5% AB serum and 3000 IU/ml IL-2 (for the complete 250 ml) was added. On day 11, 150 ml of AIM-V with IL-2 was added to each flask. On the 14th day of rapid expansion, TILs were collected and counted. TILs were frozen in aliquots of 40×10^6 in freezing media A (first) and B (second).

4.3.3 TIL activity measurement

As TILs can lose their activity upon rapid expansion, their IFN- γ production was validated on day 8 of REP. Therefore, TILs were deprived of IL-2 for 24 hours. Afterwards, 1×10^6 T2 cells were pulsed with MART-1, gp100 or unrelated Influenza peptides (1 μ g/ml) together with β 2-microglobulin (10 μ g/ml) in RPMI medium (10% FCS) for 1 hour at 37°C. Subsequently, T2 cells were washed two times with RPMI medium. TILs (20,000) and T2/ tumor cells (10,000) were co-cultured (in CLM) in a 96-well plate over night at 37°C. The next day, the cells were spun down and the cytokine concentrations were measured by ELISA.

4.3.4 TIL preparations

Before the usage in any assay or screening, TILs were thawed on day -3 in RPMI medium with 10% AB serum and 50 U/ml benzonase. Subsequently, they were incubated for 2 days in CLM with 6000 IU/ml IL-2 at a concentration of 6×10^5 cells/ml and kept at 37°C and 5% CO₂. 24 hours before the experiment TILs were deprived of IL-2 by resuspension in CLM (6×10^5 cells/ml) in order to prevent IL-2-mediated over-activation.

4.4 Assays

4.4.1 Proliferation assay

Tumor cells (10,000) were cultured in a 96 well plate in a final volume of 100 µl/well culture medium and incubated at 37°C for 72 hours. For the assay, 10 µl of cell proliferation reagent WST-1 (Roche) was added to each well and the cells incubated for another 4 h at 37°C. Subsequently, the cells were shaken thoroughly for 1 min on a shaker and then absorbance of the samples was measured against a blank well as background control using a microplate reader at 450 nm with a reference at 650 nm.

4.4.2 TIL-mediated killing assays

4.4.2.1 *Luciferase assay*

Target genes were knocked down with reverse siRNA transfection for 72 h as described in 4.2.4.1. The reverse siRNA transfection was performed using non-transparent 384 or 96 well OptiPlates (PerkinElmer). In parallel the respective TILs (e.g., TIL412 for M579-A2-luc) were thawed and prepared as described in 4.3.4. After 72 h the TILs were counted, added to the target cells (TILs in CLM and target cells in transfection medium) at the appropriate effector to target ratio (E:T) and co-cultured at 37 °C. For viability controls the according amount of CLM without TILs was added. After 20 h the supernatant containing TILs and dead tumor cells was removed and the remaining tumor cells lysed with 40 µl of Luciferase assay lysis buffer (for 96 well plates) for 10 min. Subsequently, 60 µl luciferase buffer was added and the luciferase intensity was measured using the Infinite M200 plate reader (Tecan) with a counting time of 100 msec.

4.4.2.2 Chromium-release assay

Target genes were knocked down with reverse siRNA transfection (6 well format) for 72 h as described in 4.2.4.1. In parallel, the respective TILs (e.g., TIL412 for M579-A2-luc) were thawed and prepared as described in 4.3.4. Tumor cells were detached using enzyme-free cell dissociation buffer (Gibco) in order to prevent protein shedding from the cell surface. After washing the tumor cells were labeled with approximately 100 μCi of ^{51}Cr per 1×10^6 target cells (PerkinElmer) for 60 min at 37 °C. After three washing steps with CLM the cells were incubated in PBS-EDTA (1:20 dilution) for 10 min at 37 °C to prevent clumping. The labeled target cells were seeded in a 96 well plate (3000 M579 per well in 100 μl CLM) and co-cultured with the respective TIL (100 ml CLM) in different effector to target ratios (ranging from 100:1 to 1:1) for 4 h at 37 °C. After the co-culture the plates were spun down and 100 μl supernatant of each well was transferred to LumaPlates (PerkinElmer) and dried overnight. The next day the radioactivity was measured in a Cobra counter Packard (PerkinElmer). As a spontaneous release control labeled tumor cells were incubated with CLM without TILs. Furthermore, labeled cells were treated with 10% Triton X-100 in CLM instead of co-culture with TILs for maximum release control. The percentage of specific lysis was calculated according to the formula given below:

$$\% \text{specific lysis} = \frac{(\text{experimental release} - \text{spontaneous release})}{(\text{maximum release} - \text{spontaneous release})} \times 100$$

4.4.2.3 YoYo-1 live-image killing assay

Target genes were knocked down with reverse siRNA transfection for 72 h as described in 4.2.4.1. The reverse siRNA transfection was performed using transparent 96 well microplates (TPP). In parallel, the respective TILs (e.g., TIL412 for M579-A2-luc) were thawed and prepared as described in 4.3.4. After 72 h the TILs were counted, added to the target cells at the appropriate E:T in CLM with yoyo-1 (final concentration 1:10,000) and co-cultured at 37 °C. For viability controls the according amount of CLM with YoYo-1 (final concentration 1:10,000) was added. TIL-mediated tumor lysis was imaged on the green channel (yoyo-1) using an IncuCyte ZOOM live cell imager (ESSEN BioScience) with an image every 20-45 min at a 10x magnification. Image analysis was performed using following parameters:

Table 4: Incucyte signal detection parameters

Parameter	Setting
Background Subtraction	Top-hat
Radius (μm)	30.0
Threshold (GCU)	30.0
Edge Split	Off
Hole Fill (μm^2)	50.0
Filter: min Area (μm^2)	50.0

4.4.3 Flow cytometry

If applicable, tumor cells were detached using enzyme-free cell dissociation buffer (Gibco) in order to prevent protein shedding from the cell surface. If needed the cells were labeled using DDAO-SE in PBS (1:1000) for 15 min at 37 °C followed by two washing steps. FC receptors were blocked with 166 μg Kiovig (Baxter) in 100 μl FACS buffer for 20 min on ice combined with dead cell staining with 0.1 μl Pacific Orange (Thermo Scientific). The cells were washed and stained either with fluorophore-conjugated or unconjugated target specific or isotype antibody. After two washing steps with FACS buffer the cells were stained with fluorophore-conjugated secondary antibodies if necessary. Cells were washed and resuspended in 100 μl FACS buffer. All samples were acquired with a FACS Canto II Flow cytometer (BD Bioscience) and data was analyzed using FlowJo (Tree Star).

4.5 RNAi Screening

4.5.1 Screening

Two screenings were performed using different arrayed siRNA libraries (derived from the siGENOME library; Dharmacon, GE Life Science) containing 2888 genes (1288 genes for GPCR/kinase library and 1600 genes for custom library; **Supplementary list 1**) associated with the cell surface. Each gene is targeted by a SMARTpool consisting of four synthetic siRNA duplexes. Each RNAi screening was performed in duplicates. The screening procedure was

adopted from *Khandelwal et al* [240]. Sample and control siRNAs (5 μ l of 250 nM concentration) were distributed to 384-well plates and subsequently 0.05 μ l of RNAiMAX in 15 μ l of RPMI were added to each well for reverse transfection (see 4.2.4.1). After 30 minutes of incubation 5,000 M579-A2-luc cells (in 30 μ l DMEM + 10% FCS) were plated to each well. The plates were incubated for 72 h at 37°C. TIL412 were expanded (see 4.3.2) and deprived of IL-2 24h before the co-culture. After 72h of transfection M579-A2-luc cells were either co-cultured with 25,000 TIL412 in 40 μ l CLM (cytotoxicity setup, effector to target ratio of 5:1) or CLM alone (viability setup) for 20 hours. The next day the supernatant was removed and the remaining tumor cells were lysed by adding 20 μ l Luciferase assay lysis buffer for 10 min at RT. Afterwards, 30 μ l of Luciferase buffer were added and the remaining luciferase intensity (inverse of tumor lysis) was quantified using Mithras LB 940 microplate Reader with a counting time of 100 msec. The screening procedure was run in parallel with a CellTiter-Glo luminescent cell viability (CTG) assay on luciferase-negative M579-A2 cells without the addition of TILs in order to exclude genes affecting cell viability in general.

4.5.2 Screening analysis

Screening data was analyzed using the cellHTS2 and Bioconductor packages for R [245]. The general R script for the first Screening (GPCR/kinase library) was kindly provided by Dr. Marco Breinig (DKFZ, Heidelberg, **Supplementary R code**). Raw luciferase intensity data was logarithmic transformed and per-plate normalized using the median method. The replicates were scored using the Z score method:

$$x_{ki}^Z = \frac{x_{ki} - \mu_i}{\sigma_i}$$

Here the Z score for each k -th value (x) within the i -th result file (replicate plate) is calculated by subtracting the plate average (μ_i) from each value (x_{ki}) divided by the according standard deviation (σ_i) estimated from all values on the plate [245].

As an induction of TIL-mediated killing (or apoptosis by gene knock-down) results in decrease in luciferase intensity compared to the average of the plate (assuming normal distribution), the option 'sign = -' is used. Therefore, a reduced luciferase intensity results in higher Z scores. In order to distinguish genes impacting the TIL-mediated tumor lysis but not the tumor viability per se, the cytotoxicity Z scores were fitted to the viability Z scores using the LOESS method

(LOcal regrESSion) included in R. The function `normalizeQuantileRank` from the `aroma.light` package in R was used to perform quantile normalization on the Z scores. The resulting LOESS score was used to rank the genes, taking in consideration the ranges of the according cytotoxicity and viability Z scores. The data from the CTG assay was analyzed as described above (without LOESS fitting) and an additional CTG score (Z score) was calculated.

The thresholds for hit calling were set according to the immune checkpoint controls (PD-L1, Gal-3 and Casp-3) and viability controls (UBC and cell death). Negative control siRNA 1 and 2 served as negative controls, which should not impact cytotoxicity or viability. Genes scoring < -1.5 and > 1.5 in the CTG screen were filtered out due to their general viability impact. Finally, remaining genes which had a LOESS score above 1 were considered potential negative immune checkpoints, whereas genes with a loess score below -1 were considered potential immune activators.

4.6 Mode of action analysis

4.6.1 TIL extraction after co-culture

In order to separate tumor cells and TILs without affecting TIL signaling, M579-A2 were harvested and labeled with DDAO-SE (1:1000 in PBS) for 15 min at 37 °C. M579-A2 were washed twice and co-cultured with TIL412 at an E:T ratio of 10:1 for 2 hours at 37 °C. After incubation, cells were pelleted at 1500 rpm for 10 min and resuspended in 300 μ l MACS buffer. For separation, 100 μ l of Kiovig blocking reagent and 100 μ l of Anti-Melanoma (MCSP) micro beads (Miltenyi Biotech) were added and the cells incubated another 30 min at 4 °C under gentle rotation. Cells were then washed with 5 ml MACS buffer, centrifuged and resuspended in 500 μ l of MACS buffer. Magnetic columns were placed in the magnetic field of an MACS separator and equilibrated with 500 μ l of MACS buffer. The cell suspensions were applied onto the columns and left to pass through by gravitational flow. The columns were washed once with 500 μ l of MACS buffer. The flow-through containing the TILs was centrifuged and resuspended in FACS buffer. The cells were labeled for CD4 and CD8 (see 4.4.3) and subsequently acquired with a FACS Canto II Flow cytometer.

4.6.2 Phosphoprotein analysis

OR10H1 was knocked-down in M579-A2 cells (compared to sc siRNA control) using reverse siRNA transfection in 6 well plates (see 4.2.4.1) and TILs were prepared according to 4.3.4. The supernatant of the tumor cell transfection was removed and TIL412 were added in CLM (10:1 E:T ratio). As controls TILs were treated with Ionomycin (diluted 1:15.000) and PMA (diluted 1:20.000) or not stimulated. The TILs were removed after 0, 1, 5, 30 and 120 min and directly chilled on ice. Remaining melanoma cells were removed according to 4.6.1. After separation, the TILs were spun down and lysed according to 4.2.2.3. The protein concentration was quantified using the BCA Protein Assay Kit (Thermo Scientific) according to manufacturer's instructions. Phosphorylation levels of key kinases was assessed with phospho-protein specific Western blots (see 4.2.3) or Phosphoplex analysis. For the latter, we used a general pathway (MILLIPLEX MAP Multi-Pathway Magnetic Bead 9-Plex, Millipore) and a TCR specific pathway kit (MILLIPLEX MAP Multi-Pathway Magnetic Bead 9-Plex, Millipore). Beads specific for β -tubulin served as normalization controls. The kits were used as instructed by the manufacturer. Measurements were performed using the Luminex100 Bio-Plex System (Luminex) and the data were analyzed using the Bio-Rad Bio-Plex Manager software version 4.1.1 (Bio-Rad).

4.6.3 Calcium imaging

Before transfection, round glass slides were placed in 6-well plates and incubated with poly-D-lysine (50 μ g/ml) with pen/strep in PBS for 2 hours at 37 °C. Afterwards, OR10H1 was knocked-down in M579-A2 cells (compared to sc siRNA control) using reverse siRNA transfection in the aforementioned 6-well plates (modified from 4.2.4.1) and TILs were prepared according to 4.3.4. On the day of measurement, medium was replaced with RINGER's solution and Fura-2-AM was added to a final concentration of 10 μ M. After 45 min incubation (37 °C), the glass slides (in RINGER's solution) were used for imaging. TILs were spun down and resuspended in RINGER's solution. After around 10 min of imaging, TILs were added to the glass slides in a ratio of 5:1 (E:T). RINGER's solution was added to samples without TILs. Calcium signals were detected by measuring the 340/380 nm wavelength ratio. Imaging was performed by the group of Prof. Christian Wetzel (Molecular Neuroscience, University of Regensburg).

4.6.4 cAMP imaging

Before transfection, round glass slides were placed in 6-well plates and incubated with poly-D-lysine (50 µg/ml) with pen/strep in PBS for 2 hours at 37 °C. Afterwards, OR10H1 was knocked-down in M579-A2 cells (compared to sc siRNA control) using reverse siRNA transfection in 6-well plates (modified from 4.2.4.1) and TILs were prepared according to 4.3.4. After 24 hours, medium was replaced and the cells were transfected with a cAMP reporter plasmid (EPAC_H187, kindly provided by Kees Jalink; Netherland Cancer Institute) according to 4.2.4.2. Before imaging, medium was replaced by RINGER's solution. After around 10 min of imaging, TILs were added to the glass slides in a ratio of 5:1 (E:T). RINGER's solution was added to samples without TILs. Ratiometric FRET analysis was performed by detection of the donor and acceptor emission simultaneously with two photomultipliers, using a 505 nm beamsplitter and optical filters: 470 ± 20 nm (CFP) and 530 ± 25 nm (YFP). Signals were digitized and FRET was expressed as the ratio between donor and acceptor signals. Imaging was performed by the group of Prof. Christian Wetzel (Molecular Neuroscience, University of Regensburg).

4.6.5 Differential gene expression analysis

4.6.5.1 RNA Sequencing

OR10H1 was knocked-down in M579-A2 cells (compared to sc siRNA control) using reverse siRNA transfection in 6 well plates (see 4.2.4.1) and TILs were prepared according to 4.3.4. The supernatant of the tumor cell transfection was removed and TIL412 were added in CLM (10:1 E:T ratio). The TILs were removed after 10 h and directly chilled on ice. Remaining melanoma cells were removed according to 4.6.1. After separation, the TILs were spun down and total RNA was extracted using the RNeasy Micro kit (Qiagen) per manufacturer's protocol. RNA quality and concentration was analyzed using the RNA 6000 Nano kit (Agilent). Subsequently, RNA deep sequencing was performed by the GPCF of DKFZ with following parameters:

Table 5: RNA sequencing parameters

Parameter	Setting
Machine	Illumina Hiseq 2500
Application	RNA Seq with TruSeq

Sequencing type	single read
Read length	50 bp
Sequencing depth [reads]	~40 Mio

4.6.5.2 Differential gene expression analysis

Raw data was provided by the core facility in the fastq format. The analysis workflow was adopted from *Anders et al* [246]. The reads were aligned to a reference genome, reference transcriptome and a gene information file (GRCh37, iGenomes, Illumina) using tophat2:

```
tophat -G genes.gtf --no-novel-juncs --transcriptome-index=... -p 7 -o ... genome file.fastq
```

The resulting BAM files were sorted, indexed and formatted into SAM files using SAMtools:

```
samtools sort -n accepted_hits.bam ..._sn
```

```
samtools view -o ..._sn.sam ..._sn.bam
```

The features were counted from the reads using HTSeq-count:

```
htseq-count -s no -a 10 ..._sn.sam genes.gtf > ..._sn.count
```

Finally, the differential gene expression of TILs co-cultured with OR10H1⁻ M579-A2 was compared to TILs co-cultured with sc siRNA transfected M79-A2 cells using edgeR. Weakly and noninformative (e.g., non-aligned) features were filtered out and the normalization factors were estimated and used for the differential expression test.

4.6.5.3 Pathway analysis

Based on the differential gene expression data generated in 4.6.5.2, enrichment analysis on pathways, functions and upstream regulators was performed. Genes were filtered for a gene expression fold change >0.5 or <-0.5 and a false discovery rate smaller than 0.05. Only experimentally validated observations were considered.

4.7 Mouse experiments

Approval for the animal work was obtained from the relevant regulatory authorities (Regierungspräsidium, Karlsruhe). For assessing the *in vivo* effect of tumor-restricted OR10H1 upon the anti-tumor cytotoxicity of T cells, a xenograft mouse model based on immunodeficient NOD/SCID gamma (NSG) mice was used. Mice were ordered from the animal core facility at DKFZ, Heidelberg. Stable OR10H1 knock-down M579-A2 and the respective NTS control (see 4.1.3) were resolved in matrigel (BD Bioscience) on ice. Mice were shaved at the flank regions, anesthetized with isoflurane and subcutaneously injected (0.4 mm x 20 mm needles) with 3×10^5 M579-A2 OR10H1 knock-down tumor cells in the left flank and 3×10^5 respective NTS tumor cells in the right flank at day 0. At days 2 and 9, the treatment group received adoptive cell transfer with TIL412 (9×10^6 cells/100 μ l PBS/mouse) intravenously into the tail vein. For growth control, the other group remained untreated. Tumor growth of all mice was measured twice a week with a sliding caliper gauge. Mice were sacrificed via cervical dislocation at the end of the experiment.

4.8 Statistical evaluation

Statistical differences between the test and the control groups were analyzed by the two-sided student's t-test, unless indicated otherwise. In all statistical tests, a p-value ≤ 0.05 was considered significant with * = $p \leq 0.05$, ** = $p \leq 0.01$, *** = $p \leq 0.001$ and **** = $p \leq 0.0001$.

5 Results

5.1.1 Screening setup

The main goal of this thesis was the characterization of TIL-tumor cell interactions and the subsequent identification of novel immune checkpoints using a high-throughput RNAi screening. A robust read-out system, identification of suitable negative controls and positive controls for increased TIL-mediated lysis (immune checkpoints) and robust tumor killing (e.g., HLA-A2-dependent, independent of TIL batch) are key factors for this endeavor. The screening approach was adopted from a related RNAi screening ascertaining T cell-mediated killing of breast cancer cells by measuring residual luciferase intensity [240]. This thesis focuses on the interactions between melanoma and TILs (a mixture of CD4⁺ and CD8⁺ T cells), as the main immune cell subtype infiltrating tumors. We mainly used the M579 melanoma culture in combination with tumor-infiltrating lymphocytes 412 (TIL412). All melanoma and TIL cultures were kindly provided by Dr. Michal Lotem (Hadassah Medical Center, Jerusalem, Israel).

5.1.2 Characterization of M579 melanoma cultures

The HLA-A2-negative melanoma culture M579 was generated from a metastatic melanoma patient at the Sharett Institute of Oncology (Hadassah Medical Organization Jerusalem, Israel) and stably transfected with a pcDNA3-HLA-A2 plasmid [247]. Subsequently, the HLA-A2⁺ M579 (M579-A2) cell culture was transduced to express luciferase (M579-A2-luc). This work was done in the laboratory of Dr. Lotem. Transfection parameters need to be optimized for any siRNA transfection. A reverse transfection of 5000 M579-A2-luc cells in a 384 well plate for 72 h was shown to be optimal in terms of cell growth, luciferase intensity and gene knockdown [data not shown]. Different cell types vary in their susceptibility towards transfection reagents commonly used in reverse siRNA transfection. This susceptibility is important to guarantee efficient knockdown of target genes. Therefore, several transfection reagents (Dharmafect 1 and 2, HiPerFect and RNAiMAX) were tested in combination with negative control (sc) siRNAs, siRNAs targeting cell survival genes (ubiquitin C, cell death) and siRNA targeting luciferase (Fluc). Successful knockdown using UBC (ubiquitin C) or cell death (targets unknown) siRNA would lead to a decrease in cell viability correlating with a strong reduction in residual luciferase intensity. Fluc siRNA targets luciferase and thus directly correlates with the transfection efficacy

without affecting viability. RNAiMAX showed superior transfection efficacy in M579-A2-luc compared to all other transfection reagents (**Figure 9A**). Therefore, RNAiMAX was used for reverse siRNA transfection in all subsequent experiments. Furthermore, transfection of M579-A2-luc with Fluc siRNA strongly reduced luciferase intensity (more than 90%), suggesting sufficient transfection and knockdown efficacies in this setup. Therefore, Fluc siRNA was used as a further control for transfection efficacy in the RNAi screening. Knockdown of the essential gene ubiquitin C (UBC siRNA) reduced cell viability by approximately 65%. This luciferase intensity reduction by UBC siRNA was used as a cut off to classify genes which have a strong viability impact. A proprietary siRNA mixture (cell death) showed a similar effect on cell viability (**Figure 9A**). Both siRNAs were included in the RNAi screening.

All TILs which were used in this project recognize antigens presented by HLA-A2. As mentioned before, M579-A2-luc (and M579-A2) were stably transfected with a HLA-A2 plasmid. Cell surface expression of HLA-A2 was validated using FACS (**Figure 9B**). As expected, M579-A2-luc were found to be highly positive, whereas M579 did not express HLA-A2.

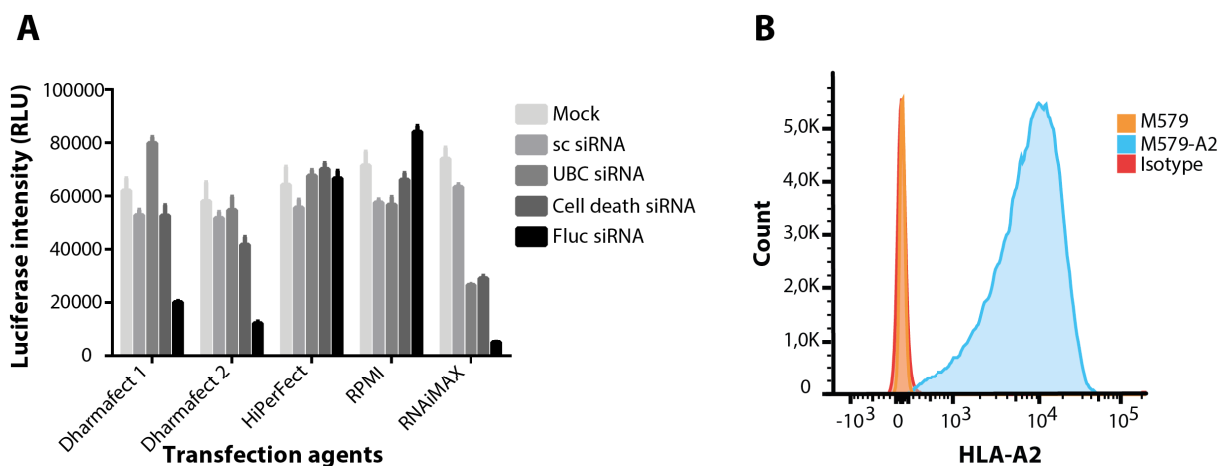


Figure 9: Characterization and optimization of M579 for RNAi screening. **A.** Luciferase assay determining transfection and knockdown efficacies. M579-A2 cells (5000) were reverse transfected with control (Mock, scrambled and Fluc) or lethal (UBC and Cell death) siRNAs in 384 well plates using different transfection agents (Dharmafect 1, Dharmafect 2, HiPerFect and RNAiMAX). Residual luciferase intensity (correlating with cell numbers and viability) was measured after 72 h. Mean luciferase intensities \pm SEM of a representative experiment are shown. **B.** HLA-A2 surface expression of M579 and M579-A2-luc. Cells were harvested and stained with HLA-A2 specific antibody or the according isotype control.

5.1.3 Tumor-infiltrating lymphocytes 412 kill M579-A2 in an antigen-specific and HLA-restricted manner

Generation and expansion of antigen-specific tumor-infiltrating lymphocytes is a challenging part of cancer immunotherapy against melanoma. The group of Dr. Lotem isolated and

expanded several TIL cultures (TIL209, TIL412 and TIL615) according to the “rapid expansion protocol” (REP) of *Dudley et al* [244]. Because high-throughput screening and subsequent validation require vast numbers of TILs the generated TIL cultures were expanded one more time using an improved REP protocol (see paragraph 4.3.2). TIL phenotype, exhaustion state and functionality were assessed after this point as a massive expansion of TILs using feeder cells, IL-2 addition and CD3 stimulation can alter these parameters. In average TIL numbers increased around 3000-fold after rapid expansion [data not shown]. Analysis revealed that the TIL cultures differ in composition, exhaustion state and functionality (**Figure 10** and **Figure 11**). Tumor-infiltrating lymphocyte culture 412 (TIL412) is a mixture of cytotoxic (CD8⁺) and helper (CD4⁺) T cells, whereas TIL209 contains predominantly cytotoxic (83.3% CD8⁺) and no helper T cells (**Figure 10**). Cytotoxic T cells are supposed to be the main effector T cell subpopulation mediating an anti-tumor immune response. For this reason, the memory and effector phenotypes of the CD3⁺CD8⁺ T cell subsets were examined by expression of the surface markers CD62L and CD45RA. Interestingly, CD8⁺ T cell populations in both TILs show a strong memory phenotype. Around half of the cells have a central memory (CD8⁺CD62L⁺CD45RA⁻) or an effector memory (CD8⁺CD62L⁻CD45RA⁻) phenotype, whereas there are no naïve (CD8⁺CD62L⁺CD45RA⁺) or terminal effector memory (CD8⁺CD62L⁻CD45RA⁺) T cells. In concordance with their memory phenotype, CD8⁺ TILs express high levels of exhaustion markers (CTLA-4, PD-1, TIM-3 and LAG-3) suggesting a state of strong exhaustion. Exhausted TILs have a higher probability to express receptor/ligands for potential immune checkpoints revealed by the RNAi screening.

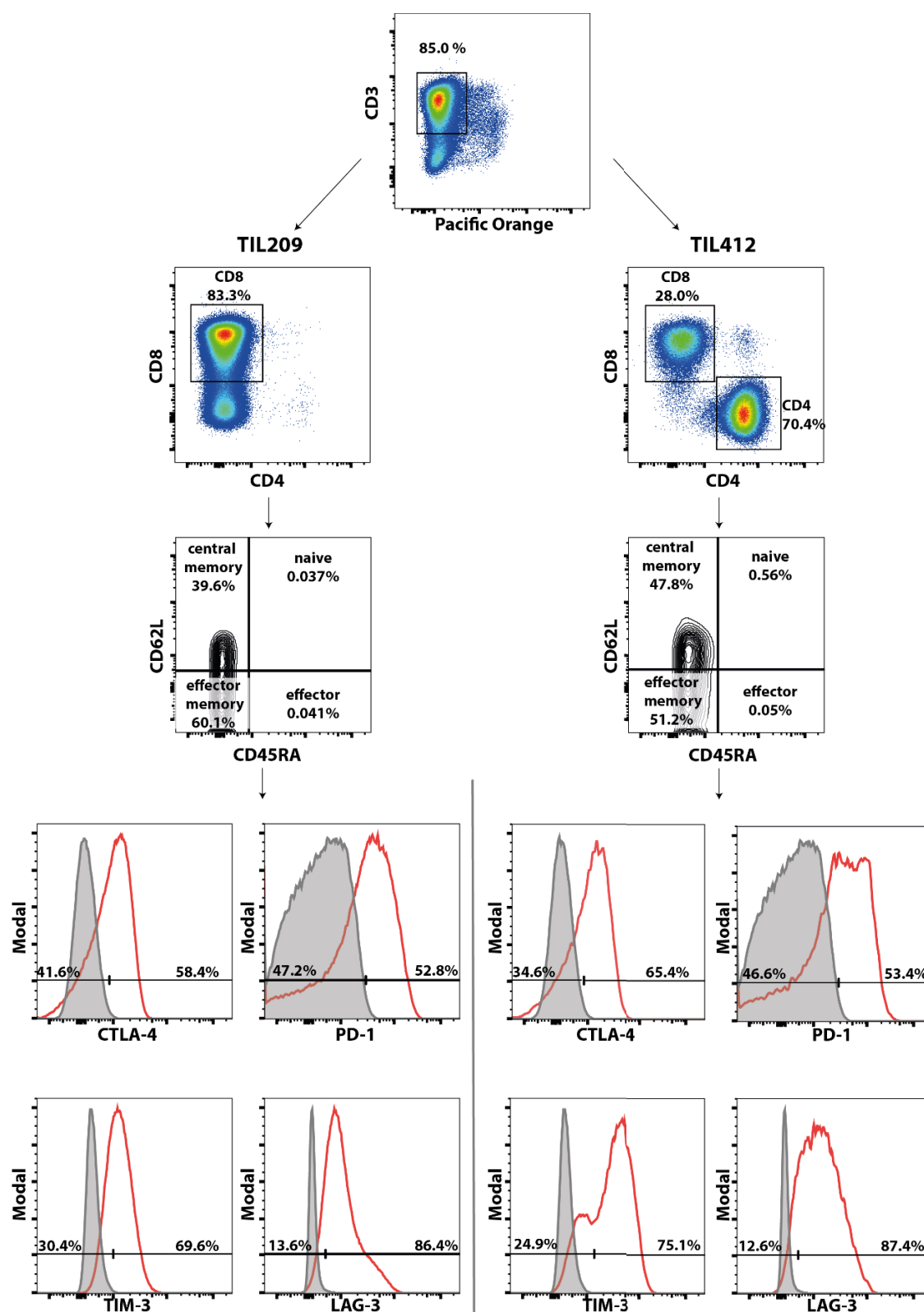


Figure 10: Tumor-infiltrating lymphocytes are a mixture of CD4⁺ and CD8⁺ T cells with highly exhausted memory phenotypes. Representative surface staining for CD3, CD4, CD8, CD62L, CD45RA, CTLA-4, PD-1, TIM-3 and LAG-3 on TIL209 and TIL412 after rapid expansion. Exhaustion markers were gated on effector memory CD3⁺ CD8⁺ T cells based on the respective isotype control antibodies (depicted in red). Experiments were performed in collaboration with Valentina Volpin (Group Prof. Beckhove, DKFZ).

Expandability of TILs is a major concern for the RNAi screening. Depending on the effector to target ratio necessary for sufficient basal tumor cell killing, huge numbers of TILs would be needed for the screening and subsequent validation. TIL412 showed a favorable expandability compared to TIL209 and was chosen as the T cell source for the RNAi screening. Thus, TIL412 were tested for their HLA-A2-restricted activity against M579-A2-luc (**Figure 11**). TIL412 showed a strong induction of cytokine secretion after co-culture with the HLA-A2-positive M579-A2-luc but not against the HLA-A2-negative melanoma cell line MaMel 33. The antigen-specificity of this cytokine secretion was tested using T2 cells pulsed with the common melanoma antigens melanoma-associated antigen recognized by T cells 1 (MART-1) and glycoprotein 100 (gp100) against an unrelated influenza antigen). TIL412 show a strong reactivity against MART-1 and to a lower degree against the epitope from gp100, but no activity against the influenza antigen. This suggest an antigen-specific and HLA-A2-restricted activity. In order to exclude any HLA-independent reactivity against M579-A2 (which might not occur against MaMel 33) TIL412 were tested against the HLA-A2-negative parental cell line M579. Furthermore, the melanoma cells were cultured and transfected (with scrambled control siRNA) similar to the conditions in the RNAi screening. TIL412 showed a strong cytokine secretion after co-culture with M579-A2 but not with M579. This elucidates the HLA-A2-restriction of TIL412 activity against M579-A2(-luc). Another important factor for the setup of the RNAi screening is the optimal effector-to-target ratio. On one hand, a basal TIL412-mediated killing is needed to assure TIL activity for the RNAi screening. A strong killing- on the other hand- would reduce the window of opportunity for intervention by immune checkpoint knockdown. Therefore, different effector-to-target ratios (50:1 to 1:1) were tested in a luciferase-cytotoxicity assay similar to the high-throughput RNAi screening. High E:T ratios lead to a dramatic reduction in residual luciferase intensity (strong TIL412-mediated killing) comparable to the treatment of M579-A2-luc with the maximum lysis control (Triton X). Interestingly, the addition of TIL412 to M579-A2-luc in low (< 5:1) E:T ratios strongly increases residual luciferase intensity after 20 hours. This effect was observed with several tumor-TIL co-cultures in different tumor entities [data not shown]. An effector-to-target ratio of 5:1 appeared to offer the best ratio between basal killing and residual luciferase intensity. Therefore, it was selected for further use in the primary RNAi screening and all subsequent validation steps (if not indicated otherwise).

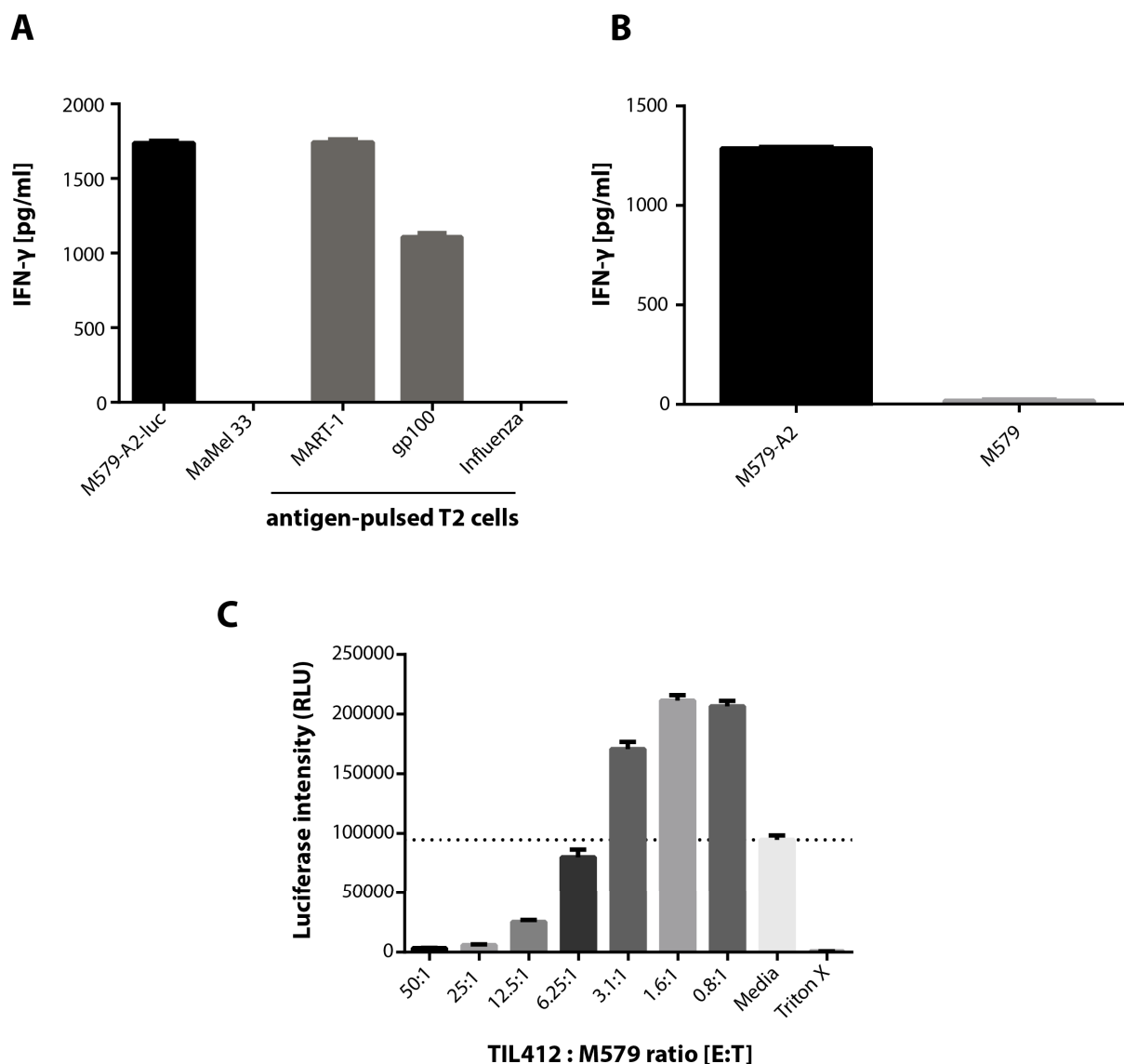


Figure 11: TIL412 recognize and kill M579-A2-luc cells in an antigen-specific, effector-to-target ratio- and HLA-A2-dependent manner. Antigen specificity (A) and HLA-dependency (A and B) of TIL412 were tested using IFN- γ secretion ELISA. **A.** T2 cells were pulsed with the according melanoma (MART-1 or gp100) or unrelated influenza peptide for 1 hour. HLA-A2-positive M579-A2-luc, negative MaMel 33 or the pulsed T2 cells were co-cultured with TIL412 (5:1 effector-to-target ratio) for 20 hours. **B.** HLA-A2-positive M579-A2 or negative M579 were transfected with negative control siRNA and cultured for 72 h before co-culture with TIL412 (5:1 E:T) for 20 hours. **C.** Luciferase cytotoxicity assay was performed using different effector-to-target ratios of TIL412 and M579-A2-luc for 20 hours. CLM medium served as a negative control, whereas Triton X represents maximum lysis. All graphs depict representative experiments with mean cytokine secretion (A and B) or mean luciferase intensity (C). Error bars denote \pm SEM.

5.1.4 PD-L1 and Galectin-3 protect M579-A2 against TIL412-mediated lysis

Selection of positive immune checkpoint controls is of uttermost importance for the high-throughput RNAi screening. Without proper checkpoint controls it is not possible to estimate any potential knockdown impact on TIL-mediated lysis. Furthermore, such controls are needed to set thresholds for hit calling. Only genes having a higher impact on TIL-mediated tumor lysis compared to the checkpoint control while having a similar minor impact on general cell

viability were considered as novel immune checkpoint candidates. Hence, we tested several known immune checkpoints (PD-L1, galectin-3, RCAS1 and CEACAM6) for their impact on TIL-mediated tumor lysis in our system (**Figure 12**). RCAS1 and CEACAM6 did not show either expression or immune-inhibitory effect in M579-A2 [data not shown]. PD-L1 and galectin-3 were detected in M579-A2 and gene-specific knockdown after 72 h was verified with qPCR (PD-L1; **Figure 12A**) and western blot (galectin-3: **Figure 12B**). Knockdown of PD-L1 or galectin-3 increased TIL-mediated lysis of M579-A2-luc in the luciferase cytotoxicity assay, while knockdown of caspase-3 (Casp-3) prevented lysis of M579-A2-luc (**Figure 12C**). Without TILs, neither the knockdown of PD-L1, galectin-3 or caspase-3 had an impact on M579-A2-luc viability, whereas the knockdown of ubiquitin C strongly reduced cell viability. Interestingly, the knockdown of PD-L1 prevented the induction of tumor cell proliferation in low effector-to-target ratios observed with control siRNA transfected M579-A2-luc. Overall our data confirmed the immune checkpoint function of PD-L1 and galectin-3 in melanoma. Both genes (PD-L1 and galectin-3) can be used as positive immune checkpoint controls for the RNAi screening. Caspase-3 knockdown prevents tumor lysis and therefore can be used as a control for potential immune activators. As mentioned before, control siRNA served as a negative and UBC or cell death as viability controls. Firefly luciferase siRNA is used to determine transfection efficacy. All these controls were used in the high-throughput RNAi screening for performance analysis and hit calling.

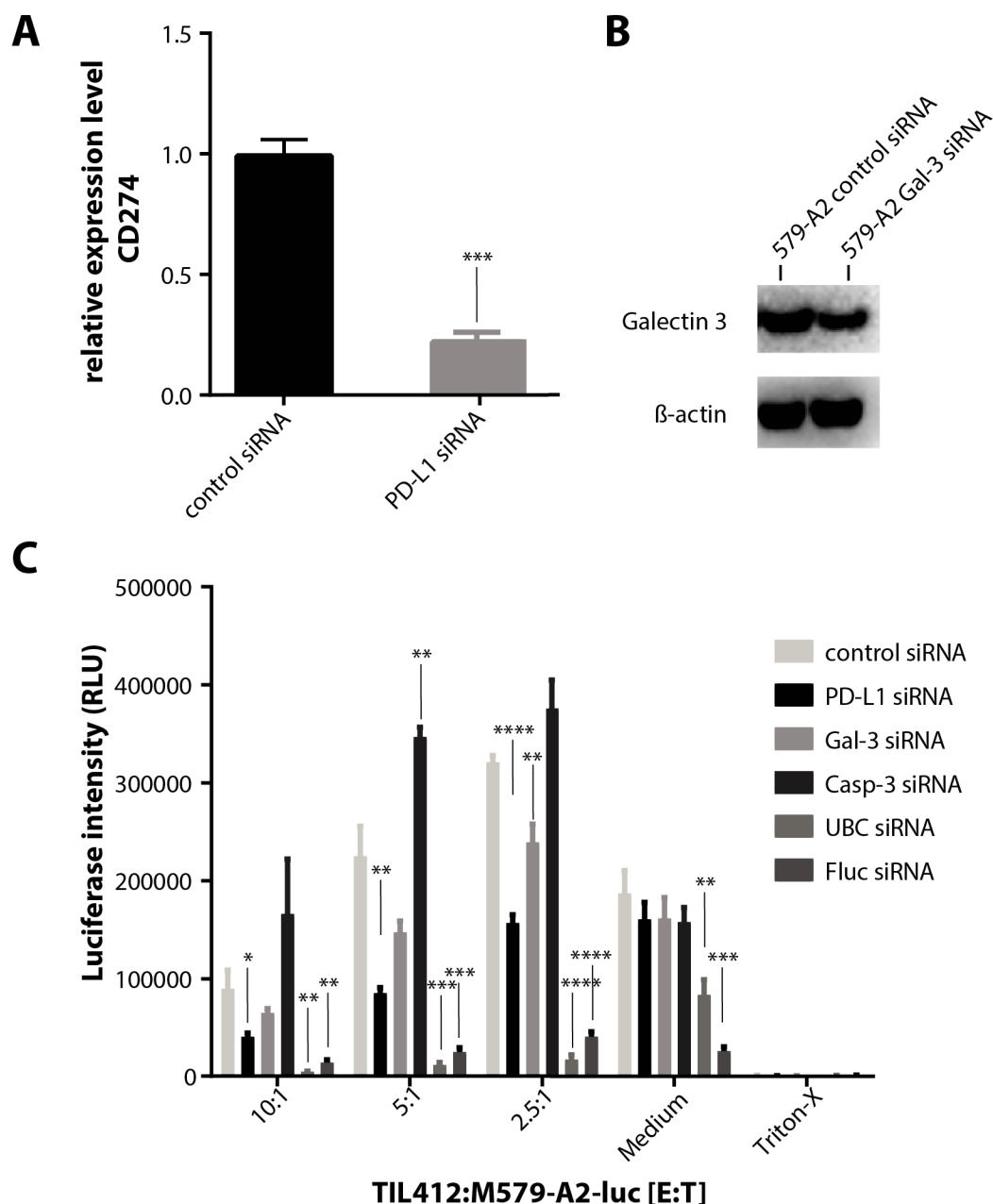


Figure 12: PD-L1, galectin-3 and caspase-3 increased or decreased TIL-mediated tumor lysis, respectively. M579-A2-luc cells were transfected with indicated siRNAs for 72 h before measurement of knockdown efficacy (A and B) or 20 h measurement of T cell-mediated cytotoxicity. A, B. Immune checkpoint expression and knockdown was verified with qPCR (PD-L1) or western blot (galectin-3). Control siRNA served as negative control siRNA. C. Luciferase cytotoxicity assay for immune inhibitory or activatory controls. M579-A2-luc cells transfected with siRNAs directed against, PD-L1 (PD-L1 siRNA), galectin-3 (Gal-3 siRNA), caspase-3 (Casp-3 siRNA), ubiquitin C (UBC siRNA), firefly luciferase (Fluc siRNA) or control siRNA were co-cultured with TIL412 in different effector-to-target ratios for 20 hours. Knockdown cells with CLM medium served as a negative control, whereas Triton X represents maximum lysis. A-C. Graphs show representative data of at least two independent experiments. A, C. Error bars denote \pm SEM, and statistical significance was calculated (compared to the according control siRNA) using unpaired, two-tailed Student's t-test with * $p \leq 0.05$; ** $p \leq 0.01$; *** $p \leq 0.001$; **** $p \leq 0.0001$.

5.2 High-throughput RNAi screen performance

Known immune checkpoints like PD-L1 are located at the cell surface and transmit inhibitory signals towards cytotoxic T cells. For this reason, a siRNA library containing all genes of the so-

called “surfaceome” would be optimal to screen for novel immune checkpoint candidates. Unfortunately, there is no such library commercially available. We checked the distribution of all surfaceome genes [248] in the whole-genome library and compiled two sub-libraries enriched for surface-associated genes (**Figure 13A**). The initial screening was performed with a library consisting of GPCRs, kinases and GPCR-associated genes. The performance and results of this screening will be described in the following paragraphs. The results of the follow-up screening (additional surface-associated genes) can be found in the supplementary information (**Supplementary figure 1**). The RNAi screening procedure is depicted in **Figure 13**. Melanoma M79-A2-luc were reverse transfected with a GPCR/kinase library containing 1288 genes and subsequently co-cultured with TIL412 (knockdown impact on cytotoxicity) or cultured in lymphocyte medium alone (knockdown impact on viability). An additional luciferase-independent CellTiter-Glo (CTG) screening was performed with M579-A2 in order to filter out genes, the knockdown of which affected cell viability. All sets (cytotoxicity, viability, CTG) were run in duplicates. The correlation in between the sample replicates (excluding control siRNAs) showed a high robustness in the screening (**Figure 14A**). The Pearson’s correlation coefficient for the cytotoxicity was $r = 0.96$, although two TIL412 batches were expanded and added separately. The coefficient for the viability set was $r = 0.98$. The performance of all negative, immune checkpoint and viability controls was satisfactory in the screening (**Figure 14B**). Overall, the residual luciferase intensities in the screening were normally distributed around the mean of the respective plate in all setups [data not shown]. Therefore, Z-scoring could be used for normalizing the data as standard deviations from the plate mean to reduce inter plate variations. As expected, negative scrambled siRNA controls 1 and 2 did not reduce or increase residual luciferase intensity. Knockdown of firefly luciferase on the other hand strongly reduced luciferase intensity proving sufficient reverse transfection efficacy and siRNA delivery. This effect was independent of the presence of TIL412. Knockdown of the known immune checkpoints PD-L1 and galectin-3 led to an increase in TIL412-mediated lysis of M579-A2-luc without affecting their viability. Knockdown of caspase-3 prevented T-cell mediated induction of apoptosis in melanoma cells but had no effect on melanoma cells alone. Transfection with cell death siRNA or siRNA directed against ubiquitin C reduced cell viability measured by the CTG viability assay.

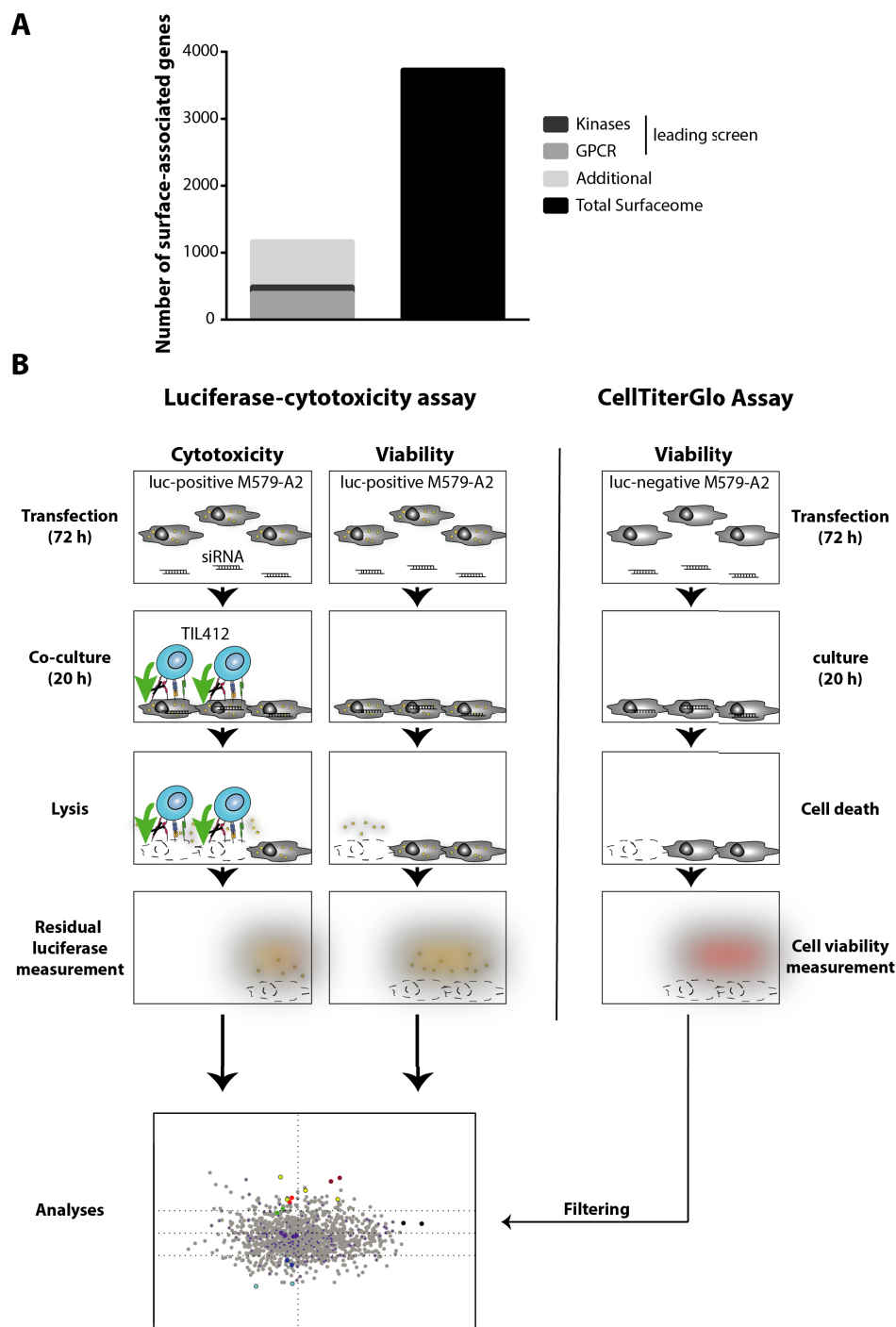


Figure 13: Libraries and workflow of the high-throughput RNAi screening. **A.** Overview of surface-associated genes in the two sub-libraries of the RNAi screen compared to the whole surfaceome. Around 30% of all genes associated to the cell surface are included in the screening. In total 2514 genes were included in the screening process. **B.** Workflow of the screening process. Three different sets were run in duplicates. The cytotoxic set is used to measure the impact of gene knockdown on TIL-mediated lysis. The viability set verifies the impact of gene knockdown without TILs and the CTG set is used to exclude genes affecting melanoma cell survival independent of luciferase expression. Screening analyses were performed using the cellHTS2 package of Bioconductor for R.

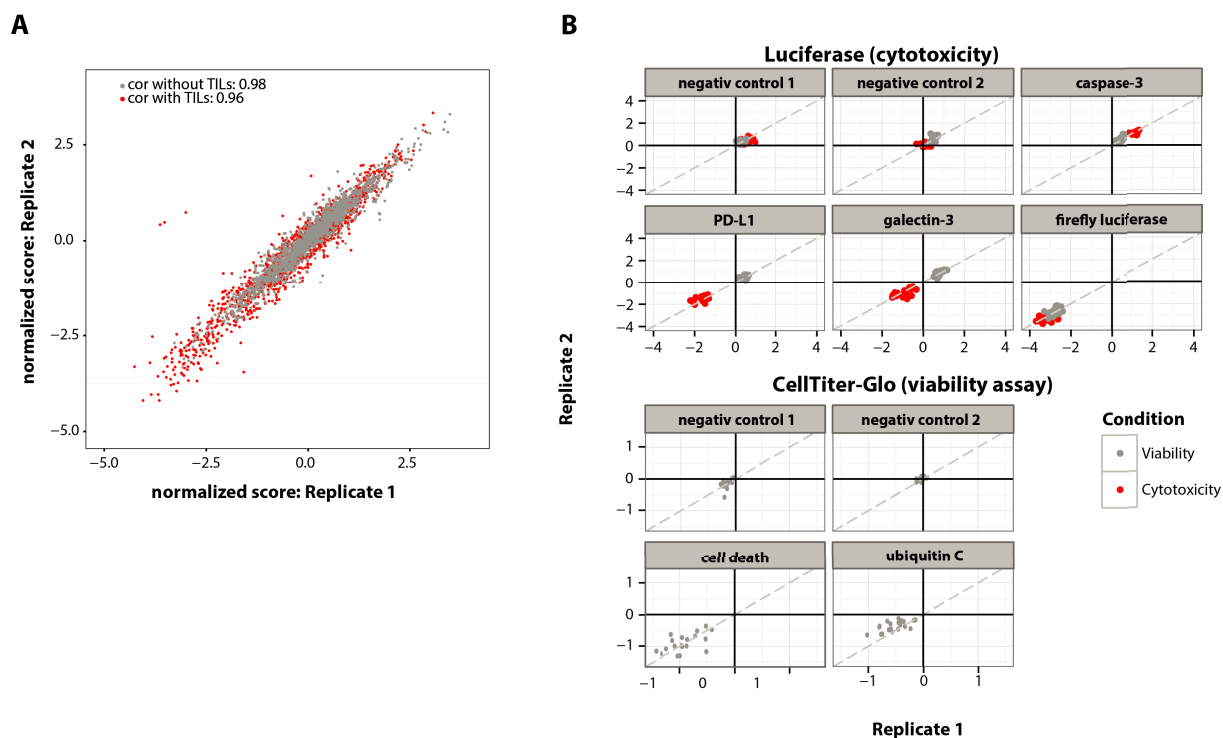


Figure 14: Overall screening and control performance. Graphical representation of normalized Z-scores for gene knockdown effects on cytotoxicity or viability (**A** and **B**). Raw residual luciferase intensities were transformed logarithmically and per-plate normalization was performed by mean normalization and Z-scoring (cellHTS2 for Bioconductor). Z-scores for all samples (**A**) or specific controls (**B**) are shown for the cytotoxicity (red) and the viability (grey) set. The CellTiter-Glo viability assay was analyzed accordingly. The Pearson's correlation coefficients for cytotoxicity and viability were calculated using the "cor" function of R on the library samples only (without controls).

5.3 The high-throughput RNAi screens reveals novel immune checkpoint candidates in melanoma

The results of the high-throughput RNAi screen are depicted in **Figure 15**. Scores for cytotoxicity and viability were quantile normalized before comparison. Finally, local regression was used to calculate LOESS-normalized cytotoxicity scores. These scores are a measurement of the cytotoxicity versus the viability impact of a gene knockdown. So-called "quadrant plots" (**Figure 15A**) represent the impact on immune-susceptibility (y-axis) and cell viability (x-axis). As expected the negative control siRNAs did not affect cytotoxicity or viability, whereas knockdown of PD-L1 and galectin-3 increased cytotoxicity but did not affect viability. Caspase-3 knockdown decreased cytotoxicity but not viability. Interestingly, genes marked as having an impact on gene viability by the CTG screening do not necessarily show a high score for viability in the luciferase screening.

The performances of the controls were used to calculate thresholds for hit-calling. The calculated LOESS scores of the immune checkpoint controls PD-L1 and galectin-3 were used as thresholds for potential immune inhibitors. Only genes having a higher LOESS score than

galectin-3 were considered as potential immune checkpoints. Ranking of the genes (**Figure 15B**) from lowest to highest - according to LOESS score - revealed several genes whose knockdown either decreased killing more than a knockdown of caspase-3 (negative LOESS score; potential immune activators) or increased TIL-mediated tumor lysis more than knockdown of galectin-3 or PD-L1 (high LOESS score; potential immune inhibitors). On the other hand, the majority of genes did not affect TIL-mediated tumor lysis (plateau between LOESS scores ± 1). Knockdown of genes which had a Z score higher than ubiquitin C in the CTG screen were excluded from hit calling. Also, knockdowns which were beneficial for tumor cell growth (Z score < -1.5 in viability or CTG) were excluded from hit calling. This also excludes genes which have a high LOESS score because of positive effects on tumor growth but no major effect on TIL-mediated lysis. The exact thresholding parameters can be derived from the R script (**Supplementary R code**). The hit-calling identified 48 candidate genes with immunomodulatory function (GPCR/kinase library). In total (both screenings), 75 (around 2.6%) out of 2888 genes were classified as candidates.

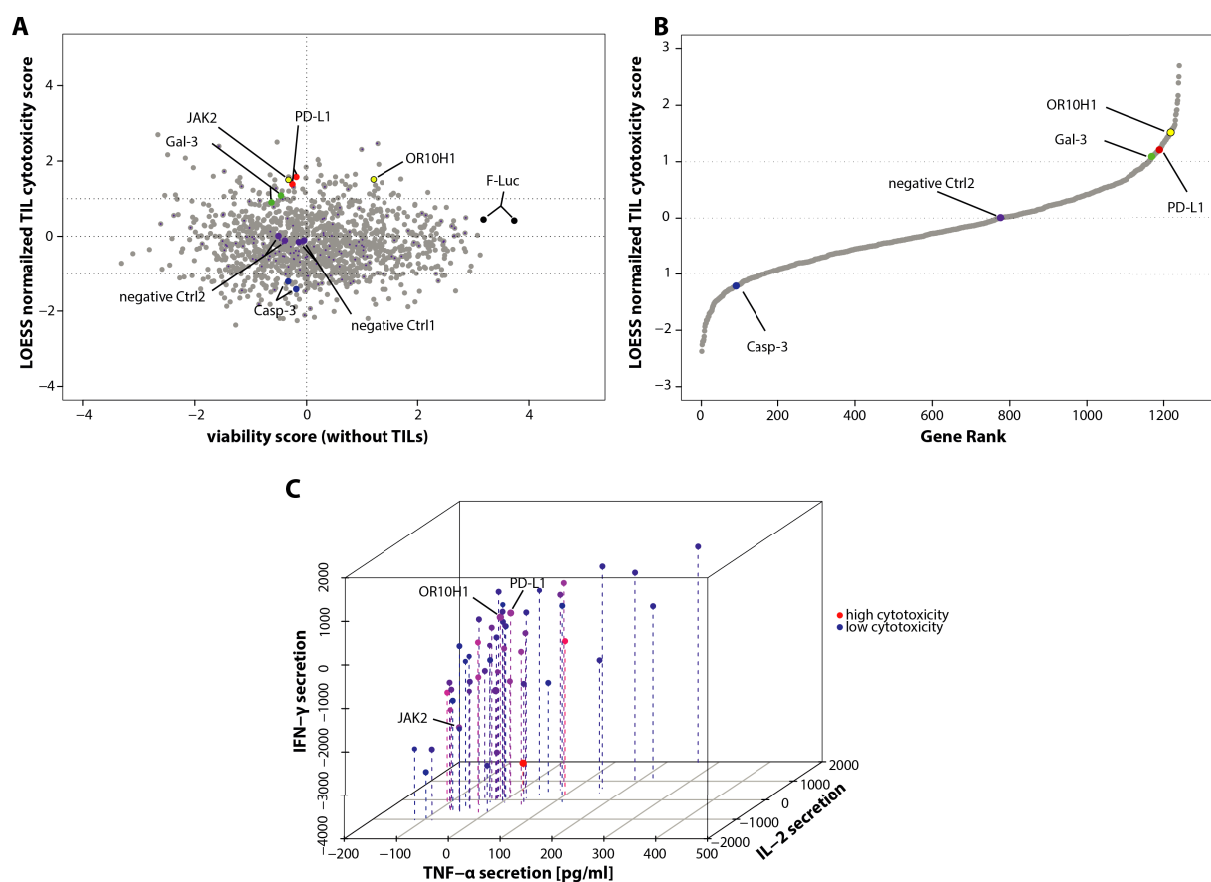


Figure 15: Results from the high-throughput RNAi screening. Graphical summary of screening results in quadrant plot format (**A**) or ranked according to LOESS cytotoxicity score (**B**). Normalized cytotoxicity Z scores (see Figure 14) were fitted to viability Z scores by local regression and the resulting LOESS scores were plotted against the viability Z scores (**A**). Representatives for negative controls 1 (light purple), 2 (dark purple), the immune activator control caspase-3 (blue), the

immune checkpoint controls PD-L1 (red) and galectin-3 (green) and the transfection control firefly luciferase (black) are labeled. Genes excluded by the CTG screen because of decreased cell viability are marked with a small purple dot. **B.** Genes were ordered according to LOESS scores. **C.** Graphical summary of the secondary screening enriched for candidates from the primary screening. The screening was run in duplicates. Luciferase values were normalized to the negative control and differential scores were calculated and ranked (cytotoxicity score – viability score). The differential cytotoxicity is indicated by colors from weak (blue) to strong (red). Cytokine secretion (TNF, IL-2 and IFN- γ) was measured after 20 h co-culture and the cytokine levels from knockdowns in tumors only were subtracted. The difference in cytokine secretion compared to the negative control are plotted on the x-, y-, and z-axis.

Notably, several confirmed immune checkpoints were detected as strong candidates in the screening. The C-C motif chemokine receptor 9 (CCR9) has been shown to desensitize MCF-7 breast cancer cells towards antigen-specific lysis by inhibiting T cell function [240]. Janus kinase 2 (JAK2) mediates target cell resistance to NK cell-mediated killing in melanoma as identified by RNAi screening [237]. This effect might be mediated by JAK-dependent upregulation of PD-L1 in response to IFN- γ [238, 249]. A similar mode of action was described for the strongest candidate protein kinase D isoform 2 (PRKD2) [250]. The rediscovery of such validated immune checkpoints in combination with good immune checkpoint control performance advocate the robustness and sensitivity of our screening approach.

An important determinant for potential immune checkpoints is the discrimination between genes desensitizing tumor cells towards TIL-mediated lysis and genes facilitating an inhibitory signal to TILs. The aim of this thesis was the discovery of novel immune checkpoints which protect melanoma cells from immune cell destruction by inhibiting TIL activity. To streamline the high-throughput immune checkpoint discovery platform, a secondary RNAi screening focusing on both TIL-mediated lysis and cytokine secretion was developed. In general, the screening was performed analogously to the primary screening but with a final siRNA concentration of 50 nM. Melanoma cells were reverse-transfected with a library of 48 genes identified as candidates in the primary GPCR/kinase screening. As the genes were enriched for their potential immune checkpoint function, per-plate normalization must be performed according to the negative control. Type I cytokine concentrations (TNF, IL-2 and IFN- γ) were measured by Luminex after 20 h co-culture in the cytotoxicity and the viability set. Notably, there was no cytokine secretion by the tumor cells, independent of any gene knockdown. Analysis was done using a modified script for cellHTS2 and R. Cytotoxicity and cytokine secretion compared to the negative control are shown in **Figure 15C**. Many of the candidate genes (~75%) improved TIL-mediated lysis compared to the negative control. A rank based

comparison of the candidate performance in the primary and secondary screening is shown in **Table 6**.

Table 6: Ranked hit-list of potential immune checkpoints in the primary and secondary screening

Gene	Ranking screening		Gene	Ranking screening		Gene	Ranking screening	
	Primary	Secondary		Primary	Secondary		Primary	Secondary
PRKD2	1	1	PSKH1	23	17	GPR55	7	33
CAMK1	3	2	PRKCG	15	18	TSSK1B	43	34
PMVK	21	3	PRKCB	38	19	DGKQ	47	35
OR3A2	27	4	PRKAG3	30	20	GPR15	31	36
OR10H1	16	5	NPY	10	21	GPR92	6	37
AMHR2	25	6	GPR30	45	22	GPRC5B	9	38
IPPK	40	7	F2R	11	23	MLN	24	39
RGS14	29	8	CDK5R2	13	24	GPR8	28	40
JAK2	17	9	AK3	39	25	ACVR1	37	41
TK1	33	10	GPR97	8	26	HCK	12	42
TTBK2	36	11	AGK	26	27	PTHR1	32	43
CDKN2B	19	12	PRPF4B	4	28	CCL25	18	44
CDK9	34	13	PTPN5	48	29	PRB4	22	45
CCR9	5	14	CDKN1C	42	30	TAS2R3	2	46
SIK3	14	15	GPR41	44	31	EDG1	41	47
CSF1R	46	16	GPR7	35	32	GPR21	20	48

Candidates are ranked according to the LOESS cytotoxicity score in the primary screening and according to the differential score (cytotoxicity score – viability score) in the secondary screening. Candidate genes with no positive effect on TIL-mediated cytotoxicity in the secondary screening are marked in red.

Several knockdowns increased the secretion of one or multiple cytokines. Interestingly, as for the primary screening the knockdown of PRKD2 showed the strongest increase in TIL-mediated lysis of M579-A2-luc but did not improve the secretion of type I cytokines. The same effect was observed for JAK2 suggesting that these kinases are important for the resistance of M579-A2-luc to TIL-mediated lysis but did not affect the functionality of the TILs per se. Overall, the secondary screening can be used as a first step of validation and a way to distinguish between tumor susceptibility genes and genes affecting TIL activation.

5.4 The immunomodulatory repertoire of solid tumors overlaps

So far, breast cancer (performed by Nisit Khandelwal), melanoma, pancreatic ductal adenocarcinoma (performed by Antonio Sorrentino) and multiple myeloma (performed by Valentina Volpin) were screened for novel immune checkpoints utilizing our high-throughput RNAi screening approach (breast cancer, PDAC and multiple myeloma screenings are not described in this thesis). Therefore, analysis of shared or distinct repertoires of potential immune checkpoints might unravel classes of genes with a strong impact on TIL-mediated tumor lysis or underlying modes of action. Due to big differences in data variance, performance and hit-calling any comparative analysis must be approached with caution. In **Figure 16A** the overlap of candidate genes from different tumor entities (excluding breast cancer) is shown. The tumor-specific immune checkpoint repertoire does not overlap greatly between different tumor entities. Only one gene – regulator of G-protein signaling 14 (RGS14) – was a common hit in all three screenings.

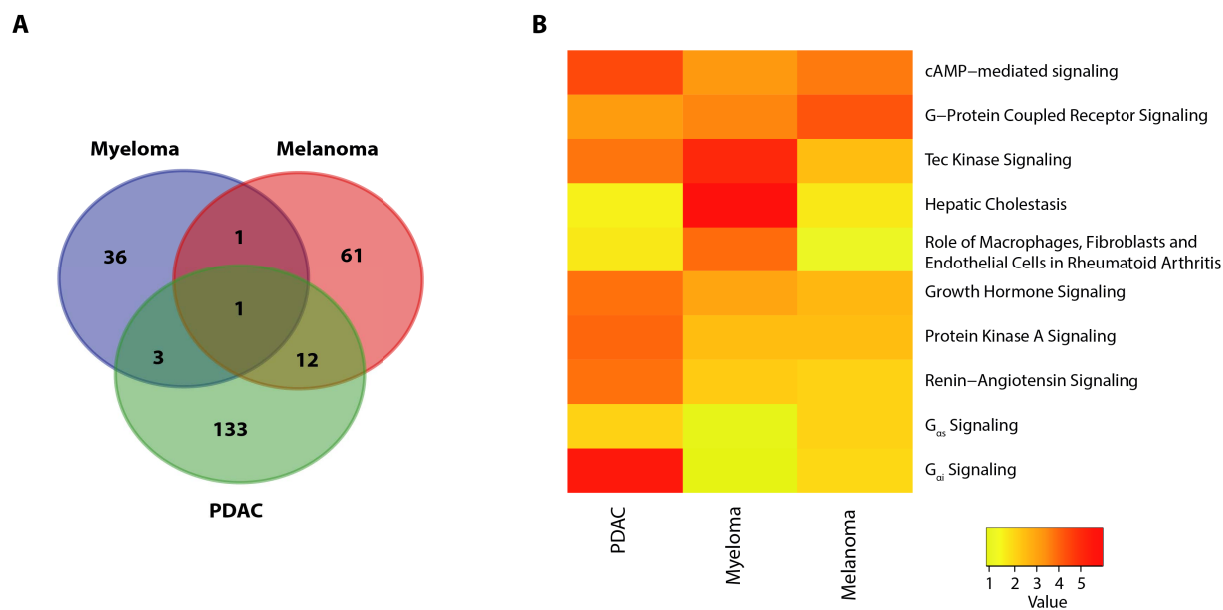


Figure 16: Immune checkpoint candidate genes are enriched in the (G_{αs})/ cAMP/ PKA pathway in solid tumors. A. Venn diagram representation of the overlap in candidate genes (after primary screening) from three different tumor entities. Breast cancer was excluded due to the difference in the used library. Only exact matches in gene names (not family members) were counted as overlapping. **B.** Heat map representing the top 10 pathways without clustering and normalization. Enrichment analysis were run on each tumor entity hit-list using ingenuity pathway analysis with standard parameters (IPA). IPA does not normalize for the background (all genes in the library). Comparative analysis was run using the melanoma, PDAC and multiple myeloma core analysis.

The solid tumors melanoma and PDAC shared 13 candidate genes (~17% of all melanoma hits), whereas they only share 2 or 4 genes with multiple myeloma, respectively. Different gene family members could exert the same immune inhibitory function in different tumor entities. Calcium/calmodulin-dependent protein kinase type 1 alpha (CAMK1) was a strong hit in melanoma, whereas Calcium/calmodulin-dependent protein kinase type 1 delta (CAMK1D) played a major role in multiple myeloma. Interestingly, different GPCRs (varying between tumor entities) from the same family (e.g., olfactory receptors) were hits in all screenings. In order to find common immune inhibitory pathways in the different tumor entities, pathway enrichment analysis was performed on the combined candidate list (**Figure 16B**). The library used for the screenings is enriched for GPCRs, kinases and surface-associated genes. Thus, enrichment analysis was prone to find pathways associated with the aforementioned gene classes. As expected, GPCR signaling was found to be a major pathway among the candidate genes. The enriched pathways hinted towards an involvement of the G-protein alpha S (G_{αs})/cAMP/protein kinase alpha (PKA) pathway in the inhibition of TIL-mediated tumor lysis, particular in melanoma. The opposing G-protein alpha I (G_{αi}) pathway was particularly enriched in PDAC. The analysis of the tumor-specific candidate repertoire and the potential

underlying mechanisms suggest a major role of GPCRs and their associated pathways (e.g., Gαs/cAMP/ PKA) in the inhibition of TIL-mediated lysis in solid tumors.

5.5 OR10H1 inhibits TIL-mediated lysis of solid tumors

Olfactory receptor family 10 subfamily H member 1 (OR10H1) is a member of the olfactory GPCR gene family. As for most olfactory receptors, its exact function is unknown. Until recently, functional descriptions of olfactory receptors were limited to olfactory neurons but roles in other tissues and functions are emerging. Out of the two olfactory receptors candidates (OR3A2 and OR10H1) OR10H1 was discovered (PDAC RNAi screen, Antonio Sorrentino) to play a major role in TIL-mediated lysis of PDAC as well [data not shown].

5.5.1 OR10H1 is expressed in solid tumors

Expression analysis is a major obstacle in the description of olfactory receptor functionality outside the olfactory system. Due to the low abundance of olfactory receptor mRNA, widely used gene expression detection methods (e.g., RNA-Sequencing) fail to give an insight in the expression profile of olfactory receptors. We used a specialized RT-PCR protocol for the detection of low abundant olfactory receptor mRNA [243]. Olfactory receptors are single exon genes preventing the use of exon-spanning primers for expression analysis. Thus, it is important to check for potential DNA contamination in the mRNA using controls without reverse transcriptase (-RT). The closest gene family member to OR10H1 is OR10H5 with 93.6% sequence similarity. Due to the sequence similarities between OR10H1 and OR10H5 it is extremely difficult to generate specific primers, siRNAs or shRNA to distinguish between the paralogues. The used primers show a preference for OR10H1 or OR10H5 (one mismatch in the forward and the reverse primer each) and are indicated accordingly. Expression of OR10H1/5 in different tumor cell lines was validated by traditional PCR (**Figure 17**). The bands were measured at the expected sizes for OR10H1 (~720 bp) and OR10H5 (~240 bp). Interestingly, OR10H1 was expressed in the solid tumors melanoma (M579-A2), PDAC (PANC-1) and colorectal cancer (SW480) but not in the hematological multiple myeloma (KMM-1). This expression pattern is in accordance with the results of the siRNA screenings. OR10H1 was found to be a candidate in multiple melanoma and PDAC but not in multiple myeloma. No bands were visible in the -RT controls.

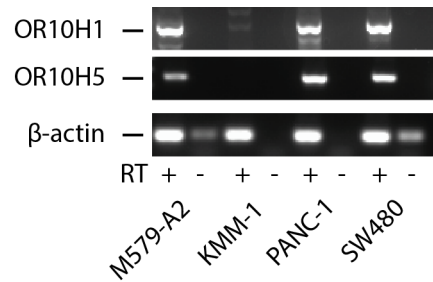


Figure 17: OR10H1/5 expression in solid tumors. OR10H1 and OR10H5 expression was measured in different tumor entities (melanoma, multiple myeloma, PDAC and colorectal cancer) by RT-PCR. Beta-actin served as a house keeping control. DNA contamination was checked using controls without reverse transcriptase (indicated by RT). PCR was run according to the protocol for low abundance gene expression (40 cycles). Expected transcript sizes are ~720 bp for OR10H1 primers and ~240 bp for OR10H5 primers.

5.5.2 OR10H1 prevents TIL-mediated lysis of melanoma *in vitro*

Single siRNA sequences out of the siRNA pools (derived from the screening library) can target unrelated genes (off-target effect) producing false-positive candidates from the screening [251, 252]. Consequently, the siRNA pool was “deconvoluted” and a correlation between candidate knockdown and the impact on TIL-mediated melanoma lysis was tested (**Figure 18**). Knockdown efficacy was tested by checking the OR10H1 mRNA levels (as before) and the impact on TIL-mediated melanoma lysis was validated with the luciferase-based killing assay. All siRNA sequences induced a knockdown of OR10H1 mRNA as validated by two different primer pairs. The individual siRNAs 1 and 3 and the pooled siRNA induced the strongest knockdown, whereas siRNA 2 and 4 mediated knockdowns were slightly weaker (**Figure 18A**). These knockdowns correlate with the respective impact on tumor killing. All siRNA-mediated knockdowns of OR10H1 had a significant impact on TIL412-mediated killing of M579-A2-luc as measured by residual luciferase intensity (**Figure 18B**). Some siRNAs (OR10H1 siRNA 1 and OR10H1 siRNA pool) increased TIL-mediated killing more (~70% over control siRNA) than the knockdown of PD-L1 (~60% over control siRNA). Only one siRNA (OR10H1 siRNA 3) showed an impact on cell viability as measured by residual luciferase intensity (**Figure 18C**). Therefore, all siRNAs induced a knockdown of the target combined with a functional phenotype suggesting a direct participation of OR10H1 in immune cell inhibition instead of an

off-target effect. The individual OR10H1 siRNA 1 showed the strongest effect in knockdown and phenotype and was used as a model siRNA for following studies.

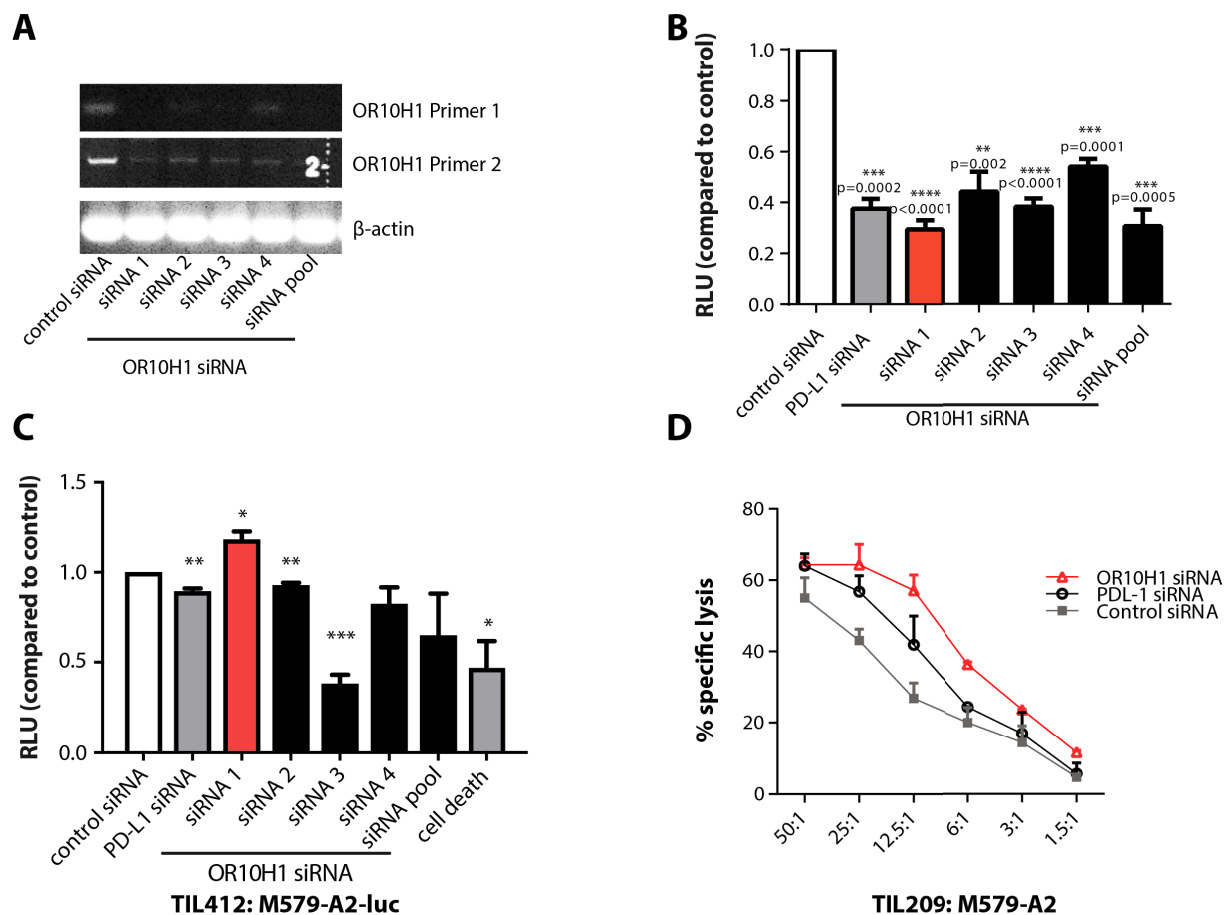


Figure 18: OR10H1 knockdown increases TIL-mediated lysis of melanoma without affecting tumor cell viability. A. Knockdown efficacy of deconvoluted siRNA sequences on OR10H1 mRNA levels was measured by RT-PCR after 72 h of transfection. Two different primer pairs were used to validate OR10H1 mRNA abundance. Beta-actin served as a house keeping control. B, D. M579-A2 killing assays with different TIL-cultures. B, C. M579-A2-luc cells were reverse-transfected with individual (s1-s4), pooled OR10H1 or control siRNAs (PD-L1 as positive immune checkpoint, cell death as positive viability and scrambled siRNA as negative control) and co-cultured with TIL412 (B, cytotoxicity, effector-to-target ratio 5:1) or CLM (C, viability) for 20 h. TIL-mediated lysis or viability impact of target knockdown was measured by luciferase assay (cumulative data, n=3). D. Representative chromium-release assay showing specific lysis of M579-A2 by TIL209 at different E:T ratios after reverse-transfection with OR10H1 siRNA 1 (Δ), positive control PD-L1 siRNA (\circ) or control siRNA (\bullet). Error bars denote \pm SEM, and statistical significance was calculated using unpaired, two-tailed Student's t-test with * $p \leq 0.05$; ** $p \leq 0.01$; *** $p \leq 0.001$; **** $p \leq 0.0001$. B-D. Experiments were performed by Christina Hartl (Group Prof Beckhove, DKFZ) under my supervision.

The lysis of M579-A2 by an independent melanoma T cell source (TIL209) was validated by chromium-release assay to exclude methodology- or TIL-restricted effects of OR10H1 knockdown with siRNA 1 (Figure 18D). Furthermore, this method excludes any prior proliferation/viability effects of the siRNA by using the same cell numbers for all co-cultures. As assumed, knockdown of OR10H1 increased TIL209-mediated lysis of M579-A2. This effect

is clearly visible at effector-to-target ratios from 50:1 to 6:1. The induction of TIL-mediated cytotoxicity surpassed the impact of PD-L1 knockdown after a co-culture period of 4 hours.

5.5.3 OR10H1-mediated inhibition of TIL cytotoxicity against melanoma is depending on HLA-A2/TCR interactions

TIL412 are a mixture of CD4⁺ and CD8⁺ T cells, whereas TIL209 consist almost exclusively of CD8⁺ TCs (see Figure 2). Therefore, we wanted to know whether the OR10H1-dependent inhibition of TIL-mediated tumor lysis is dependent on the interaction between CD8⁺ cytotoxic T cells and the tumor cell and if it is relying on TCR (T cell side) and antigen-MHC I (tumor side) binding. HLA-A2 restriction of OR10H1-mediated TIL412 inhibition was evaluated using HLA-A2⁺ M579-A2 and HLA-A2⁻ M579 (Figure 19). As expected from the secondary screening, TIL412 secreted more IFN- γ when co-cultured with OR10H1⁻ M579-A2 compared to OR10H1⁺ M579-A2 cells for 6 hours (trend, not significant). The concentration of IFN- γ was 18% higher if OR10H1 was knocked down on the M579-A2 (Figure 19A). M579 do not express HLA-A2 and thus cannot be recognized by HLA-A2-restricted TIL412 (see Figure 11). The knockdown of OR10H1 in M579 did not lead to a measurable increase in IFN- γ secretion suggesting a dependence on TCR-antigen/HLA-A2 interactions irrespective of the presence of OR10H1. M579-A2 were generated by lentiviral transduction to stably express HLA-A2. The random insertion of the HLA-A2 plasmid can lead to altered expression of adjacent genes. In theory, the immune inhibitory effect of OR10H1 could be HLA-A2-independent but depending on the random insertion of HLA-A2 in the genome of M579-A2 leading to the differential expression of immune-related genes. We ruled out that possibility by using a system in which the TC-mediated lysis of target cells is depending on the addition of flu peptide. This system was established by Ayse Nur Menevse (AG Beckhove, RCI). In short, TCs specific for flu-derived peptides presented by HLA-A2 are generated from donors, by means of antigen specific expansion, followed by sorting of the flu specific cells and a standard REP (rapid expansion protocol) to obtain the necessary cell numbers and purity. Target cells can be pulsed with the according flu-derived peptide before co-culture with TCs. In this setup, the presence or absence of the peptide ensures the interaction of the TCR and HLA-A2. M579-A2-luc melanoma were pulsed with flu-derived peptide in different concentrations and co-cultured with flu-specific T cells (Figure 19B) in different effector-to-target (E:T) ratios. These TCs are enriched for flu-specific CD8⁺ cytotoxic TCs [data not shown]. The addition of different concentrations of peptide to the M579-A2-luc without the presence of TCs did not have any effect on cell viability

[data not shown]. The 20 h co-culture of M579-A2-luc and TCs in low E:T ratios in the absence of TCR/HLA-A2 interaction (no peptide added) induced tumor cells proliferation. The presence of TCs increased cell proliferation in M579-A2-luc cells by 18% (2:1 E:T ratio) or ~30% (1:1 E:T ratio) in a HLA-A2-independent manner. This effect was OR10H1-knockdown independent. In the setup with the lowest effector-to-target ratio (1:1) the addition of 0.01 – 1 µg/ml flu-derived peptide increased the proliferation by up to 70% suggesting an additional HLA-A2-dependent induction of proliferation. In the co-culture with peptide-pulsed OR10H1⁻ M579-A2-luc the TC-mediated tumor lysis counteracts the induction of proliferation. The efficacy of the TC-mediated tumor lysis correlated with increasing concentration of flu peptides. At a higher effector-to-target ratio (2:1) the activation of TCs (flu peptide present) resulted in substantially higher lysis of OR10H1⁻ M579-A2-luc (**Figure 19B**, right). The knockdown of OR10H1 strongly increased TC-mediated tumor lysis depending on the peptide concentration. Without peptide, no tumor lysis was observed. With 0.01 µg/ml flu-derived peptide 50% of OR10H1⁻ M579-A2-luc cells were lysed, whereas the highest concentration (1 µg/ml) led to a kill of 75%, indicating that the increase in TC-mediated tumor lysis by OR10H1 knockdown is indeed HLA-A2 dependent.

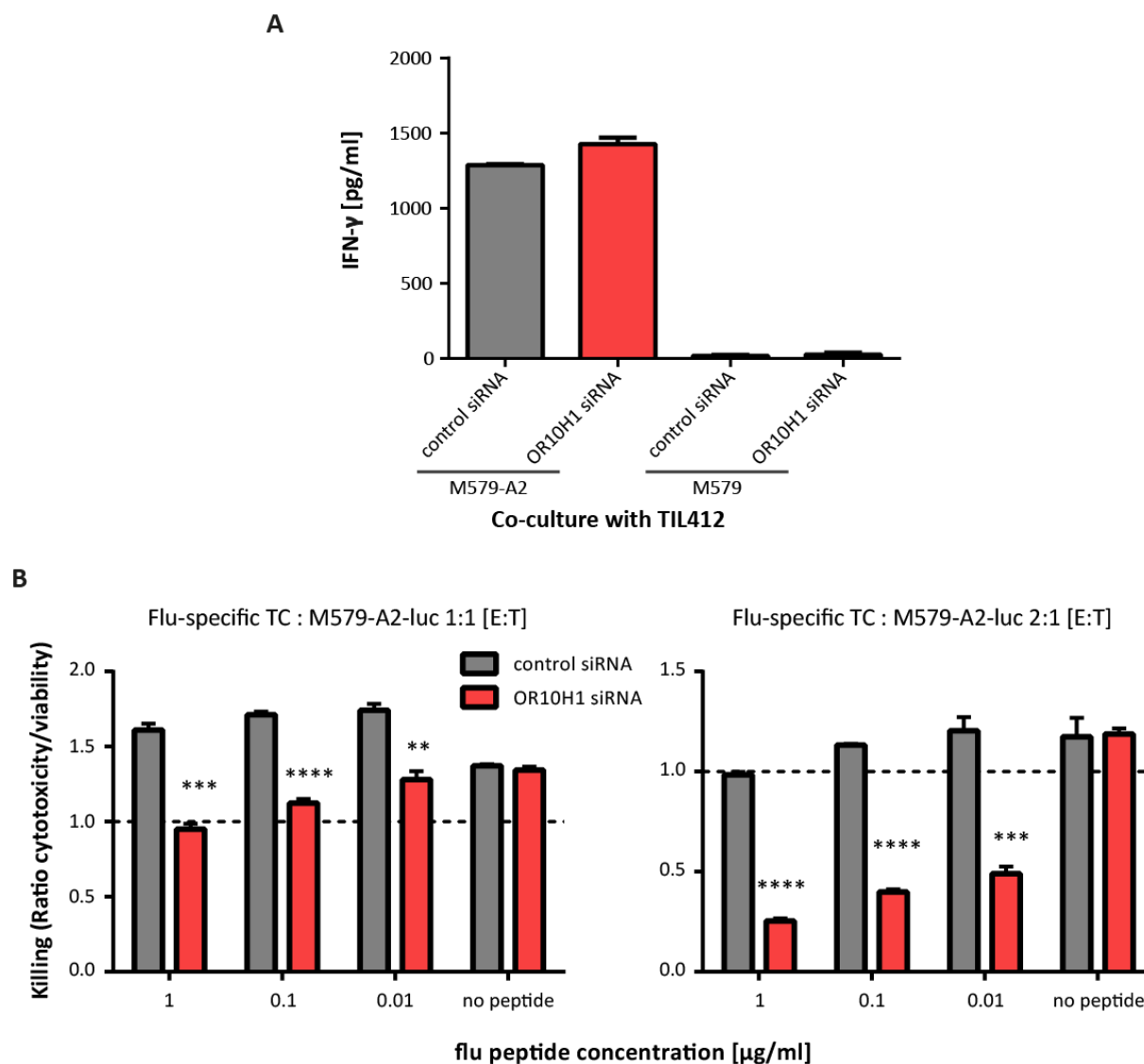


Figure 19: Increase in TIL-mediated lysis of melanoma by OR10H1 knockdown is HLA-A2-restricted. **A, B.** Representative cytokine secretion (**A**) and killing assays (**B**) with HLA-A2⁻ M579 (**A**) and HLA-A2⁺ M579-A2-luc (**A, B**) cells. M579 and M579-A2-luc cells were reverse-transfected as before. **A** Cells were co-cultured with TIL412 (5:1 E:T) for 6 h after transfection and IFN- γ levels were measured by ELISA. **B.** Cells were pulsed with different concentrations of flu-derived peptides for 1 hour before co-culture with flu-specific T cells or CLM (viability) for 20 h. TC-mediated lysis or viability impact of target knockdown was measured by luciferase assay. Flu-specific T cells and peptides were generated by Ayse Nur Menevse (RCI, Regensburg) and prepared in parallel to TILs. All experiments were performed in triplicates (means are shown) and are representative of at least three independent experiments. Error bars denote \pm SEM, and statistical significance was calculated using unpaired, two-tailed Student's t-test with * $p \leq 0.05$; ** $p \leq 0.01$; *** $p \leq 0.001$; **** $p \leq 0.0001$. **B** Experiments were performed in collaboration with Ayse Nur Menevse (AG Beckhove, RCI Regensburg).

5.5.4 OR10H1 inhibits TIL-mediated lysis of PDAC and CRC

As mentioned, OR10H1 was discovered as an immune checkpoint candidate in melanoma and PDAC. Furthermore, it was found to be expressed in several solid tumors (melanoma, PDAC and CRC) suggesting an immune inhibitory function in the respective diseases. We validated the impact of OR10H1 knockdown on TIL#1-mediated lysis of luciferase-positive PANC-1 (PDAC) and SW480 (CRC) cells (**Figure 20**). The generation of PDAC-derived TIL cultures and the co-culture setup with reverse-transfected PANC-1 was established by Antonio Sorrentino (RCI, Regensburg) and is not further discussed in this thesis. TIL#1 are a mixture of CD4⁺ and CD8⁺ TCs which can recognize and kill PANC-1 and SW480 cells in a HLA-A2-dependent manner. As for melanoma-derived TILs, TIL#1 contain a combination of highly exhausted effector and central memory T cells. They express PD-1 and TIM-3 and PANC-1 express the immune checkpoints PD-L1 and CCR9. We deconvoluted the OR10H1 siRNA pool and validated the impact of each siRNA sequence on TIL#1-mediated lysis of PANC-1 in the luciferase assay (**Figure 20A**).

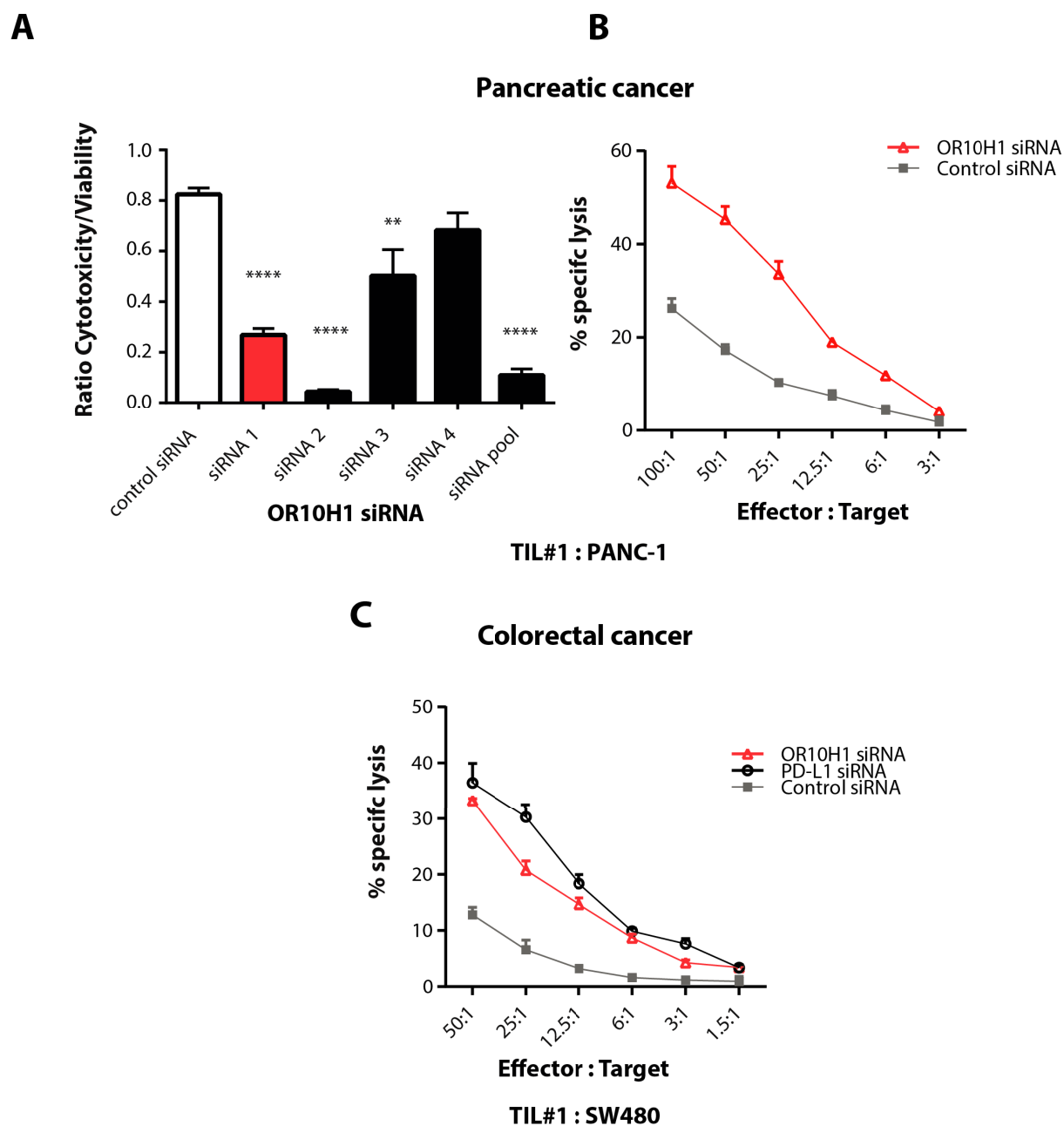


Figure 20: OR10H1 abrogation induces TIL-mediated lysis of pancreatic adenocarcinoma and colorectal cancer cell lines by patient-derived TILs. **A, B** Cytotoxicity assays with PANC-1 tumor cells and PDAC-derived TIL#1 after the knockdown of OR10H1. PANC-1 were reverse-transfected with single OR10H1 siRNA sequences or the according pool for 72 h before co-culture with TIL#1 for 20 (**A**) or 4 h (**B**). **A.** Luciferase assay with deconvoluted siRNA sequences. PANC-1 were co-cultured with TIL#1 in a 50:1 E:T ratio (cytotoxicity) or cultured with CLM only (viability). The TIL-mediated killing of PANC-1 cells is represented as the ratio between cytotoxicity and viability normalized for any potential viability or proliferation impact of gene knockdown. Scrambled siRNA and PD-L1 serve as controls. **B.** Chromium release assay with OR10H1-positive (•) or negative (Δ) PANC-1 cells and TIL#1 in different effector-to-target ratios (4 h). **C.** Chromium release assay run in analog to **B** with SW480 as target cells including PD-L1 knockdown (○). Experiments were performed by Antonio Sorrentino (RCI, Regensburg). All experiments were performed in triplicates (means are shown) and are representative of at least two independent experiments. Error bars denote \pm SEM, and statistical significance was calculated using unpaired, two-tailed Student's t-test with * $p \leq 0.05$; ** $p \leq 0.01$; *** $p \leq 0.001$; **** $p \leq 0.0001$.

Three out of four siRNA sequences and the siRNA pool show a significant induction of killing compared to the negative control. Without OR10H1 knockdown only 20% of tumor cells are killed after 20 h co-culture with TIL#1, whereas OR10H1 knockdown with siRNA sequence 2 induced killing of around 90%. Sequences 1, 3 and the pool induced killing of around 70, 50 and 85% of the tumor cells, respectively. Sequence 4 did not increase killing compared to the negative control. Knockdown of the known immune checkpoints PD-L1 and CCR9 increased the killing of PANC-1 to 74 and 69%, respectively. Knockdown of OR10H1 (siRNA sequence 1) was compared to control siRNA in a chromium release assay with different effector to target ratios (**Figure 20B**). After 4 h of co-culture with TIL#1 at a 100:1 ratio only 30% of wild type PANC-1 were lysed. This lysis was increased to around 55% in OR10H1⁻ PANC-1. The knockdown of OR10H1 strongly increased TIL#1-mediated lysis of PANC1 over the complete effector-to-target ratio range (except for the 3:1 ratio). Interestingly, the knockdown of PD-L1 did not increase TIL-mediated lysis of PANC-1 in the 4 h chromium release assay [data not shown]. As mentioned, TIL#1 can recognize and kill the CRC cell line SW480 in a HLA-A2-dependent manner. Therefore, we optimized the transfection parameters for this luciferase-negative cell line and validated the impact of OR10H1 knockdown by chromium release assay (**Figure 20C**). SW480 transfected with the negative control siRNA only showed weak lysis by TIL#1. Knockdown of OR10H1 however increased TIL-mediated lysis almost as efficiently as the knockdown of PD-L1.

Taken together these experiments indicated that OR10H1 acts as a potential immune checkpoint in several solid tumors by impeding TIL-mediated lysis of tumor cells thus underlining its appeal as a target for cancer immunotherapy.

5.6 OR10H1 inhibition augments TIL-mediated anti-tumor responses after adoptive T cell transfer *in vivo*

After validating the role of OR10H1 as an inhibitor of TIL-mediated tumor lysis in melanoma and other solid tumors *in vitro* we aimed to evaluate its immunosuppressive function *in vivo*. We used the immunodeficient NOD.Cg-Prkdc^{scid} Il2rgt^{m1Wjl}/SzJ (NSG) mouse strain for xenotransplantation of M579-A2 in combination with adoptive T cell transfer (TIL412).

5.6.1 Generation of stable OR10H1 knockdown cell lines

A stable M579-A2 OR10H1 deficient cell line was required for the *in vivo* analysis of the OR10H1 functionality. Therefore, we generated stable knockdown cell lines using lentiviral particles with OR10H1-specific shRNAs or control cell lines transduced with lentiviral particles containing non-targeting sequence (NTS) shRNA (all from Sigma Aldrich). All sequences were cloned in the pLKO.1-puro vector. First, we validated the optimal multiplicity of infection (MOI) for this setup by using GFP-coding particles. We tested MOIs ranging from 1 to 10 and found 2 to be the optimal MOI for the transduction of M579-A2 [data not shown]. We tested four different shRNA sequences for their OR10H1 knockdown compared to NTS control. Two out of four sequences showed a strong OR10H1 knockdown with shRNA 4 being the strongest [data not shown]. Before using these cell lines *in vivo*, we compared OR10H1⁺ M579-A2 (NTS) and OR10H1⁻ M579-A2 (shRNA sequence 4) on their proliferation potential and resistance towards TIL412-mediated lysis *in vitro* (**Figure 21**). The effect of stable OR10H1 knockdown on the proliferative capacity in M579 was tested by a WST-1 proliferation assay (**Figure 21A**). Only a minor proliferation advantage (~3% proliferation increase) was measured in OR10H1 knockdown cells compared to control 72 h after seeding suggesting no impact on general cell proliferation. TIL-mediated lysis of OR10H1⁻ M579 (shRNA 4) was strongly increased compared to OR10H1⁺ NTS control cells (**Figure 21B**). These results are comparable with the results obtained by transiently knocking down OR10H1 with siRNAs. Therefore, OR10H1 shRNA 4-transduced M579-A2 and the according NTS control cells were used in the following *in vivo* experiments.

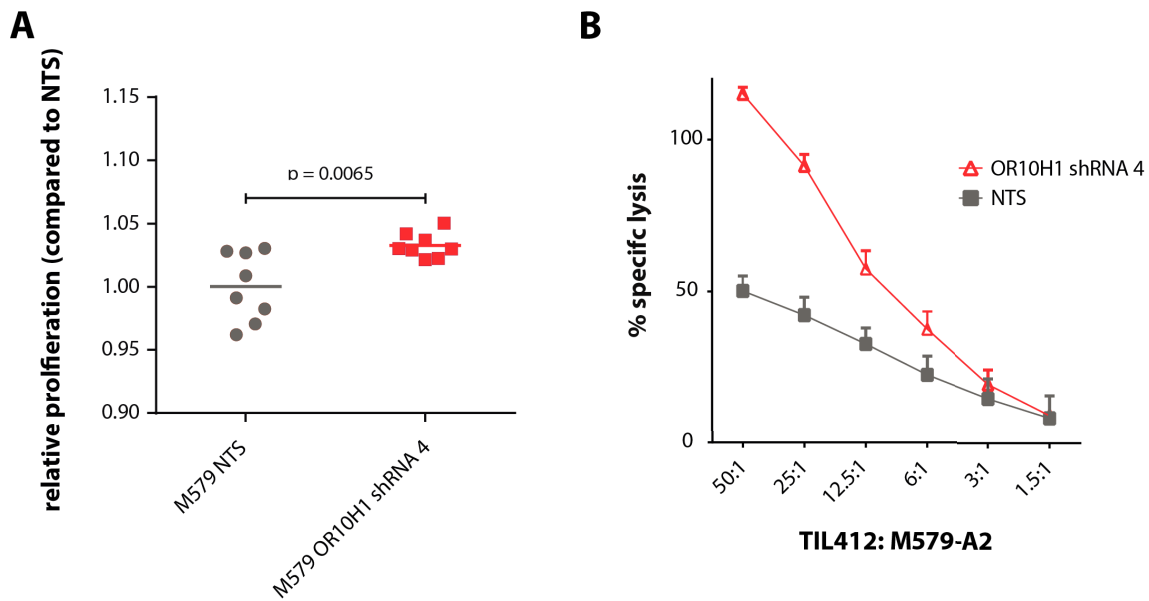


Figure 21: In vitro validation of stable OR10H1 knockdown M579-A2. The stable OR10H1 knockdown cell line (generated with shRNA 4) was evaluated for proliferation (**A**) and susceptibility towards TIL412-mediated lysis (**B**) compared to negative control (NTS shRNA). **A.** Representative cell proliferation analysis comparing mean relative proliferation of M579-A2 OR10H1 shRNA 4 (•) and M579-A2 NTS (○). Cells were grown for 72 h before an additional 4 h incubation with WST-1 at 37 °C. **B.** Representative chromium-release assay depicting mean TIL412-mediated lysis (4 h) of OR10H1 stable knockdown M579-A2 (Δ) or NTS shRNA control M579-A2 (•). Error bars denote ±SEM. Experiments were performed by Christina Hartl (Group Prof Beckhove, DKFZ) under my supervision.

5.6.2 Adoptive T cell transfer reduced tumor growth in OR10H1⁻ melanomas in a xenograft NSG mouse model

In order to evaluate the OR10H1 role as an immune checkpoint *in vivo*, we subcutaneously injected immunodeficient NSG mice with 3×10^5 OR10H1⁺ (control) and OR10H1⁻ M579-A2 in the right and left flank, respectively. One group of mice received adoptive cell transfer with 9×10^6 TIL412 on day 2 and 9 after tumor injection, whereas others did not receive adoptive cell transfer (tumor growth control). Tumor size was measured three times a week (see paragraph 4.7). The experimental and treatment setup is depicted in **Figure 22** (upper panel). Growth measurement of stable OR10H1 knockdown or control tumors without adoptive cell transfer did not reveal a growth disadvantage for OR10H1⁻ melanoma cells *in vivo* (lower right panel). On the contrary, after around 16 days OR10H1⁻ tumors grew slightly (but non-significant) more than the NTS control tumors. Overall, these results are in accordance with the *in vitro* data of transient OR10H1 knockdown. Tumor size differences based on TIL412-mediated anti-tumor response became visible at early time points in the group of mice treated with adoptive cell transfer (day 2 and 9). After the first ACT treatment growth of OR10H1⁻ tumors was delayed compared to the control tumors. The second ACT treatment (day 9) lead to a significant

reduction in tumor size of OR10H1-deficient tumors. This effect was not observable in control tumors, which continued to grow. After day 19 OR10H1⁻ tumors started to grow again but tumor growth kept being delayed compared to the NTS control. Analysis of tumor infiltration by TILs revealed that their survival and therefore their anti-tumor effect is limited in the NSG mouse model [data not shown]. Interestingly, tumor growth curves for ATC-treated or untreated NTS control tumors were fairly similar suggesting a marginal effect of TIL412-mediated anti-tumor responses against OR10H1⁺ melanoma cells *in vivo*. The knockdown of OR10H1 in the tumor on the other side dramatically increased the therapeutic window of adoptive T cell transfer.

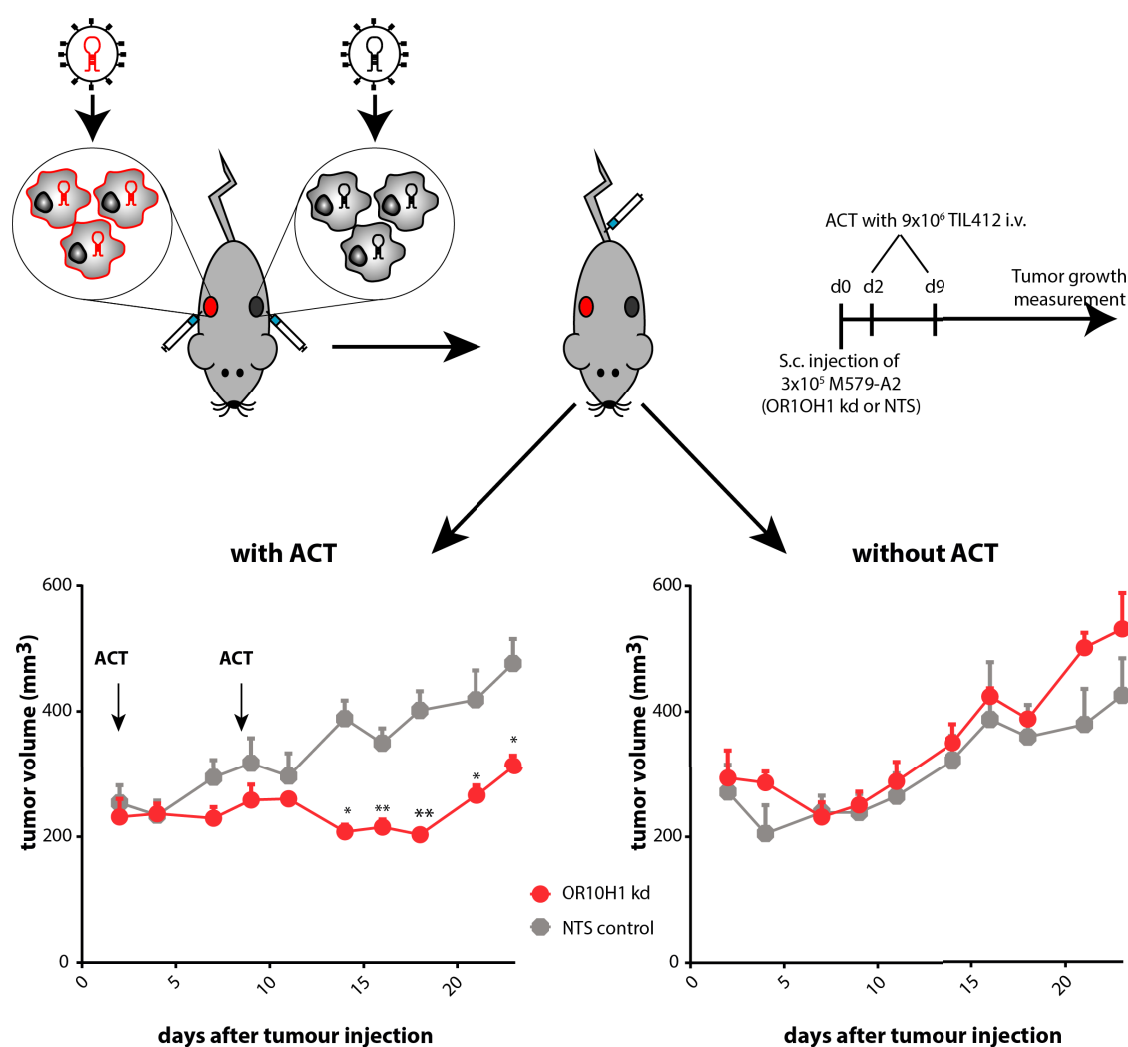


Figure 22: OR10H1 functions as an immune checkpoint in vivo. (upper panel) Experimental layout for in vivo experiments. Mice were s.c. injected with OR10H1⁺ and OR10H1⁻ M579-A2 in the left and right flank on day 0. The treated group (n=6) received adoptive T cell transfer (i.v.) on day 2 and 9. The tumor growth control group (n=4) did not receive any treatment. Tumor growth was measured three times a week for 23 days. (lower panel) Representative tumor growth curves showing mean \pm SEM tumor volumes of OR10H1-negative (i.e. OR10H1 knockdown; kd) or OR10H1-positive (i.e. NTS shRNA control) M579-A2 tumors in ACT-treated mice (lower left panel) or in the growth control group without ACT (lower right panel). The growth curves are representatives of at least two independent in vivo experiments. The values represent mean tumor volume. Statistical difference was calculated using the Mann-Whitney U test.

Taken together, our results indicate that the transient or stable knockdown of OR10H1 improved TIL-mediated killing of tumor cells *in vitro* or *in vivo*, respectively suggesting an important role for OR10H1 in T cell inhibition.

5.7 Tumor-restricted OR10H1 inhibits TIL activity and survival

The goal of this project is the discovery of novel immune checkpoints regulating T cell signaling and their subsequent activity. Some of the strongest candidates from our primary screening (namely PRKD2) seem to regulate TIL-induced apoptosis in melanoma without affecting the T cells directly. OR10H1 inhibits TIL-mediated lysis of melanoma, PDAC and CRC in an HLA-dependent manner. Therefore, we aimed to survey the effects of OR10H1 knockdown (on melanoma) on other determinants of T cell activity besides measurement of tumor lysis. A first hint of an OR10H1 inhibition of T cell activity beyond tumor lysis was found in the secondary screening (see **Figure 15** and **Figure 19**). OR10H1 knockdown increased TIL-mediated lysis and secretion of IFN- γ and IL-2. Following up on this, we tested the impact of OR10H1 knockdown on the secretion of a variety of type I (T-helper-1) and type II (T-helper-2) cytokines (27 measured by Luminex) as well as other markers of T cell activation (**Figure 23**).

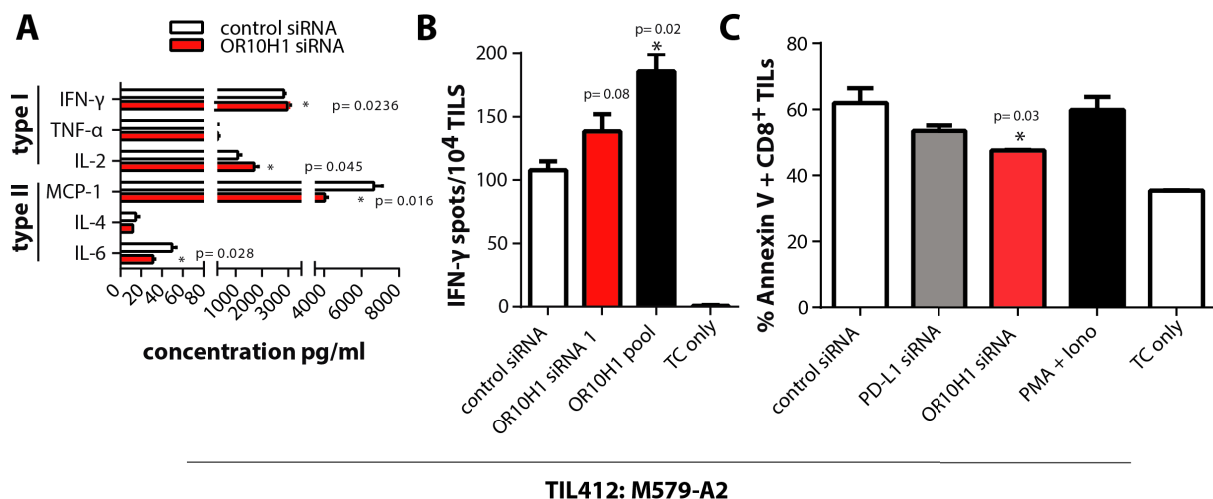


Figure 23: OR10H1 alters T cell cytokine production from anti-tumor type I to pro-tumor type II and induces TIL apoptosis. **A.** Cumulative cytokine secretion data of T helper type I and II cytokines of 20 h co-culture from TIL412 with OR10H1⁺ or OR10H1⁻ M579-A2 (measured by Luminex). **B.** ELISpot assay showing spot numbers of IFN- γ secreting TILs after co-culture with OR10H1 knockdown M579-A2 (or control siRNA). TILs without melanoma encounter were used as a negative control (TC only). **C.** Cumulative data of apoptosis induction (measured by FACS staining for Annexin V+) in CD8⁺ TILs after co-culture (6h) with OR10H1-positive or -negative M579-A2. TILs stimulated with PMA/Iono and unstimulated TILs were used as positive and negative controls, respectively. Gating strategy is shown in Supplementary figure 2. **A** and **C** show cumulative data (mean) from three independent experiments. **B** shows representative data of two independent experiments (mean shown, performed in triplicates). Error bars denote \pm SEM, and statistical significance was calculated using unpaired, two-tailed Student's t-test. (**B**, **C**) Experiments were performed in collaboration with Antonio Sorrentino (Group Prof Beckhove, DKFZ).

Overstimulation of TIL412 with PMA and Ionomycin (PMA/Iono) served as a maximum secretion control for all cytokines [data not shown]. Ten cytokines including IL-7, IL-10, and IL-12 were not secreted during the co-culture of M579-A2 and TIL412 independent of the OR10H1 knockdown. Other cytokines (GM-CSF, IL-13, IL-5, IL-8, MIP-1 α , MIP-1 β , VEGF, PDGF-BB and RANTES) were secreted during the co-culture but did not show any differential secretion upon OR10H1 knockdown.

On the other hand, knockdown of OR10H1 in M579-A2 increased the secretion of the type I cytokines IFN- γ and IL-2 while decreasing the secretion of type II cytokines IL-4, IL-6 and MCP-1 (**Figure 23A**). We validated the small but significant increase in IFN- γ secretion observed during co-culture of TIL412 with OR10H1⁻ M579-A2 (Luminex and ELISA) using ELISpot. This method focuses on the number of cytokine secreting cells rather than the concentration of secreted cytokine. The knockdown of OR10H1 significantly increased the number of IFN- γ -secreting TCs from around 105 to 185 spots/10⁴ TILs (**Figure 23B**) whereas over stimulation with PMA and Ionomycin (PMA/Iono) resulted in ~370 spots/10⁴ TILs [data not shown]. Without any stimulation or co-culture with M579-A2 (TC only) no spots were observed. This implies a need for interactions with tumor cells to trigger T cell IFN- γ secretion. Another way in which OR10H1 could inhibit T cell functionality is the induction of apoptosis. We investigated the effect of the presence or absence of OR10H1 on T cells apoptosis during co-culture with OR10H1-positive or -negative M579-A2 (**Figure 23C**) by measuring binding of Annexin V to phosphatidylserine on the membrane of apoptotic T cells (flow cytometry). The gating strategy for apoptotic CD8⁺ cells is shown in **Supplementary figure 2**. As expected, a high percentage of CD8⁺ TCs (~30%) were Annexin V-positive without an additional stimulation by PMA/Iono or co-culture with target cells. This is in accordance with the high exhaustion status of melanoma-derived TILs. Over-activation (PMA/Iono) of TILs increased the percentage of Annexin V-positive CD8⁺ TCs to around 60%. The same level of apoptosis was induced by co-culture with OR10H1⁺ M579-A2. Knockdown of OR10H1 in M579-A2 resulted in only 47% apoptotic cytotoxic T cells. Thus, knockdown of OR10H1 on tumor cells led to a reduced induction of apoptosis in exhausted T cells during co-culture.

Taken together, these results underline the relevance of OR10H1 as a potential immune checkpoint. OR10H1 did not only prevent TIL-mediated lysis of tumor cells *in vivo* and *in vitro* but reduced the secretion of anti-tumor type I cytokines and increased the secretion of

inhibitory type II cytokines. Furthermore, OR10H1 increased apoptosis induction in exhausted TILs upon co-culture.

5.8 Tumor-restricted OR10H1 induces TIL gene expression associated with negative regulation of T cell activation

After establishing the inhibitory function of OR10H1 on TIL-mediated tumor lysis (*in vitro* and *in vivo*) as well as TIL activity and survival, we aimed to understand the underlying mode of action by dissecting the involved signaling pathways. Changes of genes expressed in TIL412 co-cultured with OR10H1 knockdown M579-A2 (or control siRNA) could give an indication of signaling pathways involved in TIL inhibition.

5.8.1 Separation of TIL412 and M579-A2 after co-culture

An important requirement of pathway and gene expression analysis is the separation of tumor and TILs after co-culture without influencing target cell signaling. Most methods of cell separation use antibodies directed against proteins expressed on the cell surface of one cell type but not on the other. Here, so called melanoma beads – using antibodies binding Melanoma-associated Chondroitin Sulfate Proteoglycan (MCSP) – were used to positively select melanoma cells without affecting T cell signaling. In a first step, melanoma cells were pre-stained with a cell tracker (DDAO-SE) before co-culture (2-10 h) with TILs (10:1 effector-to-target-ratio). After the co-culture the cells were separated by magnetic cell sorting, where the melanoma cells were captured in the magnetized column and the T cells were collected as a negative fraction. Additionally, the remaining (adherent) tumor cells were detached and added to the mixture to simulate extreme conditions in which all tumor cells have to be removed. Flow cytometry was used to verify the purity of enriched T cells after separation (**Figure 24**). Isotype control beads were used as a negative control. By using melanoma beads TILs were enriched to a purity of 99.9% underlining a high specificity of the beads towards melanoma cells. In the case of control isotype beads, 7.4% of the obtained cells were M579-A2 (DDAO-SE positive). The separation process did not alter the CD4 to CD8 ratio of the enriched T cells. Using this method, we could enrich TILs to a high purity without induction of signaling by antibody binding to cell surface markers.

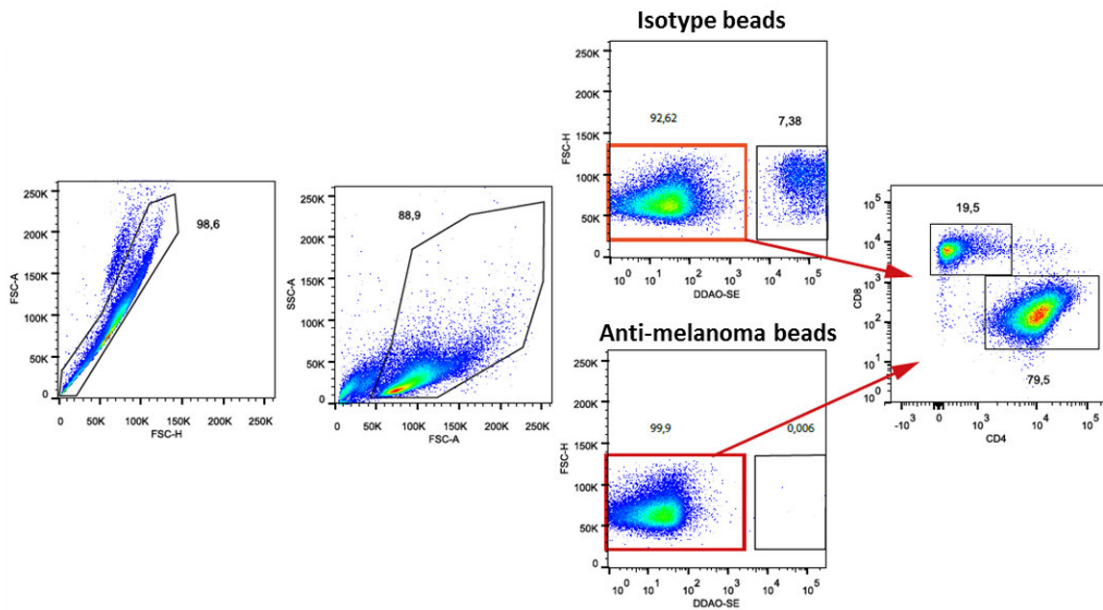


Figure 24: Successful separation of TIL412 and M479-A2 by melanoma beads. Representative flow cytometry staining of TIL412 and M579-A2 after separation. Tumor cells were stained with DDAO-SE for 30 min at 37 °C before 2 h co-culture with TIL412 (10:1 E:T). Cells were separated using anti-melanoma (MCSP) beads and subsequently stained with CD4 and CD8 antibodies. Purity was measured by FACS. Isotype beads were used as a negative control.

5.8.2 OR10H1 induces differential gene expression in TILs

In order to measure the inhibitory effect of OR10H1 on gene expression of TILs we co-cultured OR10H1-positive and -negative M579-A2 with TIL412 (10:1 E:T) for 10 h and enriched the TILs with melanoma beads. Subsequently, total RNA was isolated from the TILs and the transcriptome was analyzed by RNA sequencing. Parameters for sequencing are shown in **Table 5**. The differential gene expression of TIL412 co-cultured with OR10H1 knockdown M579-A2 compared to TIL412 co-cultured with control siRNA M79-A2 was calculated in accordance to literature [246]. In short, all reads were aligned to a reference genome, reference transcriptome and a gene information file (GRCh37) using tophat2 before sorting, indexing and formatting with SAMtools. Transcripts were counted (counts per million) using HTSeq-count. The exact parameters for alignment, formatting and counting are shown in paragraph 4.6.5.2. Gene expression values of TILs co-cultured with OR10H1 knockdown M579-A2 or control siRNA M579-A2 were compared using the edgeR package for R [253]. Features with less than one count per million in both biological replicates of a group (knockdown or control) were excluded from the analysis. The expression differences between all samples are depicted in the multidimensional scaling plot (**Figure 25**). The distances between the samples are calculated with a principal component analysis (PCA). A clear separation between gene expression of TILs co-cultured with OR10H1⁻ M579-A2 (KD) and TILs co-cultured with OR10H1⁺ M579-A2

(CTL) was observed in dimension 1 (x-axis), whereas the replicates lie close together. Dimension 2 (y-axis) accounts for the inter-experimental variation. The first dimension accounts for the major variances (distances between knockdown and control) and therefore inter-experimental variance (dimension 2) should not affect downstream analysis.

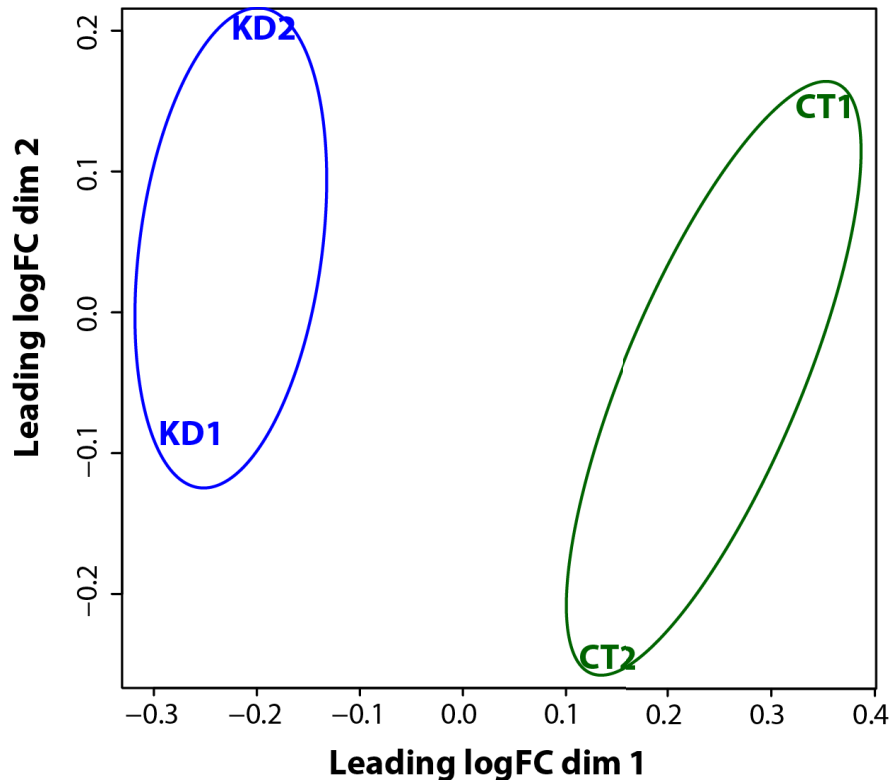


Figure 25: Multidimensional scaling plot (MDS) of RNA sequencing data. MDS plot illustrating the relations (distances) between all samples. Gene expression from TIL412 co-cultured (10 h) with OR10H1 knockdown M579-A2 (KD) is depicted in blue and gene expression from TIL412 co-cultured with control siRNA M579-A2 is depicted in green. The x-axis represents the dimension (similar to principal component) showing the variance in the dataset, followed by the dimension 2 (y-axis). Sequencing was performed on quality verified total RNA from two independent experiments. The MDS plot was generated using the plotMDS function of edgeR for R.

After establishing the quality [data not shown] and relation of all RNA sequencing samples we assessed the effect of OR10H1 knockdown (tumor side) on TIL gene expression and the associated functions (**Figure 26**). Differentially expressed genes of TILs co-cultured with OR10H1⁻ vs. OR10H1⁺ (control siRNA) M579-A2 are shown in a smear plot (**Figure 26A**). The log₂ fold change of each identified transcript in the TILs is plotted against the average count (log of counts per million), thereby representing the differential induction of gene expression in TILs upon co-culture with OR10H1 knockdown or control siRNA M579-A2. Only genes with a log₂-fold-change above/below ± 0.5 ($\log_{2}FC > 0.5$ and $\log_{2}FC < -0.5$) and a false discovery rate (corrected p-value) below 0.05 ($FDR < 0.05$) were considered differentially expressed. In

total 82 transcripts were differentially regulated in TIL412 after co-culture with OR10H1 knockdown M579-A2 (73 upregulated and 9 downregulated, respectively). As an additional representation, a heatmap was generated of all differentially expressed genes by unsupervised hierarchical clustering on the expression values in all samples (**Figure 26B**). As expected, samples from the two conditions (OR10H1 knockdown or control siRNA M579-A2 co-cultured with TIL412) clustered together. Furthermore, two clusters based on similarity of gene expression could be observed. The first cluster (upper) contains all transcripts which are more induced (upregulated) in TIL412 after 10 h co-culture with OR10H1⁺ M579-A2 (depicted in red). The second cluster (lower) contains those transcripts which are downregulated, respectively (depicted in blue). Overall, the heatmap representation of the differentially expressed genes is in accordance with the log₂-fold-change data. **Table 7** shows the top 20 upregulated and all 9 downregulated genes (for all differentially expressed genes see **Supplementary table 1**).

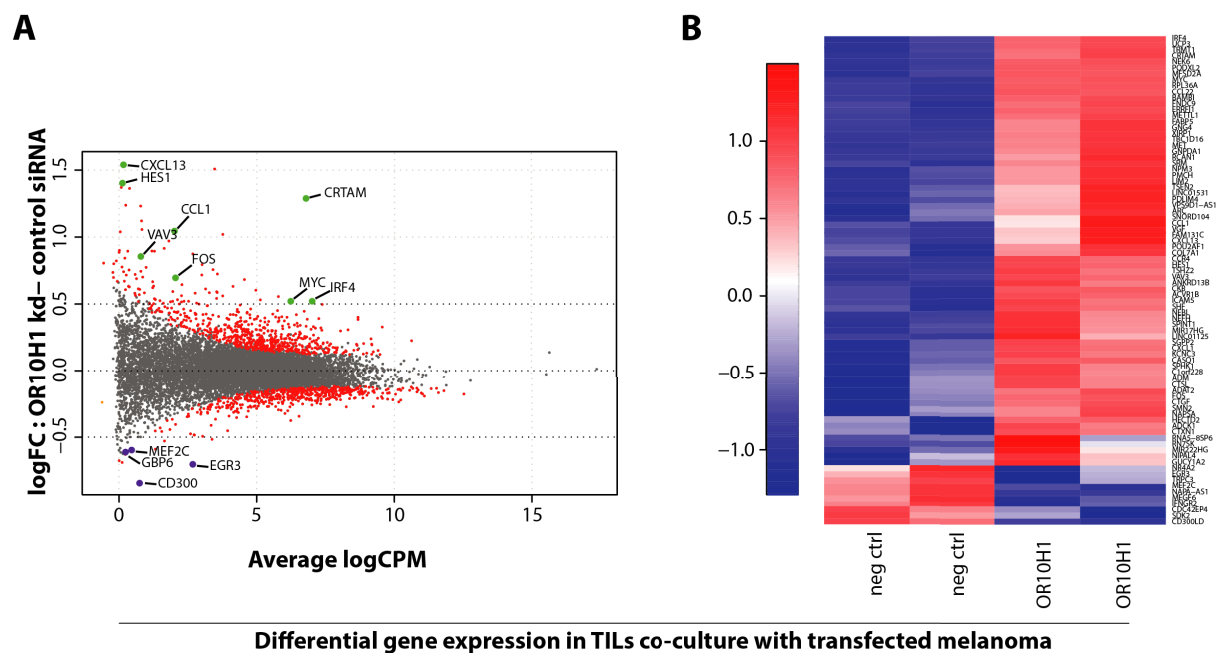


Figure 26: Overview of OR10H1 induced gene expression in TILs after co-culture. Differential gene expression visualized by smear plot (A) and heat map (B). A. Smear plot showing the log₂ fold change (TILs co-cultured with OR10H1⁻ vs. OR10H1⁺ M579A) of all sequenced transcripts plotted against the normalized read counts (CPM). Transcripts with a FDR < 0.05 are indicated by a red dot. Only transcripts with a log FC > 0.5 or < -0.5 are considered differentially expressed (indicated by dotted lines). Upregulated genes of interest are marked in green and downregulated in purple, respectively. B. Heatmap generated by unsupervised hierarchical clustering on the expression values of all differentially expressed genes. The color intensity indicates the level of gene expression ranging from low (blue) to high (red). Differential gene expression analysis was performed using edgeR. Clustering and heatmap generation was performed using hclust and regHeatmap. All tools are available via Bioconductor for R. RNA Sequencing was performed on samples from two independent experiments.

Table 7: List of genes differentially regulated by tumor-restricted *OR10H1* (top 20).

Gene	logFC	FDR	Description
CXCL13	1.55	1.36E-07	Chemokine (C-X-C motif) ligand 13
LINC01125	1.51	0.00265749	Long intergenic non-protein coding RNA 1125
HES1	1.39	4.32E-08	Hes family bHLH transcription factor 1
LINC01531	1.36	3.30E-06	Long intergenic non-protein coding RNA 1531
RN7SK	1.35	9.31E-05	RNA, 7SK small nuclear
CRTAM	1.29	8.06E-87	Cytotoxic and regulatory T cell molecule
BAMBI	1.24	5.77E-07	BMP and activin membrane-bound inhibitor
VEGF	1.24	2.13E-07	VEGF nerve growth factor inducible
COL7A1	1.22	3.89E-05	Collagen, type VII, alpha 1
MIR17HG	1.11	1.76E-07	MiR-17-92 cluster host gene
CCL1	1.05	4.81E-07	Chemokine (C-C motif) ligand 1
GUCY1A2	1.02	0.00166179	Guanylate cyclase 1, soluble, alpha 2
NEK6	1.02	1.52E-40	NIMA-related kinase 6
GNG4	0.97	4.91E-11	Guanine nucleotide binding protein (G protein), gamma 4
FAM131C	0.91	0.00384536	Family with sequence similarity 131, member C
PDLIM4	0.90	1.14E-05	PDZ and LIM domain 4
NAPSA	0.89	0.00117344	Napsin A aspartic peptidase
CXCL1	0.89	1.11E-06	Chemokine (C-X-C motif) ligand 1
XIRP1	0.88	4.55E-14	Xin actin binding repeat containing 1
VAV3	0.85	0.00010174	Vav 3 guanine nucleotide exchange factor
NR4A2	-0.51	0.00414285	Nuclear receptor subfamily 4, group A, member 2
CDC42EP4	-0.53	0.0039477	CDC42 effector protein (Rho GTPase binding) 4

MEF2C	-0.59	0.03680576	Myocyte enhancer factor 2C
SDK2	-0.59	0.00707349	Sidekick cell adhesion molecule 2
MEGF6	-0.61	0.04111638	Multiple EGF-like-domains 6
IFNGR2	-0.67	0.03615516	Interferon gamma receptor 2
TRPC3	-0.68	0.03478056	Transient receptor potential cation channel, subfamily C, member 3
EGR3	-0.70	0.0010135	Early growth response 3
CD300LD	-0.83	0.00011753	CD300 molecule-like family member d

Gene expression analysis revealed several genes associated with T cell function, anergy and survival that were differentially regulated in TILs depending on the presence of OR10H1 on melanoma cells. Several genes associated with impaired T cell responses were downregulated in TILs co-cultured with OR10H1 knockdown M579-A2. Downregulated genes associated with T cell anergy, apoptosis and exhaustion included EGR3 (Early Growth Response 3) [254], IFNGR2 (Interferon Gamma Receptor 2) [255] and NR4A2 (Nuclear Receptor Subfamily 4 Group A Member 2) [48, 256], respectively. Interestingly, the transcription factor MEF2C (Myocyte Enhancer Factor 2C) can induce the transcription factor family members NUR77 (NR4A1; Nuclear Receptor Subfamily 4 Group A Member 1) and NURR1 (NR4A2), which in turn induce apoptosis in T cells [257, 258]. NR4A1 was excluded from the analysis as it had a log₂-fold-change of -0.47 (logFC > -0.5).

Among the genes upregulated in TILs after co-culture with OR10H1 knockdown M579-A2 were genes associated with improved T cell function. For example, HES1 (Hes Family BHLH Transcription Factor 1) [259], CRTAM (Cytotoxic And Regulatory T-Cell Molecule) [260] and VAV3 (Vav Guanine Nucleotide Exchange Factor 3) [261] are involved in T cell activation, proliferation and TCR activation. The common transcription factors FOS (Fos Proto-Oncogene, AP-1 Transcription Factor Subunit) and MYC (V-Myc Avian Myelocytomatosis Viral Oncogene Homolog) are upregulated and associated with T cell activation [262, 263]. Another transcription factor, which is upregulated in TILs after co-culture with OR10H1⁻ M579-A2 compared to TILs after co-culture with OR10H1⁺ M579-A2 is IRF4 (Interferon Regulatory Factor 4). IRF4 is important for translating TCR affinity-mediated CD8⁺ T cell

responses and metabolic programming of T cells [264, 265]. These differential gene expression patterns between TILs co-cultured with OR10H1⁻ and OR10H1⁺ melanoma cells suggest a beneficial change of gene expression in TILs when OR10H1 is knocked down in the tumor cells. To further characterize these patterns of gene expression we performed pathway analysis using IPA (Ingenuity Pathway Analysis software, Qiagen).

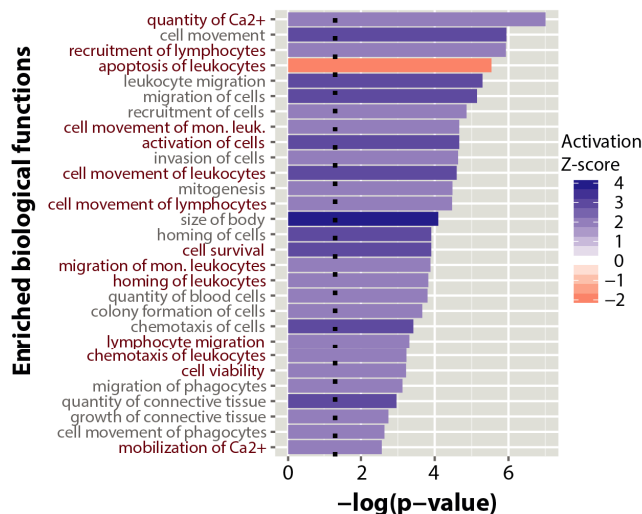
5.8.3 OR10H1 knockdown increased expression of genes positively associated with immune function downstream of TCR in TILs

Aiming to connect biological processes to observed changes in gene expression in TILs depending on the presence of OR10H1 on tumor cells during co-culture, we performed IPA Downstream Effects Analysis (DEA) (**Figure 27**) on all differential expressed genes ($\log_{2}FC > 0.5/ < -0.5$ and $FDR < 0.05$). This analysis approach associates the differential expression pattern to biological functions and/or diseases. Furthermore it predicts whether these functions are activated or inhibited based on the gene expression changes in the datasets [266]. Query of diseases associated with the observed gene pattern were excluded from the current analysis. DEA revealed several activated or inhibited biological functions correlating with the gene expression changes. The p-value ($-\log(p\text{-value})$) represents the statistical significance of the correlation between the gene dataset and the genes associated with biological functions from the Ingenuity knowledge database. Based on the direction of differential expression – \log_{2} -fold-change between TILs co-cultured with OR10H1⁻ or OR10H1⁺ M579-A2 – an activation Z-score is calculated predicting the activation or inhibition of the according biological function. **Figure 27A** shows all biological functions with an activation Z-score >2 or <-2 and a p-value < 0.05 . Some enriched biological functions were associated with leukocytes/lymphocytes and their activation or survival. The biological function ‘apoptosis of leukocytes’ was highly enriched in the dataset and predicted to be inhibited in TILs after co-culture with OR10H1 knockdown M579-A2, whereas the functions ‘cell survival’ and ‘cell viability’ were predicted to be activated, respectively. Other functions associated with lymphocytes were ‘recruitment of lymphocytes’, ‘cell movement of lymphocytes’ and ‘lymphocyte migration’. Enriched and activated functions associated with activation of cells included ‘quantity of Ca²⁺’, ‘activation of cells’ and ‘mobilization of Ca²⁺’. In summary, biological functions associated with the differential gene expression suggest increased viability/ reduced apoptosis of the TILs, increased functionality of lymphocytes and activated Ca²⁺ signaling activity.

Upstream Regulator Analysis (URA) was run to predict upstream regulators that are associated with the observed changes in gene expression [data not shown]. The TCR complex was found to be the upstream regulator with the strongest predicted activation (Z-score = 2.9) and enrichment (p-value = 9.5×10^{-10}) in the data set, suggesting an important role in differential gene expression induced in TILs co-cultured with OR10H1 knockdown M579-A2. In a final step, the URA and DEA were combined by Regulator Effect Analysis (REA) to generate a causal hypothesis for the (gene expression patterns). This connects the potential upstream molecules, the genes they regulate and the associated biological functions. REA predicted that the TCR complex together with associated Ras [267] and ERK1/2 [268] and several cytokines differentially regulates 16 genes leading to enhanced cell functionality (**Figure 27B**).

In summary, the pathway analyses predicted that knockdown of OR10H1 on melanoma cells induces a beneficial gene expression pattern – including reduced apoptosis and increased functionality – in TILs after co-culture. Furthermore, the TCR complex was predicted to regulate these gene expression changes and the associated biological functions implying an inhibitory role of OR10H1 on TCR signaling.

A



B

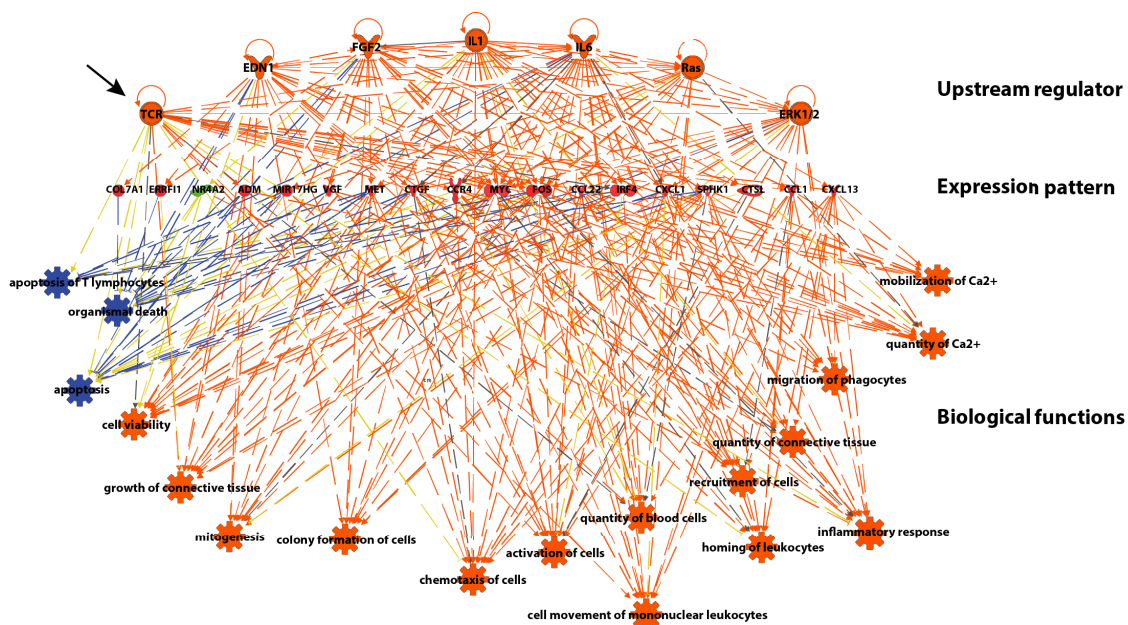


Figure 27: Knockdown of OR10H1 induces gene expression associated with TCR-mediated leukocyte functionality. A. Functional enrichment analysis (Ingenuity IPA) based on top upregulated ($\log_{2}FC > 0.5$) and downregulated ($\log_{2}FC < 0.5$) genes with $FDR \leq 0.05$. Differential gene expression-associated functions were selected based on enrichment p-value ($-\log_{10}$ of p-value; threshold = -1.3) and activation Z-score (threshold ± 2). Activation Z-score is color coded from deactivated (red) to activated (purple) functions. T cell-associated functions are marked in red. **B.** Causal network combining URA and DEA to match potential upstream regulators to associated downstream functions. Positive associated functions and regulations are indicated in orange and negative in blue. Biased associations are indicated in yellow. Downregulated genes are depicted in green and upregulated in red, respectively.

5.9 Tumor-associated OR10H1 impairs anti-tumor activity by activation of CREB and inhibition of Lck in TILs

Differential gene expression and subsequent pathway analysis revealed a role of OR10H1 in alteration of TCR-associated signaling leading to impaired T cell function. Affected pathways include kinases (e.g., TCR-associated) and other proteins activated/inactivated by phosphorylation. Therefore, we aimed to decipher the immune-inhibitory mode of action by delineating the signaling pathways in TCs altered by OR10H1 on the tumor side. In a first step, TIL412 were co-cultured with M579-A2 (OR10H1 knockdown or control siRNA) for 2 hours, separated (see paragraph 5.8.1) and the phosphorylation levels of 8 proteins were measured by Phosphoplex. The pathways tested for activation or inhibition were represented by CREB, ERK, NFκB, JNK, p70 S6K, STAT3, STAT5 and Akt (**Table 8** upper part). Induction (or reduction) of protein phosphorylation was calculated as log₂ ratio to unstimulated TILs (no tumor cells added) and compared to TILs stimulated with PMA/Iono (**Figure 28**).

Table 8: Phosphoproteins included in pathway analyses

Gene	Name	Phosphorylation side
General pathway overview		
CREB	cAMP response element-binding protein	pSerine133
ERK1/2	Extracellular-signal regulated kinases	pThreonine185/ pTyrosine187
NFκB	Nuclear factor kappa-light-chain-enhancer of activated B cells	pSerine536
JNK	c-Jun N-terminal kinase	pThreonine183/ pTyrosine185
p70 S6K	Ribosomal protein S6 kinase beta-1	pThreonine412
STAT3	Signal transducer and activator of transcription 3	pSerine727
STAT5	Signal transducer and activator of transcription 5	pTyrosine694/ pTyrosine699
Akt	Protein kinase B	pSerine473
TCR-associated		
CREB	cAMP response element-binding protein	pSerine133

CD3ε	CD3ε chain	pan pTyrosine
ERK1/2	Extracellular-signal regulated kinases	pThreonine185/ pTyrosine187
LAT	Linker for activation of T cells	pan pTyrosine
Lck	Lymphocyte-specific protein tyrosine kinase	pan pTyrosine
Syk	Spleen tyrosine kinase	pan pTyrosine
ZAP-70	Zeta-chain-associated protein kinase 70	pan pTyrosine

**pan indicates site-unspecific antibodies against all phospho-tyrosines of a given protein*

Phosphorylation levels of most proteins remained unchanged (compared to unstimulated TIL412) after a 2 h co-culture with M579-A2 independent of the presence of OR10H1 (**Figure 28A**). Overstimulation of TIL412 with PMA/Iono induced phosphorylation of ERK, STAT3 and Akt. Phosphorylation levels of CREB – on the activator phosphorylation site serine 133 – were strongly increased in TIL412 after co-culture with control siRNA M579-A2 (5-fold change). In TILs, co-cultured with OR10H1⁻ M579-A2 the induction of CREB is significantly smaller (2-fold change). Over-activation of TILs induced a 4-fold change in CREB phosphorylation. These data suggest a role of CREB activation in OR10H1-mediated alterations in signaling. CREB is a transcription factor positively and negatively involved in TCR signaling and function [269-271]. The differential phosphorylation of CREB in combination with the predicted differential gene expression (TCR associated; see 5.8.3) indicated an OR10H1-mediated dysregulation of TCR signaling upon co-culture with melanoma cells. We analyzed the kinetics of OR10H1-related effects on TCR signaling by measuring phosphorylation changes in distinct signaling nodes at 0, 5, 30 and 120 min co-culture. The analysis was performed as before measuring phosphorylation of CREB, CD3ε, ERK1/2, LAT, Lck, Syk and ZAP-70 (**Table 8** lower part). **Figure 28B** and **C** show phosphorylation kinetics of CREB, Lck and ZAP-70 in TILs co-cultured with OR10H1 knockdown or control siRNA M579-A2 or stimulated with PMA/Iono.

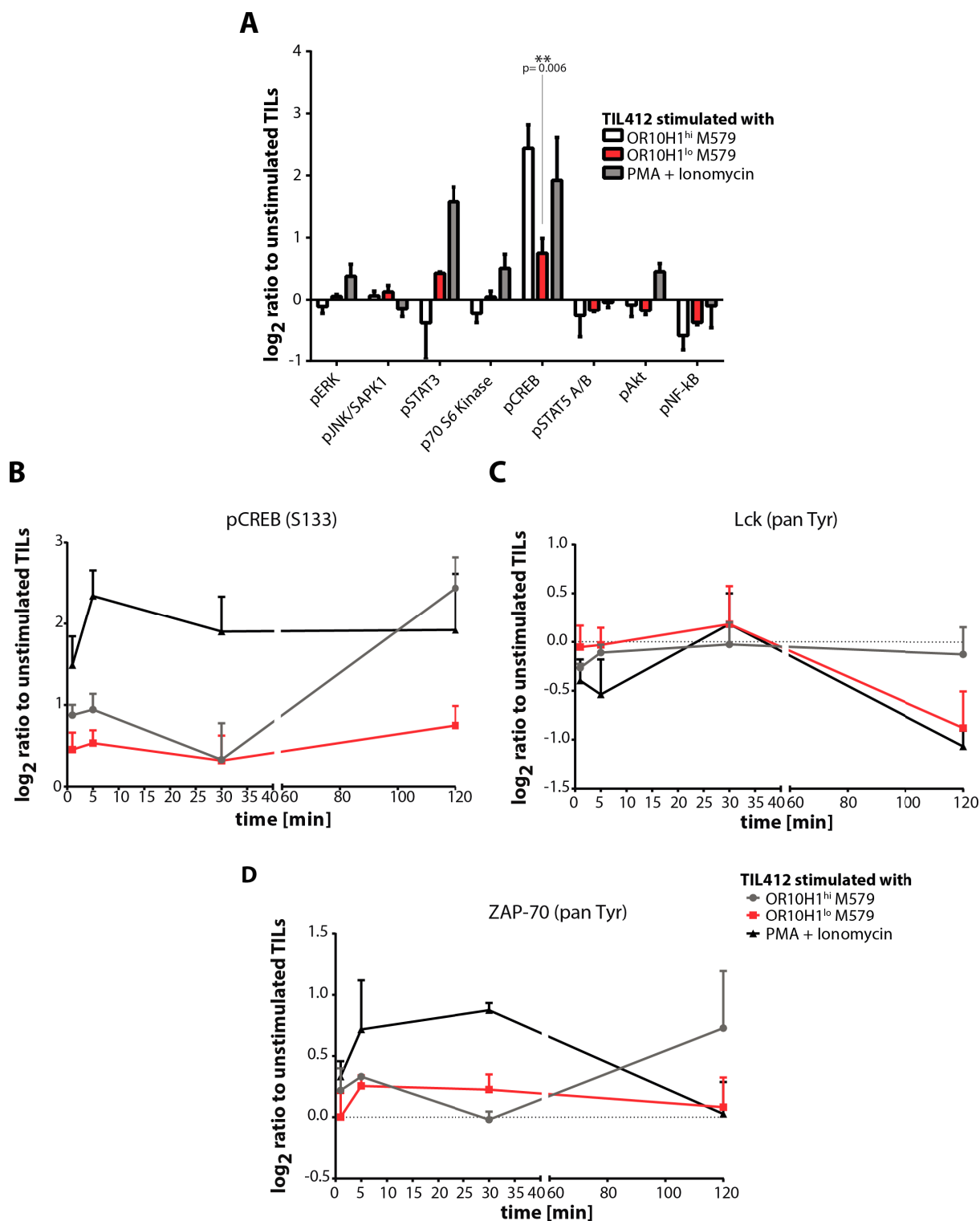


Figure 28: OR10H1 reduces Lck and increases CREB activity in TILs during co-culture. A, B, C, D Phospho pathway analysis for general (A) and TCR-associated (B, C, D) key signaling proteins in TILs after co-culture (up to 2 hours) with OR10H1-positive or -negative M579-A2. TILs without re-stimulation (unstimulated) and overstimulated with PMA/Iono serve as negative and positive control, respectively. Total protein content was normalized using beta-tubulin. A. Cumulative phosphoplex data ($n = 3$) of key proteins involved in general pathways after 2 h co-culture. (De)phosphorylation are indicated by \log_2 fold-change compared to TILs without re-stimulation. Co-culture and separation was performed as described in Figure 24. B, C, D. Cumulative phosphoplex data ($n = 3$) of CREB, Lck and ZAP-70 phosphorylation kinetics in TILs upon co-culture with OR10H1-positive (\bullet) or -negative (\square) M579-A2 or TILs stimulated with PMA/Iono (Δ) for 0, 5 30 and 120 min. Mean \pm SEM are shown, unless stated otherwise, and statistical significance was calculated using unpaired, two-tailed Student's t-test. Experiments were performed by Christina Hartl (Group Prof Beckhove, DKFZ) under my supervision.

Phosphoplex analysis for phosphorylation of CD3 ϵ , ERK1/2, LAT and Syk did not show a distinguishable kinetic pattern between TIL412 co-cultured with OR10H1 knockdown or control siRNA M579-A2 [data not shown]. As expected, knockdown of OR10H1 on tumor cells altered the kinetics for CREB phosphorylation in TILs upon co-culture (**Figure 28B**). For the first 30 min, the phosphorylation levels of CREB were similar in both settings with a raise in phosphorylation in the first 5 min, followed by a decrease at 30 min. After 2 h, CREB became highly phosphorylated in TILs co-cultured with OR10H1-positive M579-A2 but stayed similar in the OR10H1 knockdown setting. Interestingly, stimulation with PMA/Iono led to a strong phosphorylation of CREB already after 5 min and remained high for 2 hours. The kinetics of Lck phosphorylation showed a different pattern (**Figure 28C**). Co-culture with OR10H1-positive M579-A2 did not induce (de)phosphorylation of Lck over the time period of 2 hours. Knockdown of tumor-restricted OR10H1 on the other hand led to a strong dephosphorylation of Lck in TILs compared to TILs without stimulation between 30 and 120 min. Interestingly, the kinetics of Lck phosphorylation upon stimulation with PMA/Iono were similar to the one induced by OR10H1⁻ M579-A2. Finally, in the first 5 min the induction of ZAP-70 phosphorylation was similar in the ORH10 knockdown and control siRNA setup. After 30 min, TILs co-cultured with OR10H1⁺ M579-A2 have the same phosphorylation level of ZAP-70 as unstimulated TILs, whereas TILs in the OR10H1 knockdown setting show increased ZAP-70 phosphorylation. After 120 min co-culture induction of ZAP-70 phosphorylation was higher in TILs co-cultured with OR10H1-positive M579-A2 compared to the knockdown setting. Stimulation with PMA/Iono induced ZAP-70 phosphorylation up to 30 min followed by dephosphorylation reaching the levels of unstimulated TILs after 120 min (**Figure 28D**).

In summary, knockdown of OR10H1 in tumor cells led to differential phosphorylation of key nodes involved in TCR-mediated signaling. Induction of CREB phosphorylation is reduced whereas Lck becomes dephosphorylated. Induction of ZAP-70 phosphorylation is higher at first (OR10H1 knockdown setting) but strongly reduced after 120 min compared to TILs co-cultured with control siRNA M579-A2. Lck and ZAP-70 have several tyrosine residues which can activate or inhibit their downstream kinase functionality upon phosphorylation [272, 273]. The Lck and ZAP-70 antibodies used by phosphoplex analysis are site unspecific (pan-tyrosine) measuring overall tyrosine phosphorylation without revealing site-specific phosphorylation patterns. We performed site-specific western blot analysis for phosphorylation of CREB, PKA and Lck to detect activation or inhibition of the respective kinase (**Figure 29**). As expected,

phosphorylation of CREB at serine 133 was reduced in TILs co-cultured with OR10H1 knockdown M579-A2 compared to TILs co-cultured with control siRNA M579-A2 (**Figure 29A**, left panel). Interestingly, phosphorylation of activating transcription factor 1 (ATF1) – a gene family member of CREB – was also reduced (lower band). ATF1 and CREB share the same activation site phosphorylated by PKA [274] suggesting a role for PKA in OR10H1-mediated inhibition of T cell function. In accordance with this, knockdown of OR10H1 in M579-A2 reduced the induction of PKA phosphorylation in TILs compared to the control siRNA setting (**Figure 29A**, right panel). Stimulation with PMA/Iono did not induce phosphorylation of PKA. ZAP70 is a critical node in TCR-mediated signaling but it contains at least 11 phosphorylation sites with activatory, inhibitory or unknown functionality [275] making a site-specific phosphorylation analysis difficult. Therefore, we focused on Lck as a key regulator of T cell activation. The spatial and regulatory kinetics of Lck phosphorylation and function were reviewed by *Rossy et al.* [276]. In short, Lck can be either phosphorylated on tyrosine Tyr394 (activation) or tyrosine Tyr505 (inhibition). Phosphorylation of Tyr505 leads to its interaction with the SH2 domain of Lck and subsequent stabilization of the inactive “closed” conformation. Phosphorylation on Tyr394 stabilizes the activation loop in an active formation. We measured phosphorylation of the main inhibitory site (Tyr505) and found it to be highly increased in TILs co-cultured with OR10H1⁺ M579-A2 compared to TILs co-cultured with OR10H1⁻ M579-A2 or stimulated with PMA/Iono.

Several groups reported inhibitory pathways in T cells inducing cAMP-mediated activation of PKA, its phosphorylation/ activation of CREB and C-terminal Src kinase (Csk) and the subsequent inhibition of Lck by phosphorylation at Tyr505 (mediated by Csk) [277-281]. We validated Lck as the functional joint of OR10H1-mediated TCR inhibition by using the Lck-specific inhibitor 7-Cyclopentyl-5-(4-phenoxyphenyl)-7H-pyrrolo[2,3-d]pyrimidin-4-ylamine. This class of Lck inhibitors (pyrrolo[2,3-d]pyrimidines) shows a stronger inhibition of the inactive form of Lck [282] and increased inhibition of lower avidity effector cells [283]. We used different concentrations of the Lck inhibitor to measure the functional outcome of differential Lck phosphorylation (structural conformation) induced by OR10H1 on the tumor side (**Figure 29B**). The addition of 2 μ M Lck greatly abrogated killing of M579-A2-luc transfected with control siRNA. Only 8% of all tumor cells were lysed by TIL412. The knockdown of OR10H1 in melanoma cells strongly reduced the sensitivity of TIL412-mediated killing towards Lck inhibition (70% killing). At higher concentrations of the Lck inhibitor

(5 μM) the TIL412-mediated killing of M579-A2-luc was completely abrogated independent of the presence of OR10H1. We validated this effect by real-time imaging and checked the impact of the inhibitor concentrations on TIL survival and behavior (**Supplementary figure 3**). None of the used concentrations of inhibitor induced apoptosis in TILs or prevented their binding to tumor cells. Therefore, the data suggest that tumor-restricted OR10H1 leads to the phosphorylation of Lck on tyrosine 505 inducing an inactive form. This inactive form is more prone to Lck inhibition compared to the more active Lck in a setting with OR10H1 knockdown. In summary, OR10H1 promotes an inhibitor pathway in TILs via activation of PKA phosphorylation of CREB and Csk and subsequent phosphorylation/inhibition of Lck abrogating TIL functionality.

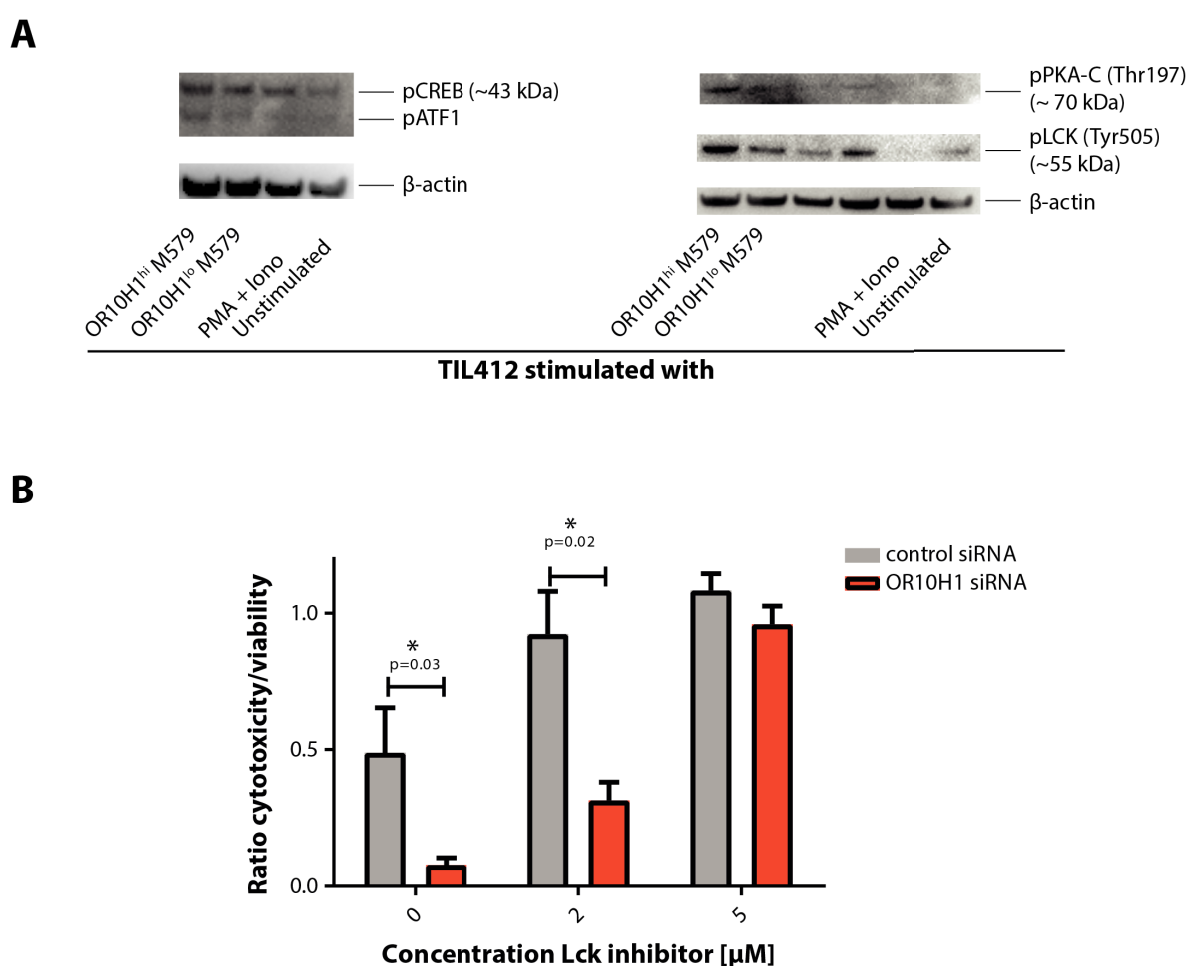


Figure 29: OR10H1 reduces Lck activity via PKA and Csk leading to impaired TIL function. **A.** Representative immunoblot analysis showing phospho-CREB (Ser133), phospho-ATF1, phospho-PKA (Thr197) and phospho-Lck (Tyr505) levels in OR10H1⁺-treated, OR10H1⁻-treated, PMA/Iono-treated or unstimulated TIL412 using the according phospho-specific antibodies. Beta-actin was used as a loading control. **B.** Cumulative data (n = 3) of Lck inhibition sensitivity of TIL412 co-cultured with OR10H1⁺ or OR10H1⁻ M579-A2-luc. M579-A2-luc and TIL412 were co-cultured for 20 h in the presence of different concentrations of the Lck inhibitor 7-Cyclopentyl-5-(4-phenoxyphenyl)-7H-pyrrolo[2,3-d]pyrimidin-4-ylamine. TIL-mediated tumor lysis is represented by the luciferase intensity ratio between cytotoxicity and viability (no TILs). Mean \pm SEM are shown, unless stated otherwise, and statistical significance was calculated using unpaired, two-tailed Student's t-test.

5.10 OR10H1-mediated TIL inhibition involves cAMP transport via gap junctions

Induction of Lck inhibition via cAMP-PKA-Csk could either be triggered by binding of soluble factors (e.g., adenosine, PGE₂) to T cell-restricted receptors [284-286] – inducing the production of cAMP – or the transport of cAMP from regulatory T cells or tumor cells into effector T cells via gap junctions [118, 279]. Connexins CX31.1, CX32, CX43, CX45, and CX46 are expressed by regulatory and effector T cells and their expression increases after T cell activation [118]. Interestingly, CX32 (connexin 32; GJB1) was found to be a potential immune checkpoint in our follow-up primary screening (**Supplementary figure 1, Supplementary table 2**), whereas the knockdown of other connexins (e.g., the more common CX43) did not impact on T cell-mediated lysis of melanoma cells [data not shown]. CX32 gap-junctions are permeable to the secondary messenger adenosine [287], cAMP [288] and Inositoltrisphosphat (IP₃) [289]. Therefore, we validated the expression of connexins 32 and 43 in several tumor entities by RT-PCR (**Figure 30A**). Melanoma (M579-A2) and colorectal cancer (SW480) expressed high level of CX32, whereas multiple myeloma (KMM-1, RPMI8226), pancreatic cancer (PANC-1) and breast cancer (MCF-7) expressed connexin 43 only, respectively.

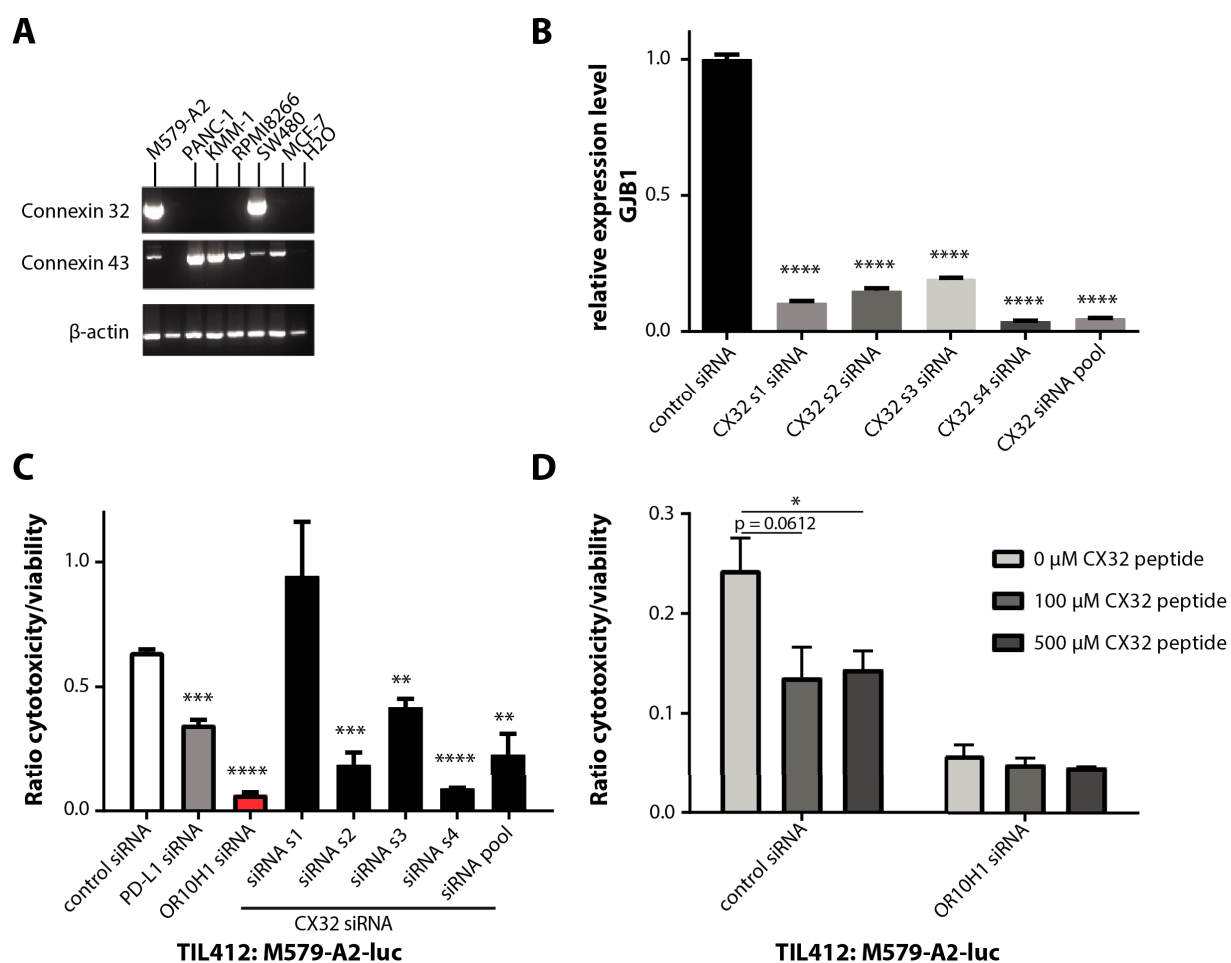


Figure 30: Intercellular communication via connexin 32 is needed for OR10H1-mediated inhibition of TIL412. **A.** Representative agarose gel of CX 32 and 43 expression in different tumor entities (melanoma, PDAC, multiple myeloma, colorectal and breast cancer) by RT-PCR. Beta-actin served as a house keeping control. PCR was run according to the protocol for normal abundance gene expression (35 cycles). Expected transcript sizes are ~386 bp for CX32 primers and ~354 bp for CX43 primers. **B.** Knockdown efficacy of deconvoluted siRNA sequences on CX32 (GJB1) mRNA levels was measured by qPCR (representative data of at least two independent experiments) after 72 h of transfection. qPCR-optimized primers were used to validate CX32 (GJB1) mRNA abundance. Beta-actin served as a house keeping control. **C, D.** Luciferase killing assays with CX32 knockdown (**C**) or peptide-based blockade (**D**). **C.** M579-A2-luc cells were reverse-transfected with individual (s1-s4), pooled CX32 or control siRNAs (PD-L1 and OR10H1 as positive immune checkpoint scrambled siRNA as negative control) and co-cultured with TIL412 (effector-to-target ratio 5:1) or CLM for 20 h. TIL-mediated lysis or viability impact of target knockdown was measured by luciferase assay (cumulative data, n=3). TIL-mediated tumor lysis is represented by the luciferase intensity ratio between cytotoxicity and viability (no TILs). **D.** M579-A2-luc were transfected with OR10H1 or control siRNA (as in C). CX32-blocking peptide was added for one hour before co-culture with TIL412 or CLM FOR 20 h. TIL-mediated lysis or viability impact of peptide-mediated blockade was measured by luciferase assay (representative data of at least two independent experiments). TIL-mediated tumor lysis is represented by the luciferase intensity ratio between cytotoxicity and viability (no TILs). Mean \pm SEM are shown, unless stated otherwise, and statistical significance was calculated using unpaired, two-tailed Student's t-test.

We further validated the involvement of gap junctions in OR10H1-mediated TIL inhibition by siRNA knockdown of CX32 (**Figure 30B** and **C**) and peptide-based inhibition of gap junction formation (**Figure 30D**). Transfection of M579-A2 with siRNAs showed a significant knockdown of CX32 with all four designated sequences and the pooled siRNA compared to the negative control (**Figure 30B**). Knockdown with siRNA 4 and pooled siRNA reduced CX32

mRNA levels more than 90%. The knockdown efficacy (on mRNA level) of the different siRNA sequences correlates strongly with the impact on TIL-mediated tumor lysis, except for siRNA s1 (**Figure 30C**). This exception was dependent on a major impact on TIL-independent M579-A2-luc survival. Transfection with siRNA s1 reduced TIL-independent survival by more than 80% [data not shown] suggesting a strong off-target effect of this particular siRNA sequence. CX32 knockdown with the other three siRNAs improved TIL-mediated killing of M579-A2-luc strongly. These data suggested a strong role of connexins (here CX32; GJB1) in tumor inhibition of TIL functionality, but does not imply a role in the mode of action of OR10H1-mediated inhibition. In order to explore the potential role of CX32 in OR10H1-dependent TIL inhibition we combined siRNA knockdown of OR10H1 with small peptide blockade of gap junction formation between tumor and T cells (**Figure 30D**). Peptides partially mimicking functional domains of connexins have been used to block connexin-based gap junctions and hemichannels (reviewed in [290]). CX32 mimicking peptide (SRPTEKTVFTV) was added to tumor cells one hour before co-culture with TILs resulting in an increased lysis of M579-A2-luc transfected with control siRNA but not of those transfected with OR10H1 siRNA. Therefore, we conclude that CX32 has an inhibitory effect on T cell-mediated tumor lysis only in the presence of OR10H1. In summary, connexin 32 is important for the intercellular cAMP transport and depending on the activity of OR10H1.

5.11 OR10H1 regulates the balance between $G\alpha_i$ and $G\alpha_{\text{Olf}}/G\alpha_s$ signaling in tumor cells upon TIL encounter

Our data suggest that OR10H1 is involved in the inhibition of TIL function indirectly by transport of cAMP into TILs and not via direct interaction with a ligand on the T cell surface. Therefore, it is important to understand the signaling downstream of OR10H1 in melanoma cells. Olfactory receptors initiate signaling cascades by activation of different types of heterotrimeric G-proteins [291]. Normally, olfactory receptors activate olfactory G protein α subunit ($G\alpha_{\text{Olf}}$) – a homolog of stimulatory G protein α subunit ($G\alpha_s$) – which in turn activates adenylate cyclase 3 (ADYC3). The expression of olfactory receptors and their associated machinery in non-olfactory tissues can be associated with a chemoreceptor function [292]. We found that both $G\alpha_{\text{Olf}}$ and ADYC3 are expressed in M579-A2 (**Figure 31**). Adenylate cyclase 3 is equally expressed among all tested tumor entities whereas $G\alpha_{\text{Olf}}$ is expressed in melanoma, PDAC and CRC and it is detected at lower levels in multiple myeloma and breast cancer. $G\alpha_s$

is highly expressed in M579-A2 [data not shown]. Interestingly, tumors with an OR10H1-dependent inhibition of TIL-mediated tumor lysis also express the olfactory machinery. As M579-A2 express genes associated with olfactory receptor function we aimed to detect signaling events inside tumor cells upon contact with TILs. Activation of olfactory receptors in melanocytes can be measured by the secondary messengers calcium (Ca^{2+}) and cAMP [243]. Therefore, we adopted imaging based assays to measure the release of calcium and the generation of cAMP in M579-A2 depending on the interaction with TILs. As mentioned, the inhibitory effect of OR10H1 is HLA-A2-dependent. Therefore, we assumed that OR10H1-dependent signaling is triggered mainly by CD8^+ TILs. Consequently, we used TIL209 (only consisting of CD8^+ TILs) for the following pathway analysis.

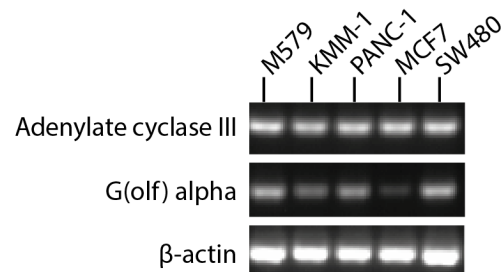


Figure 31: Expression of the olfactory machinery in different tumor entities. GNAL and ADCY3 expression was measured in different tumor entities (melanoma, multiple myeloma, PDAC, breast cancer and CRC by RT-PCR. Beta-actin served as a house keeping control. PCR was run according to the protocol for normal abundance gene. Expected transcript sizes are ~100 bp.

5.11.1 OR10H1-dependent calcium signaling

The secondary messenger calcium propagates signaling in waves. This can occur inter- and intracellularly [293]. Due to the wave nature of the signal it is important to measure the amplitude, frequency and intercellular propagation of calcium signals on a single-cell resolution. Particularly, in a system where the unselected interaction/proximity of a T cell is supposed to trigger the signaling event instead of a single specific receptor-ligand interaction, activation is induced simultaneously in all cells. We used the fluorescent dye Fura-2-AM to measure intracellular calcium concentrations in tumor cells. The ratiometric nature of this dye prevents imaging-based side-effects (e.g., photobleaching). M579-A2 cells were labeled with Fura-2-AM and a basal level of signal was measured before co-culture with TIL209 or RINGER buffer as a control (**Figure 32**). The basal levels of calcium concentrations were stable in both OR10H1^+ and OR10H1^- M579-A2 for the whole measurement (1 hour). The addition of

RINGER buffer did not induce any calcium signal either (**Figure 32C and D**). The addition of TIL209 induced distinct calcium signaling peaks (up to a ratio of 1.3) after 10 min of co-culture (**Figure 32A**). We observed several distinct peaks in those cells where calcium signals occur, suggesting an interplay of promoting and limiting factors for signal transduction leading to fluctuation of calcium waves. Surprisingly, the knockdown of OR10H1 on M579-A2 before the co-culture with TIL209 dramatically enhanced the calcium signal in every aspect (**Figure 32B**). More cells showed signaling events in general. Calcium signaling could be observed as early as 7 min after addition of TIL209. Most strikingly, the signaling was stronger (amplitudes up to a ratio of 1.8) and more frequent in the reacting cells. Cumulative data (integrated calcium signal normalized to basal levels) revealed a more than 2-fold increase in calcium signal in OR10H1 knockdown cells compared to control after co-culture with TIL209 (**Figure 32C**). This translated into increases in intracellular calcium signals. An increase in calcium levels was not detected in the control setup. We observed intercellular calcium waves in both setups but could not apply an algorithm for intercellular calcium signal transduction due to the dynamic nature of our settings (dynamic interactions of tumor cells and TCs in terms of signal fluctuation). The observed increase in calcium signaling upon knockdown of OR10H1 dissents with the literature on olfactory neurons [294]. The binding of odorants to the receptor led to the generation of cAMP which in turn activates calcium channels resulting in an influx of calcium. The observed results might be depending on the nature of interactions between melanoma cells and TILs. Therefore, we analyzed cAMP production as the primary step of olfactory receptor activation.

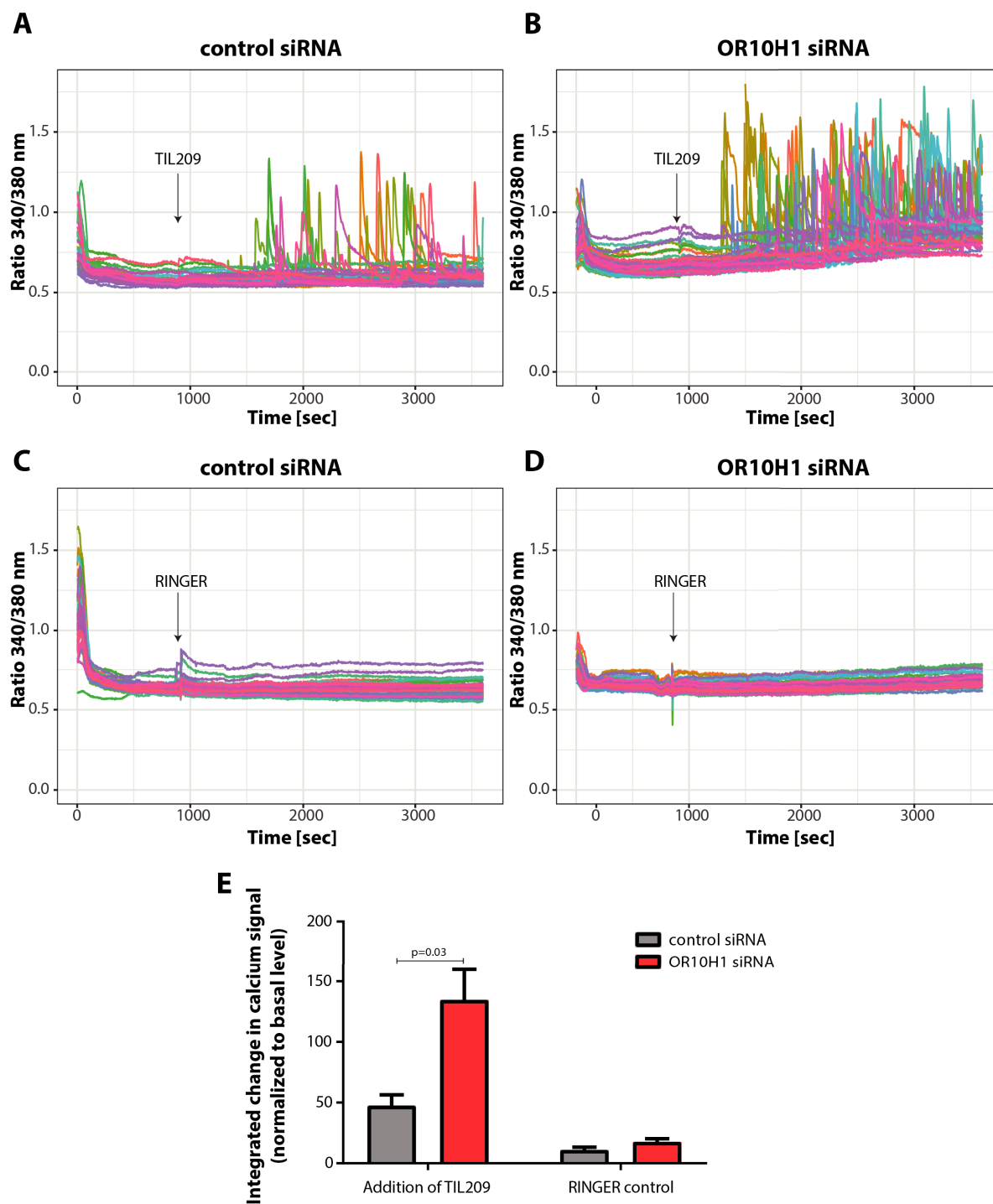


Figure 32: Knockdown of OR10H1 increases TIL-induced calcium signaling in M579-A2. A-D. Representative calcium measurements in control siRNA (A, C) or OR10H1 siRNA-transfected (B, D) M579-A2 upon co-culture with TIL209 (A, B) or RINGER buffer (C, D). M579-A2-luc cells were reverse-transfected (as before) on D-Lysine-treated glass slides for 72 h, incubated in RINGER buffer before measurement. Basal levels of 340/380 nm ratio were measured for 15 min before co-culture with TIL209 or RINGER buffer. Each color-coded line represents the signal inside a single region of interest (manually adopted to cell outlines). Around 40 cells were measured per setup. E. Cumulative data (n = 3) of overall calcium signal changes. Ratiometric data was normalized to the basal level (subtraction) and integrated over 60 min. Mean ± SEM are shown, unless stated otherwise, and statistical significance was calculated using unpaired, two-tailed Student's t-test.

5.11.2 OR10H1-dependent cAMP signaling

As mentioned, activation of adenylate cyclase (predominantly ADYC3) and subsequent production of cAMP is the main pathway of olfactory receptor-mediated signaling. Olfactory receptors are associated with the olfactory G protein α subunit ($G\alpha_{olf}$) an olfactory-neuron restricted homolog to the common $G\alpha_s$. We found expression of both homologs in M579-A2 (**Figure 31**) and will refer to them as $G\alpha_{olf/s}$. Detection and measurement of dynamic cAMP signals in a system depending on cell-cell interactions (M579-A2 and TIL209) is difficult. Particularly, if the detection should be restricted to one of the interaction partners (here M579-A2). We took advantage of a state-of-the-art EPAC-based FRET sensor [295]. These sensors contain the cAMP binding domain of EPAC with a FRET (CFP and YFP) signal in the closed conformation. Binding of cAMP stretches the binding domain and induces loss of FRET signal increasing CFP signal. The respective plasmid was kindly provided by Kees Jalink (Netherlands Cancer Institute, Netherlands). Using this system, we were able to analyze cAMP production on a single-cell resolution and in a time-lapsed fashion. Double transfected M579-A2 (FRET sensor and control or OR10H1 siRNA) were co-cultured with TIL209 and the resulting cAMP production was detected using the ratio between CFP and YFP (**Figure 33**). Addition of the phosphodiesterase inhibitor 3-isobutyl-1-methylxanthine (IBMX) prevented the degradation of cAMP. Basal levels were measured for 10 min before the addition of TIL209. Representative pictures for basal level, shortly after co-culture and end of measurement are shown in **Figure 33A**. Before the co-culture levels of cAMP were similar in OR10H1-positive and -deficient cells. After addition of TIL209, control siRNA-transfected M579-A2 showed an increased induction of cAMP. OR10H1 knockdown however decreased the TIL-mediated induction of cAMP production (**Figure 33B**) but did not abolish it completely. This might be based on the activity of OR10H1-independent $G\alpha_s$. We concluded that M579-A2 produce cAMP upon TIL209 co-culture in an OR10H1-dependent manner. This cAMP production is triggered by OR10H1-dependent activation of $G\alpha_{olf/s}$ and adenylate cyclase 3.

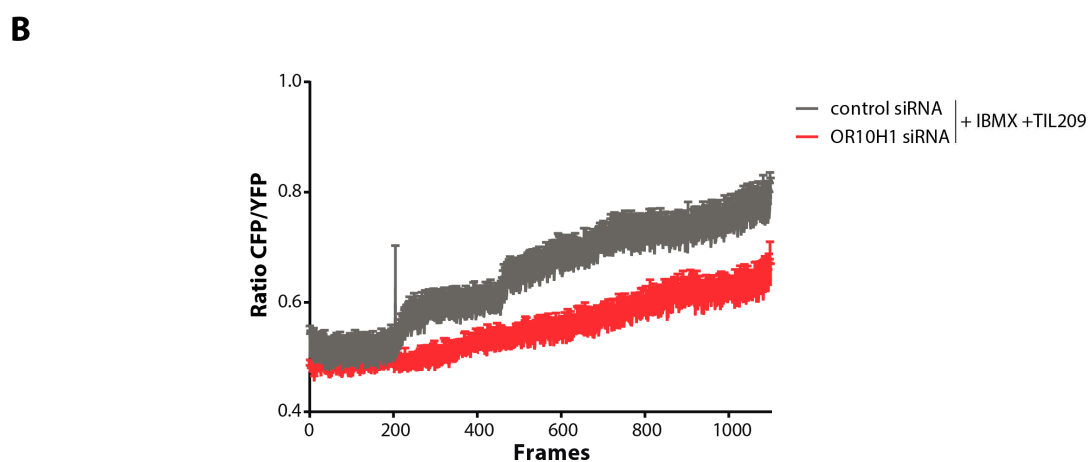
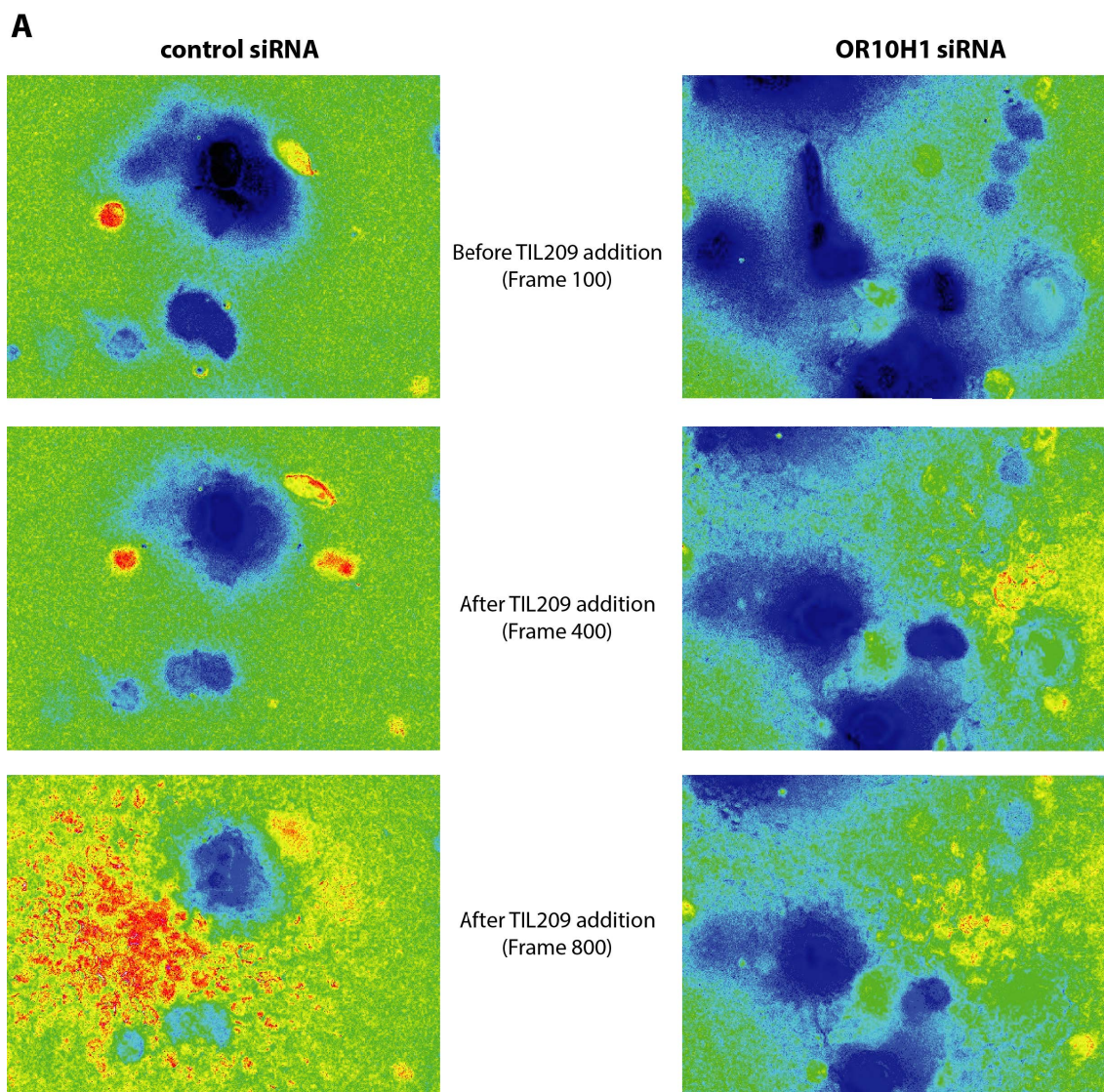


Figure 33: Knockdown of OR10H1 decreases TIL-induced cAMP signaling in M579-A2. **A.** Representative pictures of OR10H1-mediated M579-A2 cAMP production induced by TIL209 co-culture. M579-A2-luc cells were reverse-transfected (as before) on D-Lysine-treated glass slides for 24 h before an additional transfection with the EPAC-based FRET sensor. Basal levels of CFP/YFP were measured for 10 min before co-culture with TIL209. IBMX (25 μ M) was added to all setups at the beginning. The ratio between CFP/YFP is shown. Signals are represented by lookup tables reaching from blue (low) to red (high). **B.** Representative data (from at least two independent experiments) of overall cAMP signal induction. Signals of regions of interest (manually adopted to cell outlines) were integrated and Mean \pm SEM is shown.

5.12 Improved TIL-mediated lysis of M579-A2 after OR10H1 knockdown can be reversed by cholera toxin (CTX)

After detecting differential TIL-mediated activation of the calcium and cAMP pathways depending on the presence of OR10H1 we aimed to validate the functional implications. Therefore, the impact of pertussis (PTX) and cholera toxin (CTX) on TIL-mediated tumor lysis was measured. Pertussis toxin (derived from *Bordetella pertussis*) inhibits the inhibitory G protein α subunit ($G\alpha_i$) which is thus prevented from inhibiting the adenylate cyclase [296]. Cholera toxin on the other hand inhibits the GTPase function of $G\alpha_s$ keeping it in its activated state leading to increased activation of ADY3. This effect is also observed with $G\alpha_{olf}$ [297]. The addition of cholera but not pertussis toxin abrogated the OR10H1 knockdown-mediated increase in TIL-mediated tumor lysis (**Figure 34**). Here, tumor cells were pretreated with the toxins followed by vigorous washing to prevent any direct effect on the TILs.

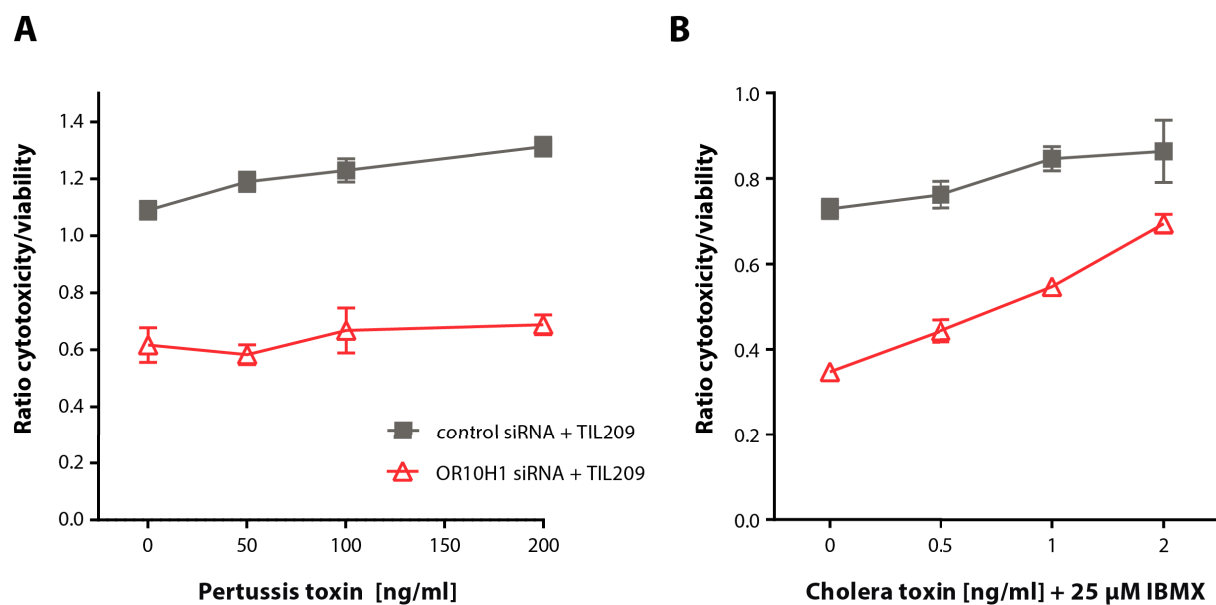


Figure 34: Pretreatment with cholera but not pertussis toxin abrogates killing of OR10H1-deficient melanoma. A, B. Representative luciferase killing assays (of at least three independent experiments) after pretreatment with pertussis (A) or cholera toxin +IBMX (B). M579-A2-luc cells were reverse transfected as before. Before co-culture with TIL209 cells were pretreated with different concentrations of pertussis (6 h) and cholera toxin (1 hour). Treated OR10H1⁺ or OR10H1⁻ M579-A2-luc were co-cultured with TIL209 for 20 h. TIL-mediated tumor lysis is represented by the luciferase intensity ratio between cytotoxicity and viability (no TILs).

The 6-hour pretreatment with pertussis toxin slightly decreased the TIL-mediated tumor lysis in control siRNA transfected M579-A2-luc (**Figure 34A**). This was not observed in cells transfected with OR10H1 siRNA. The pretreatment with cholera toxin and 25 μ M IBMX led to a slight decrease in TIL-mediated tumor lysis in the control setup but dramatically impaired killing of OR10H1⁻ M579-A2-luc (**Figure 34B**). This decrease in killing occurred in a cholera

toxin concentration-dependent manner. Without cholera toxin pretreatment (but with IBMX) around 65-70% of OR10H1-negative M579-A2-luc cells got lysed (20-25% in the control setup). At a concentration of 2 ng/ml, cholera toxin pretreatment decreased TIL-mediated lysis to around 30%. At this concentration, the effect of OR10H1 knockdown on TIL-mediated lysis is almost completely abrogated (compared to the negative control). This data suggests a major role for the $G\alpha_{s/Olf}$ pathway in OR10H1-mediated inhibition of TIL cytotoxicity.

In summary, co-culture with TILs triggers differential signaling in OR10H1-deficient M579-A2. On one hand, calcium signaling is strongly increased in terms of amplitude and frequency. On the other hand, cAMP production is reduced in OR10H1 knockdown M579-A2 during co-culture. Finally, the increase in TIL-mediated lysis of OR10H1-deficient M579-A2 can be abrogated by the pretreatment with cholera toxin but not with pertussis toxin. This suggest a direct involvement of $G\alpha_{s/Olf}$ in OR10H1-mediated TIL inhibition.

6 Discussion

Immune checkpoint blockade tremendously improved cancer immunotherapy [206] but a large proportion of cancer patients cannot benefit from blockade of anti-PD-1/PD-L1 antibody therapies [219]. Therapies can for example be improved by synergistically combining immune checkpoint blockades [222-224]. Many unknown immune checkpoint pathways might be used by non-responsive tumors (to anti-PD-1/PD-L1 antibody therapy) in order to shut down antitumor immune responses. Thus, there is a strong demand to systematically identify novel immune checkpoint axes.

Here, we developed a high-throughput screening platform for the detection of novel immune checkpoint pathways. Our setup closely resembles the situation in cancer patients' due to the usage of patient-derived melanoma cultures in combination with HLA-matched TILs. In the first of two rounds of screening (performed with different libraries) we found 75 candidate genes. After a secondary screening, 35 genes (from the first primary screening) potentially mediated T cell-inhibition. We chose the olfactory receptor OR10H1 for further validation and mode of action analysis. So far, no role of OR10H1 has been described in tumor-mediated T cell inhibition. OR10H1 prevents TIL-mediated killing of solid tumors in a HLA-dependent manner and reduces T cell activity. This inhibitory effect was observed *in vitro* and *in vivo*. OR10H1-dependent inhibition of T cell function is mediated via a pathway involving cAMP activation of PKA which in turn activates CREB and thus alters T cell gene expression. Furthermore, PKA activates Csk, which in turn shuts down TCR-dependent signaling of Lck. We hypothesize that cAMP is produced in the tumor cell upon T cell encounter and transported into T cells via CX32 gap junctions. OR10H1 regulates the production of cAMP by altering the balance between $G\alpha_i$ and $G\alpha_s$ signaling towards $G\alpha_s$. The inhibitory pathway described here is independent from PD-L1-mediated T cell inhibition and thus might be used as a target for immune checkpoint blockade as a single treatment or synergistically with other blockades.

6.1 High-throughput RNAi screening for tumor-restricted immune checkpoints

The importance of immune checkpoint blockade for modern antitumor immunotherapy and cancer treatment in general drove the development of several high-throughput immune checkpoint discovery platforms. Bellucci and colleagues used an arrayed shRNA library (around 1000 genes) in multiple myeloma [237]. They measured IFN- γ secretion as a marker

of natural killer cell activity and found that JAK2 knockdown improved IFN- γ secretion. The group of Kai Wucherpfennig developed an elegant *in vivo* shRNA screening for negative regulators in tumor-infiltrating T cells [239]. OT-1 T cells were transduced with a pooled shRNA library and the abundance of enriched shRNAs was measured inside the tumor. Mainly genes involved in T cell resistance to the tumor microenvironment were enriched. Recently, Patel and colleagues performed a CRISPR/Cas screening for the identification of essential genes for cancer immunotherapy [298]. They used a lentiviral-based pooled library of 123,000 gRNA and transduced melanoma cells before co-culture with TCR-transduced primary human T cells. Genes identified for being essential for cancer immunotherapy have key roles in antigen presentation and the IFN- γ signaling. These findings correlated with loss-of-function mutations in cancer patients. All mentioned approaches give valuable information about pathways important for the interaction of tumor and immune cells but lack a focus on improvement of tumor-lysis. In our opinion, reduction of tumor burden by T cell-mediated lysis of tumor cells is the most important goal of antitumor immunotherapy and pathways preventing tumor killing are of uttermost importance. All mentioned screenings either focus on immune activators – genes necessary for tumor lysis/T cell function – or use cytokine secretion/T cell proliferation as a readout system. Recently, the group of Nicholas Haining developed a CRISPR/Cas *in vivo* screening for genes that synergize with or induce resistance to PD-1 checkpoint blockade in mice [299]. B16 melanoma was transduced with sgRNAs against 2,368 genes and transplanted into immune-competent or -deficient mice in combination with PD-1 therapy. This study resulted in the observation that the deletion of genes involved in antigen presentation, inhibition of kinase signaling, ubiquitin-proteasome pathway and NF- κ B activation sensitized melanoma to immunotherapy.

Our group developed a high-throughput RNAi screening to dissect pathways inhibiting T cell-mediated tumor lysis [240] in human cancer. This screening focused on HLA/TCR interaction independent lysis of breast cancer cells using a bispecific antibody to create an artificial immunological synapse. Later on, it was validated using survivin-specific T cells. In this thesis, the approach developed by Dr. Nisit Khandelwal was adopted and improved to resemble more closely the situation in cancer patients.

- The current study focused on melanoma as a tumor entity. Melanoma represents the perfect target for immune checkpoint blockade. On one hand, melanoma-derived tumors show a high level of TIL-infiltration. On the other hand, melanoma uses several

immune inhibitory pathways to prevent TIL-mediated tumor lysis. More importantly, blockade of PD-L1 and CTLA-4 have been shown to improve patient survival in melanoma proving the concept of immune checkpoint blockade (see paragraph 1.6.3 for details). From a technical point of view, it is possible to extract and expand TIL as well as tumor cultures *ex vivo* [18, 193]. This was a requirement for this study as high numbers of TILs were needed for the screening approach and the subsequent validations.

- The current study was performed with TILs instead of PBMCs or antigen-specific lymphocytes. TILs combined with patient-derived melanoma cultures closely resemble the situation in patients thus improving aforementioned approaches using artificial setups. TILs are highly exhausted and show functional impairment (see paragraph 1.4). Improvement of exhausted functionality and subsequent TIL-mediated tumor cell killing is the main goal of antitumor immunotherapy. Exhausted TILs express high levels of exhaustion markers (e.g., PD-1 and TIM-3) compared to PBMCs. These exhaustion markers in turn can function as receptors for inhibitory ligands (e.g., PD-L1/PD-1 axis) [300]. Therefore, highly exhausted TILs have the highest probability to express potential receptors for tumor-associated immune checkpoints identified by our screening approach.
- So far, our screening approaches were limited to a library of around 500 GPCRs. GPCRs are interesting targets because many are orphan receptors and for most of them no role in immune inhibition has been described. The long-term goal of our group is to screen all genes associated to the cell surface (surfaceome) for their potential role as immune checkpoints. Candidates derived from the surfaceome might directly mediate immune suppression by interaction with a receptor/ligand on the T cell. These pathways are perfect targets for antibody-mediated blockade. Here, we used two libraries enriched for genes associated with the surfaceome. In a first screening, we used a library of GPCRs and kinases. In the second screening, we used plates from Dharmacon's "whole-genome library" which were enriched for surfaceome genes. In total, we screened around 2800 genes (around 50% surfaceome) for their potential role as immune checkpoints.

6.2 Setup and performance of the high-throughput RNAi screen

Screening for novel immune checkpoints using our RNAi approach needs vigorous preparation due to the need to identify optimal level of TIL-mediated tumor lysis. The read-out of a cell-cell interaction can only be meaningful if the appropriate cells and controls have been set up. We tested several combinations of melanoma cells and TIL cultures for the RNAi screening. We identified the combination of M579-A2-luc melanoma cells and TIL412 as optimal for the screening. We generated M579-A2-luc cells which were altered to express HLA-A2 and luciferase. We optimized the siRNA transfection protocol and found RNAiMAX to have the best efficacy (see paragraph 5.1.2). We found that TIL412 are highly exhausted and can kill M579-A2-luc in an HLA-A2-dependent manner (see paragraph 5.1.3). Furthermore, killing of M579-A2-luc by TIL412 can be significantly improved by knockdown of known immune checkpoints (see paragraph 5.1.4). We identified PD-L1 and galectin-3 as positive controls for immune checkpoints. Knockdown of PD-L1 and to a lesser degree galectin-3 improved TIL-mediated lysis of M579-A2-luc without affecting viability. The knockdown of ubiquitin C (UBC) only partially killed melanoma cells. Therefore, we included the commercial siRNA pool “cell death” as an additional viability control. To exclude any effect of siRNAs and underlying processing mechanisms in the cells per se we chose “select negative control no. 2” as control siRNA. Lacking proper immune activator controls – genes essential for TIL-mediated tumor lysis – we used caspase-3. The knockdown of caspase-3 prevented killing of M579-A2-luc but might be representative of a decrease in general apoptosis [301], rather than reducing TIL functionality as expected from an immune activator.

The screen itself was run in two sets. Transfected tumor cells were co-cultured with TIL412 to measure cytotoxicity (set 1) or cultured without TILs to measure the general impact of gene knockdown on cell viability (set 2). Each set was used in duplicates. We ran two screenings: 1. GPCR/kinase library; 2. surfaceome enriched library. Here, only the first screening will be discussed but the performance of the second screening was comparable. The correlation between the two duplicates was robust (0.96 for cytotoxicity and 0.98 for viability, respectively) and the positive controls performed well (see paragraph 5.2). Unfortunately, the viability controls did not induce high levels of apoptosis. This was observed before and might be related to the melanoma intrinsic resistance towards apoptosis [302]. We included an additional “CellTiter-Glo” assay to exclude genes affecting cell viability. In this assay cytotoxicity is measured by ATP concentration in the tumor cells instead of target cell lysis [303]. After

normalization cytotoxicity scores were fitted to viability scores using local regression (LOESS). Additionally, genes scoring high in the CTG screen were excluded. Overall 48 candidate genes (75 with both primary screens) had a bigger impact on TIL-mediated tumor lysis than PD-L1 (paragraph 5.3 and **Supplementary figure 2**). Interestingly, knockdown of around 50 genes abrogated tumor killing more than caspase-3. Among genes increasing TIL-mediated lysis were members of the phosphatidylinositol 3-kinase family (PIK3C2G, PIK3CA) and interleukin-1 receptor associated kinase-2 (IRAK2). IRAK2 is a mediator of apoptosis via ER stress signaling [214]. The PI3K/Akt pathway is normally associated with the blockade of cell death [304] but it was shown that rapid elevation of intracellular calcium activated PI3K/Akt and induced apoptosis [305]. On the other hand, several recently described immune checkpoints were among the genes ranked higher than PD-L1. As mentioned, the kinases JAK1 and PRKD2 were shown to upregulate PD-L1 expression in response to IFN- γ [238, 249, 250]. The inhibitory role of colony stimulating factor-1 receptor (CSF1R) on T-Cell mediated melanoma therapy is associated with the function of TAMs [306] but CSF1R is also aberrantly expressed in melanoma cells [307]. Neuropeptide Y (NPY) has shown some anti-inflammatory effects. NPY induces a T_H2 polarization and impairs T cell proliferation [308, 309]. Melanoma cells might utilize NPY to impair the secretion of antitumor T_H1 cytokines and proliferation of TILs. The kinases tau tubulin kinase 2 (TTBK2) and acylglycerol kinase (AGK) are known to prevent apoptosis in cancer and might play a general role in tumor resistance to therapy [310, 311]. Interestingly, some candidate kinases impair apoptosis induced by pathways directly associated with T cell function. Cyclin-dependent kinase 9 (CDK9) was found to be responsible for TRAIL resistance in cancer [312]. Overexpression of inositol-pentakisphosphate 2-kinase (IPPK) prevent the induction of TNF- and Fas-induced apoptosis in HEK293 [313]. Additionally, our group recently discovered that salt-inducible kinase 3 (SIK3) shifts the PDAC and melanoma response to TIL-secreted TNF from apoptosis to proliferation [Dr. Antonio Sorrentino, manuscript in preparation]. Finally, C-C motif chemokine receptor 9 (CCR9) was identified as an immune checkpoint in breast cancer and melanoma [240]. In summary, several genes known to inhibit TIL function and/or prevent TIL-mediated tumor lysis were among the candidate genes from the primary melanoma RNAi screening. Other genes seem to be important for the improvement of TIL-mediated tumor killing (immune activators). Our laboratory is adopting the high-throughput screening approach to autoimmune diseases model (Ayse Nur Menevse). Multiple sclerosis (MS) is a severe autoimmune disease of the brain and involves the attack of oligodendrocytes by antigen-specific CD8⁺ T cells [314, 315]. We will use this screen to identify

genes increasing T cell-mediated killing of oligodendrocytes as potential candidates for the fight against MS. Furthermore, we will analyze the loss-of-function of identified immune checkpoints in this autoimmune disease.

High-throughput RNAi screenings are prone to produce false positive hits due to off-target effects compromising any detectable phenotypic consequences from unintended interactions (dependent and independent from the nucleotide sequence). Echeverri and colleagues argue that the uniqueness of a reported RNAi phenotype is crucial for the number of false positive hits [252]. This factor is difficult to determine in our screening approach in particular due to cell-cell interactions. On one hand, TIL-mediated tumor lysis is a reasonable specific unique phenotype. On the other hand, TILs can use several mechanisms (some might still be unknown) to kill melanoma cells. We therefore conducted a secondary screening with an enriched library (48 candidates derived from the first primary screening). Around 28% of the candidates did not show the expected immune checkpoint phenotype as tested by the luciferase-based killing assay. We included effector cytokine secretion (TNF, IL-2 and IFN- γ) as an additional marker for immune checkpoint discovery. This allows distinguishing between genes affecting melanoma susceptibility towards TIL-mediated lysis from genes altering the functionality of TILs. Furthermore, this allows probing of the phenotype in an independent way revealing genes of particular relevance [228]. Genes, which impair cytokine secretion, are likely to alter T cell signaling and therefore interesting targets for immune checkpoint blockade. In the future, one could include a setting with the addition of supernatant from stimulated TILs (e.g., CD3/CD28 beads) in order to identify genes desensitizing tumor cells towards soluble effector molecules (e.g., TNF). Reduced luciferase intensity would correlate with the ability of an effector molecule to induce apoptosis. This might become important in cases of acquired resistance to cancer immunotherapy [316]. Additionally, to the secondary screening we used extensive validation to exclude false positives and identify real immune checkpoints.

6.3 The immune checkpoint repertoire of cancer

So far, our lab performed high-throughput RNAi screenings in several tumor entities. Dr. Nisit Khandewal established the screening approach using a GPCR siRNA library in breast cancer combined with antigen-specific and -unspecific T cell sources. This thesis described the screening in patient-derived melanoma in conjunction with antigen-specific TILs. Afterwards similar screenings have been adopted to PDAC (performed by Dr. Antonio Sorrentino) and

multiple myeloma (performed by Valentina Volpin). Both screenings used the same library as the melanoma screen. Recently, we generated a new library covering the whole “surfaceome” together with known immune checkpoints. We screened lung cancer for novel immune checkpoints using this library (performed by Dr. Anchana Rathinasamy). Due to the differences in T cell sources and libraries only the results from melanoma, PDAC and multiple myeloma can be directly compared. We found little overlap between the hematological disease (multiple myeloma) and the solid tumors (**Figure 16**). Nevertheless, there was a considerable overlap in the immune checkpoint repertoire of melanoma and PDAC. Among the genes utilized by both tumor entities to avoid destruction by the immune system were JAK2, SIK3 and CCR9. The only candidate overlapping in all three screenings was regulator of G protein signaling 14 (RGS14). Noteworthy, different members of a gene family class could be found as targets in different entities. For example, the two calcium/calmodulin-dependent protein kinase 1 family members alpha (CAMK1) and delta (CAMK1D) were found to be candidates in melanoma and multiple myeloma, respectively. Expression analysis revealed that CAMK1 is expressed in melanoma but not in multiple myeloma and the other way around for CAMK1D (work of Valentina Volpin). We therefore assume that two family members exert similar functions in different tumor entities. Members of certain larger gene families (e.g., olfactory receptors) were found in all screenings (including breast cancer and lung cancer). This suggests that the underlying pathways leading to TIL inhibition or abrogation of TIL-mediated lysis are related. Pathway analysis revealed that melanoma-derived candidates are enriched in (G α _s/cAMP/PKA-signaling. Therefore, we aimed to dissect the role of this pathway on TIL inhibition. In summary, we found that the repertoire of immune checkpoint is tumor entity-restricted. Nonetheless, the underlying modes of action might be similar.

After selection from the primary and secondary screening we chose interesting candidates for further validation by their novelty, differential expression and their potential drugability. As mentioned, several genes identified by our screening are known to play a role in tumor immune escape. We focused on genes which were not associated with immune escape so far. We looked for a potential differential expression (tumor vs. normal tissue) of candidate genes using databases for gene expression (e.g., TCGA). Systematic expression of an immune checkpoint in healthy tissue can lead to severe immune-mediated side effects upon antibody blockade (see paragraph 1.6.3). Furthermore, candidate genes should not play a pivotal role in cellular functions beside their impact on immune responses. Finally, we aimed to generate a platform

to discover immune checkpoints that can be targets for a therapeutic intervention. Therefore, our candidates should be potentially drugable. For example, kinases can be targeted with small molecules whereas cell surface receptors/ligands can be blocked by antibodies.

The first step of any target validation is the exclusion of potential off-target effects of the siRNA used in the RNAi screening. There are several ways on how a given siRNA sequence can have an effect on an un-related mRNA (off-target) [317]. Particularly, sequence similarities in the so called “seed sequence” (2nd to 7/8th nucleotide of the siRNA) can lead to binding of the siRNAs to several unrelated mRNAs. The usage of several non-overlapping siRNA sequences reduces the risk of measuring off-target effects [252]. The library of our RNAi screening was optimized to avoid off-target effects [318]. The siRNAs against each target were delivered as a pool of four non-overlapping sequences in each well. This approach should maximize knockdown efficacy and reduce dose-dependent off-target effects at the same time [319]. After candidate selection, siRNA pools need to be “deconvoluted” as a first step of target validation. Candidates were considered for functional and mode of action analysis only if at least two non-overlapping siRNAs (from the pool) show on-target effects. The most interesting targets were validated using deconvoluted siRNAs. Knockdown was confirmed by RT-PCR/qPCR and the functional phenotype by luciferase-based cytotoxicity assay. Several genes dropped out in this early stage of validation due to strong off-target effects of single siRNA sequences. Genes which passed this step were further validated. This thesis focuses on one particular target: olfactory receptor family 10 subfamily H member 1 (OR10H1).

6.4 OR10H1 as an immune checkpoint in cancer

6.4.1 Olfactory receptors outside of olfactory neurons

Olfactory receptors are members of the seven transmembrane G protein-coupled receptor (GPCR) class A (rhodopsin-like) [320]. They sense the chemical environment and can be distinguished by the chemostimuli to which they respond. Olfactory receptors signal mainly via a unique G protein-coupled adenylyl cyclase cascade [321-323]. Subsequently, cAMP is the key messenger of olfactory G protein signaling [321, 324-326]. Olfactory signaling leads to cAMP production by adenylyl cyclase type III (ADYC3) [327, 328]. ADYC3 in turn is activated by the olfactory-restricted G protein alpha subunit $G\alpha_{\text{Olf}}$ [329, 330]. It was shown that olfactory receptors can couple *in vitro* to $G\alpha_s$ and $G\alpha_{15}$ G proteins [331], which might alter the specificity

of the receptor [332]. Furthermore, olfactory receptors can signal via other mechanisms. Olfactory receptor activation leads to production of cGMP, opens cyclic nucleotide-gated channels (CNC) by cAMP and cGMP, stimulates the production of Inositol-1,4,5-trisphosphate (IP₃) and increases influx of calcium (reviewed by *Ronnet et al.*) [333].

Olfactory receptors are a highly divergent group of receptors ranging in a length of 300-350 amino acids, depending on the length of the N- and C-terminal stretches. They are coded by single coding-exon genes, but exons in the 5' untranslated region may undergo alternative splicing [334-336]. Due to a high number of degenerated pseudogenes only about 390 human functional OR genes are known (compared to 855 OR genes in total) [337-339]. Human ORs are organized in 18 families (sequence similarity >40%) and around 300 subfamilies (similarity >60%) [339-341]. As mentioned before, ORs contain seven hydrophobic membrane-spanning domains and belong to the GPCR class A. Several characteristic conserved amino acids motifs distinguish ORs from other GPCRs (e.g., extracellular NXS/T consensus for N-linked glycosylation) [342, 343]. Interestingly, published data suggest that the transmembrane domains (e.g., amino acids in TM3, TM5 and TM6) are essential for the specificity of odorant binding pockets (reviewed by *Fleischer et al.*) [343].

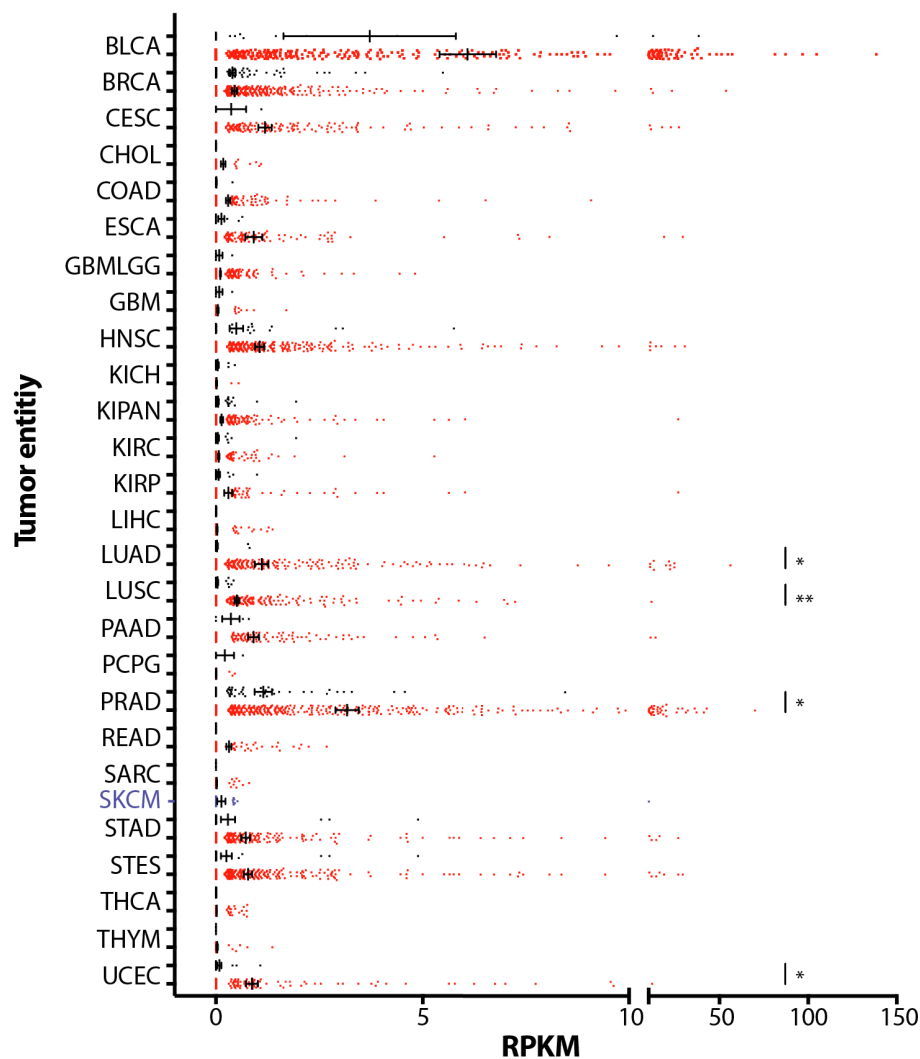
The olfactory receptor family 10 contains 29 subfamilies and the subfamily H consists of five functional OR genes (no pseudogenes) [339]. Olfactory receptor family 10 subfamily H member 1 (OR10H1), is also known as AC004510, OR19-27, HSOR19.4.4, ORL733, ORL525. The OR10H1 gene (on chromosome 19: 15,807,003-15,808,126) is 1124 base pairs long and codes for a protein of 318 amino acids [344, 345]. OR10H1 has two paralogous OR10H2 (89.6% similarity) and OR10H5 (93.6% similarity) [346].

The role of olfactory receptors outside the olfactory system is relatively unknown but recent literature suggest that they can function as chemosensory receptors in other tissues [347]. Olfactory receptors are expressed in and associated with many tumors [348-352]. OR15E2 was found in melanocytes and its stimulation with β -ionone leads to melanogenesis and dendritogenesis via calcium and cAMP signaling [243]. Recently, it was shown that OR51E2 is overexpressed in melanoma [352]. Interestingly, OR10H1/5 was among the olfactory receptors that were found to be expressed in melanocytes.

We validated expression of OR10H1 in RNA-Seq data from around 11,500 tumor samples from 36 tumor entities (TCGA; doi:10.7908/C11G0KM9) using TCGA2STAT for R [353]. In

Figure 35A, OR10H1 expression values (RPKM) from different tumor entities and the respective healthy tissue are shown. For skin cutaneous melanoma (SKCM), no healthy control tissue was available. Overall, OR10H1 was weakly expressed in many tumor entities. The highest levels of OR10H1 expression were found in bladder urothelial carcinoma (BLCA) and prostate adenocarcinoma (PRAD). In general, subsets of cancer patients show expression of OR10H1 whereas others do not show any expression. OR10H1 is significantly overexpressed in lung adenocarcinoma (LUAD), lung squamous cell carcinoma (LUSC), PRAD and uterine corpus endometrial carcinoma (UCEC). We found that OR10H1 expression levels correlated with patient survival in pancreatic adenocarcinoma (PAAD or PDAC). Patients with high expression of OR10H1 had a worse survival probability (non-significant; $p = 0.061$) than patients with low expression (**Figure 35B**). The expression patterns of OR10H1 made it an interesting candidate for further validation.

A



B

OR10H1 correlation with patient survival (PDAC)

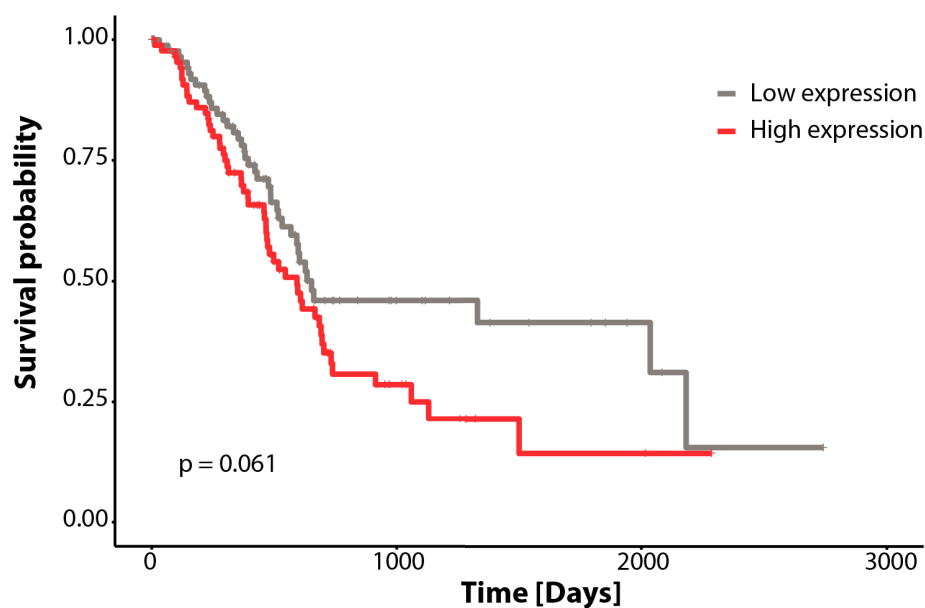


Figure 35: OR10H1 is expressed in different tumor entities. **A.** Subsets of tumor samples express OR10H1. TCGA data was imported using TCGA2STAT for R and RPKM values of OR10H1 expressed in tumor (indicated in red) were compared to healthy tissues (except SKCM, indicated in blue). Tumor entities were: Bladder urothelial carcinoma (BLCA), Breast invasive carcinoma (BRCA), Cervical and endocervical cancers (CESC), Cholangiocarcinoma (CHOL), Colon adenocarcinoma (COAD), Esophageal carcinoma (ESCA), Glioblastoma multiforme (GBM), Glioma (GBMLGG), Head and Neck squamous cell carcinoma (HNSC), Kidney Chromophobe (KICH), Pan-kidney cohort (KIPAN), Kidney renal clear cell carcinoma (KIRC), Kidney renal papillary cell carcinoma (KIRP), Liver hepatocellular carcinoma (LIHC), Lung adenocarcinoma (LUAD), Lung squamous cell carcinoma (LUSC), Pancreatic adenocarcinoma (PAAD), Pheochromocytoma and Paranglioma (PCPG), Prostate adenocarcinoma (PRAD), Rectum adenocarcinoma (READ), Sarcoma (SARC), Skin Cutaneous Melanoma (SKCM), Stomach adenocarcinoma (STAD), Stomach and Esophageal carcinoma (STES), Thyroid carcinoma (THCA), Thymoma (THYM) and Uterine Corpus Endometrial Carcinoma (UCEC). Error bars denote \pm SEM, and statistical significance was calculated (compared to the respective healthy tissue) using unpaired, two-tailed Student's t-test with * $p \leq 0.05$; ** $p \leq 0.01$. **B.** Correlation of OR10H1 expression and patient survival in PAAD. Patients were divided into high and low expression groups by the median of OR10H1 expression. The clinical data provided by TCGA (death status, overall survival) was used to draw a Kaplan-Meier curve using the survival package for R [354]. Significance was calculated using the log-rank test.

6.4.2 OR10H1 prevents tumor lysis by inhibiting TIL function

OR10H1 was the 16th candidate in the primary and 4th in the secondary screening of melanoma as well as one of the top candidates in the PDAC screen. Furthermore, we found that the knockdown of OR10H1 increased T cell-mediated lysis of oligodendrocytes in a RNAi screening for multiple sclerosis (performed by Ayse Nur Menevse, RCI). OR10H1 was expressed in several tumor cell lines. As expected, this olfactory receptor expression was weak and the RT-PCR protocols had to be modified for low abundance genes [243]. We sequenced the PCR products to validate OR10H1 specificity of the primers [data not shown]. Unfortunately, the primers generated against OR10H1 could not distinguish between the close family members OR10H1 and OR10H5. In the meantime, OR10H1-specific expression assays were generated by iOmx Therapeutics and confirmed the expression of this particular gene in melanoma. We could show that at least three different siRNA sequences reduced OR10H1 expression and dramatically increased TIL-mediated tumor lysis of melanoma, PDAC and colorectal cancer (**Figure 18-20**). This effect was independent of a particular T cell source as it could be reproduced with different TIL cultures as well as PBMC-derived flu-specific CD8⁺ T cells. On the other hand, OR10H1 inhibition of TIL-mediated tumor lysis requires activation of T cells via the MHC-peptide complex. Xenograft mouse model experiments together with adoptive cell transfer of TILs confirmed the role of OR10H1 as an inhibitor of tumor lysis *in vivo* (see paragraph 5.6).

Our experiments showed that OR10H1 proficient tumor cells prevent TIL-mediated lysis. As explained in the introduction there are several ways in which tumor cells can evade destruction by the immune system (paragraph 1.5). In the context of tumor cell-TIL co-culture, candidate

genes could either mediate resistance towards TIL-mediated killing or inhibit TIL activation/functionality. We validated the function of OR10H1 by assessing several factors of TIL functionality during co-culture with tumor cells. As expected from the secondary screening, co-culture with OR10H1 proficient cells reduced type I effector cytokine secretion of TILs (paragraph 5.7). The recovery of effector cytokine secretion after co-culture with OR10H1-deficient melanoma cells (compared to proficient) indicates a less exhausted phenotype of TILs [355]. Additionally, OR10H1 induces higher levels of apoptosis in TILs after co-culture. Our data suggest that OR10H1 actively impairs T cell function and induces a more exhausted phenotype.

6.4.3 OR10H1 impairs TCR signaling via PKA-mediated Lck inhibition

In this study, it was shown that a signaling cascade involving PKA, CREB, Csk and Lck (on the T cell side) leads to OR10H1-mediated inhibition of TIL functionality. We found that TILs differentially express genes depending on the presence of OR10H1 on the tumor cells. TILs co-cultured with OR10H1-deficient cells showed a gene expression profile associated with increased T cell function/viability and decreased anergy (see paragraph 5.8). This differential gene expression was associated with TCR-mediated signaling. In depth phosphoprotein analysis revealed that CREB, PKA and Lck are differentially activated in TILs when co-cultured with OR10H1-deficient or –proficient cells. CREB is an important transcription factor in T cells inducing the expression of different effector cytokines [356]. Noteworthy, most studies on the role of CREB on effector cytokine secretion of T cells were performed using PBMCs or T cell hybridomas and did not focus on its role in TILs with exhausted memory phenotype. Furthermore, several transcription factors (including CREB) work together to induce cytokine production [357-359]. We found that CREB is strongly activated in TIL412 after 2-hour co-culture with OR10H1-proficient melanoma cells (paragraph 5.9) compared to unchallenged (unstimulated) TIL412. This strong induction of CREB phosphorylation was not observed in TILs co-cultured with OR10H1-deficient melanoma. CREB activation in T cells is mainly regulated by phosphorylation of the serine133 by protein kinases C (PKC) and/or A (PKA) [356]. As mentioned before, several groups described an inhibitory pathway in T cells involving cAMP-mediated activation of PKA and subsequent phosphorylation of the inhibitory tyrosine 505 of Lck. We were able to validate that Lck is less phosphorylated on this inhibitory domain when TILs are co-cultured with OR10H1-deficient melanoma. This phosphorylation pattern was similar to TILs stimulated with PMA/Iono. Furthermore, TILs co-cultured with OR10H1-

proficient melanoma were sensitive to a Lck inhibitor (7-Cyclopentyl-5-(4-phenoxyphenyl)-7H-pyrrolo[2,3-d]pyrimidin-4-ylamine) which shows a higher inhibition to the inactive (Tyr505 phosphorylated) form of Lck [282]. Our data suggest, that tumor-associated OR10H1 inhibits TCR-mediated activation of Lck via a pathway involving cAMP-activated PKA. This inhibition of Lck induces a more exhausted T cell state and impairs T cell functionality.

6.4.4 Tumor-associated OR10H1 activation leads to the transport of cAMP via gap junctions

As mentioned, the cAMP-mediated activation of PKA in TILs could either be the result of ligand binding to TIL-restricted receptors and subsequent AC activation [284-286] or the result of cAMP transport via gap junctions [118, 279]. We hypothesized that OR10H1-mediated inhibition of TILs utilizes the transport of cAMP through gap junction as CX32 was one of the strongest candidate genes from our follow-up primary screen in melanoma. CX32 is expressed by melanoma and CRC whereas CX43 is expressed by PDAC and multiple myeloma. Furthermore, we found that TILs express CX32 as well. Transport of cAMP into T cells is normally associated with gap junctions build up by CX43. The role of CX32 in cAMP transport needed to be elucidated. Validation experiments underlined the immune checkpoint function of CX32 (see paragraph 5.10). Furthermore, blockade of CX32 hemichannels or gap junctions increased TIL-mediated lysis of OR10H1-proficient but not -deficient melanoma cells suggesting that OR10H1 and CX32 function on the same inhibitory pathway. Interestingly, CX32 and other gap junction proteins can be phosphorylated by cAMP-activated PKA increasing gap junction permeability [360]. Thus, increased cAMP concentrations inside melanoma cells can activate PKA which in turn could phosphorylate connexins increasing the flux of cAMP into TILs and inhibiting their function. As mentioned, olfactory receptors are associated with an olfactory machinery including $G\alpha_{\text{Olf}}$ (GNAL) and adenylylate cyclase 3 (ADCY3). We found that this olfactory machinery is expressed in melanoma, PDAC and CRC but not in breast cancer. Consistently, an immune inhibitory function of OR10H1 was not found in our screening with MCF-7 [240]. We assessed OR10H1-associated signaling in tumor cells upon TIL encounter by validating calcium and cAMP activity. Surprisingly, OR10H1-deficient melanoma cells showed dramatically increased calcium signaling waves compared to OR10H1-proficient cells. Inside olfactory neurons, activation of olfactory receptors induces cAMP production which opens cAMP-gated ion channels for calcium increasing its intracellular concentration [294]. Therefore, the observed increase in cytoplasmic calcium after

OR10H1 knockdown might be independent from this pathway. T cells could induce calcium signaling inside tumor cells independent from olfactory signaling. For example, granzyme B (secreted by T cells) induces neurotoxicity by activation of protease-activated receptor-1 (PAR1) and subsequent IP3-associated calcium signaling [361]. OR10H1-mediated activation of PKA could inhibit PLC function and thus decrease calcium flux into the cytoplasm [362, 363]. Increased calcium signaling inside tumor cells could be a sign of improved TIL functionality as well. The combined function of perforin and granzyme B counteracted by cell membrane repair mechanisms was shown to induce fluctuating calcium waves inside the target cell [364]. We did not observe any calcium signaling inside melanoma cells upon treatment with the supernatant from activated (anti-CD3/CD8 beads) T cells. This might be dependent on the concentration of perforin and granzyme B or the necessary proximity of T cell and target cell. The outcome of different calcium waves inside tumor cells upon TIL encounter are an interesting topic for further investigations. In this study, we focused on the production of cAMP inside tumor cells during interactions with TILs. We detected induction of cAMP production in tumor cells during co-culture with TILs. This cAMP production was decreased in OR10H1-deficient cells. Additional functional assays with cholera toxin (activation of $G\alpha_{olf/s}$) confirmed the role of OR10H1 in cAMP-mediated inhibition of TIL functionality. Activation of $G\alpha_{olf/s}$ rescued OR10H1-deficient cells from TIL-mediated lysis. Interestingly, inhibition of $G\alpha_i$ with cholera toxin reduced killing of OR10H1-proficient but not -deficient cells. As mentioned, $G\alpha_i$ inhibits the activation of adenylate cyclase. In the absence of OR10H1-mediated adenylate cyclase activation the inhibition of $G\alpha_i$ does not rescue melanoma cells. Our data suggest that tumor-associated OR10H1 induces cAMP production via $G\alpha_{olf/s}$ upon TIL encounter. Unfortunately, the ligand for OR10H1 remains unknown. One could use fractions of T cell-primed supernatants for their induction of cAMP in OR10H1-positive cells. Deciphering the ligand repertoire of OR10H1 would help to uncover its immune inhibitory function. The suggested OR10H1 mode of action is depicted in **Figure 36**.

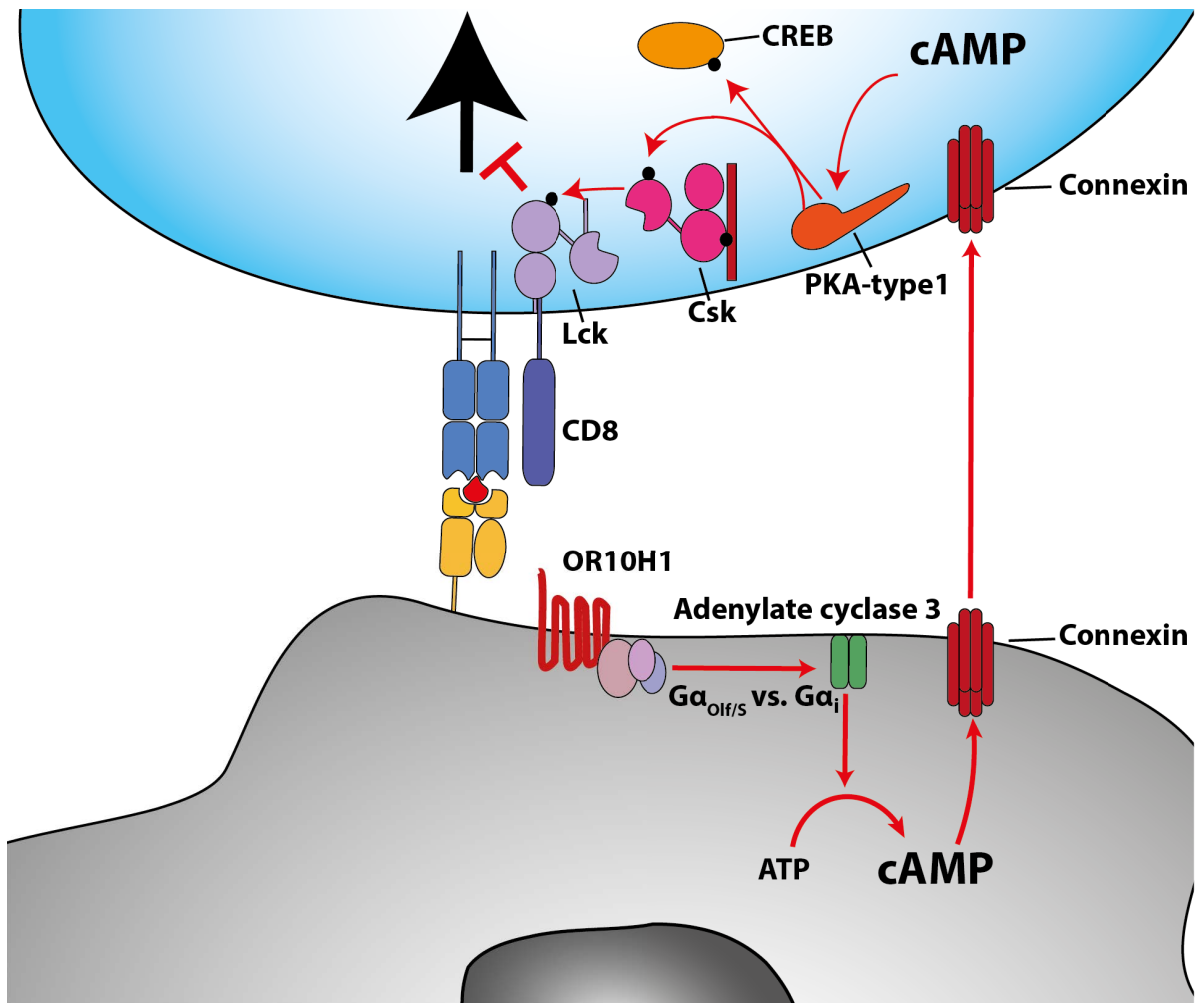


Figure 36: Proposed mode of action for OR10H1-mediated inhibition of CD8⁺ TIL functionality. T cell recognition of tumor cells results in TCR-mediated activation of Lck and subsequent killing of the target cell. Binding of an unknown ligand to the olfactory receptor OR10H1 induces the dissociation of $G\alpha_{olf/s}$ from the trimeric G-protein complex. $G\alpha_{olf/s}$ activates adenylate cyclase 3 increasing cAMP concentration. Potentially, cAMP activates tumor-associated PKA which in turn phosphorylates CX32 and increased permeability. cAMP diffuses through CX32 gap junctions into CD8⁺ TILs and activates TIL-associated PKA. PKA phosphorylates/activates Csk and CREB. The transcription factor CREB induces gene expression associated with an exhausted TIL phenotype. Csk phosphorylates Lck at an inhibitory tyrosine residue and thus abrogates TCR-mediated signaling.

6.5 Translational implications of OR10H1 as a target for cancer immunotherapy

The main task of this project was the discovery of novel immune checkpoints as targets for cancer immunotherapy. We established a high-throughput discovery platform and identified OR10H1 as a potential target for immunotherapeutic interventions in melanoma and other cancers.

6.5.1 Anti-OR10H1 therapy as monotherapy

Olfactory receptors in general and OR10H1 in particular are interesting targets as no important role outside the olfactory system was found so far. Thus, inhibition of these receptors could offer improved TIL-mediated tumor lysis without the strong side effects observed with anti-CTLA-4 therapy (see paragraph 1.6.3). On the other hand, olfactory signaling might have a yet unknown role in healthy tissues. For example, OR51E2 was found to regulate melanogenesis and dendritogenesis in melanocytes [243]. Therefore, any therapy directed against olfactory receptors has to be carefully evaluated regarding its effects on healthy tissue. Another important factor to be considered for OR10H1 therapy is the development of biomarkers to stratify patients for therapy. As seen in **Figure 35**, OR10H1 expression can be detected in different tumor entities but OR10H1 abundance is low. In general, patient stratification based on target gene expression showed poor prediction of the outcome of immune checkpoint blockade [365]. Biomarkers for anti-OR10H1 therapy could be based on a mixture of immune cell infiltration and expression of the olfactory machinery (e.g., GNAL and ADCY3). Olfactory receptors are difficult targets for drug development due to their complicated conformational structure. Promising approaches to target olfactory receptors are blocking antibodies [366] and small molecule inhibitors [367, 368]. Both approaches are currently tested to produce inhibitory compounds directed against OR10H1. Despite the hurdles, OR10H1 remains an interesting target for immune checkpoint blockade particularly in tumor entities where anti-CTLA or anti-PD-1/PD-L1 therapies fail.

6.5.2 Anti-OR10H1 therapy combined with other immune checkpoint blockades

Most researchers agree that the combination of different immunotherapies in general and the combination of immune checkpoint blockades in particular is the best way to treat most cancers in the future. Many different combination therapies (mostly anti-CTLA-4 combined with anti-PD-1/PD-L1) are being tested in the clinic and show superior outcome compared to monotherapies (see paragraph 1.6.3). Combination of therapies directed against OR10H1 with anti-PD-1/PD-L1 or anti-CTLA-4 could offer great improvement of cancer immunotherapy. As mentioned, PD-L1 binding to PD-1 recruits the phosphatase SHP2 which in turn dephosphorylates/inhibits nodes of TCR-mediated and costimulatory signaling [142-144] whereas OR10H1 function results in deactivation of Lck by Csk. Therefore, combination therapy could improve TIL functionality by increasing Lck activity and further prevent the

inhibitory function of PD-1-mediated SHP2. Supporting this hypothesis, recent findings underline the interactions of Lck activity and PD-1/SHP2-mediated dephosphorylation of TCR-mediated and costimulatory signaling [369]. Interestingly, the presence of Csk increased the inhibitory function of PD-1/SHP2. Therefore, a double intervention against OR10H1 and PD-1/PD-L1 could result in more active and less exhausted TILs with stronger antitumor activity.

7 Conclusion

Immune checkpoint blockade is a promising approach to fight many different cancer types. Unfortunately, only a fraction of patients can benefit from current therapies due to the numerous immune inhibitory mechanisms employed by the tumor and its immune inhibitory microenvironment. In this study, we aimed to generate a high-throughput discovery platform to identify novel immune checkpoints as targets for immune checkpoint blockade. We established the screening procedure in melanoma using patient-derived tumor and TIL cultures. We found melanoma to be optimal to establish the RNAi screening and subsequent target validation. Interestingly, the overlap with other screening in other tumor entities was limited underlining the heterogeneity of the immune interactions between TILs and tumor cells among different entities. This cancer-specific repertoire of immune checkpoints highlights the challenges of current immunotherapy and cancer therapy in general.

We discovered a broad spectrum of different pathways as potentially involved in the inhibition of TIL-mediated tumor lysis. Among the genes identified as potential immune checkpoints were kinases, gap junction proteins and GPCRs. In this regard, olfactory signaling is a particularly interesting pathway as it was never associated with immune function before. Overall, the diversity of candidates discovered by our screenings could explain why only a small fraction of patients respond to current immune checkpoint blockade. The majority of immune escape mechanisms might still be unknown.

We found that OR10H1 inhibits TIL functionality by a mode of action involving cAMP-mediated activation of PKA and subsequent inhibition of Lck. OR10H1 and its associated pathway offer an interesting target for intervention with blocking antibodies or small molecule inhibitors. Based on the differences in the modes of action of OR10H1 and PD-L1/PD-1 a combination therapy might offer a great improvement compared to monotherapies currently used in cancer immunotherapy.

8 References

1. Gabriel, J., *What is Cancer?*, in *The Biology of Cancer*. 2007, John Wiley & Sons Ltd. p. 3-9.
2. Stewart, B.W. and C.P. Wild, *World Cancer Report 2014*, I.A.f.R.o. Cancer, Editor. 2014: Lyon, France.
3. American Cancer Society. *American Cancer Society: Cancer Facts and Figures 2016*. 2016 [cited 2017 22.06.2017]; Available from: <https://www.cancer.org/content/dam/cancer-org/research/cancer-facts-and-statistics/annual-cancer-facts-and-figures/2016/cancer-facts-and-figures-2016.pdf>.
4. Hanahan, D. and R.A. Weinberg, *The hallmarks of cancer*. *Cell*, 2000. **100**(1): p. 57-70.
5. Quail, D.F. and J.A. Joyce, *Microenvironmental regulation of tumor progression and metastasis*. *Nat Med*, 2013. **19**(11): p. 1423-37.
6. Hanahan, D. and R.A. Weinberg, *Hallmarks of cancer: the next generation*. *Cell*, 2011. **144**(5): p. 646-74.
7. Burnet, F.M., *The concept of immunological surveillance*. *Prog Exp Tumor Res*, 1970. **13**: p. 1-27.
8. Clemente, C.G., et al., *Prognostic value of tumor infiltrating lymphocytes in the vertical growth phase of primary cutaneous melanoma*. *Cancer*, 1996. **77**(7): p. 1303-10.
9. Galon, J., et al., *Type, density, and location of immune cells within human colorectal tumors predict clinical outcome*. *Science*, 2006. **313**(5795): p. 1960-4.
10. van Houdt, I.S., et al., *Favorable outcome in clinically stage II melanoma patients is associated with the presence of activated tumor infiltrating T-lymphocytes and preserved MHC class I antigen expression*. *Int J Cancer*, 2008. **123**(3): p. 609-15.
11. Sato, E., et al., *Intraepithelial CD8+ tumor-infiltrating lymphocytes and a high CD8+/regulatory T cell ratio are associated with favorable prognosis in ovarian cancer*. *Proc Natl Acad Sci U S A*, 2005. **102**(51): p. 18538-43.
12. Coulie, P.G., et al., *Tumour antigens recognized by T lymphocytes: at the core of cancer immunotherapy*. *Nat Rev Cancer*, 2014. **14**(2): p. 135-46.
13. Robbins, P.F., et al., *Mining exomic sequencing data to identify mutated antigens recognized by adoptively transferred tumor-reactive T cells*. *Nat Med*, 2013. **19**(6): p. 747-52.
14. van Rooij, N., et al., *Tumor exome analysis reveals neoantigen-specific T-cell reactivity in an ipilimumab-responsive melanoma*. *J Clin Oncol*, 2013. **31**(32): p. e439-42.
15. Ferguson, T.A., J. Choi, and D.R. Green, *Armed response: how dying cells influence T-cell functions*. *Immunol Rev*, 2011. **241**(1): p. 77-88.
16. Franciszewicz, K., et al., *Role of chemokines and chemokine receptors in shaping the effector phase of the antitumor immune response*. *Cancer Res*, 2012. **72**(24): p. 6325-32.
17. Chen, D.S. and I. Mellman, *Oncology meets immunology: the cancer-immunity cycle*. *Immunity*, 2013. **39**(1): p. 1-10.
18. Dudley, M.E. and S.A. Rosenberg, *Adoptive-cell-transfer therapy for the treatment of patients with cancer*. *Nat Rev Cancer*, 2003. **3**(9): p. 666-75.
19. Dunn, G.P., et al., *Cancer immunoediting: from immunosurveillance to tumor escape*. *Nat Immunol*, 2002. **3**(11): p. 991-8.
20. Mittal, D., et al., *New insights into cancer immunoediting and its three component phases—elimination, equilibrium and escape*. *Curr Opin Immunol*, 2014. **27**: p. 16-25.
21. Beatty, G.L. and W.L. Gladney, *Immune escape mechanisms as a guide for cancer immunotherapy*. *Clin Cancer Res*, 2015. **21**(4): p. 687-92.

22. Shankaran, V., et al., *IFN[gamma] and lymphocytes prevent primary tumour development and shape tumour immunogenicity*. *Nature*, 2001. **410**(6832): p. 1107-1111.
23. Dudley, M.E., et al., *Cancer regression and autoimmunity in patients after clonal repopulation with antitumor lymphocytes*. *Science*, 2002. **298**(5594): p. 850-4.
24. Dudley, M.E., et al., *CD8+ enriched "young" tumor infiltrating lymphocytes can mediate regression of metastatic melanoma*. *Clin Cancer Res*, 2010. **16**(24): p. 6122-31.
25. Djenidi, F., et al., *CD8+CD103+ tumor-infiltrating lymphocytes are tumor-specific tissue-resident memory T cells and a prognostic factor for survival in lung cancer patients*. *J Immunol*, 2015. **194**(7): p. 3475-86.
26. Mahmoud, S.M., et al., *Tumor-infiltrating CD8+ lymphocytes predict clinical outcome in breast cancer*. *J Clin Oncol*, 2011. **29**(15): p. 1949-55.
27. Reiser, J. and A. Banerjee, *Effector, Memory, and Dysfunctional CD8(+) T Cell Fates in the Antitumor Immune Response*. *J Immunol Res*, 2016. **2016**: p. 8941260.
28. Thompson, E.D., et al., *Tumor masses support naive T cell infiltration, activation, and differentiation into effectors*. *J Exp Med*, 2010. **207**(8): p. 1791-804.
29. Wolkers, M.C., et al., *Redundancy of Direct Priming and Cross-Priming in Tumor-Specific CD8+ T Cell Responses*. *The Journal of Immunology*, 2001. **167**(7): p. 3577-3584.
30. Kalia, V., et al., *Prolonged interleukin-2Ralpha expression on virus-specific CD8+ T cells favors terminal-effector differentiation in vivo*. *Immunity*, 2010. **32**(1): p. 91-103.
31. Pipkin, M.E., et al., *Interleukin-2 and inflammation induce distinct transcriptional programs that promote the differentiation of effector cytolytic T cells*. *Immunity*, 2010. **32**(1): p. 79-90.
32. Usharauli, D. and T. Kamala, *Brief antigenic stimulation generates effector CD8 T cells with low cytotoxic activity and high IL-2 production*. *J Immunol*, 2008. **180**(7): p. 4507-13.
33. Andersen, M.H., et al., *Cytotoxic T cells*. *J Invest Dermatol*, 2006. **126**(1): p. 32-41.
34. Voskoboinik, I., J.C. Whisstock, and J.A. Trapani, *Perforin and granzymes: function, dysfunction and human pathology*. *Nat Rev Immunol*, 2015. **15**(6): p. 388-400.
35. Weant, A.E., et al., *Apoptosis regulators Bim and Fas function concurrently to control autoimmunity and CD8+ T cell contraction*. *Immunity*, 2008. **28**(2): p. 218-30.
36. Wojciechowski, S., et al., *Bim/Bcl-2 balance is critical for maintaining naive and memory T cell homeostasis*. *J Exp Med*, 2007. **204**(7): p. 1665-75.
37. Hughes, P.D., et al., *Apoptosis regulators Fas and Bim cooperate in shutdown of chronic immune responses and prevention of autoimmunity*. *Immunity*, 2008. **28**(2): p. 197-205.
38. Obar, J.J. and L. Lefrancois, *Memory CD8+ T cell differentiation*. *Ann N Y Acad Sci*, 2010. **1183**: p. 251-66.
39. Hamann, D., et al., *Phenotypic and functional separation of memory and effector human CD8+ T cells*. *J Exp Med*, 1997. **186**(9): p. 1407-18.
40. Sallusto, F., et al., *Two subsets of memory T lymphocytes with distinct homing potentials and effector functions*. *Nature*, 1999. **401**(6754): p. 708-12.
41. Lanzavecchia, A. and F. Sallusto, *Progressive differentiation and selection of the fittest in the immune response*. *Nat Rev Immunol*, 2002. **2**(12): p. 982-7.
42. Wherry, E.J., *T cell exhaustion*. *Nat Immunol*, 2011. **12**(6): p. 492-9.
43. Wherry, E.J. and M. Kurachi, *Molecular and cellular insights into T cell exhaustion*. *Nat Rev Immunol*, 2015. **15**(8): p. 486-99.
44. Wherry, E.J., et al., *Viral persistence alters CD8 T-cell immunodominance and tissue distribution and results in distinct stages of functional impairment*. *J Virol*, 2003. **77**(8): p. 4911-27.

45. Schietinger, A. and P.D. Greenberg, *Tolerance and exhaustion: defining mechanisms of T cell dysfunction*. Trends Immunol, 2014. **35**(2): p. 51-60.
46. Fuertes Marraco, S.A., et al., *Inhibitory Receptors Beyond T Cell Exhaustion*. Front Immunol, 2015. **6**: p. 310.
47. Liu, J., et al., *Targeting PD-1 and Tim-3 Pathways to Reverse CD8 T-Cell Exhaustion and Enhance Ex Vivo T-Cell Responses to Autologous Dendritic/Tumor Vaccines*. J Immunother, 2016. **39**(4): p. 171-80.
48. Wherry, E.J., et al., *Molecular signature of CD8+ T cell exhaustion during chronic viral infection*. Immunity, 2007. **27**(4): p. 670-84.
49. Baitsch, L., et al., *Exhaustion of tumor-specific CD8(+) T cells in metastases from melanoma patients*. J Clin Invest, 2011. **121**(6): p. 2350-60.
50. Paley, M.A., et al., *Progenitor and terminal subsets of CD8+ T cells cooperate to contain chronic viral infection*. Science, 2012. **338**(6111): p. 1220-5.
51. Martinez, G.J., et al., *The transcription factor NFAT promotes exhaustion of activated CD8(+) T cells*. Immunity, 2015. **42**(2): p. 265-278.
52. Macian, F., et al., *Transcriptional mechanisms underlying lymphocyte tolerance*. Cell, 2002. **109**(6): p. 719-31.
53. Shin, H., et al., *A role for the transcriptional repressor Blimp-1 in CD8(+) T cell exhaustion during chronic viral infection*. Immunity, 2009. **31**(2): p. 309-20.
54. Quigley, M., et al., *Transcriptional analysis of HIV-specific CD8(+) T cells shows that PD-1 inhibits T cell function by upregulating BATF*. Nature Medicine, 2010. **16**(10): p. 1147-U127.
55. Staron, M.M., et al., *The transcription factor FoxO1 sustains expression of the inhibitory receptor PD-1 and survival of antiviral CD8(+) T cells during chronic infection*. Immunity, 2014. **41**(5): p. 802-14.
56. Stephen, T.L., et al., *Transforming growth factor beta-mediated suppression of antitumor T cells requires FoxP1 transcription factor expression*. Immunity, 2014. **41**(3): p. 427-439.
57. Zarour, H.M., *Reversing T-cell Dysfunction and Exhaustion in Cancer*. Clin Cancer Res, 2016. **22**(8): p. 1856-64.
58. Schwartz, R.H., *T cell anergy*. Annu Rev Immunol, 2003. **21**(1): p. 305-34.
59. Valdor, R. and F. Macian, *Induction and stability of the anergic phenotype in T cells*. Semin Immunol, 2013. **25**(4): p. 313-20.
60. Srinivasan, M. and K.A. Frauwirth, *Reciprocal NFAT1 and NFAT2 Nuclear Localization in CD8+ Anergic T Cells Is Regulated by Suboptimal Calcium Signaling*. The Journal of Immunology, 2007. **179**(6): p. 3734-3741.
61. Pita-Lopez, M.L., et al., *Effect of ageing on CMV-specific CD8 T cells from CMV seropositive healthy donors*. Immun Ageing, 2009. **6**: p. 11.
62. Appay, V., et al., *Accelerated immune senescence and HIV-1 infection*. Exp Gerontol, 2007. **42**(5): p. 432-7.
63. Montes, C.L., et al., *Tumor-induced senescent T cells with suppressor function: a potential form of tumor immune evasion*. Cancer Res, 2008. **68**(3): p. 870-9.
64. Filaci, G., et al., *CD8+CD28- T Regulatory Lymphocytes Inhibiting T Cell Proliferative and Cytotoxic Functions Infiltrate Human Cancers*. The Journal of Immunology, 2007. **179**(7): p. 4323-4334.
65. Hofbauer, G.F., et al., *Melan A/MART-1 immunoreactivity in formalin-fixed paraffin-embedded primary and metastatic melanoma: frequency and distribution*. Melanoma Res, 1998. **8**(4): p. 337-43.

66. de Vries, T.J., et al., *Heterogeneous expression of immunotherapy candidate proteins gp100, MART-1, and tyrosinase in human melanoma cell lines and in human melanocytic lesions*. *Cancer Res*, 1997. **57**(15): p. 3223-9.
67. Garrido, F., et al., *Natural history of HLA expression during tumour development*. *Immunol Today*, 1993. **14**(10): p. 491-9.
68. Ferrone, S. and F.M. Marincola, *Loss of HLA class I antigens by melanoma cells: molecular mechanisms, functional significance and clinical relevance*. *Immunology Today*, 1995. **16**(10): p. 487-494.
69. Hicklin, D.J., et al., *beta2-Microglobulin mutations, HLA class I antigen loss, and tumor progression in melanoma*. *J Clin Invest*, 1998. **101**(12): p. 2720-9.
70. Restifo, N.P., et al., *Loss of functional beta 2-microglobulin in metastatic melanomas from five patients receiving immunotherapy*. *J Natl Cancer Inst*, 1996. **88**(2): p. 100-8.
71. Restifo, N.P., et al., *Identification of human cancers deficient in antigen processing*. *J Exp Med*, 1993. **177**(2): p. 265-72.
72. Korkolopoulou, P., et al., *Loss of antigen-presenting molecules (MHC class I and TAP-1) in lung cancer*. *Br J Cancer*, 1996. **73**(2): p. 148-53.
73. Sanda, M.G., et al., *Molecular characterization of defective antigen processing in human prostate cancer*. *J Natl Cancer Inst*, 1995. **87**(4): p. 280-5.
74. Fulda, S., *Tumor resistance to apoptosis*. *Int J Cancer*, 2009. **124**(3): p. 511-5.
75. Kischkel, F.C., et al., *Cytotoxicity-dependent APO-1 (Fas/CD95)-associated proteins form a death-inducing signaling complex (DISC) with the receptor*. *EMBO J*, 1995. **14**(22): p. 5579-88.
76. Ashkenazi, A., *Targeting the extrinsic apoptosis pathway in cancer*. *Cytokine Growth Factor Rev*, 2008. **19**(3-4): p. 325-31.
77. Schulze-Osthoff, K., et al., *Apoptosis signaling by death receptors*. *European Journal of Biochemistry*, 1998. **254**(3): p. 439-459.
78. Wajant, H., K. Pfizenmaier, and P. Scheurich, *Tumor necrosis factor signaling*. *Cell Death Differ*, 2003. **10**(1): p. 45-65.
79. Kroemer, G., L. Galluzzi, and C. Brenner, *Mitochondrial membrane permeabilization in cell death*. *Physiol Rev*, 2007. **87**(1): p. 99-163.
80. Gordon, N., et al., *Fas expression in lung metastasis from osteosarcoma patients*. *J Pediatr Hematol Oncol*, 2005. **27**(11): p. 611-5.
81. Liu, K., E. McDuffie, and S.I. Abrams, *Exposure of human primary colon carcinoma cells to anti-Fas interactions influences the emergence of pre-existing Fas-resistant metastatic subpopulations*. *J Immunol*, 2003. **171**(8): p. 4164-74.
82. Worth, L.L., et al., *Fas expression inversely correlates with metastatic potential in osteosarcoma cells*. *Oncol Rep*, 2002. **9**(4): p. 823-7.
83. Liu, K., S.A. Caldwell, and S.I. Abrams, *Immune selection and emergence of aggressive tumor variants as negative consequences of Fas-mediated cytotoxicity and altered IFN-gamma-regulated gene expression*. *Cancer Res*, 2005. **65**(10): p. 4376-88.
84. Petak, I., et al., *Hypermethylation of the gene promoter and enhancer region can regulate Fas expression and sensitivity in colon carcinoma*. *Cell Death Differ*, 0000. **10**(2): p. 211-217.
85. Dechant, M.J., et al., *Mutation analysis of the apoptotic "death-receptors" and the adaptors TRADD and FADD/MORT-1 in osteosarcoma tumor samples and osteosarcoma cell lines*. *Int J Cancer*, 2004. **109**(5): p. 661-7.
86. Thomas, D.A. and J. Massague, *TGF-beta directly targets cytotoxic T cell functions during tumor evasion of immune surveillance*. *Cancer Cell*, 2005. **8**(5): p. 369-80.

87. Lin, R., et al., *Targeting miR-23a in CD8+ cytotoxic T lymphocytes prevents tumor-dependent immunosuppression*. J Clin Invest, 2014. **124**(12): p. 5352-67.
88. Chen, W., et al., *Conversion of peripheral CD4+CD25- naive T cells to CD4+CD25+ regulatory T cells by TGF-beta induction of transcription factor Foxp3*. J Exp Med, 2003. **198**(12): p. 1875-86.
89. Roncarolo, M.G., et al., *Type 1 T regulatory cells*. Immunological Reviews, 2001. **182**(1): p. 68-79.
90. Hamidullah, B. Changkija, and R. Konwar, *Role of interleukin-10 in breast cancer*. Breast Cancer Res Treat, 2012. **133**(1): p. 11-21.
91. Kim, Y.J., S.J. Park, and H.E. Broxmeyer, *Phagocytosis, a potential mechanism for myeloid-derived suppressor cell regulation of CD8+ T cell function mediated through programmed cell death-1 and programmed cell death-1 ligand interaction*. J Immunol, 2011. **187**(5): p. 2291-301.
92. McKallip, R., R. Li, and S. Ladisch, *Tumor gangliosides inhibit the tumor-specific immune response*. J Immunol, 1999. **163**(7): p. 3718-26.
93. Das, T., et al., *Renal cell carcinoma tumors induce T cell apoptosis through receptor-dependent and receptor-independent pathways*. Journal of Immunology, 2008. **180**(7): p. 4687-4696.
94. Rayman, P., et al., *Effect of renal cell carcinomas on the development of type 1 T-cell responses*. Clin Cancer Res, 2004. **10**(18 Pt 2): p. 6360S-6S.
95. Lee, H.C., et al., *Ganglioside inhibition of CD8+ T cell cytotoxicity: interference with lytic granule trafficking and exocytosis*. J Immunol, 2012. **189**(7): p. 3521-7.
96. Liu, B., L. Qu, and S. Yan, *Cyclooxygenase-2 promotes tumor growth and suppresses tumor immunity*. Cancer Cell Int, 2015. **15**: p. 106.
97. Marvel, D. and D.I. Gabrilovich, *Myeloid-derived suppressor cells in the tumor microenvironment: expect the unexpected*. J Clin Invest, 2015. **125**(9): p. 3356-64.
98. Gabrilovich, D.I. and S. Nagaraj, *Myeloid-derived suppressor cells as regulators of the immune system*. Nature Reviews Immunology, 2009. **9**(3): p. 162-174.
99. Srivastava, M.K., et al., *Myeloid-derived suppressor cells inhibit T-cell activation by depleting cystine and cysteine*. Cancer Res, 2010. **70**(1): p. 68-77.
100. Lindau, D., et al., *The immunosuppressive tumour network: myeloid-derived suppressor cells, regulatory T cells and natural killer T cells*. Immunology, 2013. **138**(2): p. 105-15.
101. Huang, B., et al., *Gr-1+CD115+ immature myeloid suppressor cells mediate the development of tumor-induced T regulatory cells and T-cell anergy in tumor-bearing host*. Cancer Res, 2006. **66**(2): p. 1123-31.
102. Mosser, D.M. and J.P. Edwards, *Exploring the full spectrum of macrophage activation*. Nat Rev Immunol, 2008. **8**(12): p. 958-69.
103. Noy, R. and J.W. Pollard, *Tumor-associated macrophages: from mechanisms to therapy*. Immunity, 2014. **41**(1): p. 49-61.
104. Tran Janco, J.M., et al., *Tumor-infiltrating dendritic cells in cancer pathogenesis*. J Immunol, 2015. **194**(7): p. 2985-91.
105. Kuwana, M., *Induction of anergic and regulatory T cells by plasmacytoid dendritic cells and other dendritic cell subsets*. Hum Immunol, 2002. **63**(12): p. 1156-63.
106. Steinbrink, K., et al., *Interleukin-10-treated human dendritic cells induce a melanoma-antigen-specific anergy in CD8(+) T cells resulting in a failure to lyse tumor cells*. Blood, 1999. **93**(5): p. 1634-42.
107. Sakaguchi, S., et al., *Regulatory T cells and immune tolerance*. Cell, 2008. **133**(5): p. 775-87.

108. Tanaka, A. and S. Sakaguchi, *Regulatory T cells in cancer immunotherapy*. Cell Res, 2017. **27**(1): p. 109-118.
109. Shang, B., et al., *Prognostic value of tumor-infiltrating FoxP3+ regulatory T cells in cancers: a systematic review and meta-analysis*. Sci Rep, 2015. **5**: p. 15179.
110. Knol, A.C., et al., *Prognostic value of tumor-infiltrating Foxp3+ T-cell subpopulations in metastatic melanoma*. Exp Dermatol, 2011. **20**(5): p. 430-4.
111. Facciabene, A., G.T. Motz, and G. Coukos, *T-regulatory cells: key players in tumor immune escape and angiogenesis*. Cancer Res, 2012. **72**(9): p. 2162-71.
112. Qureshi, O.S., et al., *Trans-endocytosis of CD80 and CD86: a molecular basis for the cell-extrinsic function of CTLA-4*. Science, 2011. **332**(6029): p. 600-3.
113. Vignali, D.A.A., L.W. Collison, and C.J. Workman, *How regulatory T cells work*. Nat Rev Immunol, 2008. **8**(7): p. 523-532.
114. Gondek, D.C., et al., *Cutting edge: contact-mediated suppression by CD4+CD25+ regulatory cells involves a granzyme B-dependent, perforin-independent mechanism*. J Immunol, 2005. **174**(4): p. 1783-6.
115. Ren, X., et al., *Involvement of cellular death in TRAIL/DR5-dependent suppression induced by CD4(+)CD25(+) regulatory T cells*. Cell Death Differ, 2007. **14**(12): p. 2076-84.
116. Garin, M.I., et al., *Galectin-1: a key effector of regulation mediated by CD4+CD25+ T cells*. Blood, 2007. **109**(5): p. 2058-65.
117. Deaglio, S., et al., *Adenosine generation catalyzed by CD39 and CD73 expressed on regulatory T cells mediates immune suppression*. J Exp Med, 2007. **204**(6): p. 1257-65.
118. Bopp, T., et al., *Cyclic adenosine monophosphate is a key component of regulatory T cell-mediated suppression*. J Exp Med, 2007. **204**(6): p. 1303-10.
119. Munn, D.H., et al., *GCN2 kinase in T cells mediates proliferative arrest and anergy induction in response to indoleamine 2,3-dioxygenase*. Immunity, 2005. **22**(5): p. 633-42.
120. van Baren, N. and B.J. Van den Eynde, *Tumoral Immune Resistance Mediated by Enzymes That Degrade Tryptophan*. Cancer Immunology Research, 2015.
121. Lob, S., et al., *IDO1 and IDO2 are expressed in human tumors: levo- but not dextro-1-methyl tryptophan inhibits tryptophan catabolism*. Cancer Immunol Immunother, 2009. **58**(1): p. 153-7.
122. Moon, Y.W., et al., *Targeting the indoleamine 2,3-dioxygenase pathway in cancer*. J Immunother Cancer, 2015. **3**(1): p. 51.
123. Yu, C.P., et al., *Targeting TDO in cancer immunotherapy*. Med Oncol, 2017. **34**(5): p. 73.
124. Koshiba, M., et al., *Patterns of A2A and A2B Extracellular Adenosine Receptor Expression in Different Functional Subsets of Human Peripheral T Cells. Flow Cytometry Studies with Anti-A2A and A2B Receptor Monoclonal Antibodies*. Molecular Pharmacology, 1999. **55**(3): p. 614.
125. Lukashev, D.E., et al., *Analysis of A2a receptor-deficient mice reveals no significant compensatory increases in the expression of A2b, A1, and A3 adenosine receptors in lymphoid organs*. Biochemical Pharmacology, 2003. **65**(12): p. 2081-2090.
126. Ohta, A., et al., *A2A Adenosine Receptor May Allow Expansion of T Cells Lacking Effector Functions in Extracellular Adenosine-Rich Microenvironments*. Journal of Immunology, 2009. **183**(9): p. 5487-5493.
127. Ohta, A., et al., *A2A adenosine receptor protects tumors from antitumor T cells*. Proc Natl Acad Sci U S A, 2006. **103**(35): p. 13132-7.
128. Ma, S.R., et al., *Blockade of adenosine A2A receptor enhances CD8+ T cells response and decreases regulatory T cells in head and neck squamous cell carcinoma*. Mol Cancer, 2017. **16**(1): p. 99.

129. Allard, B., et al., *Immunosuppressive activities of adenosine in cancer*. *Curr Opin Pharmacol*, 2016. **29**: p. 7-16.
130. Allard, D., et al., *CD73-adenosine: a next-generation target in immuno-oncology*. *Immunotherapy*, 2016. **8**(2): p. 145-63.
131. Antonioli, L., et al., *CD39 and CD73 in immunity and inflammation*. *Trends Mol Med*, 2013. **19**(6): p. 355-67.
132. Blay, J., T.D. White, and D.W. Hoskin, *The extracellular fluid of solid carcinomas contains immunosuppressive concentrations of adenosine*. *Cancer Res*, 1997. **57**(13): p. 2602-5.
133. Hatfield, S.M., et al., *Systemic oxygenation weakens the hypoxia and hypoxia inducible factor 1alpha-dependent and extracellular adenosine-mediated tumor protection*. *J Mol Med (Berl)*, 2014. **92**(12): p. 1283-92.
134. Zhu, Y., S. Yao, and L. Chen, *Cell surface signaling molecules in the control of immune responses: a tide model*. *Immunity*, 2011. **34**(4): p. 466-78.
135. Chen, L. and D.B. Flies, *Molecular mechanisms of T cell co-stimulation and co-inhibition*. *Nat Rev Immunol*, 2013. **13**(4): p. 227-42.
136. Ishida, Y., et al., *Induced Expression of Pd-1, a Novel Member of the Immunoglobulin Gene Superfamily, Upon Programmed Cell-Death*. *Embo Journal*, 1992. **11**(11): p. 3887-3895.
137. Dong, H., et al., *B7-H1, a third member of the B7 family, co-stimulates T-cell proliferation and interleukin-10 secretion*. *Nat Med*, 1999. **5**(12): p. 1365-9.
138. Freeman, G.J., et al., *Engagement of the PD-1 immunoinhibitory receptor by a novel B7 family member leads to negative regulation of lymphocyte activation*. *J Exp Med*, 2000. **192**(7): p. 1027-34.
139. Oestreich, K.J., et al., *NFATc1 regulates PD-1 expression upon T cell activation*. *Journal of Immunology*, 2008. **181**(7): p. 4832-4839.
140. Youngblood, B., et al., *Chronic virus infection enforces demethylation of the locus that encodes PD-1 in antigen-specific CD8(+) T cells*. *Immunity*, 2011. **35**(3): p. 400-12.
141. Ahn, E., et al., *Demethylation of the PD-1 Promoter Is Imprinted during the Effector Phase of CD8 T Cell Exhaustion*. *J Virol*, 2016. **90**(19): p. 8934-46.
142. Chemnitz, J.M., et al., *SHP-1 and SHP-2 associate with immunoreceptor tyrosine-based switch motif of programmed death 1 upon primary human T cell stimulation, but only receptor ligation prevents T cell activation*. *Journal of Immunology*, 2004. **173**(2): p. 945-954.
143. Yokosuka, T., et al., *Programmed cell death 1 forms negative costimulatory microclusters that directly inhibit T cell receptor signaling by recruiting phosphatase SHP2*. *J Exp Med*, 2012. **209**(6): p. 1201-17.
144. Sheppard, K.A., et al., *PD-1 inhibits T-cell receptor induced phosphorylation of the ZAP70/CD3zeta signalosome and downstream signaling to PKCtheta*. *FEBS Lett*, 2004. **574**(1-3): p. 37-41.
145. Boussiotis, V.A., P. Chatterjee, and L. Li, *Biochemical signaling of PD-1 on T cells and its functional implications*. *Cancer J*, 2014. **20**(4): p. 265-71.
146. Okazaki, T., et al., *A rheostat for immune responses: the unique properties of PD-1 and their advantages for clinical application*. *Nat Immunol*, 2013. **14**(12): p. 1212-8.
147. Barber, D.L., et al., *Restoring function in exhausted CD8 T cells during chronic viral infection*. *Nature*, 2006. **439**(7077): p. 682-7.
148. Mazanet, M.M. and C.C.W. Hughes, *B7-H1 is expressed by human endothelial cells and suppresses T cell cytokine synthesis*. *Journal of Immunology*, 2002. **169**(7): p. 3581-3588.

149. Hino, R., et al., *Tumor cell expression of programmed cell death-1 ligand 1 is a prognostic factor for malignant melanoma*. *Cancer*, 2010. **116**(7): p. 1757-66.
150. Liu, J., et al., *Plasma cells from multiple myeloma patients express B7-H1 (PD-L1) and increase expression after stimulation with IFN- γ and TLR ligands via a MyD88-, TRAF6-, and MEK-dependent pathway*. *Blood*, 2007. **110**(1): p. 296-304.
151. Wang, X., et al., *PD-L1 expression in human cancers and its association with clinical outcomes*. *Onco Targets Ther*, 2016. **9**: p. 5023-39.
152. Xu, W., et al., *The upregulation of immune checkpoint ligand PD-L1 in tumour microenvironment*. *Scand J Immunol*, 2014. **80**(1): p. 71-2.
153. Spranger, S., et al., *Up-regulation of PD-L1, IDO, and T(regs) in the melanoma tumor microenvironment is driven by CD8(+) T cells*. *Sci Transl Med*, 2013. **5**(200): p. 200ra116.
154. Chambers, C.A., et al., *CTLA-4-mediated inhibition in regulation of T cell responses: mechanisms and manipulation in tumor immunotherapy*. *Annu Rev Immunol*, 2001. **19**(1): p. 565-94.
155. Walker, L.S. and D.M. Sansom, *Confusing signals: recent progress in CTLA-4 biology*. *Trends Immunol*, 2015. **36**(2): p. 63-70.
156. Leach, D.R., M.F. Krummel, and J.P. Allison, *Enhancement of antitumor immunity by CTLA-4 blockade*. *Science*, 1996. **271**(5256): p. 1734-6.
157. Takahashi, H., et al., *RCAS1 antigen is highly expressed in extramammary Paget's disease and in advanced stage squamous cell carcinoma of the skin*. *Journal of Dermatological Science*, 2001. **26**(2): p. 140-144.
158. Zhang, Y., et al., *The membrane molecule RCAS1 induces immune cell apoptosis via the RCAS1-RCAS1R pathway*. *Int J Mol Med*, 2013. **31**(6): p. 1319-26.
159. Thies, A., et al., *CEACAM1 expression in cutaneous malignant melanoma predicts the development of metastatic disease*. *J Clin Oncol*, 2002. **20**(10): p. 2530-6.
160. Witzens-Harig, M., et al., *Tumor cells in multiple myeloma patients inhibit myeloma-reactive T cells through carcinoembryonic antigen-related cell adhesion molecule-6*. *Blood*, 2013. **121**(22): p. 4493-503.
161. Gray-Owen, S.D. and R.S. Blumberg, *CEACAM1: contact-dependent control of immunity*. *Nat Rev Immunol*, 2006. **6**(6): p. 433-46.
162. Liu, F.T. and G.A. Rabinovich, *Galectins as modulators of tumour progression*. *Nat Rev Cancer*, 2005. **5**(1): p. 29-41.
163. Braeuer, R.R., et al., *Galectin-3 contributes to melanoma growth and metastasis via regulation of NFAT1 and autotaxin*. *Cancer Res*, 2012. **72**(22): p. 5757-66.
164. Peng, W., et al., *Tumor-associated galectin-3 modulates the function of tumor-reactive T cells*. *Cancer Res*, 2008. **68**(17): p. 7228-36.
165. Stillman, B.N., et al., *Galectin-3 and galectin-1 bind distinct cell surface glycoprotein receptors to induce T cell death*. *J Immunol*, 2006. **176**(2): p. 778-89.
166. Hsu, D.K., H.Y. Chen, and F.T. Liu, *Galectin-3 regulates T-cell functions*. *Immunol Rev*, 2009. **230**(1): p. 114-27.
167. Chapoval, A.I., et al., *B7-H3: a costimulatory molecule for T cell activation and IFN- γ production*. *Nat Immunol*, 2001. **2**(3): p. 269-74.
168. Hofmeyer, K.A., A. Ray, and X. Zang, *The contrasting role of B7-H3*. *Proc Natl Acad Sci U S A*, 2008. **105**(30): p. 10277-8.
169. Suh, W.K., et al., *The B7 family member B7-H3 preferentially down-regulates T helper type 1-mediated immune responses*. *Nat Immunol*, 2003. **4**(9): p. 899-906.
170. Wang, J., et al., *B7-H3 associated with tumor progression and epigenetic regulatory activity in cutaneous melanoma*. *J Invest Dermatol*, 2013. **133**(8): p. 2050-8.

171. Sun, Y., et al., *B7-H3 and B7-H4 expression in non-small-cell lung cancer*. Lung Cancer, 2006. **53**(2): p. 143-51.
172. Liu, C., et al., *B7-H3 expression in ductal and lobular breast cancer and its association with IL-10*. Mol Med Rep, 2013. **7**(1): p. 134-8.
173. Zang, X., et al., *B7x: A widely expressed B7 family member that inhibits T cell activation*. Proceedings of the National Academy of Sciences, 2003. **100**(18): p. 10388-10392.
174. Prasad, D.V.R., et al., *B7S1, a novel B7 family member that negatively regulates T cell activation*. Immunity, 2003. **18**(6): p. 863-873.
175. Choi, I.H., et al., *Genomic organization and expression analysis of B7-H4, an immune inhibitory molecule of the B7 family*. J Immunol, 2003. **171**(9): p. 4650-4.
176. Zang, X. and J.P. Allison, *The B7 family and cancer therapy: costimulation and coinhibition*. Clin Cancer Res, 2007. **13**(18 Pt 1): p. 5271-9.
177. Zhao, R., et al., *HHLA2 is a member of the B7 family and inhibits human CD4 and CD8 T-cell function*. Proc Natl Acad Sci U S A, 2013. **110**(24): p. 9879-84.
178. Anderson, A.C., et al., *T-bet, a Th1 transcription factor regulates the expression of Tim-3*. Eur J Immunol, 2010. **40**(3): p. 859-66.
179. Zhu, C., et al., *The Tim-3 ligand galectin-9 negatively regulates T helper type 1 immunity*. Nat Immunol, 2005. **6**(12): p. 1245-52.
180. Huang, Y.H., et al., *CEACAM1 regulates TIM-3-mediated tolerance and exhaustion*. Nature, 2015. **517**(7534): p. 386-90.
181. Lucca, L.E. and D.A. Hafler, *Co-inhibitory blockade while preserving tolerance: checkpoint inhibitors for glioblastoma*. Immunol Rev, 2017. **276**(1): p. 9-25.
182. Kouo, T., et al., *Galectin-3 Shapes Antitumor Immune Responses by Suppressing CD8+ T Cells via LAG-3 and Inhibiting Expansion of Plasmacytoid Dendritic Cells*. Cancer Immunol Res, 2015. **3**(4): p. 412-23.
183. Dougall, W.C., et al., *TIGIT and CD96: new checkpoint receptor targets for cancer immunotherapy*. Immunol Rev, 2017. **276**(1): p. 112-120.
184. Guo, C., et al., *Therapeutic cancer vaccines: past, present, and future*. Adv Cancer Res, 2013. **119**: p. 421-75.
185. Hanna, M.G. and L.C. Peters, *Specific immunotherapy of established visceral micrometastases by BCG-tumor cell vaccine alone or as an adjunct to surgery*. Cancer, 1978. **42**(6): p. 2613-2625.
186. Baars, A., et al., *Metastasectomy and active specific immunotherapy for a large single melanoma metastasis*. Hepatogastroenterology, 2002. **49**(45): p. 691-3.
187. Mach, N., et al., *Differences in dendritic cells stimulated in vivo by tumors engineered to secrete granulocyte-macrophage colony-stimulating factor or Flt3-ligand*. Cancer Res, 2000. **60**(12): p. 3239-46.
188. Hu, Z., *Overcome the Impairment of NK Cells for Icon and Antibody Immunotherapy of Cancer*. Journal of Immune Based Therapies, Vaccines and Antimicrobials, 2013. **02**(01): p. 1-8.
189. Sondak, V.K., M.S. Sabel, and J.J. Mulé, *Allogeneic and Autologous Melanoma Vaccines: Where Have We Been and Where Are We Going?* Clinical Cancer Research, 2006. **12**(7): p. 2337s.
190. Longo, D.L., *New therapies for castration-resistant prostate cancer*. N Engl J Med, 2010. **363**(5): p. 479-81.
191. Kreiter, S., et al., *Targeting the tumor mutanome for personalized vaccination therapy*. Oncoimmunology, 2012. **1**(5): p. 768-769.

192. Rosenberg, S.A., P. Spiess, and R. Lafreniere, *A New Approach to the Adoptive Immunotherapy of Cancer with Tumor-Infiltrating Lymphocytes*. *Science*, 1986. **233**(4770): p. 1318-1321.
193. Jin, J., et al., *Simplified method of the growth of human tumor infiltrating lymphocytes in gas-permeable flasks to numbers needed for patient treatment*. *J Immunother*, 2012. **35**(3): p. 283-92.
194. Phan, G.Q. and S.A. Rosenberg, *Adoptive cell transfer for patients with metastatic melanoma: the potential and promise of cancer immunotherapy*. *Cancer Control*, 2013. **20**(4): p. 289-97.
195. Radvanyi, L.G., et al., *Specific lymphocyte subsets predict response to adoptive cell therapy using expanded autologous tumor-infiltrating lymphocytes in metastatic melanoma patients*. *Clin Cancer Res*, 2012. **18**(24): p. 6758-70.
196. Pilon-Thomas, S., et al., *Efficacy of adoptive cell transfer of tumor-infiltrating lymphocytes after lymphopenia induction for metastatic melanoma*. *J Immunother*, 2012. **35**(8): p. 615-20.
197. Rosenberg, S.A. and N.P. Restifo, *Adoptive cell transfer as personalized immunotherapy for human cancer*. *Science*, 2015. **348**(6230): p. 62-68.
198. de Witte, M.A., et al., *Targeting self-antigens through allogeneic TCR gene transfer*. *Blood*, 2006. **108**(3): p. 870.
199. Robbins, P.F., et al., *Single and dual amino acid substitutions in TCR CDRs can enhance antigen-specific T cell functions*. *Journal of Immunology*, 2008. **180**(9): p. 6116-6131.
200. Maher, J., *Clinical Immunotherapy of B-Cell Malignancy Using CD19-Targeted CAR T-Cells*. *Current Gene Therapy*, 2014. **14**(1): p. 35-43.
201. Heslop, H.E., *Safer CARs*. *Mol Ther*, 2010. **18**(4): p. 661-2.
202. Carpenito, C., et al., *Control of large, established tumor xenografts with genetically retargeted human T cells containing CD28 and CD137 domains*. *Proc Natl Acad Sci U S A*, 2009. **106**(9): p. 3360-5.
203. Sharpe, M. and N. Mount, *Genetically modified T cells in cancer therapy: opportunities and challenges*. *Dis Model Mech*, 2015. **8**(4): p. 337-50.
204. Maus, M.V., et al., *Antibody-modified T cells: CARs take the front seat for hematologic malignancies*. *Blood*, 2014. **123**(17): p. 2625-35.
205. Maude, S.L., et al. *Efficacy and Safety of CTL019 in the First US Phase II Multicenter Trial in Pediatric Relapsed/Refractory Acute Lymphoblastic Leukemia: Results of an Interim Analysis*. in *ASH*. 2016. San Diego, CA.
206. Couzin-Frankel, J., *Breakthrough of the year 2013. Cancer immunotherapy*. *Science*, 2013. **342**(6165): p. 1432-3.
207. U.S. Food and Drug Administration. *Avelumab (BAVENCIO)*. 2017 [cited 2017 25.07]; Available from: <https://www.fda.gov/Drugs/InformationOnDrugs/ApprovedDrugs/ucm547965.htm>.
208. Brahmer, J.R., et al., *Phase I study of single-agent anti-programmed death-1 (MDX-1106) in refractory solid tumors: safety, clinical activity, pharmacodynamics, and immunologic correlates*. *J Clin Oncol*, 2010. **28**(19): p. 3167-75.
209. Topalian, S.L., et al., *Safety, activity, and immune correlates of anti-PD-1 antibody in cancer*. *N Engl J Med*, 2012. **366**(26): p. 2443-54.
210. Sharma, P., et al., *Nivolumab in metastatic urothelial carcinoma after platinum therapy (CheckMate 275): a multicentre, single-arm, phase 2 trial*. *Lancet Oncol*, 2017. **18**(3): p. 312-322.
211. Topalian, S.L., et al., *Survival, durable tumor remission, and long-term safety in patients with advanced melanoma receiving nivolumab*. *J Clin Oncol*, 2014. **32**(10): p. 1020-30.

212. Robert, C., et al., *Nivolumab in previously untreated melanoma without BRAF mutation*. N Engl J Med, 2015. **372**(4): p. 320-30.
213. Rizvi, N.A., et al., *Activity and safety of nivolumab, an anti-PD-1 immune checkpoint inhibitor, for patients with advanced, refractory squamous non-small-cell lung cancer (CheckMate 063): a phase 2, single-arm trial*. Lancet Oncol, 2015. **16**(3): p. 257-65.
214. Benosman, S., et al., *Interleukin-1 receptor-associated kinase-2 (IRAK2) is a critical mediator of endoplasmic reticulum (ER) stress signaling*. PLoS One, 2013. **8**(5): p. e64256.
215. Kaufman, H.L., et al., *Avelumab in patients with chemotherapy-refractory metastatic Merkel cell carcinoma: a multicentre, single-group, open-label, phase 2 trial*. Lancet Oncol, 2016. **17**(10): p. 1374-1385.
216. Massard, C., et al., *Safety and Efficacy of Durvalumab (MEDI4736), an Anti-Programmed Cell Death Ligand-1 Immune Checkpoint Inhibitor, in Patients With Advanced Urothelial Bladder Cancer*. J Clin Oncol, 2016. **34**(26): p. 3119-25.
217. Peters, S., et al., *Phase II Trial of Atezolizumab As First-Line or Subsequent Therapy for Patients With Programmed Death-Ligand 1-Selected Advanced Non-Small-Cell Lung Cancer (BIRCH)*. J Clin Oncol, 2017. **35**(24): p. 2781-2789.
218. Buque, A., et al., *Trial Watch: Immunomodulatory monoclonal antibodies for oncological indications*. Oncoimmunology, 2015. **4**(4): p. e1008814.
219. Carbognin, L., et al., *Differential Activity of Nivolumab, Pembrolizumab and MPDL3280A according to the Tumor Expression of Programmed Death-Ligand-1 (PD-L1): Sensitivity Analysis of Trials in Melanoma, Lung and Genitourinary Cancers*. PLoS One, 2015. **10**(6): p. e0130142.
220. Pardoll, D.M., *The blockade of immune checkpoints in cancer immunotherapy*. Nat Rev Cancer, 2012. **12**(4): p. 252-64.
221. Nirschl, C.J. and C.G. Drake, *Molecular pathways: coexpression of immune checkpoint molecules: signaling pathways and implications for cancer immunotherapy*. Clin Cancer Res, 2013. **19**(18): p. 4917-24.
222. Kleponis, J., R. Skelton, and L. Zheng, *Fueling the engine and releasing the break: combinational therapy of cancer vaccines and immune checkpoint inhibitors*. Cancer Biol Med, 2015. **12**(3): p. 201-8.
223. Wolchok, J.D., et al., *Nivolumab plus ipilimumab in advanced melanoma*. N Engl J Med, 2013. **369**(2): p. 122-33.
224. Larkin, J., et al., *Combined Nivolumab and Ipilimumab or Monotherapy in Untreated Melanoma*. N Engl J Med, 2015. **373**(1): p. 23-34.
225. Postow, M.A., et al., *Nivolumab and ipilimumab versus ipilimumab in untreated melanoma*. N Engl J Med, 2015. **372**(21): p. 2006-17.
226. Antonia, S.J., et al., *Phase I/II study of nivolumab with or without ipilimumab for treatment of recurrent small cell lung cancer (SCLC): CA209-032*. Journal of Clinical Oncology, 2015. **33**(15).
227. Fire, A., et al., *Potent and specific genetic interference by double-stranded RNA in *Caenorhabditis elegans**. Nature, 1998. **391**(6669): p. 806-11.
228. Boutros, M. and J. Ahringer, *The art and design of genetic screens: RNA interference*. Nat Rev Genet, 2008. **9**(7): p. 554-66.
229. Cerutti, H. and J.A. Casas-Mollano, *On the origin and functions of RNA-mediated silencing: from protists to man*. Curr Genet, 2006. **50**(2): p. 81-99.
230. Wilson, R.C. and J.A. Doudna, *Molecular mechanisms of RNA interference*. Annu Rev Biophys, 2013. **42**: p. 217-39.
231. Hannon, G.J., *RNA interference*. Nature, 2002. **418**(6894): p. 244-51.

232. Paddison, P.J., et al., *Short hairpin RNAs (shRNAs) induce sequence-specific silencing in mammalian cells*. Genes Dev, 2002. **16**(8): p. 948-58.
233. Echeverri, C.J. and N. Perrimon, *High-throughput RNAi screening in cultured cells: a user's guide*. Nat Rev Genet, 2006. **7**(5): p. 373-84.
234. Possik, P.A., et al., *Parallel in vivo and in vitro melanoma RNAi dropout screens reveal synthetic lethality between hypoxia and DNA damage response inhibition*. Cell Rep, 2014. **9**(4): p. 1375-86.
235. Diehl, P., D. Tedesco, and A. Chenchik, *Use of RNAi screens to uncover resistance mechanisms in cancer cells and identify synthetic lethal interactions*. Drug Discov Today Technol, 2014. **11**: p. 11-8.
236. Agaesse, G., et al., *A large-scale RNAi screen identifies LCMR1 as a critical regulator of Tspan8-mediated melanoma invasion*. Oncogene, 2017. **36**(4): p. 446-457.
237. Bellucci, R., et al., *Tyrosine kinase pathways modulate tumor susceptibility to natural killer cells*. J Clin Invest, 2012. **122**(7): p. 2369-83.
238. Bellucci, R., et al., *Interferon-gamma-induced activation of JAK1 and JAK2 suppresses tumor cell susceptibility to NK cells through upregulation of PD-L1 expression*. Oncoimmunology, 2015. **4**(6): p. e1008824.
239. Zhou, P., et al., *In vivo discovery of immunotherapy targets in the tumour microenvironment*. Nature, 2014. **506**(7486): p. 52-7.
240. Khandelwal, N., et al., *A high-throughput RNAi screen for detection of immune-checkpoint molecules that mediate tumor resistance to cytotoxic T lymphocytes*. EMBO Mol Med, 2015. **7**(4): p. 450-63.
241. Pittet, M.J., et al., *Melan-A/MART-1-specific CD8 T cells: from thymus to tumor*. Trends Immunol, 2002. **23**(7): p. 325-8.
242. Machlenkin, A., et al., *Capture of tumor cell membranes by trogocytosis facilitates detection and isolation of tumor-specific functional CTLs*. Cancer Res, 2008. **68**(6): p. 2006-13.
243. Gelis, L., et al., *Functional Characterization of the Odorant Receptor 51E2 in Human Melanocytes*. J Biol Chem, 2016. **291**(34): p. 17772-86.
244. Dudley, M.E., et al., *Generation of tumor-infiltrating lymphocyte cultures for use in adoptive transfer therapy for melanoma patients*. Journal of Immunotherapy, 2003. **26**(4): p. 332-342.
245. Boutros, M., L.P. Bras, and W. Huber, *Analysis of cell-based RNAi screens*. Genome Biol, 2006. **7**(7): p. R66.
246. Anders, S., et al., *Count-based differential expression analysis of RNA sequencing data using R and Bioconductor*. Nat Protoc, 2013. **8**(9): p. 1765-86.
247. Eisenberg, G., et al., *Imprinting of lymphocytes with melanoma antigens acquired by trogocytosis facilitates identification of tumor-reactive T cells*. J Immunol, 2013. **190**(11): p. 5856-65.
248. da Cunha, J.P., et al., *Bioinformatics construction of the human cell surfaceome*. Proc Natl Acad Sci U S A, 2009. **106**(39): p. 16752-7.
249. Concha-Benavente, F. and R. Ferris, *JAK2 inhibition prevents NK-released IFN γ -mediated PD-L1 upregulation and enhances cetuximab mediated ADCC of HNC cells (TUM2P.1014)*. The Journal of Immunology, 2015. **194**(1 Supplement): p. 69.11-69.11.
250. Chen, J., et al., *Interferon-gamma-induced PD-L1 surface expression on human oral squamous carcinoma via PKD2 signal pathway*. Immunobiology, 2012. **217**(4): p. 385-93.
251. Cullen, B.R., *Enhancing and confirming the specificity of RNAi experiments*. Nat Methods, 2006. **3**(9): p. 677-81.

252. Echeverri, C.J., et al., *Minimizing the risk of reporting false positives in large-scale RNAi screens*. Nat Methods, 2006. **3**(10): p. 777-9.
253. Robinson, M.D., D.J. McCarthy, and G.K. Smyth, *edgeR: a Bioconductor package for differential expression analysis of digital gene expression data*. Bioinformatics, 2010. **26**(1): p. 139-40.
254. Safford, M., et al., *Egr-2 and Egr-3 are negative regulators of T cell activation*. Nat Immunol, 2005. **6**(5): p. 472-480.
255. Bernabei, P., et al., *Interferon- γ receptor 2 expression as the deciding factor in human T, B, and myeloid cell proliferation or death*. Journal of Leukocyte Biology, 2001. **70**(6): p. 950-960.
256. Parish, I.A., et al., *The molecular signature of CD8⁺ T cells undergoing deletional tolerance*. Blood, 2009. **113**(19): p. 4575-85.
257. Woronicz, J.D., et al., *Requirement for the orphan steroid receptor Nur77 in apoptosis of T-cell hybridomas*. Nature, 1994. **367**(6460): p. 277-81.
258. Okabe, T., et al., *cDNA cloning of a NGFI-B/nur77-related transcription factor from an apoptotic human T cell line*. J Immunol, 1995. **154**(8): p. 3871-9.
259. Tomita, K., et al., *The bHLH gene Hes1 is essential for expansion of early T cell precursors*. Genes & Development, 1999. **13**(9): p. 1203-1210.
260. Boles, K.S., et al., *The tumor suppressor TSLC1/NECL-2 triggers NK-cell and CD8⁺ T-cell responses through the cell-surface receptor CRTAM*. Blood, 2005. **106**(3): p. 779.
261. Zakaria, S., et al., *Differential regulation of TCR-mediated gene transcription by Vav family members*. J Exp Med, 2004. **199**(3): p. 429-34.
262. Yaseen, N.R., et al., *A central role for Fos in human B- and T-cell NFAT (nuclear factor of activated T cells): an acidic region is required for in vitro assembly*. Molecular and Cellular Biology, 1994. **14**(10): p. 6886-6895.
263. Wang, R., et al., *The transcription factor Myc controls metabolic reprogramming upon T lymphocyte activation*. Immunity, 2011. **35**(6): p. 871-82.
264. Man, K., et al., *The transcription factor IRF4 is essential for TCR affinity-mediated metabolic programming and clonal expansion of T cells*. Nature Immunology, 2013. **14**(11): p. 1155-U79.
265. Yao, S., et al., *Interferon regulatory factor 4 sustains CD8(+) T cell expansion and effector differentiation*. Immunity, 2013. **39**(5): p. 833-45.
266. Kramer, A., et al., *Causal analysis approaches in Ingenuity Pathway Analysis*. Bioinformatics, 2014. **30**(4): p. 523-30.
267. Downward, J., et al., *Stimulation of P21ras Upon T-Cell Activation*. Nature, 1990. **346**(6286): p. 719-723.
268. Li, D., J.J. Molldrem, and Q. Ma, *LFA-1 regulates CD8⁺ T cell activation via T cell receptor-mediated and LFA-1-mediated Erk1/2 signal pathways*. J Biol Chem, 2009. **284**(31): p. 21001-10.
269. Gao, M.H. and P.B. Kavathas, *Functional importance of the cyclic AMP response element-like decamer motif in the CD8 alpha promoter*. J Immunol, 1993. **150**(10): p. 4376-85.
270. Barton, K., et al., *Defective thymocyte proliferation and IL-2 production in transgenic mice expressing a dominant-negative form of CREB*. Nature, 1996. **379**(6560): p. 81-5.
271. Solomou, E.E., Y.T. Juang, and G.C. Tsokos, *Protein kinase C-theta participates in the activation of cyclic AMP-responsive element-binding protein and its subsequent binding to the -180 site of the IL-2 promoter in normal human T lymphocytes*. J Immunol, 2001. **166**(9): p. 5665-74.

272. McNeill, L., et al., *The differential regulation of Lck kinase phosphorylation sites by CD45 is critical for T cell receptor signaling responses*. *Immunity*, 2007. **27**(3): p. 425-37.
273. Wang, H., et al., *ZAP-70: an essential kinase in T-cell signaling*. *Cold Spring Harb Perspect Biol*, 2010. **2**(5): p. a002279.
274. Thomson, D.M., et al., *AMP-activated protein kinase phosphorylates transcription factors of the CREB family*. *J Appl Physiol* (1985), 2008. **104**(2): p. 429-38.
275. Szabo, M., et al., *Fine-tuning of proximal TCR signaling by ZAP-70 tyrosine residues in Jurkat cells*. *Int Immunol*, 2012. **24**(2): p. 79-87.
276. Rossy, J., D.J. Williamson, and K. Gaus, *How does the kinase Lck phosphorylate the T cell receptor? Spatial organization as a regulatory mechanism*. *Frontiers in Immunology*, 2012. **3**: p. 167.
277. Vang, T., et al., *Activation of the C-terminal Src Kinase (Csk) by Camp-Dependent Protein Kinase Inhibits Signaling through the T Cell Receptor*. *The Journal of Experimental Medicine*, 2001. **193**(4): p. 497-508.
278. Moreno-Fernandez, M.E., et al., *Regulatory T cells control HIV replication in activated T cells through a cAMP-dependent mechanism*. *Blood*, 2011. **117**(20): p. 5372-80.
279. Ye, J., et al., *TLR8 signaling enhances tumor immunity by preventing tumor-induced T-cell senescence*. *EMBO Mol Med*, 2014. **6**(10): p. 1294-311.
280. Su, Y., E.K. Jackson, and E. Gorelik, *Receptor desensitization and blockade of the suppressive effects of prostaglandin E(2) and adenosine on the cytotoxic activity of human melanoma-infiltrating T lymphocytes*. *Cancer Immunol Immunother*, 2011. **60**(1): p. 111-22.
281. Chen, J.H., et al., *Prostaglandin E2 and programmed cell death 1 signaling coordinately impair CTL function and survival during chronic viral infection*. *Nat Med*, 2015. **21**(4): p. 327-34.
282. Arnold, L.D., et al., *Pyrrolo[2,3-d]pyrimidines containing an extended 5-substituent as potent and selective inhibitors of lck I*. 2000. p. 2167-2170.
283. Holbrook, B.C., et al., *In vivo modulation of avidity in highly sensitive CD8(+) effector T cells following viral infection*. *Viral Immunol*, 2013. **26**(5): p. 302-13.
284. Huang, S., et al., *Role of A2a extracellular adenosine receptor-mediated signaling in adenosine-mediated inhibition of T-cell activation and expansion*. *Blood*, 1997. **90**(4): p. 1600-10.
285. Linnemann, C., et al., *Adenosine regulates CD8 T-cell priming by inhibition of membrane-proximal T-cell receptor signaling*. *Immunology*, 2009. **128**(1 Suppl): p. e728-37.
286. Plaut, M., G. Marone, and E. Gillespie, *The role of cyclic AMP in modulating cytotoxic T lymphocytes. II. Sequential changes during culture in responsiveness of cytotoxic lymphocytes to cyclic AMP-active agents*. *J Immunol*, 1983. **131**(6): p. 2945-52.
287. Goldberg, G.S., A.P. Moreno, and P.D. Lampe, *Gap junctions between cells expressing connexin 43 or 32 show inverse permselectivity to adenosine and ATP*. *J Biol Chem*, 2002. **277**(39): p. 36725-30.
288. Bedner, P., et al., *Selective permeability of different connexin channels to the second messenger cyclic AMP*. *J Biol Chem*, 2006. **281**(10): p. 6673-81.
289. Niessen, H., et al., *Selective permeability of different connexin channels to the second messenger inositol 1,4,5-trisphosphate*. *J Cell Sci*, 2000. **113** (Pt 8)(8): p. 1365-72.
290. Schulz, R., et al., *Connexin 43 is an emerging therapeutic target in ischemia/reperfusion injury, cardioprotection and neuroprotection*. *Pharmacol Ther*, 2015. **153**: p. 90-106.

291. Luttrell, L.M., *Transmembrane Signaling by G Protein-Coupled Receptors*, in *Transmembrane Signaling Protocols*, H. Ali and B. Haribabu, Editors. 2006, Humana Press: Totowa, NJ. p. 3-49.
292. Ferrer, I., et al., *Olfactory Receptors in Non-Chemosensory Organs: The Nervous System in Health and Disease*. *Front Aging Neurosci*, 2016. **8**: p. 163.
293. Leybaert, L. and M.J. Sanderson, *Intercellular Ca(2+) waves: mechanisms and function*. *Physiol Rev*, 2012. **92**(3): p. 1359-92.
294. Menini, A., *Calcium signaling and regulation in olfactory neurons*. *Curr Opin Neurobiol*, 1999. **9**(4): p. 419-26.
295. Klarenbeek, J., et al., *Fourth-generation epac-based FRET sensors for cAMP feature exceptional brightness, photostability and dynamic range: characterization of dedicated sensors for FLIM, for ratiometry and with high affinity*. *PLoS One*, 2015. **10**(4): p. e0122513.
296. Mangmool, S. and H. Kurose, *G(i/o) protein-dependent and -independent actions of Pertussis Toxin (PTX)*. *Toxins (Basel)*, 2011. **3**(7): p. 884-99.
297. Jones, D.T., et al., *Biochemical characterization of three stimulatory GTP-binding proteins. The large and small forms of Gs and the olfactory-specific G-protein, Golf*. *J Biol Chem*, 1990. **265**(5): p. 2671-6.
298. Patel, S.J., et al., *Identification of essential genes for cancer immunotherapy*. *Nature*, 2017. **548**(7669): p. 537-542.
299. Manguso, R.T., et al., *In vivo CRISPR screening identifies Ptpn2 as a cancer immunotherapy target*. *Nature*, 2017. **547**(7664): p. 413-+.
300. Pauken, K.E. and E.J. Wherry, *Overcoming T cell exhaustion in infection and cancer*. *Trends Immunol*, 2015. **36**(4): p. 265-76.
301. McIlwain, D.R., T. Berger, and T.W. Mak, *Caspase functions in cell death and disease*. *Cold Spring Harb Perspect Biol*, 2013. **5**(4): p. a008656.
302. Soengas, M.S. and S.W. Lowe, *Apoptosis and melanoma chemoresistance*. *Oncogene*, 2003. **22**(20): p. 3138-51.
303. Crouch, S.P.M., et al., *The Use of Atp Bioluminescence as a Measure of Cell-Proliferation and Cytotoxicity*. *Journal of Immunological Methods*, 1993. **160**(1): p. 81-88.
304. Shaw, R.J. and L.C. Cantley, *Ras, PI(3)K and mTOR signaling controls tumour cell growth*. *Nature*, 2006. **441**(7092): p. 424-30.
305. Liu, Z.M., et al., *Calcium-mediated activation of PI3K and p53 leads to apoptosis in thyroid carcinoma cells*. *Cell Mol Life Sci*, 2007. **64**(11): p. 1428-36.
306. Sluijter, M., et al., *Inhibition of CSF-1R supports T-cell mediated melanoma therapy*. *PLoS One*, 2014. **9**(8): p. e104230.
307. Giricz, O., et al., *Abstract 3332: Aberrant expression of CSF1R in melanoma is driven through an endogenous viral promoter and it contributes to malignant growth and the acquisition of resistance against BRAF inhibition*. *Cancer Research*, 2017. **77**(13 Supplement): p. 3332.
308. Buttari, B., et al., *Neuropeptide Y induces potent migration of human immature dendritic cells and promotes a Th2 polarization*. *FASEB J*, 2014. **28**(7): p. 3038-49.
309. Wheway, J., H. Herzog, and F. Mackay, *The Y1 receptor for NPY: a key modulator of the adaptive immune system*. *Peptides*, 2007. **28**(2): p. 453-8.
310. Bender, C. and A. Ullrich, *PRKX, TTBK2 and RSK4 expression causes Sunitinib resistance in kidney carcinoma- and melanoma-cell lines*. *Int J Cancer*, 2012. **131**(2): p. E45-55.

311. Cui, Y., et al., *AGK enhances angiogenesis and inhibits apoptosis via activation of the NF-kappaB signaling pathway in hepatocellular carcinoma*. *Oncotarget*, 2014. **5**(23): p. 12057-69.
312. Lemke, J., et al., *Selective CDK9 inhibition overcomes TRAIL resistance by concomitant suppression of cFlip and Mcl-1*. *Cell Death Differ*, 2014. **21**(3): p. 491-502.
313. Verbsky, J. and P.W. Majerus, *Increased levels of inositol hexakisphosphate (InsP6) protect HEK293 cells from tumor necrosis factor (alpha)- and Fas-induced apoptosis*. *J Biol Chem*, 2005. **280**(32): p. 29263-8.
314. Gobel, K., et al., *Collateral neuronal apoptosis in CNS gray matter during an oligodendrocyte-directed CD8(+) T cell attack*. *Glia*, 2010. **58**(4): p. 469-80.
315. Friese, M.A. and L. Fugger, *Autoreactive CD8+ T cells in multiple sclerosis: a new target for therapy?* *Brain*, 2005. **128**(Pt 8): p. 1747-63.
316. Sharma, P., et al., *Primary, Adaptive, and Acquired Resistance to Cancer Immunotherapy*. *Cell*, 2017. **168**(4): p. 707-723.
317. Sharma, S. and A. Rao, *RNAi screening: tips and techniques*. *Nat Immunol*, 2009. **10**(8): p. 799-804.
318. Reynolds, A., et al., *Rational siRNA design for RNA interference*. *Nat Biotechnol*, 2004. **22**(3): p. 326-30.
319. Jackson, A.L. and P.S. Linsley, *Recognizing and avoiding siRNA off-target effects for target identification and therapeutic application*. *Nat Rev Drug Discov*, 2010. **9**(1): p. 57-67.
320. Jacoby, E., et al., *The 7 TM G-protein-coupled receptor target family*. *ChemMedChem*, 2006. **1**(8): p. 761-82.
321. Pace, U., et al., *Odorant-Sensitive Adenylate-Cyclase May Mediate Olfactory Reception*. *Nature*, 1985. **316**(6025): p. 255-258.
322. Pace, U. and D. Lancet, *Olfactory GTP-binding protein: signal-transducing polypeptide of vertebrate chemosensory neurons*. *Proc Natl Acad Sci U S A*, 1986. **83**(13): p. 4947-51.
323. Spehr, M. and S.D. Munger, *Olfactory receptors: G protein-coupled receptors and beyond*. *J Neurochem*, 2009. **109**(6): p. 1570-83.
324. Sklar, P.B., R.R. Anholt, and S.H. Snyder, *The odorant-sensitive adenylate cyclase of olfactory receptor cells. Differential stimulation by distinct classes of odorants*. *J Biol Chem*, 1986. **261**(33): p. 15538-43.
325. Ronnett, G.V., et al., *Odorant-Sensitive Adenylate-Cyclase - Rapid, Potent Activation and Desensitization in Primary Olfactory Neuronal Cultures*. *Proceedings of the National Academy of Sciences of the United States of America*, 1991. **88**(6): p. 2366-2369.
326. Jaworsky, D.E., et al., *Calcium modulates the rapid kinetics of the odorant-induced cyclic AMP signal in rat olfactory cilia*. *J Neurosci*, 1995. **15**(1 Pt 1): p. 310-8.
327. Wong, S.T., et al., *Disruption of the type III adenylyl cyclase gene leads to peripheral and behavioral anosmia in transgenic mice*. *Neuron*, 2000. **27**(3): p. 487-97.
328. Bakalyar, H.A. and R.R. Reed, *Identification of a Specialized Adenylyl Cyclase That May Mediate Odorant Detection*. *Science*, 1990. **250**(4986): p. 1403-1406.
329. Jones, D.T. and R.R. Reed, *Golf: an olfactory neuron specific-G protein involved in odorant signal transduction*. *Science*, 1989. **244**(4906): p. 790-5.
330. Belluscio, L., et al., *Mice Deficient in Golf Are Anosmic*. *Neuron*, 1998. **20**(1): p. 69-81.
331. Kajiya, K., et al., *Molecular bases of odor discrimination: Reconstitution of olfactory receptors that recognize overlapping sets of odorants*. *Journal of Neuroscience*, 2001. **21**(16): p. 6018-6025.

332. Shirokova, E., et al., *Identification of specific ligands for orphan olfactory receptors. G protein-dependent agonism and antagonism of odorants.* J Biol Chem, 2005. **280**(12): p. 11807-15.
333. Ronnett, G.V. and C. Moon, *G proteins and olfactory signal transduction.* Annual Review of Physiology, 2002. **64**: p. 189-222.
334. Linardopoulou, E., et al., *Transcriptional activity of multiple copies of a subtelomerically located olfactory receptor gene that is polymorphic in number and location.* Human Molecular Genetics, 2001. **10**(21): p. 2373-2383.
335. Hoppe, R., et al., *Sequence analyses of the olfactory receptor gene cluster mOR37 on mouse chromosome 4.* Genomics, 2000. **66**(3): p. 284-95.
336. Bulger, M., et al., *Comparative structural and functional analysis of the olfactory receptor genes flanking the human and mouse beta-globin gene clusters.* Proc Natl Acad Sci U S A, 2000. **97**(26): p. 14560-5.
337. Glusman, G., et al., *The complete human olfactory subgenome.* Genome Res, 2001. **11**(5): p. 685-702.
338. Zozulya, S., F. Echeverri, and T. Nguyen, *The human olfactory receptor repertoire.* Genome Biol, 2001. **2**(6): p. RESEARCH0018.
339. Olender, T., D. Lancet, and D.W. Nebert, *Update on the olfactory receptor (OR) gene superfamily.* Hum Genomics, 2008. **3**(1): p. 87-97.
340. Malnic, B., P.A. Godfrey, and L.B. Buck, *The human olfactory receptor gene family.* Proc Natl Acad Sci U S A, 2004. **101**(8): p. 2584-9.
341. Glusman, G., et al., *The olfactory receptor gene superfamily: data mining, classification, and nomenclature.* Mamm Genome, 2000. **11**(11): p. 1016-23.
342. Liu, A.H., et al., *Motif-based construction of a functional map for mammalian olfactory receptors.* Genomics, 2003. **81**(5): p. 443-56.
343. Fleischer, J., H. Breer, and J. Strotmann, *Mammalian olfactory receptors.* Front Cell Neurosci, 2009. **3**: p. 9.
344. Ensembl. [cited 2016 16.02]; Available from: http://www.ensembl.org/Homo_sapiens/Gene/Summary?db=core;g=ENSG00000186723;r=19:15807003-15808126;t=ENST00000334920.
345. UniProtKB. [cited 2016 16.02]; Available from: <http://www.uniprot.org/uniprot/Q9Y4A9>.
346. HORDE. [cited 2016 16.02]; Available from: <http://genome.weizmann.ac.il/horde/card/index/symbol:OR10H1/term:OR10X1>.
347. Abaffy, T., *Human Olfactory Receptors Expression and Their Role in Non-Olfactory Tissues A Mini-Review.* Journal of Pharmacogenomics & Pharmacoproteomics, 2015. **06**(04).
348. Ranzani, M., et al., *Revisiting olfactory receptors as putative drivers of cancer.* Wellcome Open Res, 2017. **2**: p. 9.
349. Weng, J., et al., *Increased expression of prostate-specific G-protein-coupled receptor in human prostate intraepithelial neoplasia and prostate cancers.* Int J Cancer, 2005. **113**(5): p. 811-8.
350. Sanz, G., et al., *Promotion of Cancer Cell Invasiveness and Metastasis Emergence Caused by Olfactory Receptor Stimulation.* PLoS ONE, 2014. **9**(1): p. e85110.
351. Wei, P., H. Tang, and D. Li, *Insights into pancreatic cancer etiology from pathway analysis of genome-wide association study data.* PLoS One, 2012. **7**(10): p. e46887.
352. Gelis, L., et al., *Functional expression of olfactory receptors in human primary melanoma and melanoma metastasis.* Exp Dermatol, 2017. **26**(7): p. 569-576.

-
353. Wan, Y.W., G.I. Allen, and Z. Liu, *TCGA2STAT: simple TCGA data access for integrated statistical analysis in R*. Bioinformatics, 2016. **32**(6): p. 952-4.
354. Therneau, T.M. *A Package for Survival Analysis in S*. 2015; Available from: <https://cran.r-project.org/package=survival>.
355. Jiang, Y., Y. Li, and B. Zhu, *T-cell exhaustion in the tumor microenvironment*. Cell Death Dis, 2015. **6**: p. e1792.
356. Wen, A.Y., K.M. Sakamoto, and L.S. Miller, *The role of the transcription factor CREB in immune function*. J Immunol, 2010. **185**(11): p. 6413-9.
357. Falvo, J.V., et al., *A stimulus-specific role for CREB-binding protein (CBP) in T cell receptor-activated tumor necrosis factor alpha gene expression*. Proc Natl Acad Sci U S A, 2000. **97**(8): p. 3925-9.
358. Samten, B., et al., *CREB, ATF, and AP-1 transcription factors regulate IFN-gamma secretion by human T cells in response to mycobacterial antigen*. J Immunol, 2008. **181**(3): p. 2056-64.
359. Hsueh, Y.P., et al., *CD28-costimulation activates cyclic AMP-responsive element-binding protein in T lymphocytes*. J Immunol, 1997. **158**(1): p. 85-93.
360. Pogoda, K., et al., *Regulation of gap junction channels and hemichannels by phosphorylation and redox changes: a revision*. BMC Cell Biol, 2016. **17 Suppl 1**(Suppl 1): p. 11.
361. Lee, P.R., et al., *Protease-activated receptor-1 activation by granzyme B causes neurotoxicity that is augmented by interleukin-1beta*. J Neuroinflammation, 2017. **14**(1): p. 131.
362. Nalli, A.D., et al., *Regulation of Gbetagammai-dependent PLC-beta3 activity in smooth muscle: inhibitory phosphorylation of PLC-beta3 by PKA and PKG and stimulatory phosphorylation of Galphai-GTPase-activating protein RGS2 by PKG*. Cell Biochem Biophys, 2014. **70**(2): p. 867-80.
363. Huang, J., et al., *Inhibition of Galphaq-dependent PLC-beta1 activity by PKG and PKA is mediated by phosphorylation of RGS4 and GRK2*. Am J Physiol Cell Physiol, 2007. **292**(1): p. C200-8.
364. Keefe, D., et al., *Perforin triggers a plasma membrane-repair response that facilitates CTL induction of apoptosis*. Immunity, 2005. **23**(3): p. 249-62.
365. Patel, S.P. and R. Kurzrock, *PD-L1 Expression as a Predictive Biomarker in Cancer Immunotherapy*. Molecular Cancer Therapeutics, 2015. **14**(4): p. 847-856.
366. Jo, M. and S.T. Jung, *Engineering therapeutic antibodies targeting G-protein-coupled receptors*. Exp Mol Med, 2016. **48**(2): p. e207.
367. Vaidehi, N., J.E. Pease, and R. Horuk, *Chapter 13 Modeling Small Molecule-Compound Binding to G-Protein-Coupled Receptors*, in *Chemokines, Part A*. 2009, Academic Press. p. 263-288.
368. Grigoriadis, D.E., et al., *Drugability of extracellular targets: discovery of small molecule drugs targeting allosteric, functional, and subunit-selective sites on GPCRs and ion channels*. Neuropsychopharmacology, 2009. **34**(1): p. 106-25.
369. Hui, E.F., et al., *T cell costimulatory receptor CD28 is a primary target for PD-1-mediated inhibition*. Science, 2017. **355**(6332): p. 1428-+.

Supplementary Data

Supplementary R code: RNAi screening analysis script

```
#####
## CTL_modifier screens ...cellHTS
#####
#load cellHTS2 first and load other packages later
# looks like cellHTS2 annotation does not work adequately when other packages are loaded together
with it?
library('cellHTS2')
## CellHTS2 report
## set all parameters
## setwd for analysis
setwd("...")
path=getwd()
Name="cellline_xx_CTLversusnoCTL"
Outdir_report="..."
LogTransform=TRUE
Annotation="GeneID_NEWdouble_1_2_3_67_68.txt"
PlateList="Platelist_CTL_noCTL.txt"
# the file PlateConfig_2013-07-29.txt was incorrectly annotated...
# therefore use PlateConfig_2013-08-12.txt
Plateconf="PlateConfig_2013-08-12.txt"
Screenlog="Screenlog.txt"
Description="Description_GPCR.txt"
NormalizationMethod="median"
NormalizationScaling="multiplicative"
VarianceAdjust="none"
SummaryMethod="mean"
Score="zscore"
## run the first analysis
x = readPlateList(PlateList,name=Name)
x = configure(x, descripFile=Description, confFile=Plateconf, logFile=Screenlog, path=path)
xp = x
xp = normalizePlates(x, log=LogTransform, scale=NormalizationScaling,
method=NormalizationMethod, varianceAdjust=VarianceAdjust)
xp@state["normalized"] = TRUE
xsc = scoreReplicates(xp, sign = "-", method = Score)
xsc = summarizeReplicates(xsc, summary = SummaryMethod)
xsc = annotate(xsc, geneIDFile = Annotation)
out = writeReport(raw = x, normalized = xp, scored = xsc, outdir=Outdir_report, force=TRUE)

#####
#analysis of screen from cellHTS2 output
#####
# load all other libraries that can be useful
library('car')
library('lattice')
library('limma')
library('gplots')
library('ggplot2')
library('reshape2')
```

```
df_xx = read.delim(...)
head(df_xx)
# define which plates are withCTL versus noCTL
# first order the df based on plates and well
df = df_xx
df <- df[order(df$plate, df$well),]
head(df)
df$condition <- recode(df$plate, "1:5='Tcells_Luc'; 6:10='noTcells_Luc'")
# split df into 2 based on condition:
tcells <- subset(df, df$condition == 'Tcells_Luc')
notcells <- subset(df, df$condition == "noTcells_Luc")
head(tcells)
dim(tcells)
head(notcells)
dim(notcells)
# calculate correlation:
corr_tcells = cor(tcells$normalized_r1_ch1, tcells$normalized_r2_ch1, use= "complete.obs")
corr_tcells
corr_notcells = cor(notcells$normalized_r1_ch1, notcells$normalized_r2_ch1, use= "complete.obs")
corr_notcells
corr_all = cor(df$normalized_r1_ch1, df$normalized_r2_ch1, use= "complete.obs")
corr_all
df_compare = tcells
head(df_compare)
df_compare$score_noTcells = notcells$score
head(df_compare)
df_compare = df_compare[, c("wellAnno", "Gene", "score", "score_noTcells")]
head(df_compare)
df_compare = df_compare[order(df_compare$Gene),]
head(df_compare)
df_forquant = df_compare
head(df_forquant)

df_forquant$diff_score = df_forquant$score - df_forquant$score_noTcells
head(df_forquant)
df_forquant = df_forquant[order(df_forquant$diff_score),]
head(df_forquant)
dim(df_forquant)
# check if NA need to be removed
df_forquant$diffscoreRank = c(1:1920)
head(df_forquant)
df_forquant = df_forquant[order(df_forquant$Gene),]
head(df_forquant)
## plot the data as quadrant overview based on scores
# reduce plotting of interesting genes...
# check for high and low
#####
head(df_forquant)
df_forquant_x = df_forquant
head(df_forquant_x)
df_forquant_x$wellAnno = NULL
df_forquant_x$Gene = NULL
df_forquant_x$diff_score = NULL
```

```

df_forquant_x$diffscoreRank = NULL
head(df_forquant_x)
df_forquant_x = data.matrix(df_forquant_x)
library("aroma.light")
normalizeQuantileRank(df_forquant_x, xTarget=NULL)-> A1_1_quant
head(A1_1_quant)
class(A1_1_quant)
A1_1_quant = as.data.frame(A1_1_quant)
A1_1_quant$Gene = df_compare$Gene
head(A1_1_quant)
df_quant_diff = A1_1_quant
head(df_quant_diff)
df_quant_diff$diff_score = df_quant_diff$score - df_quant_diff$score_noTcells
head(df_quant_diff)
df_quant_diff = df_quant_diff[order(df_quant_diff$diff_score),]
head(df_quant_diff)
dim(df_quant_diff)
df_quant_diff$diffscoreRank = c(1:1920)
df_forquant2 = df_quant_diff
head(df_forquant2)
# reduce plotting of interesting genes...
# check for high and low

#####
##### try loess fitting:
#head(df_forquant)
#head(df_forquant2)
# fit loess in:
## learn curve
x <- df_forquant2$score_noTcells
y <- df_forquant2$score
I <- which(is.finite(x) & is.finite(y))
model1 <- loess(y[I] ~ x[I], span=0.99)
x2 = seq(-4,4,length.out=1000)
p1 = predict(model1, x2)
#plot the loess learned curve
lines(x2, p1, col="blue", lwd=2, lty="dotdash")
#####
## apply loess fit to data
p = predict(model1, df_forquant2$score_noTcells) # some p's will be NA!!!
res1 = df_forquant2$score - p
#make res1 from loess fitting a dataframe
res1_df <- as.data.frame(res1)
head(res1_df)
dim(res1_df)
# add the res1 data to the toget_merge2 dataframe
df_forquant2$loess_resi <- res1
head(df_forquant2)
# sort df based on loes residulas:
df_forquant2 = df_forquant2[order(df_forquant2$loess_resi),]
head(df_forquant2)
dim(df_forquant2)
df_forquant2$loess_resiRank = c(1:1920)

```

```
head(df_forquant2)
# here comes the analysis of the CTG screen
#####
## CTL_modifier screens ...cellHTS
### CTG cell viability to be used as a filter for Tcell tox...###
#####
#load cellHTS2 first and load other packages later
# looks like cellHTS2 annotation does not work adequately when other packages are loaded together
with it?
library('cellHTS2')
## CellHTS2 report
## set all parameters
## setwd for analysis setwd(...)
path=getwd()
Name="cellline_xx_CTGviability"
Outdir_report="... "
LogTransform=TRUE
Annotation="GeneID_NEWdouble_1_2_3_67_68.txt"
PlateList="Platelist_CTL_noCTL.txt"
Plateconf="PlateConfig_2013-08-23.txt"
Screenlog="Screenlog.txt"
Description="Description_GPCR.txt"
NormalizationMethod="median"
NormalizationScaling="multiplicative"
VarianceAdjust="none"
SummaryMethod="mean"
Score="zscore"
## run the first analysis
x = readPlateList(PlateList,name=Name)
x = configure(x, descripFile=Description, confFile=Plateconf, logFile=Screenlog, path=path)
xp = x
xp = normalizePlates(x, log=LogTransform, scale=NormalizationScaling,
method=NormalizationMethod, varianceAdjust=VarianceAdjust)
xp@state["normalized"] = TRUE
xsc = scoreReplicates(xp, sign = "-", method = Score)
xsc = summarizeReplicates(xsc, summary = SummaryMethod)
xsc = annotate(xsc, geneIDFile = Annotation)
out = writeReport(raw = x, normalized = xp, scored = xsc, outdir=Outdir_report, force=TRUE)
#####
#analysis of screen from cellHTS2 output
#####
# load all other libraries that can be useful
library('car')
library('lattice')
library('limma')
library('gplots')
library('ggplot2')
library('reshape2')
## get the dataframe and check the data in an explorative manner
df = read.delim(...)
head(df)
dim(df)
# get the controls from the dataframe and plot them
```

```

df_ctrls = subset(df, ! df$wellAnno == "sample")
head(df_ctrls)
dim(df_ctrls)
## get the modified dataframe with median for ctrl and check the data in an explorative manner
df = read.delim(...)
head(df)
# calculate correlation:
# for all data
corr_all = cor(df$normalized_r1_ch1, df$normalized_r2_ch1, use= "complete.obs")
corr_all
corr_all = cor(df$raw_r1_ch1, df$raw_r2_ch1, use= "complete.obs")
corr_all
corr_samples = cor(samples$normalized_r1_ch1, samples$normalized_r2_ch1, use= "complete.obs")
corr_samples
corr_samples = cor(samples$raw_r1_ch1, samples$raw_r2_ch1, use= "complete.obs")
corr_samples
df_filterout = subset(df, df$score > 1.5 | df$score < -1.5)
dim(df_filterout)
df_filterout
#####
filterout = df_filterout$Gene
controlneg1 <- as.character(filterout)
#####
# get all important dataframes!
#load dataframe of analyzed and normalized screen
df_1 = read.delim(...)
head(df_1)
# plot quadrant
## plot the data as quadrant overview based on score noTcells and loess fitted score
df_score_noTcells_filterout = subset(df_1, df_1$score_noTcells > 2.5 | df_1$score_noTcells < -2.5)
dim(df_score_noTcells_filterout)
head(df_score_noTcells_filterout, n=75)
df_score_noTcells_filterout = df_score_noTcells_filterout$Gene
df_score_noTcells_filterout = as.character(df_score_noTcells_filterout)
df_score_noTcells_filterout
### filtering of CTG and noTcell tox from screen:
dim(df_1)
df_filtered_CTG = subset(df_1, ! df_1$Gene %in% filterout)
dim(df_filtered_CTG)
head(df_filtered_CTG)
df_filterd_CTG_and_viab = subset(df_filtered_CTG, ! df_filtered_CTG$Gene %in%
df_score_noTcells_filterout)
dim(df_filterd_CTG_and_viab)
### filter further for score_Tcells... which is higher than ??
### > 0.5 & < - 0.5
df_filter_final = subset(df_filterd_CTG_and_viab_naomit,
df_filterd_CTG_and_viab_naomit$score > 0.5 |
df_filterd_CTG_and_viab_naomit$score < - 0.5 )
dim(df_filter_final)
df_filter_final_final = subset(df_filter_final,
df_filter_final$loess_resi > 1 |
df_filter_final$loess_resi < - 1 )
dim(df_filter_final_final)

```

```

df_filter_final_final
df_filter_final_ctrls_removed = subset(df_filter_final_final, ! df_filter_final_final$Gene == "ctrl1a")
df_filter_final_ctrls_removed = subset(df_filter_final_ctrls_removed, !
df_filter_final_ctrls_removed$Gene == "ubc")
df_filter_final_ctrls_removed = subset(df_filter_final_ctrls_removed, !
df_filter_final_ctrls_removed$Gene == "ccr9")
df_filter_final_ctrls_removed = subset(df_filter_final_ctrls_removed, !
df_filter_final_ctrls_removed$Gene == "cd274")
df_filter_final_ctrls_removed = subset(df_filter_final_ctrls_removed, !
df_filter_final_ctrls_removed$Gene == "cd274a")
df_filter_final_ctrls_removed = subset(df_filter_final_ctrls_removed, !
df_filter_final_ctrls_removed$Gene == "plk1")
df_filter_final_ctrls_removed = subset(df_filter_final_ctrls_removed, !
df_filter_final_ctrls_removed$Gene == "gal3")
df_filter_final_ctrls_removed = subset(df_filter_final_ctrls_removed, !
df_filter_final_ctrls_removed$Gene == "gal3")
df_filter_final_ctrls_removed = subset(df_filter_final_ctrls_removed, !
df_filter_final_ctrls_removed$Gene == "gal3a")
df_filter_final_ctrls_removed = subset(df_filter_final_ctrls_removed, !
df_filter_final_ctrls_removed$Gene == "casp3")
df_filter_final_ctrls_removed = subset(df_filter_final_ctrls_removed, !
df_filter_final_ctrls_removed$Gene == "rpm1")
df_filter_final_ctrls_removed = subset(df_filter_final_ctrls_removed, !
df_filter_final_ctrls_removed$Gene == "rpmia")
df_filter_final_ctrls_removed = subset(df_filter_final_ctrls_removed, !
df_filter_final_ctrls_removed$Gene == "ctrl1")

df_filter_final_ctrls_removed
dim(df_filter_final_ctrls_removed)
write.table(df_filter_final_ctrls_removed, file = "...", sep="\t", quote=FALSE)

```

Supplementary lists

GPCR/Kinase library

HGNC Symbol

AAK1	ADCK4	AK4	AKD1	AURKB	BMPR2
AATK	ADCK5	AK5	AKT1	AURKC	BMX
ABL1	ADK	AK7	AKT2	AVPR1A	BRAF
ABL2	ADRA1A	AK8	AKT3	AVPR1B	BRD2
ACVR1	ADRA1B	AKAP1	ALK	AXL	BRDT
ACVR1B	ADRB2	AKAP11	ALPK2	AZU1	BTK
ACVR1C	ADRBK1	AKAP13	AMHR2	BCKDK	BUB1
ACVR2A	ADRBK2	AKAP3	ANGPT4	BDKRB2	BUB1B
ACVR2B	AGK	AKAP4	ANKK1	BLK	CALM3
ACVRL1	AGTR2	AKAP5	APPL1	BLNK	CAMK1
ADAM9	AK1	AKAP6	ARAF	BMP2K	CAMK1D
ADCK1	AK2	AKAP7	ATM	BMPR1A	CAMK1G
ADCK2	AK3	AKAP8	ATR	BMPR1B	CAMK2A

CAMK2B	CDKN1A	DAPK2	EPHA1	GFRA2	RAPGEF3
CAMK2D	CDKN1B	DAPK3	EPHA2	GK	RAPGEF4
CAMK2G	CDKN1C	DBF4	EPHA3	GK2	RFK
CAMK4	CDKN2B	DCK	EPHA4	GMFB	RIPK4
CAMKK1	CDKN2C	DCLK1	EPHA5	GMFG	ROPN1L
CAMKK2	CDKN2D	DDR1	EPHA6	GNE	SCYL2
CARD10	CDKN3	DDR2	EPHA7	GRK4	SGK196
CARD14	CERK	DGKA	EPHA8	GRK5	SGK223
CASK	CHEK1	DGKB	EPHB1	GRK6	SGK494
CCL2	CHEK2	DGKD	EPHB2	GRK7	SHPK
CCL4L2	CHKA	DGKE	EPHB3	GSG2	SPEG
CD3E	CHKB	DGKG	EPHB4	GSK3A	STK32B
CD4	CHRM1	DGKI	EPHB6	GSK3B	STRADB
CD7	CHUK	DGKQ	ERBB2	GTF2H1	STYK1
CDADC1	CINP	DGKZ	ERBB3	GUCY2C	THNSL1
CDC42BPA	CIT	DGUOK	ERBB4	GUCY2D	TNK2
CDC42BPB	CKB	DLG1	ERN1	GUCY2F	TP53RK
CDC42BPG	CKM	DLG2	ETNK1	GUK1	TRIB1
CDC7	CKMT1B	DLG3	ETNK2	HCK	TRIB3
CDK1	CKMT2	DLG4	FASTK	HIPK1	TSSK4
CDK10	CKS1B	DMPK	FER	HIPK2	ULK3
CDK11B	CKS2	DNAJC3	FES	HIPK3	ULK4
CDK11A	CLK1	DOK1	FGFR1	HIPK4	YSK4
CDK12	CLK2	DTYMK	FGFR2	HK1	KIAA1399
CDK13	CLK3	DUSP1	FGFR3	HK2	ACAD10
CDK15	CLK4	DUSP10	FGFR4	HK3	ALDH18A1
CDK19	CNKSRI	DUSP2	FGR	HSPB8	ALPK1
CDK2	COL4A3BP	DUSP22	FLT1	HUNK	ALPK3
CDK20	COPB2	DUSP4	FLT3	IPPK	BRSK1
CDK3	CRKL	DUSP5	FLT4	IQCH	C9orf96
CDK4	CSF1R	DUSP6	FN3K	ITGB1BP1	CAMKV
CDK5	CSK	DUSP7	FN3KRP	LRRK1	CDK14
CDK5R1	CSNK1A1L,CSNK1A1L	DUSP8	FPGT-TNNI3K,TNNI3K	MAPK15	CDK16
CDK5R2	CSNK1D	DYRK1A	FRK	MASTL	CDK17
CDK5RAP1	CSNK1E	DYRK1B	FUK	MECOM	CDK18
CDK5RAP3	CSNK1G1	DYRK2	FXN	MLKL	COASY
CDK6	CSNK1G2	DYRK3	FYB	MTOR	CSNK1A1L
CDK7	CSNK1G3	DYRK4	FYN	FLJ32685	DCLK2
CDK8	CSNK2A1	EDN2	GAK	FLJ35107	DCLK3
CDK9	CSNK2A2	EEF2K	GALK1	NADK	EIF2AK2
CDKL1	CSNK2B	EGFR	GALK2	NUAK1	EVI5L
CDKL2	CXCL10	EIF2AK1	GAP43	PLK3	EXOSC10
CDKL3	DAK	EIF2AK3	GCK	POM121L10P,BCRCK	
CDKL5	DAPK1	EIF2AK4		PPP1R17	IGF1R

IKBKAP	MAP2K1	MARK1	NME1-NME2,NMIF	PHKFB2	PKN3
IKBKB	MAP2K2	MARK2	NME1-NME2,NMIF	PHKFB3	PLK1
IKBKE	MAP2K3	MARK3	NME3	PFKFB4	PMVK
IL2	MAP2K4	MARK4	NME4	PFKL	PNKP
ILK	MAP2K5	MAST2	NME5	PFKM	PPP1R1B
ILKAP	MAP2K6	MAST3	NME6	PFKP	PPP2CA
INSR	MAP2K7	MATK	NME7	PGK1	PPP2CB
INSRR	MAP3K1	MBIP	NPR1	PGK2	PPP4C
IP6K1	MAP3K10	MELK	NPR2	PHKA1	PRKAA1
IP6K2	MAP3K11	MERTK	NRBP1	PHKA2	PRKAA2
IP6K3	MAP3K12	MET	NRBP2	PHKG1	PRKACA
IPMK	MAP3K13	MINK1	NRG3	PHKG2	PRKACB
IRAK1	MAP3K14	MKNK1	NTRK1	PI4K2A	PRKACG
IRAK2	MAP3K2	MKNK2	NTRK2	PI4K2B	PRKAG1
IRAK3	MAP3K3	MOK	NTRK3	PI4KA	PRKAG3
IRS1	MAP3K4	MOS	OBSCN	PI4KB	PRKAR1A
ITK	MAP3K5	MPP1	OXR1	PICK1	PRKAR2A
ITPK1	MAP3K6	MPP2	PACSIN1	PIK3C2A	PRKAR2B
ITPKA	MAP3K7	MPP3	PAG1	PIK3C2B	PRKCA
ITPKB	MAP3K8	MPZL1	PAK1	PIK3C2G	PRKCB
ITPKC	MAP3K9	MRC2	PAK2	PIK3CA	PRKCD
JAK1	MAP4K1	MST1R	PAK3	PIK3CB	PRKCE
JAK2	MAP4K2	MST4	PAK4	PIK3CG	PRKCG
JAK3	MAP4K3	MUSK	PAK6	PIK3R1	PRKCH
KDR	MAP4K4	MVD	PAK7	PIK3R2	PRKCI
KHK,CGREF1	MAP4K5	MVK	PANK1	PIK3R3	PRKCQ
KIAA1804	MAPK1	MYLK	PANK3	PIK3R4	PRKCSH
KIF13B	MAPK10	MYLK2	PANK4	PIM1	PRKCZ
KIT	MAPK11	MYLK3	PAPSS1	PIM2	PRKD1
KSR2	MAPK12	MYO3A	PAPSS2	PINK1	PRKD2
LAMTOR3	MAPK13	MYO3B	PASK	PIP4K2A	PRKD3
LATS1	MAPK14	NAGK	PCK1	PIP4K2B	PRKDC
LATS2	MAPK3	NBEA	PCK2	PIP4K2C	PRKG1
LCK	MAPK4	NEK1	PDGFRA	PIP5K1A	PRKG2
LCP2	MAPK6	NEK11	PDGFRB	PIP5K1A	PRKRA
LIMK1	MAPK7	NEK2	PDIK1L	PIP5KL1	PRKX
LIMK2	MAPK8	NEK3	PDK1	PITPNM3	PRKX,PRKY
LMTK2	MAPK8IP1	NEK4	PDK2	PKIA	PRPF4B
LMTK3	MAPK8IP2	NEK6	PDK3	PKIB	PRPS1
LTK	MAPK8IP3	NEK7	PDK4	PKLR	PRPS1L1
LYN	MAPK9	NEK8	PDLIM5	PKM	PRPS2
MAGI3	MAPKAPK2	NEK9	PDPK1	PKMYT1	PRPSAP1
MAK	MAPKAPK3	NIM1	PDXK	PKN1	PRPSAP2
MALT1	MAPKAPK5	NLK	PFKFB1	PKN2	PSKH1

PSKH2	ROCK1	NME8	TNFRSF10A	ADRA2A	CCR4
PTK2	ROCK2	NUAK2	TNK1	ADRA2B	CCR5
PTK2B	ROR1	PBK	TPK1	ADRA2C	CCR6
PTK6	RPS6KA1	RBKS	TRAT1	ADRB1	CCR7
PTK7	RPS6KA2	RIOK1	TRIB2	ADRB2	CCR8
PTPN5	RPS6KA3	RNASEL	TRIO	ADRB3	CCR9
PTPRG	RPS6KA4	ROR2	TRPM6	ADRBK1	CCRL1
PTPRJ	RPS6KA5	ROS1	TRPM7	ADRBK2	CCRL2
PTPRR	RPS6KA6	RP2	TSKS	AGTR1	CD3E
PTPRT	RPS6KB1	SGK2	TSSK1B	AGTR2	CD97
PXK	RPS6KB2	SLK	TSSK1B,DGCR14,TSK1	CCRL1	CELSR1
RAC1	RPS6KC1	SOCS5	TTBK1	AKT1	CELSR2
RAF1	RPS6KL1	SPHK2	TTBK2	ARL3	CELSR3
RASGRF2	RYK	SQSTM1	TTK	ARRB1	CHAF1B
RPRD1A	SCYL1	SRC	TTN	AVPR1A	CHRM2
SCYL3	SEPHS1	SRMS	TXK	AVPR1B	CHRM3
SIK3	SEPHS2	SRPK1	TYK2	AVPR2	CMKLR1
SMAD7	SGK1	SRPK2	TYRO3	BAI1	CNR1
STK32A	SGK3	STK10	UCK1	BAI2	CNR2
STK32C	SHC1	STK17B	UCK2	BAI3	CRHR1
STK40	SIK1	STK33	UCKL1	BDKRB1	CRHR2
STRADA	SIK2	STK4	UGP2	BDKRB2	CRY1
TAOK1	SKAP1	SYK	ULK1	BLR1	CX3CR1
TAOK2	SMG1	TAF1L,TAF1	ULK2	BRS3	CXCL1
TAOK3	SNRK	TAF1L,TAF1	VRK1	C17ORF35	CXCL12
TBCK	SOCS1	TAOK2	VRK2	C3	CXCL2
TNIK	SPA17	TBK1	VRK3	C3AR1	CXCL3
TPD52L3	SPHK1	TEC	WEE1	C5	CXCL9
TWF1	SRPK3	TEK	WIF1	C5R1	CXCR3
TWF2	STK11	TESK1	XYLB	C7ORF9	CXCR4
UHMK1	STK16	TESK2	YES1	CALCA	CXCR6
WNK1	STK17A	TEX14	YWHAH	CALCR	CYSLTR1
WNK2	STK19	TGFBR1	YWHAQ	CALCRL	CYSLTR2
WNK3	STK24	TGFBR2	ZAK	CALM1	DEFB4
WNK4	STK25	TIE1	ZAP70	CASR	DRD1
CMPK1	STK3	TJP2	ADCYAP1R1	CCBP2	DRD5
KALRN	STK31	TK1	ADMR	CCL17	EBI2
ABI1	STK35	TK2	ADORA1	CCL2	ECE2
AURKA	STK36	TLK1	ADORA2A	CCL23	EDG1
BRSK2	STK38	TLK2	ADORA2B	CCL25	EDG2
CDC42SE2	STK38L	TLR1	ADORA3	CCL3	EDG3
MAST1	STK39	TLR3	ADORA1A	CCR1	EDG4
PLK2	TSSK3	TLR4	ADORA1B	CCR2	EDG5
PLK4	TSSK6	TLR6	ADORA1D	CCR3	EDG6

EDG7	GLP2R	GPR128	GPR51	GRM2	OR5P2
EDG8	GNA13	GPR132	GPR52	GRM3	OR5P3
EDNRA	GNA14	GPR14	GPR54	GRM4	TRAR5
EDNRB	GNA15	GPR141	GPR55	GRM5	GPR147
ELOVL4	GNAI1	GPR143	GPR56	GRM6	GRK1
ELTD1	GNAI3	GPR145	GPR58	GRM7	LPHN2
EMR1	GNAO1	GPR146	GPR6	GRM8	LPHN3
EMR3	GNAQ	GPR15	GPR61	GRPR	LTB4R
ENPP2	GNAS	GPR155	GPR62	H963	LTB4R2
F2R	GNAT1	GPR156	GPR63	HRH1	MAS1
F2RL1	GNAT2	GPR157	GPR64	HRH2	MAS1L
F2RL2	GNAZ	GPR160	GPR65	HRH3	MASS1
F2RL3	GNB1	GPR161	GPR68	HRH4	MBC2
FKSG79	GNB3	GPR17	GPR7	HTR1A	MC1R
FKSG83	GNB4	GPR18	GPR73	HTR1B	MC2R
FLJ10060	GNG11	GPR19	GPR73L1	HTR1D	MC3R
FLJ10458	GNG12	GPR2	GPR74	HTR1E	MC4R
FLJ11856	GNG3	GPR20	GPR75	HTR1F	MC5R
FLJ31393	GNG4	GPR21	GPR77	HTR2A	MGC24137
FPR1	GNG5	GPR22	GPR78	HTR2C	MGC26856
FPRL1	GNG7	GPR23	GPR8	HTR3A	MGC40047
FPRL2	GNRHR	GPR24	GPR80	HTR3B	MLN
FSHR	GNRHR2	GPR25	GPR81	HTR4	MRGPRF
FY	GPBAR1	GPR26	GPR82	HTR5A	MRGX1
FZD1	GPR	GPR27	GPR83	HTR6	MRGX2
FZD10	GPR1	GPR3	GPR84	HTR7	MRGX3
FZD2	GPR10	GPR30	GPR85	ICF45	MRGX4
FZD3	GPR100	GPR31	GPR86	IL8	MS4A2
FZD4	GPR101	GPR32	GPR87	IL8RA	MTNR1A
FZD5	GPR105	GPR34	GPR88	IL8RB	MTNR1B
FZD6	GPR109A	GPR35	GPR91	KCNJ3	NMBR
FZD7	GPR109B	GPR37	GPR92	KCNJ5	NMUR2
FZD8	GPR110	GPR37L1	GPR97	KCNJ6	NPR1
FZD9	GPR111	GPR39	GPRC5B	KCNJ9	NPR2
GABBR1	GPR112	GPR4	GPRC5C	LANCL1	NPR3
GALR2	GPR113	GPR40	GPRC5D	LGR7	NPY
GCG	GPR115	GPR41	GPRC6A	LGR8	NPY1R
GCGR	GPR116	GPR42	GPSM2	LHCGR	NPY2R
GHRHR	GPR119	GPR43	GRCA	LOC115131	NPY5R
GHSR	GPR119	GPR44	GRK4	LPHN1	NTSR1
GIPR	GPR12	GPR45	GRK5	MLNR	NTSR2
GIT1	GPR123	GPR48	GRK6	NMUR1	OPN1LW
GIT2	GPR124	GPR49	GRK7	OPN5	OPN1MW
GLP1R	GPR126	GPR50	GRM1	OR10A5	OPN1SW

OPN3	OR2C3	P2RY1	PTHR2	SMO	TAS2R5
OPN4	OR2F1	P2RY10	PTPN6	SORT1	TAS2R60
OPRD1	OR2H1	P2RY11	RAMP1	SREB3	TAS2R7
OPRK1	OR2H3	P2RY12	RASD1	SST	TAS2R8
OPRL1	OR2J2	P2RY2	RDS	SSTR1	TAS2R9
OPRM1	OR2S2	P2RY4	RGR	SSTR2	TBL3
OR10H1	OR2T1	P2RY5	RGS1	SSTR3	TBXA2R
OR10H2	OR2W1	P2RY6	RGS11	SSTR4	TRAR1
OR10J1	OR3A1	P2RY8	RGS12	SSTR5	TRAR3
OR11A1	OR3A2	PDC	RGS14	TACR1	TRAR4
OR12D2	OR3A3	PDCL	RGS16	TACR2	TRHDE
OR12D3	OR4D1	PIK3CB	RGS19	TACR3	TRHR
OR1A1	OR51B2	PIK3CG	RGS19IP1	TAS1R1	TSHB
OR1A2	OR51B4	PNR	RGS2	TAS1R2	TSHR
OR1C1	OR51E2	PPYR1	RGS20	TAS2R1	VIP
OR1D2	OR52A1	PRB4	RGS3	TAS2R10	VIPR1
OR1D4	OR5F1	PTAFR	RGS4	TAS2R13	VIPR2
OR1D5	OR5I1	PTGDR	RGS5	TAS2R14	VN1R1
OR1E1	OR5V1	PTGER1	RGS6	TAS2R16	VN1R2
OR1E2	OR6A2	PTGER2	RGS7	TAS2R3	VN1R3
OR1F1	OR7A17	PTGER3	RGS9	TAS2R39	VN1R4
OR1G1	OR7A5	PTGER4	RHO	TAS2R4	VN1R5
OR1J5	OR7C2	PTGFR	ROM1	TAS2R40	WDR5B
OR2A4	OR8B8	PTGIR	RRH	TAS2R41	XCR1
OR2B2	OXER1	PTH	SALPR	TAS2R46	XPR1
OR2C1	OXTR	PTHR1	SCTR	TAS2R48	

Custom library

HGNC Symbol

ACP5	CIB1	DUSP16	FCRLA	GRB14	HLA-DMB
ACPP	CLDN3	DUSP18	FLVCR1	GRB7	HLA-DOB
BCAM	CLTCL1	DUSP19	FST	GRIA1	HLA-DPA1
CANT1	CRK	DUSP23	GFRA1	GRIA2	HLA-G
CD163L1	CRLF2	DUSP26	GFRA4	GRIA3	IL11RA
CD300C	CSF2RA	DU	GHR	GRIA4	IL13RA1
CD300E	CTDSP1	SP3	GJA1	GRID2	IL18RAP
CD300LF	CTNND1	DUSP9	GOSR1	GRIK2	IL1RAPL1
CD46	DCC	EDAR	GOSR2	GRIK4	IL20RA
CDC14A	DOLPP1	EPM2A	GPD1	GRIK5	IL22RA2
CDC25A	DUSP11	F3	GPR135	GRIN3A	IL23R
CDC25B	DUSP12	FAM89B	GPR142	HAVCR2	IL28RA
CDC25C	DUSP14	FCRL1	GRAP2	HFE	INPPL1
CENPE	DUSP15	FCRL3	GRB10	HLA-B	ITPR1

ITPR3	LRP3	KIF4A	PKHD1	PTP4A3	SFRP1
KCNH2	LRP5	KIF5C	PLAUR	PTPDC1	SFRP2
KCNH3	M6PR	KIR2DL5	PLXNB3	PTPLA	SFRP4
KCNH4	MAML2	LAMR1	PPAP2B	PTPLB	SH2D1A
KCNH7	MARCO	LILRB2	PPAP2C	PTPMT1	SH3BP5
KCNH8	MINPP1	MCC	PPEF1	PTPN1	SKAP2
KDEL3	MPL	MGC26484	PPEF2	PTPN12	SSH1
KIF11	MS4A1	MPRA	PPM1A	PTPN13	SSH2
KIF12	MS4A6A	NRP2	PPM1B	PTPN14	SSH3
KIF13A	MS4A7	PLXNA3	PPM1D	PTPN18	STYXL1
KIF14	MS4A8B	PNRC2	PPM1E	PTPN21	TAB1
KIF15	MSR1	PPP1R3B	PPM1F	PTPN22	TAS2R42
KIF16B	MTM1	PRB3	PPM1G	PTPN23	TENC1
KIF17	MTMR1	PSPHL	PPM1H	PTPN3	TIMM50
KIF18A	MTMR2	PTEN	PPM1J	PTPN4	TMEM123
KIF1A	MTMR3	PTENP1	PPM1L	PTPN7	TPTE
KIF1B	MTMR4	PTPN11	PPP1CA	PTPN9	UIMC1
KIF1C	MTMR6	PTPRA	PPP1CB	PTPRB	ADM
KIF20A	MTMR7	PTPRU	PPP1R16A	PTPRC	AGRP
KIF20B	MTMR8	ROBO1	PPP1R3C	PTPRD	AKAP10
KIF22	MYOC	RTN4RL1	PPP1R3D	PTPRE	AKAP9
KIF23	ACPI	SCG3	PPP2R1A	PTPRF	ALCAM
KIF25	CDC14B	SFRP5	PPP2R1B	PTPRH	AMH
KIF26A	CLDN4	SH120	PPP2R2B	PTPRK	ANGPT1
KIF2A	CNTFR	SH3BGR	PPP2R5A	PTPRM	ANGPT2
KIF2B	CTDP1	STYX	PPP2R5B	PTPRN	ANGPTL1
KIF2C	CXADR	TPTE2	PPP2R5C	PTPRN2	ANGPTL2
KIF3A	DUSP13	NCR1	PPP2R5D	PTPRO	APOL2
KIF3B	DUSP21	NCR3	PPP2R5E	PTPRS	ASGR2
KIF3C	EBP	NGFR	PPP3CA	PTPRZ1	ASIP
KIF5A	FKBP8	NPAS4	PPP3CB	PVR	AVP
KIF5B	GRAP	NPC1	PPP3CC	PVRL2	BCL10
KIF9	GRIK3	NPTN	PPP3R2	RAMP2	BMP15
KIFC1	GRINL1A	NPTXR	PPP4R1	RAMP3	BMP2
KIFC3	HLA-A	NSMAF	PPP5C	RGS17	BMP3
LAT	HLA-C	OSCAR	PPP6C	RNGTT	BMP5
LEPR	HLA-DOA	OSMR	PPTC7	RTN4R	BMP7
LIF	HLA-DQA1	PDCD1	PROCR	RTN4RL2	BZRAP1
LILRA4	HLA-DQB1	PDP1	PSD	SCARB1	CCK
LILRB1	HLA-DRA	PDP2	PSPH	SEMA3A	CCL1
LILRB4	HLA-DRB1	PER1	PTCH1	SEMA3F	CCL11
LILRB5	HLA-DRB3	PER2	PTCH2	SEMA4D	CCL13
LMBR1L	HLA-E	PGAP2	PTP4A1	SEMA6B	CCL16
LPPR3	KIF21A	PHLPP1	PTP4A2	SEZ6L2	CCL18

CCL19	CSF2RB	FGF13	HDGF	IL1RAP	FGF9
CCL20	CSF3	FGF14	HLA-DMA	IL1RAPL2	GDF1
CCL21	CSF3R	FGF16	HMGN3	IL1RL1	GDF15
CCL22	CTF1	FGF17	IAPP	IL1RL2	GDF5
CCL24	CX3CL1	FGF18	ICAM1	IL1RN	GP6
CCL26	CXCL11	FGF19	ICAM2	IL21R	IFNA10
CCL27	CXCL13	FGF20	ICAM3	IL22	IFNA13
CCL28	CYFIP2	FGF21	IFNA14	IL22RA1	IFNA17
CCL5	CYTL1	FGF23	IFNA16	IL24	IFNA21
CCL7	DBI	FGF3	IFNA2	IL26	IFNA4
CCL8	DGCR2	FGF4	IFNA5	IL27RA	IFNB1
CD1D	DIAPH1	FGF5	IFNA6	IL2RA	IGF2
CD2	DLG5	FGF6	IFNA8	IL2RB	IK
CD247	DLL3	FGF7	IFNAR1	IL2RG	IL1F9
CD28	DMBT1	FGF8	IFNAR2	IL3	IL3RA
CD300LB	DOK2	FIGF	IFNG	IL36A	SHC3
CD302,LY75-CD300LB	DOK4	FLNA	IFNGR1	IL36B	SIVA
CD36	DOK5	FLT3LG	IFNW1	IL36RN	TAS2R38
CD3D	DVL1	FOLR1	IGF1	IL37	WNT10A
CD3G	DVL2	FOLR2	IKBKG	MSTN	WNT4
CD40	EDA	FOLR3	IL10	AREG	WNT7B
CD44	EDIL3	FRS3	IL10RA	BAG4	WNT8B
CD5	EDN1	FRZB	IL10RB	BDNF	PLIN3
CD6	EFNA1	FSHB	IL11	BMP4	RELT
CD69	EFNA2	GAB1	IL12B	BMP6	SHB
CD72	EFNA5	GAST	IL12RB1	BMP8B	SLA
CD8A	EFNB1	GDF10	IL12RB2	BZRP	SLAMF6
CD8B	EFNB2	GDF11	IL13RA2	CCL14	SNX9
CD93	EGFL6	GDF2	IL15	CCL15	SORL1
CDK2AP1	EPO	GDF9	IL15RA	CCL3L1	STAM
CGA	EPS15L1	GDNF	IL16	CD14	STMN1
CHGB	EREG	GFRA3	IL17A	CD33	TACSTD2
CKLF,CKLF-CMTM1	ESM1	GH2	IL17B	CLEC2	TFG
CLCF1	FADD	GHRH	IL17C	CNTF	TGFBRAP1
CLEC4D	FAS	GHRL	IL17RA	CSSL1	TIRAP
CLEC4M	FCAR	GIP	IL17RB	DAG1	TLR10
CMTM7	FCER1A	GLG1	IL18	DLL4	TLR5
CORT	FCER1G	GNRH1	IL18BP	EDN3	TLR7
CR1	FCER2	GNRH2	IL18R1	EGF	TLR9
CR2	FCGRT	GP1BA	IL19	FCGR1A	TNFRSF10C
CRH	FCRL2	GRB2	IL1A	FCGR2A	TNFRSF10D
CSF1	FEM1B	GRP	IL1B	FCGR2B	TNFRSF11A
CSF2	FGF10	HAMP	IL1R1	FCGR3B	TNFRSF13B
	FGF11	HBEGF	IL1R2	FGF1	TNFRSF17

TNFRSF21	CD80	GLRA2	ITGB2	HMGA1	NOTCH2
TNFRSF8	CD86	GLRA3	ITGB3	INS	NOTCH3
TNFRSF9	CHRNA1	GRIN1	ITGB3BP	IRS2	NOTCH4
TP53BP2	CHRNA10	GRIN2A	ITGB4	ITGA3	NOV
TRADD	CHRNA2	GRIN2B	ITGB5	ITGAX	NPAS1
TREM1	CHRNA3	GRIN2D	ITGB6	KAB	NPPA
TREM2	CHRNA4	HIF1A	JAG2	LGALS9	NPPB
TRPC4	CHRNA5	HIF3A	JMJD1C	LRP6	NR0B1
TRPC7	CHRNA6	HNF4G	KDELR2	LSP1	NR0B2
TRPM4	CHRNA7	HTR3C	KITLG	MRC1	NR1D1
TRPV2	CHRNA9	IL31RA	KLRAP1	MYD88	NR1D2
TRPV3	CHRN1	IL4	KLRC4- KLRK1,KLRC4	NMB	NR1H3
TYROBP	CHRN2	IL4R	KLRD1	NOTCH1	NR1H4
UNC5B	CHRN3	IL5	KLRF1	NR1H2	NR1I2
UNC5C	CHRNA10	IL5RA	LBR	NR2F2	NR1I3
WASF2	CLEC2D	IL6	LDLR	NR2F6	NR2C1
WNT1	CLOCK	IL6R	LEP	NR4A2	NR2C2
WNT10B	CNOT7	IL6ST	LRP1	NRTN	NR2E1
WNT11	CXCR7	IL7	LRP12	OPCML	NR2E3
WNT16	EPAS1	IL7R	LRP1B	PLXNB1	NR2F1
WNT2	ERG	IL9	LRP2	PMCH	NR3C1
WNT2B	ESR1	IL9R	LRP8	RXRA	NR3C2
WNT3	ESRRA	INHA	LRPAP1	SCGF	NR4A1
WNT3A	ESRRB	INHBA	LTA	TDGF1	NR4A3
WNT5B	ESRRG	INHBB	LTB	TG	NR5A1
WNT6	FASLG	INHBC	LTBP4	TLR2	NR5A2
WNT8A	GABRA1	INSL3	LTBR	TNFRSF7	NR6A1
WNT9A	GABRA2	INSL4	MDK	TNFSF12	NRBF2
WNT9B	GABRA3	INSL5	MED1	TNFSF13	NTF3
ZP2	GABRA4	INSL6	MED14	TP53I3	NTF4
ABCC9	GABRA6	IRS4	MED17	TRPV5	NTS
AHR	GABRB1	ITGA10	MED26	XCL1	OGFR
AIMP1	GABRB2	ITGA2	MED7	XCL2	OLR1
AIP	GABRB3	ITGA2B	MIA	XEDAR	OSM
APOL3	GABRD	ITGA4	CHRNE	ZP3	P2RX1
AR	GABRE	ITGA5	CUBN	NCK1	P2RX2
ARNT	GABRG1	ITGA6	EBAF	NCK2	P2RX3
ARNT2	GABRG2	ITGA7	ESR2	NCOA1	P2RX4
ARNTL	GABRG3	ITGA8	GABRA5	NCOA2	P2RX7
ARNTL2	GABRP	ITGA9	GP1BB	NCOA6	PAX8
ARPP19	GABRQ	ITGAE		NDP	PDGFA
CD180	GABRR1	ITGAL		NFKBIB	PDGFB
CD40LG	GABRR2	ITGAM		NGF	PENK
CD70	GLRA1	ITGB1		NMU	PEX5

PEX7	TAC1	ABCB7	COL7A1	HSPG2	LIG4
PF4	TAC3	ABCC1	COL8A2	KCNA1	LLGL1
PGF	TGFB1	ABCC2	COMP	KCNA3	LMNA
PGR	TGFB3	ABCC3	CORO1A	KCNAB2	LMNB2
PGRMC2	TGFBI	ABCD1	CPNE7	KCND1	LOR
PHB2	TGFBR3	ACTN1	CRB1	KCND2	LUM
PHIP	THBD	ACTN2	CTNND2	KCND3	MAP1A
PLRG1	TLR8	ACTN3	CTNS	KCNE1	MAP1B
PLXNC1	TMED1	ACTN4	CXCL14	KCNE3	MAP2
POMC	TNF	ADD3	DMD	KCNH6	MAP7
PPARA	TNFRSF11B	AFP	DRP2	KCNJ11	MAPT
PPARD	TNFRSF12A	ANK1	EED	KCNJ2	MATN3
PPARG	TNFRSF14	ANKH	ELN	KCNJ8	MATR3
PPARGC1B	TNFRSF18	ANXA7	ENAM	KCNK13	MBP
PRL	TNFRSF19	AP2B1	EPB41L1	KCNK3	MCOLN1
PROK1	TNFRSF1A	AP3B1	EPB42	KCNQ1	MCOLN3
PSPN	TNFRSF1B	APOC1	EPC1	KCNQ2	MGP
PTHLH	TNFRSF25	APOC4	ETF1	KCNQ3	MIP
PVRL1	TNFRSF4	APOM	ETFA	KCNQ4	MLC1
RARA	TNFSF10	AQP3	ETFB	KCNS2	MPZ
RARB	TNFSF11	AQP4	EVPL	KCNV2	MRPL1
RARG	TNFSF13B	AQP5	FAT1	KPNA4	MRPL13
REL	TNFSF15	AQP6	FAT2	KPNA6	MRPL28
RELA	TNFSF18	ARVCF	FAU	KRT10	MRPL32
RLN1	TNFSF4	ATP6V0A4	FBLN1	KRT12	MRPS11
RLN2	TNFSF8	BEST1	FBN1	KRT13	MTA1
RORA	TNFSF9	CACNA2D1	FBN2	KRT14	MYBPC3
RORB	TOB1	CITED4	FLG	KRT15	MYL4
RORC	TOLLIP	CLCA2	FN1	KRT19	MYOT
RXR	TRAK2	CLCN2	FXYD1	KRT2	ABCA1
RXRG	TRAP1	CLCN5	GABARAPL2	KRT20	ABCC6
RYR2	TRH	CLCN7	GADD45A	KRT35	ADD1
RYR3	TRIP6	CLDN16	GADD45G	KRT36	APOA1
S100A6	TRPV6	CLIC4	GFAP	KRT7	AQP1
S100A9	UCN	CLIC5	GJB1	KRT73	AQP2
SELPLG	VEGFA	CNOT2	GJB2	KRT75	AQP7
SLAMF1	VEGFB	CNTNAP2	GJB4	KRT76	ARP3BETA
SMAD6	VEGFC	COL14A1	GJB5	LAMA1	CATSPER2
SOCS2	VEGF	COL18A1	GJB6	LAMA3	CDC10
SORCS1	VLDLR	COL19A1	GJC1	LAMB1	CLCN1
SORCS2	WISP3	COL4A3	GTF2B	LAMB2	CLCNKA
SORCS3	WNT7A	COL4A6	GTF2E1	LAMB3	CNTNAP3
SPN	ZNHIT3	COL5A1	GTF2E2	LAMC2	COG4
SRPR	ABCB1	COL6A1	HBB	LAMC3	COL11A1

COL6A2	NTN3	SLC2A5	TRPM3	FIGLA	FLJ43692
COL6A3	NTN4	SLC2A8	TRPV4	FLJ41423	FLJ44006
CTNNA2	NUMA1	SLC2A9	TUBGCP3	FLJ42842	FLJ44796
EPB41	NUP98	SLC30A3	TUSC3	FLJ44790	FLJ45300
GJA4	NXT1	SLC39A4	UBA52	FLJ90757	FLJ45422
GJB3	PEX13	SLC4A1	USH2A	FNDC9	FLJ45966
HBG1	PHB	SLC4A3	UTRN	GATC	FLJ46010
KAL1	PIGR	SLC4A4	VCL	GGNBP1	FLJ46257
KCNAB3	PKP2	SLC5A1	VIM	HBM	FRG2
KCNK9	PKP3	SLC5A2	VPS13A	IGFL4	GPR158L1
KCNT1	PKP4	SLC5A5	XK	KATNAL2	HHCM
KRT3	PNN	SLC6A2	AK4	KCTD2	KRTAP5-1
KRT4	PPBP	SLC6A4	AMTN	LCN10	LOC163223
KRT5	PROS1	SLC7A7	ARL13A	LINC00238	LOC284757
KRT6A	RDX	SLC7A9	ASTL	LOC100130417	LOC387646
KRT6B	RPS2	SLCO1A2	BLID	LOC283174	LOC388962
KRT6C	RPS3	SLIT3	BLOC1S3	LRRC52	LOC389831
KRT8	RSC1A1,DDI2	SMAD1	C14orf37	LRRIQ1	LOC389832
LAMC1	SCAMP3	SORBS3	C16orf74	LY6G6F	LOC389834
MATN1	SCN1B	SPTB	C16orf87	LYSMD1	LOC389841
NEB	SCN2A	STATH	C1orf168	MAP1LC3C	LOC389842
NID	SCN3A	STEAP3	C1orf194	MCART6	LOC389844
PKP1	SCN4A	STX2	C1orf95	METTL10	LOC389846
PLEC1	SCNN1A	SUPT3H	C21orf119	MTHFD2L	LOC389857
RPS21	SCNN1B	TAF1A	C21orf49	ACTBL1	LOC389873
RPS5	SCNN1G	TAF1C	C8orf82	ASB18	LOC389878
SCAMP1	SLC10A1	TCAP	C9orf173	BPY2B	LOC389888
SCN1A	SLC10A2	TCIRG1	C9orf47	BPY2C	LOC389892
SCN5A	SLC11A1	TCOF1	CALHM1	BTBD7	LOC389893
SLC26A2	SLC11A2	TECTA	CCDC88A	C10ORF55	LOC389895
SLC2A3	SLC12A1	TFPI2	CHTF8	C21ORF37	LOC389896
SLC6A8	SLC12A2	THBS1	CLDN20	C4B	LOC389899
SMTN	SLC12A6	THBS4	COX4NB	CDY1B	LOC389900
STX1A	SLC14A1	TIMM8A	CXorf30	CYP2D7P1	LOC389901
THBS2	SLC14A2	TOM1L1	DBX2	DEFB108	LOC389904
TPM4	SLC16A1	TPCN2	DDI1	FLJ16124	LOC389905
NAPB	SLC17A5	TPM1	DNAJB3	FLJ16171	LOC389907
NCF2	SLC1A1	TPM2	DZANK1-AS1	FLJ16323	LOC389908
NEFH	SLC22A12	TRPC1	ETV3L	FLJ16331	LOC389910
NF2	SLC22A5	TRPC3	EVI5	FLJ16353	LOC389915
NHP2L1	SLC26A4	TRPC5	FAM116B	FLJ31132	LOC389916
NPHP1	SLC2A1	TRPC6	FAM129B	FLJ35429	LOC392425
NPHP4	SLC2A2	TRPM1	FAM149A	FLJ41170	LOC392433
NTN1	SLC2A4	TRPM2	FAM166A	FLJ42258	LOC392439

LOC392447	LOC401621	OR4F5	OR10V1	OR51G1	OR8I2
LOC392467	LOC401622	OR4M1	OR11G2	OR51G2	OR8J1
LOC392473	LOC401623	OR4Q3	OR13G1	OR52H1	OR8J3
LOC392486	LOC401624	OR51A4	OR14A16	OR56A1	OR8K1
LOC392487	LOC401625	OR52A4	OR14J1	OR5AC2	OR9G4
LOC392512	LOC401628	OR5H1	OR1L3	OR5AK2	OR9K2
LOC392517	LOC402388	OR5H15	OR2A2	OR5AP2	PATE2
LOC392528	LOC402414	OR5K2	OR2AE1	OR5B17	PLEKHG7
LOC392531	LOC402434	OR6B2	OR2AT4	OR5B2	PRR19
LOC392533	LOC402436	OR6B3	OR2B3	OR5B3	PRSS58
LOC392539	LOC402556	OR8B2	OR2G2	OR5D16	REEP3
LOC392546	LOC402558	POTE2	OR2J3	OR5H14	RNASEK
LOC392549	LOC414059	PRY2	OR2T11	OR5H2	SERBP1
LOC392559	LOC440607	PSG8	OR2T6	OR5H6	SPINK14
LOC392563	LOC474170	RBMY1B	OR2W5	OR5J2	STGC3
LOC392582	MGC12815	RBMY1D	OR2Y1	OR5K3	STX19
LOC392583	MGC35440	RBMY1E	OR3A4P	OR5K4	SUMO4
LOC392584	MGC39584	RBMY1J	OR4A15	OR5M11	SYNGAP1
LOC392586	MGC44903	TNFSF12-TNFSF13	OR4A16	OR5M8	SYPL2
LOC401577	MGC57359	TRIM6-TRIM34	OR4A47	OR5W2	TARP
LOC401579	NDUFB4	VCX-C	OR4A5	OR6C2	TM6SF2
LOC401581	NOMO3	XKRY	OR4B1	OR6C4	TRAM2
LOC401584	OR11H1	XKRY2	OR4C15	OR6C6	VHLL
LOC401589	OR1L1	NCCRP1	OR4C45	OR6C65	#
LOC401590	OR1L4	NRARP	OR4E2	OR6C68	ZBTB46
LOC401599	OR2A1	OR10A7	OR4F15	OR6C70	ZNF12
LOC401605	OR2L8	OR10AG1	OR4F6	OR6C74	ZNF429
LOC401606	OR2T2	OR10C1	OR4K1	OR6C75	ZNF69
LOC401607	OR2T3	OR10G2	OR4K13	OR6F1	ZNF721
LOC401611	OR4F16	OR10G3	OR4K15	OR6K2	ZYG11A
LOC401613	OR4F17	OR10J3	OR4K2	OR6K3	
LOC401616	OR4F21	OR10K1	OR4K5	OR6M1	
LOC401618	OR4F3	OR10K2	OR4P4	OR6N2	
LOC401620	OR4F4	OR10P1	OR51B5	OR6V1	

Supplementary tables

Supplementary table 1: Differentially expressed genes from RNA sequencing

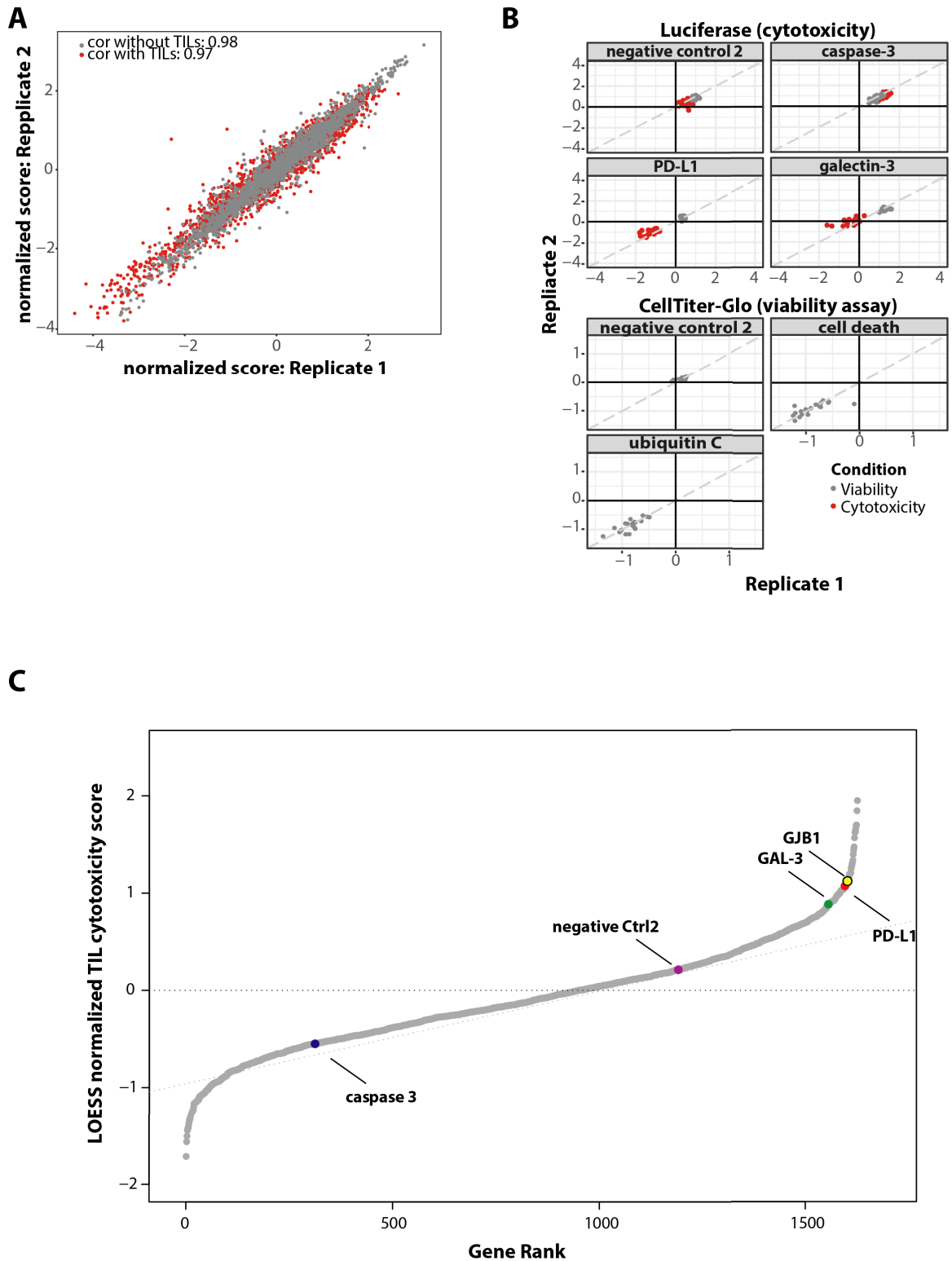
Gene	logFC	FDR	Description
CXCL13	1.55	1.36E-07	Chemokine (C-X-C motif) ligand 13
LINC01125	1.51	0.002657494	Long intergenic non-protein coding RNA 1125
HES1	1.39	4.32E-08	Hes family bHLH transcription factor 1
LINC01531	1.36	3.30E-06	Long intergenic non-protein coding RNA 1531
RN7SK	1.35	9.31E-05	RNA, 7SK small nuclear
CRTAM	1.29	8.06E-87	Cytotoxic and regulatory T cell molecule

BAMBI	1.24	5.77E-07	BMP and activin membrane-bound inhibitor
VGF	1.24	2.13E-07	VGF nerve growth factor inducible
COL7A1	1.22	3.89E-05	Collagen, type VII, alpha 1
MIR17HG	1.11	1.76E-07	miR-17-92 cluster host gene
CCL1	1.05	4.81E-07	Chemokine (C-C motif) ligand 1
GUCY1A2	1.02	0.001661791	Guanylate cyclase 1, soluble, alpha 2
NEK6	1.02	1.52E-40	NIMA-related kinase 6
GNG4	0.97	4.91E-11	Guanine nucleotide binding protein (G protein), gamma 4
FAM131C	0.91	0.003845356	Family with sequence similarity 131, member C
PDLIM4	0.90	1.14E-05	PDZ and LIM domain 4
NAPSA	0.89	0.001173444	Napsin A aspartic peptidase
CXCL1	0.89	1.11E-06	Chemokine (C-X-C motif) ligand 1
XIRP1	0.88	4.55E-14	Xin actin binding repeat containing 1
VAV3	0.85	0.000101738	Vav 3 guanine nucleotide exchange factor
LIM2	0.84	0.002967884	Lens intrinsic membrane protein 2, 19kDa
SNORD104	0.82	0.012031312	Small nucleolar RNA, C/D box 104
FNDC9	0.80	4.84E-14	Fibronectin type III domain containing 9
PODXL2	0.77	0.008513491	Podocalyxin-like 2
CTGF	0.77	0.000373029	Connective tissue growth factor
RNA5-8SP6	0.75	0.012407807	RNA, 5.8S ribosomal pseudogene 6
NEBL	0.75	3.02E-14	Nebulette
ICAM5	0.74	0.000901733	Intercellular adhesion molecule 5, telencephalin
ERRFI1	0.74	0.01068307	ERBB receptor feedback inhibitor 1
MFSD2A	0.72	4.82E-17	Major facilitator superfamily domain containing 2A
SHF	0.72	0.003246346	Src homology 2 domain containing F
METTL1	0.72	2.28E-12	Methyltransferase like 1
CTSL	0.71	0.014273157	Cathepsin L
POU2AF1	0.69	0.005322962	POU class 2 associating factor 1
NIPAL4	0.69	0.012032463	NIPA-like domain containing 4
FOS	0.69	3.09E-05	FBJ murine osteosarcoma viral oncogene homolog
CCR4	0.68	5.26E-26	Chemokine (C-C motif) receptor 4
RPL36A	0.67	0.046088185	Ribosomal protein L36a
KCNC3	0.66	0.028527333	Potassium channel, voltage gated Shaw related subfamily C, member 3
ADM	0.66	0.002126438	Adrenomedullin
CKB	0.64	0.000862595	Creatine kinase, brain
UCP3	0.63	2.82E-17	Uncoupling protein 3 (mitochondrial, proton carrier)
CTXN1	0.63	0.028483242	Cortexin 1
MIR222HG	0.62	0.045765444	MIR222 host gene
TSHZ2	0.62	0.001284676	Teashirt zinc finger homeobox 2
SGPP2	0.61	2.92E-08	Sphingosine-1-phosphate phosphatase 2
ACVR1B	0.61	0.04489157	Activin A receptor, type IB
SMN2	0.60	0.018275287	Survival of motor neuron 1, telomeric
FABP5	0.60	1.49E-18	Fatty acid binding protein 5 (psoriasis-associated)
ADAT2	0.59	3.29E-06	Adenosine deaminase, tRNA-specific 2
SPINT1	0.59	0.00010293	Serine peptidase inhibitor, Kunitz type 1
PMCH	0.59	7.74E-09	Pro-melanin-concentrating hormone
GNPDA1	0.59	8.70E-09	Glucosamine-6-phosphate deaminase 1

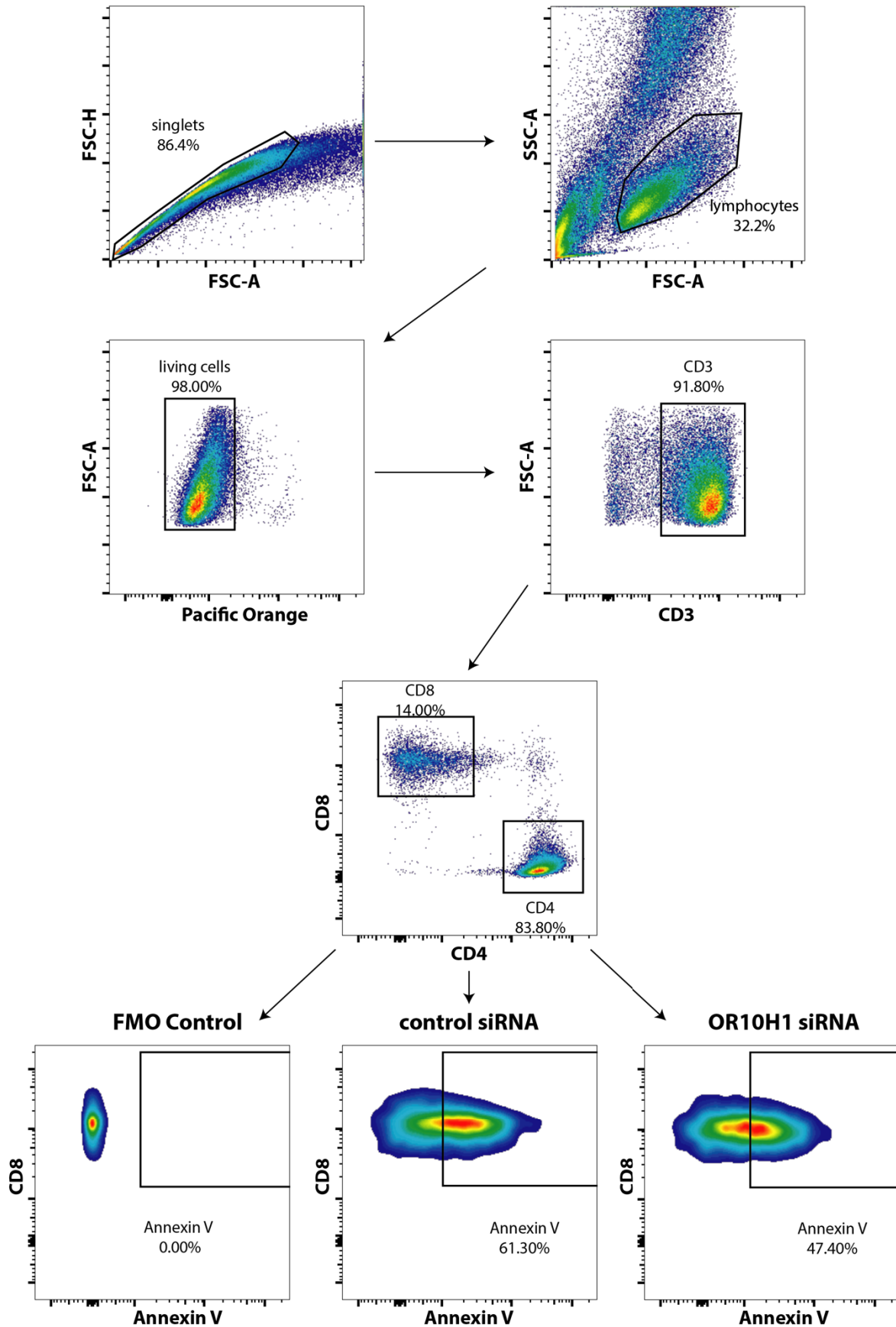
ARC	0.58	0.013190929	Activity-regulated cytoskeleton-associated protein
ANKRD13B	0.58	6.10E-07	Ankyrin repeat domain 13B
CASQ1	0.58	0.02873544	Calsequestrin 1 (fast-twitch, skeletal muscle)
MET	0.56	5.26E-05	MET proto-oncogene, receptor tyrosine kinase
NPM3	0.56	8.85E-09	Nucleophosmin/nucleoplasm 3
TRMT1	0.56	2.40E-21	tRNA methyltransferase 1 homolog (<i>S. cerevisiae</i>)
TBC1D16	0.54	0.006412811	TBC1 domain family, member 16
HECTD2	0.54	0.001173444	HECT domain containing E3 ubiquitin protein ligase 2
RCAN1	0.53	1.72E-13	regulator of calcineurin 1
TSEN2	0.52	0.000356729	TSEN2 tRNA splicing endonuclease subunit
CCL22	0.52	9.42E-05	Chemokine (C-C motif) ligand 22
C1orf228	0.52	0.006060461	Chromosome 1 open reading frame 228
IRF4	0.52	1.87E-23	Interferon regulatory factor 4
NAPA-AS1	0.52	0.046976106	NAPA antisense RNA 1
VPS9D1-AS1	0.52	0.004420594	VPS9D1 antisense RNA 1
SRM	0.52	2.71E-17	Spermidine synthase
SPHK1	0.51	0.000631147	Sphingosine kinase 1
MYC	0.51	6.13E-24	V-myc avian myelocytomatosis viral oncogene homolog
ADCK1	0.50	0.017492807	aarF domain containing kinase 1
NEFH	0.50	2.75E-05	Neurofilament, heavy polypeptide
NR4A2	-0.51	0.004142847	Nuclear receptor subfamily 4, group A, member 2
CDC42EP4	-0.53	0.003947695	CDC42 effector protein (Rho GTPase binding) 4
MEF2C	-0.59	0.036805756	Myocyte enhancer factor 2C
SDK2	-0.59	0.007073487	Sidekick cell adhesion molecule 2
MEGF6	-0.61	0.041116384	Multiple EGF-like-domains 6
IFNGR2	-0.67	0.036155163	Interferon gamma receptor 2
TRPC3	-0.68	0.034780585	Transient receptor potential cation channel, subfamily C, member 3
EGR3	-0.70	0.001013492	Early growth response 3
CD300LD	-0.83	0.000117527	CD300 molecule-like family member d

Supplementary table 2: Second primary screening hit-list

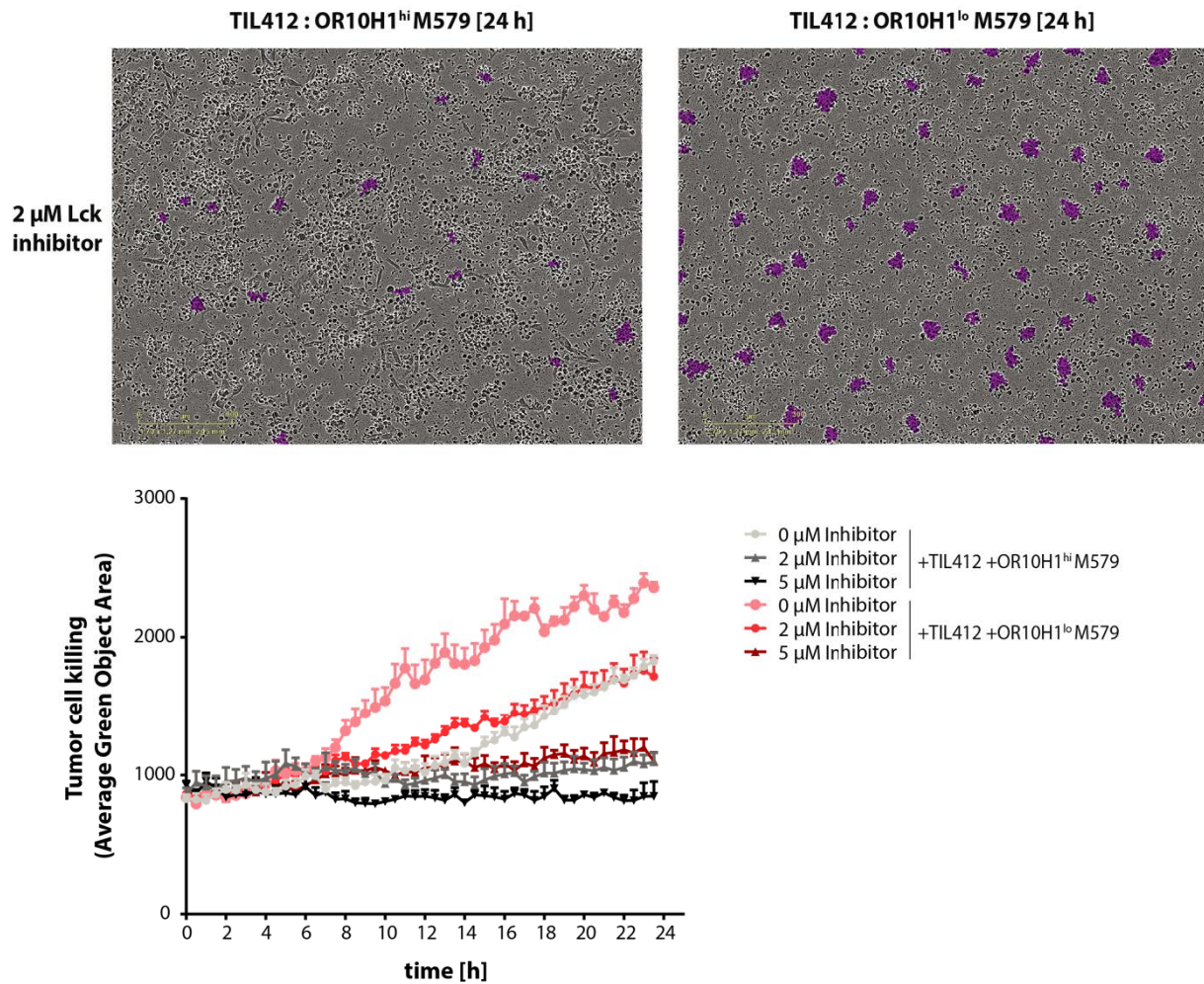
KIF15	NRARP	S100A6	SEZ6L2
SLC7A9	TPM1	KCNE1	CDK2AP1
TNFRSF19	IFNA5	GJB1	TACSTD2
PTPN4	C21orf49	KIF20A	OR6M1
PTPN13	IL12B	DDI1	CD44
MAP1A	MYL4	NCOA2	MED1
APOL3	RPS3	SCNN1B	



Supplementary figure 1: Control performance and results from the second primary screening. Graphical representation of normalized Z-scores for gene knockdown effects on cytotoxicity or viability (A and B). Raw residual luciferase intensities were transformed logarithmically and per-plate normalization was performed by mean normalization and Z-scoring (cellHTS2 for Bioconductor). Z-scores for all samples (A) or specific controls (B) are shown for the cytotoxicity (red) and the viability (grey) set. The CellTiter-Glo viability assay was analysed accordingly. The Pearson's correlation coefficients for cytotoxicity and viability were calculated using the "cor" function of R on the library samples only (without controls). C Graphical summary of screening results ranked according to LOESS cytotoxicity score. Representatives for negative control 2 (dark purple), the immune activator control caspase-3 (blue), the immune checkpoint controls PD-L1 (red) and galectin-3 (green) are labelled.



Supplementary figure 2: Gating strategy for Figure 23C. Representative data of apoptosis induction (measured by FACS staining for Annexin V+) in CD8⁺ TILs after co-culture (6h) with OR10H1-positive or -negative M579-A2. First cell aggregates were excluded and lymphocytes selected. Afterwards, living CD3⁺ lymphocytes were selected. Annexin V positivity was measured on CD8⁺ T cells.



Supplementary figure 3: Lck inhibition does not induce TIL apoptosis or alter TIL behaviour but prevents TIL-dependent tumor lysis. sM579-A2 cells were reverse transfected as before. M579-A2-luc and TIL412 were co-cultured for 20 h in the presence of different concentrations of the Lck inhibitor 7-Cyclopentyl-5-(4-phenoxyphenyl)-7H-pyrrolo[2,3-d]pyrimidin-4-ylamine. Apoptosis was measured by YoYo-1 signal in tumor and TILs by real-time imaging (Incucyte). The level of apoptosis (indicated in purple) was analysed according to paragraph 4.4.2.3.